High Linearity Broad-band Helix TWTs

Richard Owen Jenkins

MPhys, MSc

A Thesis Submitted for the degree of Doctor of Philosophy

June 2003

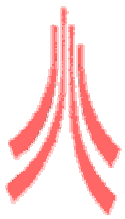

Engineering Department
Lancaster University, UK

DECLARATION

I declare that the thesis is my own work and has not been submitted in substantially the same form for the award of a higher degree elsewhere. Any sections of the thesis which have been published are clearly referenced.

ACKNOWLEDGEMENTS

The Author wishes to thank the following people and organisations for their help and involvement throughout this work:

- The Engineering and Physical Sciences Research Council for funding this project

- The collaborating industries: E2V Technologies and Astrium Space Ltd.

- My supervisor: Prof. Richard Carter, for his expert guidance and support.

- Dr Tushar Ghosh for his collector simulation which was used in Chapter 6.

- My family and April Ventricelli for their love, support and encouragement.

High Linearity Broadband Helix TWTs

Richard Owen Jenkins

A Thesis Submitted for the degree of Doctor of Philosophy

ABSTRACT

Helix travelling-wave tubes (TWTs) are extensively employed as final power amplifiers in satellites. These applications demand low spectral noise and high efficiency across a broad band. Research has been carried out to achieve these criteria in a helix TWT design.

A deeper understanding has been gained on how the basic parameters of a TWT affect its non-linear performance. By selecting and controlling the parameters that are critical to the amplifier's nonlinear performance the designs corresponding to the important and desired conditions have been identified. The main simulation tool for modelling the interaction processes in a generic helix TWT was a large-signal model (LSM).

A helix slow-wave structure is normally tapered to maintain its phase relationship with the electron beam and to maximise its output RF power. By determining the sensitivity of the helix dimensions on the nonlinear performance at different regions along the tube, a non-uniform slow-wave structure design has been developed for a more linear performance. Since the conditions of high linearity and efficiency could not be achieved simultaneously, the best trade-off was attained. The performance across the frequency band of 10.7 to 12.75GHz was computed for the uniform and tapered helix designs. With the use of a simulated multi-stage collector with optimised electrodes, the overall TWT performance was determined

Further understanding has been gained on the fundamental processes in the tube that cause the generation of nonlinear transfer curves and spectral distortion. The modelling of RF beam current and helix voltage waveforms and their characteristics provided a unique insight. In addition, the formation and deceleration of the electron beam bunches have been shown for the various important conditions; revealing the desirable physical conditions within the beam.

June 2003
Engineering Department
Lancaster University
United Kingdom

CONTENTS

Chapter One: Introduction

This introductory chapter will address the need for high linearity broadband helix TWTs in future satellite communications systems. By providing background on helix TWTs, nonlinearity and the future trends of satellite communications, this chapter will discuss the criteria of helix TWTs for future employment in these systems.

1.1 Satellite Communications

Broadband satellite systems are an integral part of communications technology [1]. Transportation of data via a satellite is the most common and preferred method of worldwide communications. There are countless applications for satellites: one such application is direct television broadcasting services for the distribution of programs directly to homes [1]. Other applications include mobile services, where a large fixed earth station communicates with a number of mobile stations on boats or aircraft etc. via a satellite [2,3].

In recent years, satellite communications technology has undergone many new developments. Much of this is due to the introduction of broadband digital technology, to cope with the ever-increasing amount of data traffic. Broadband digital communications has transformed the way information is generated, stored, processed and transported. There is a growing demand for this new technology in mobile communications, multi-media [4] and broadcasting [5].

In order to evolve systems for a full digital network, a new generation of INTELSAT satellites (INTELSATXIII) have been launched, each containing more than 44 transponders and providing a traffic-carrying capacity of 60 to 80 thousand 2-way telephone channels, together with multiple video channels [2]. INTELSAT IX and X are due to be launched at the end of 2003[6]. For these latest systems, both earth stations and satellites must provide enhanced processing and switching so that the satellite networks are fully integrated with the terrestrial networks. Inmarsat's

Broadband Global Area Network will also soon enter service in 2004 [3]. This network consists of 14 satellites supporting small personal devices linked up with handheld and notebook PCs and vehicular installations to remote base stations.

Digital signal processing in satellite communications employs various multiple accessing or multiplexing schemes to suit the application. The schemes include time, frequency and code division multiple access techniques (TDMA, FDMA and CDMA respectively)[7]. TDMA is becoming the most efficient means of processing digital bit streams for satellite systems due to availability of higher speed switching devices. The terminals required for TDMA are also becoming low cost and easy to maintain because of the increased popularity of digital technology [7].

Quadrature phase shift keying (QPSK) is widely used in present and near future systems. As communications data traffic increases however, higher order modulation schemes e.g. 16-64QAM become more desirable [8]. This is because their greater number of data nodes enable a higher bit-rate flow for information processing. Another technique is orthogonal frequency-division multiplexing (OFDM), which copes efficiently with high-speed multi-carrier transmission of digital data. OFDM is therefore used in many transmissions of services, including the European digital terrestrial television broadcasting system. This technique works by implementing an Inverse Fourier Transform to transport an input data stream with a number of tones (or carriers) whose phases are orthogonal. The approximately constant power envelope of the OFDM signal makes it desirable for satellite transmissions. The drawback however, is the large dynamic fluctuations of the signal amplitude caused by the high number of carriers (hundreds) with random phases and amplitudes [9]. 16-64QAM will be probably take place of other schemes in the longer term, due to the greater handling of very high data rates, meeting the needs of future users.

A satellite transponder initially amplifies the incoming broadband signal by about 60dB using low noise amplifiers and filters. The channels contained within the broadband signal are then separated using multiplexers and individually amplified. Another set of multiplexers then recombines the channels back into one broadband signal ready for retransmission [10]; see fig 1.1. The broadband signal sent back to Earth is normally allocated a lower frequency to prevent overpowering the weak

uplink signal. A typical example, of the uplink and downlink frequencies of an Intelsat IX satellite (IS-901) is given in table 1.1. Other examples of UK satellite uplink and downlink frequency allocations for bands L to V are in table 1.2.

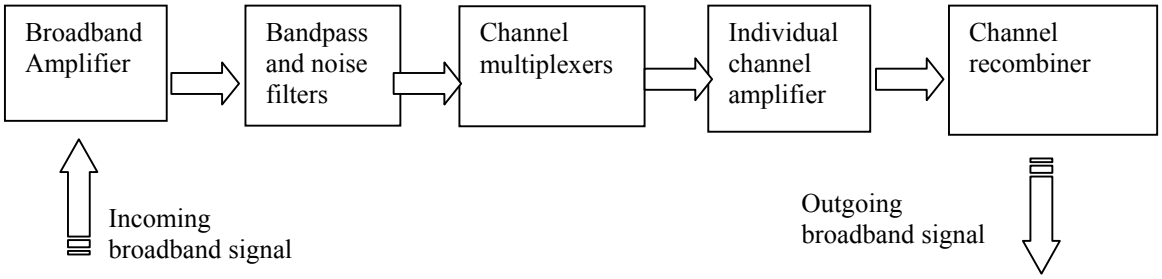

Fig 1.1 A satellite transponder

Table 1.1

Number of Transponders	Bandwidth of each unit	Band	Uplink Frequency	Downlink Frequency
72	36 MHz	C	5850 to 6425 MHz	3625 to 4200 MHz
22	36 MHz	Ku	14.0 to 14.5GHz	10.95 to 11.20GHz 11.45 to 11.70GHz

Table 1.2

Band	Uplink Frequency /GHz	Downlink Frequency /GHz
L	1.6565 to 1.6600	1.530 to 1.535
C	5.850 to 7.075	3.6 to 4.2
Ku	14.00 to 14.25	10.7 to 11.7
Ka	29.5 to 30.0	20.2 to 21.2
V	50.4 to 51.4	37.5 to 39.5

Due to the rapid growths in information traffic facing the satellite telecommunications industries, more efficient usage of their broadband spectrum allocation becomes ever more important. Higher frequency bands (e.g. Ku to V bands) provide an attractive and more accessible medium for broadband satellite systems. The Ku-band will be fully occupied by these broadband (>1GHz) systems by the early part of the 21st century [2]. Higher order modulation schemes e.g. 16 or 32QAM, will be employed in these systems to handle the very high bit flow rates more effectively. The main and essential function of the satellite is the amplification of these modulated signals, this will now be discussed.

1.2 Satellite Amplifiers

There are around 35 to 50 identical microwave power amplifiers on-board a typical modern satellite, which consume 80 to 90% of all the satellite's power [11]. The operation and efficiency of these amplifiers is therefore crucial to the overall operation of a satellite. Satellite amplifiers have to perform a demanding job of amplifying very weak signals (a few mW) to high power levels (100W or higher) continuously over many years in the outer-space environment. For the most efficient operation, they are positioned near the satellite's output antenna and near the outer surface for improved heat dissipation. They are placed well away from sensitive electronics and receivers.

There are two types of power amplifiers, Solid State Power Amplifiers (SSPAs) and Travelling Wave Tube Amplifiers (TWTAs). Travelling wave tubes have been used as final power amplifiers for communications for many decades. Space qualified TWTs can produce hundreds of watts of power consistently across a broad band (more than 1 GHz). TWTs also operate reliably over a lifetime of more than 15 years. The greatest attribute however of space TWTs, is their high efficiency whilst working at both high power (>100W) and frequency (>1GHz) levels: their maximum power added efficiency is from around 60 to 70% [11].

By the early 1980's, microwave solid-state power amplifiers began to replace the TWTA at RF power output levels of 5 to 10 Watts. Since then, the two technologies have been competing with each other. SSPAs are now used in most L-band systems and in C-band systems below say 50W, and in low powered Ku-band devices (below 20W). In C-band applications, say between 20 and 40W, the RF output power, gain and non-linear performance of an SSPA is very comparable to that of a TWTA, but the SSPA has a lower noise figure. The main difference however, which divides the two technologies apart for broadband operation is their efficiencies: the TWT can exceed 55% while the SSPA barely exceeds 40%. Another added bonus with the TWT is its lower overall payload mass as a result to its higher power added efficiency. Even so, many systems choose SSPAs on board the satellite. This is partly due cost effectiveness in manufacturing bulk quantities and also due to reliability [11].

Reliability is an important factor to consider, because more reliable amplifiers require fewer amplifiers on-board the transponder. The consequent weight reduction would considerably reduce the launching costs. In a TWTA, the major reliability problem has been the oxide cathode in the electron gun, which eventually degrades after 20 or more years. Studies carried out in 1994 on an in-orbit comparison at C-band between the TWTA and a GaAs MESFET SSPA, revealed however, that the SSPAs had a greater failure rate [11]. A single operating SSPA was reported to have just over 70% of the average lifetime of a TWTA. Other tests revealed that the failure rate of an SSPA population was higher than the TWTA population by around 15% [12].

For present and future digital satellite communications systems which demand of high frequency signal transmission (Ku band and above) continuously across a broad band. The limited power handling capability of SSPAs means that the TWT will always remain unrivalled. This is because the TWT can transmit high power signals across this band very efficiently. The continuing domination of TWTs makes their operation and properties crucial to the entire field of space communications: any improvement in their performance would enhance the whole system. The biggest problem facing all power amplifiers however is nonlinear distortion; this problem will now be addressed.

1.3 Nonlinearity and Intermodulation Distortion

All amplifiers exhibit distortion in the output signal when the amplitude of the input signal is high enough. The generation of this nonlinear distortion is a major concern in high power amplifiers, especially in space TWTs. Since this project is concerned with this type of microwave power amplifier, nonlinearity is a major issue in this report. The next section will define nonlinearity in power amplifiers and discuss the consequence this has on communications systems. This will then be followed by the techniques used to minimise intermodulaton distortion.

1.3.1 The Non-linear Response in Power Amplifiers

The main way of characterising the non-linear response of a power amplifier (at a particular frequency) is from its transfer curves. An example of a typical transfer curve is shown in fig 1.2. The amplitude (AM/AM) transfer curve is the output RF power as a function of input RF power. When the device is being operated in the linear region, the output power is directly proportional to the input signal power, shown as a straight line at 45° in the figure. The power curve then becomes non-linear as it tends towards its maximum (saturation) point. This is where RF power is actually being lost at that particular frequency, known as compression. In helix TWT amplifiers, the gradient of the AM/AM curve then usually becomes negative beyond power saturation. This is where the output RF power is lost from the circuit back into the beam; the features of the helix TWTs are in Section 1.4.

The non-linear response of a TWT power amplifier is also represented by its phase (AM/PM) transfer curve (see fig 1.2). This phase response is generally small within the linear region. But when driven in the non-linear power region, the phase shift becomes greater. The phase nonlinearity is quantified as the AM/PM conversion Kp: the phase shift in degrees per dB increase in RF input power, as shown in the figure.

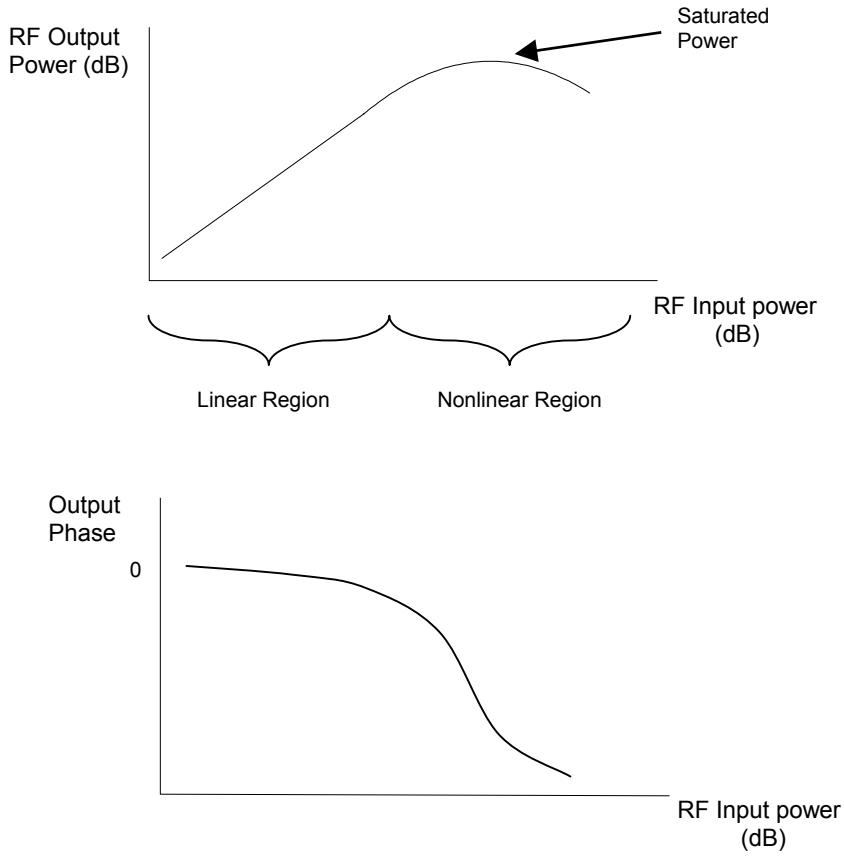

Fig 1.2 AM/AM curve with corresponding AM/PM curve (below) of a typical TWT power amplifier.

1.3.2 Non-Linear Distortion

When a single frequency (or single-carrier) signal is passed through any power amplifier at a drive level where the output RF power is nonlinear and/or is phase shifted, harmonics are generated. For a multi-carrier input signal, the non-linear processes within the amplifier cause mixing between the different carriers, resulting in intermodulation (IM) distortion.

Harmonics do not present a problem, with regards to the output performance, because they arise at multiple frequencies of the input carrier signal, thus well away from the operating band of the amplifier. For multi-carrier signals however, the unwanted spurious signals are displaced from the carrier frequencies by multiples of the

difference frequencies of the carriers, as shown in fig 1.3 for a two-carrier system. Here, the third-order intermodulation products have a much greater influence on the output performance than the other products, because they have greater amplitudes and because they lie adjacent to the carrier signals - closer to the operating band. In practical communications systems where hundreds of closely spaced carriers are used, intermodulation distortion then becomes a severe problem. This is because the IM products arise within the pass-band as well as outside of the band. The IM products may arise at the same frequencies as those of the input signal, modifying the carriers themselves. For digitally modulated signals, this phenomenon, known as spectral regrowth [13] is most problematic, resulting in a large increase in the bit-error rate.

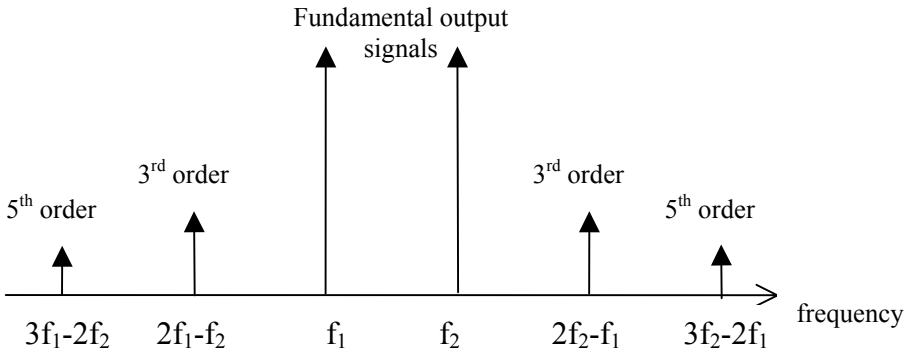

Fig. 1.3 Spectral response of a two-carrier signal

In order to keep the non-linear distortion at a tolerable level, the power amplifier must be operated at a level below (or backed-off) that of saturation where the signal response is more linear. In modern communications systems, where the input signal envelope is amplitude modulated, the output RF power of the signal is varying dynamically. For, say, a hundred carriers, the probability of the signal power occurring above or below its mean value is distributed across a range of powers as shown in fig 1.4 [14]. This dynamic variation of the output signal amplitude must be centred at a specified output backoff (or output power below saturation) so that the carrier-to-intermodulation ratio (C/I) is at a tolerable level. The problem with increased output backoff is that the conversion efficiency[1] is reduced, since the conversion efficiency is maximum at saturation.

[1] Conversion efficiency (or the basic tube efficiency) = $\frac{\text{RF output power – RF input power}}{\text{DC input power}}$

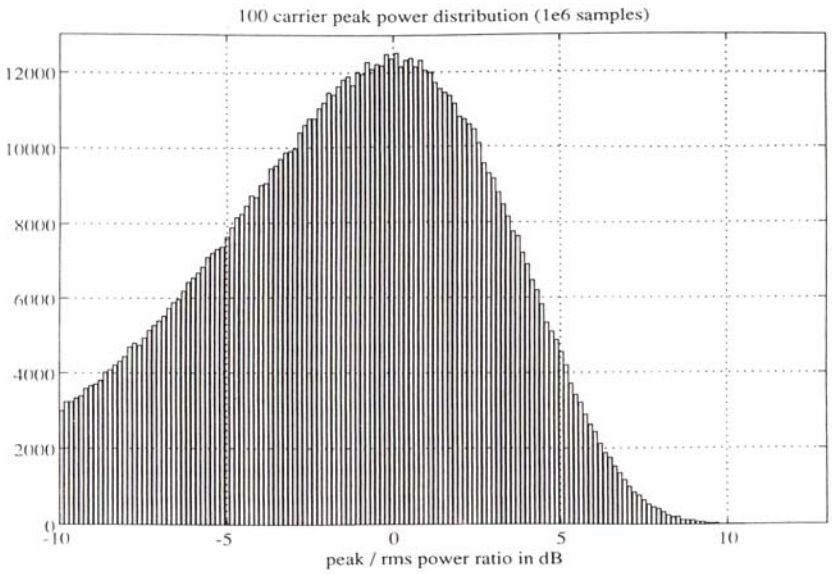

Fig 1.4 Dynamic variation of signal amplitude for a hundred carriers in a TWTA [14]

Obtaining high efficiency is of prime importance in microwave communications applications. This is especially the case in satellite systems, where the power supply is limited and excess heat from the on-board amplifiers is not easily dissipated by radiators into outer space. Satellite amplifiers must therefore be highly efficient, so that a minimum amount of the very limited supply power is dissipated as heat, otherwise resulting in overheating. The amplifier should therefore be operated at a high enough power level to maximise the conversion efficiency but without being too near saturation where the resulting distortion becomes severe.

In multi-carrier communications systems where reduced output spectral distortion is required, power amplifiers have to be operated with greater backoff from saturation. Cellular technology for example, demands highly linear power amplifiers to avoid any co-channel interference in which the reception of a much weaker distant signal may be taking place. This technology requires a carrier-to–interference (C/I) ratio from -35 to -65dBc. The output backoff for a C/I of -35dBc in a class A SSPA is 5.5dB, which can cut two-thirds off its overall efficiency. A C/I of -65dBc requires more than 15dB of output backoff [13].

The general trend of communications systems is to employ higher order modulation schemes in which to transport increasingly vast quantities of data. Since the probability of error occurrence (determined by the bit error rate) in these signal envelopes is higher [7], nonlinearity in power amplifiers will have a more detrimental on the output signal. The issue of nonlinearity therefore becomes an increasingly important topic for future systems. The next section discusses some of the ways of tackling this problem.

1.3.3 Linearisation Techniques

To improve the levels of intermodulation distortion in the output signal of power amplifiers, linearisation methods are often employed. Linearisation techniques include feedforward, feedback and pre-distortion. A basic schematic representation of the feedforward technique is shown in fig 1.5. In the first loop of the circuit, samples of the input signal are subtracted from the output signal of the main amplifier to produce a sample of the amplifier's distortion. The second loop then subtracts this amplified sampled distortion from the delayed output signal of the main amplifier. The improvement in IM distortion in decibels for this technique can be quantified by using equation 1.1.

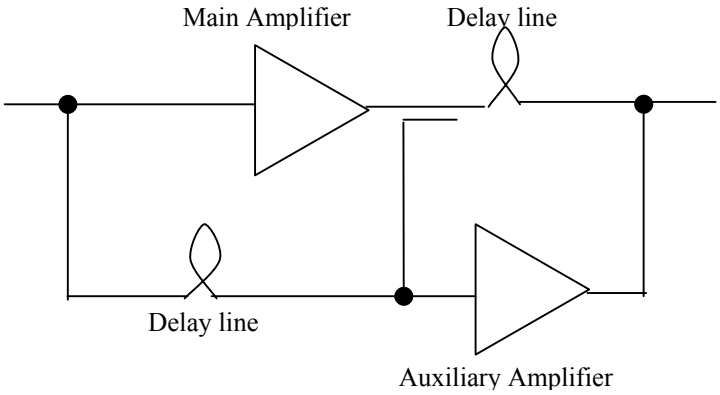

Fig 1.5 A circuit representation of a feed-forward lineariser

$$\Delta IM = -10 \log \left| 1 + 10^{\Delta G / 10} - (2 \times 10^{\Delta G / 10} \cos \Delta \phi) \right| \qquad (1.1)$$

where ΔG is the amplitude mismatch (in dB's) between the main and error paths

$\Delta \phi$ is the phase error in degrees.

This equation illustrates the limitations of the technique. For example, a 2°-phase mismatch is enough to result in a big reduction in intermodulation improvement [15]. The absolute phase must be closely matched with that of an additional auxiliary amplifier, which is required for this technique. This additional amplifier reduces the efficiency of the system and the circuitry is complex [16]. The feed-forward linearisation method is therefore not suitable for space applications.

Another approach that is now used more widely and is much preferred is the pre-distortion method. This technique generates a non-linear transfer curve, which is the reverse of the actual amplifier's transfer curve in both amplitude and phase. When this distorted signal is coupled to the original output signal, the resulting transfer characteristics resemble those of a hard power limiter. This is an effective and practical means of cancelling out the intermodulation products. The carrier-to-interference ratio can be improved by as much as 2.5dB for 8 or more signals [17]. As a consequence, the amplifier can be operated closer to power saturation for a specified carrier-to-interference ratio, enhancing its operating efficiency. The pre-distortion method is especially useful for applications where very low IM distortion (e.g. a C/I below -50dBc) is required. This will continue to gain popularity, as many future systems will require reduced levels of IM distortion. Even the most preferred linearisation method has its drawback in the eyes of industry however; which is expense and added design complexity (e.g. phase matching) and band limitations. It is therefore preferred to somehow find an alternative way of producing a highly linear TWT amplifying system without these drawbacks of an added lineariser. The methods for improving the linear performance of the helix TWT itself will be discussed in Chapter 2. It is necessary to first understand the features and operation of a helix TWT; these will now be explored.

1.4 Helix TWTs

Helix travelling wave tubes can amplify very weak signals of, say, 1mW up to more than 100W of RF power efficiently across a bandwidth greater than 1GHz. These uniquely desirable properties make the helix TWT the most attractive high power-amplifying device for broadband satellite communications. This section will describe the features of helix TWTs and the physical process within them.

1.4.1 Basic features of Helix TWT

A helix TWT consists of three main parts: the electron gun, slow-wave structure and collector. A schematic representation is shown in fig 1.6 [18]. Electrons are emitted when a DC current heats the cathode. Electrodes then accelerate and focus these electrons into a narrow beam. The beam then enters the helix slow-wave structure, where energy from the beam amplifies the RF signal. Within the slow-wave structure, the beam is kept focused by an applied magnetic field, either from a solenoid or periodic permanent magnets (PPM). The latter are more desirable in practice because they are much more compact and lightweight than the solenoid. When the electron beam exits the surrounding slow-wave structure, its energy is considerably reduced, because a proportion (e.g. 15%) of the beam energy has been transferred to the RF signal. The electron beam then enters a multistage depressed collector which collects the spent beam. The collector comprises several electrodes at different electrical potentials. The voltages of these electrodes are selected to maximise the recovery of the different electron energies.

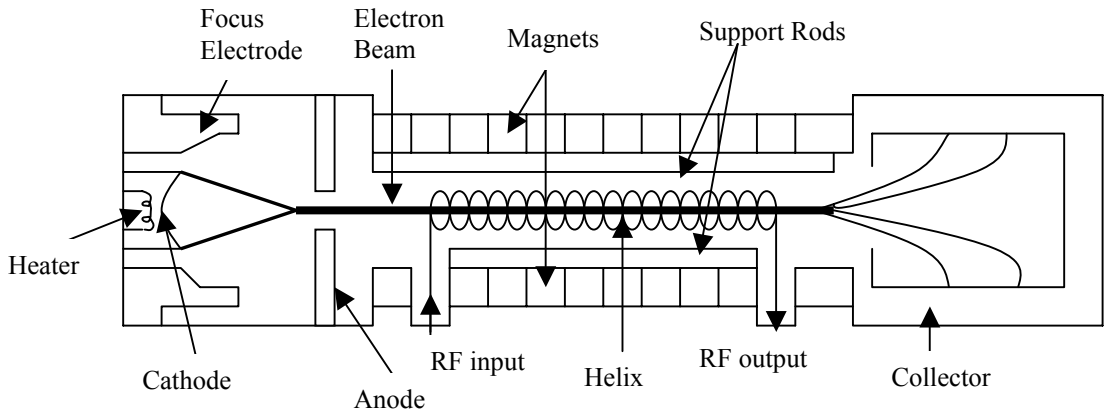

Fig 1.6 Schematic diagram of a Helix TWT

1.4.2 The Helix Slow-Wave Circuit

The helix slow-wave structure is a helical metallic tape (normally copper coated) supported by a series of identical dielectric rods. Figure 1.7 shows the case with wedge shaped supports, which rods are usually made from beryllium oxide (BeO) or anisotopic pyrolytic boron nitride (APBN) encased in an overall metal enclosure. The purpose of the vanes is to prevent circumferential currents flowing in the metal enclosure to improve the dispersive properties of the helix (further discussed in Chapter 2.4). The RF current flows through the metal tape surrounding electron beam. Amplification of the power in the RF wave results from the kinetic energy of the electrons being transferred from the beam. This transfer of energy is only effective however, if the both the electron beam and the RF wave on the helix are travelling at approximately the same velocity. The RF wave on the helix causes electrons in the beam to bunch, as shown in fig 1.8. In the region of these bunched electrons, positive charges are induced on the structure and negative elsewhere. It is these induced charges on the helix which cause the amplitude of the RF current to grow along the helix circuit.

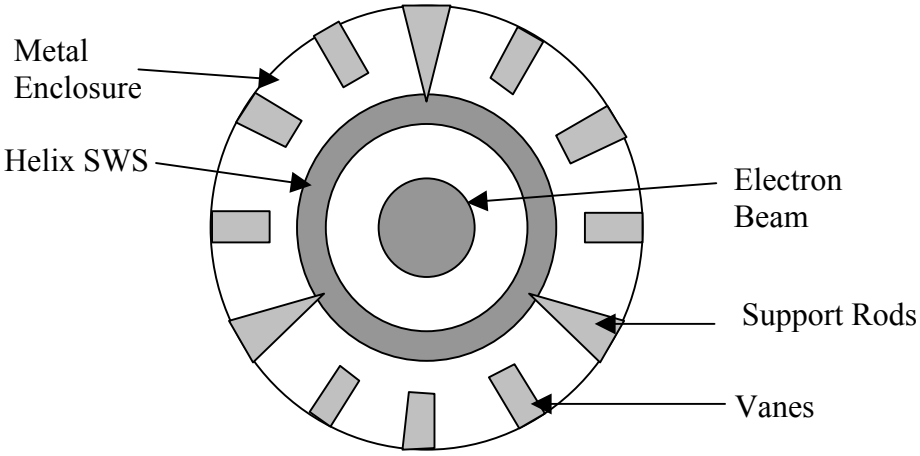

Fig 1.7 2-D (cross-section) schematic diagram of a helix TWT with wedge-shaped supports

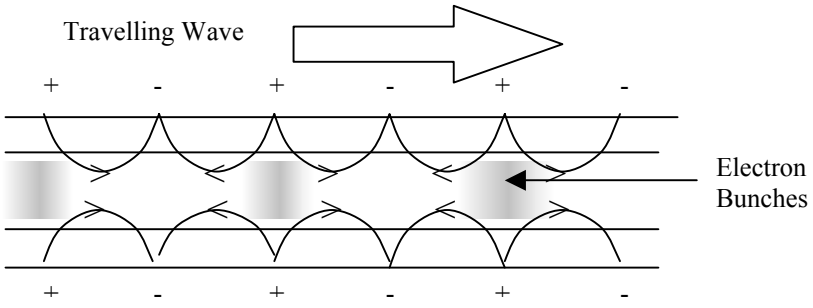

Fig 1.8 A positive charge is induced in the slow-wave structure close to the region of the electron bunches

1.4.3 Severs and Attenuators

A sever is a cut in the helix tape, it therefore represents a region of field free drift space with infinite attenuation, zero propagation and zero interaction impedance. The RF signal is carried across the sever region by the modulated electron beam. A sever ensures stability against feedback oscillations or backward waves. These oscillations are caused by signals reflected by mismatches at the input and output of the slow-wave structure and by the inherent backward wave. Regions of high attenuation lie adjacent to the sever, this eases the mismatch between the sever and RF structure, thus reducing the amplitude of the backward RF signal.

Past computer analysis [19] has shown that a sever incorporated into a slow-wave structure generally increases AM/PM conversion assuming the TWT has a gain greater than 21dB from the sever to output. Incorporating severs and attenuators to the slow-wave structure can also reduce the electronic efficiency (from say 65% to 48%). Despite these drawbacks, severs and attenuators remain essential features for maintaining a stable transmission of power through the circuit.

1.4.4 Models of the Helix

Models are used to provide a theoretical description of the helix slow-wave structure and its interaction with the electron beam. The equivalent circuit analysis is one example, which represents the helix by an equivalent transmission line (see fig 1.9) whose properties are defined by its phase velocity v_p and characteristic impedance Z_0.

The electronic behaviour of the helix can be analysed using two different approximations: the sheath model and the tape model. The sheath model approximates the helix by a helically conducting cylindrical surface of infinitesimal thickness. This provides an effective way of obtaining results for the design of inhomogeneously loaded (i.e. dielectric loading with a varying dielectric constant) helix TWTs.

The dispersion equation (1.2) obtained from the sheath helix model [20] can be separated to produce expressions for the series inductance L_0 and shunt capacitance C_0 per unit length in free space, as shown in equation (1.3).

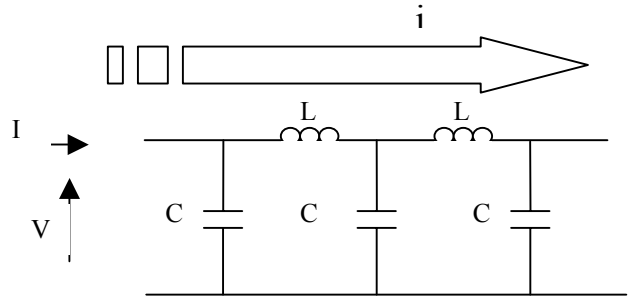

Fig 1.9 Equivalent circuit representation

$$\beta^2 = \omega^2 \varepsilon_0^2 \mu_0 \left(\frac{\beta}{\gamma}\right)^2 cot^2\psi \frac{I_1(\gamma a) K_1(\gamma a)}{I_0(\gamma a) K_0(\gamma a)} \qquad (1.2)$$

$$\gamma = \left[\beta^2 - \left(\omega/c\right)^2\right]^{1/2}$$

where

β = axial propagation constant = ω / v_p

γ = radial propagation constant

ω = angular frequency

ψ = pitch angle

a = helix radius

$$L_0 = \left(\frac{\mu_0}{2\pi}\right)\left(\frac{\beta}{\gamma}\right)^2 \cot^2\psi \,.\, I_1(\gamma a) K_1(\gamma a) \qquad (1.3)$$

$$C_0 = \frac{2\pi\varepsilon_0}{I_0(\gamma a) K_0(\gamma a)}$$

where I_m and K_m (m = 0,1) are modified Bessel functions of the first and second kind. These expressions in (1.2) can be modified to model the effect of the surrounding metal shield and the dielectric support rods.

The propagation constant of the transmission line can therefore be written as:

$$\beta = \omega\sqrt{L_0 C_0} \qquad (1.4)$$

The characteristic impedance of the transmission line is also given as [20]:

$$Z_0 = \sqrt{L_0 / C_0} \qquad (1.5)$$

The tape model represents the helix by a tape of finite width and infinitesimal thickness formed into a cylinder whose radius is the actual helix mean radius. Unlike the sheath helix model, the tape is modelled to conduct in all directions. For tubes which operate at very high voltages and frequencies, the helix circumference becomes comparable to the free space wavelength making it necessary to use the tape model. The axial periodicity of the helical structure also enables the tape model to include the effects of generated space harmonics [21]. Generally, the tape model thus provides a more accurate description of the electrical parameters in the helix, especially the interaction impedance.

1.4.5 The Electron Beam

The electron beam lies at the centre of the TWT in the radial direction, as shown in fig. 1.7. It travels through the radial centre of the helix. The beam is focussed into a uniform laminar flow as energy is being transferred from the electrons to the slow-wave structure, resulting in the amplification of the RF signal. The formation of electron bunches and the deceleration of the electron bunches by the electromagnetic field are fundamental for the electromagnetic induction of RF energy in the circuit [22]. Understanding the physical processes in the beam and its interaction with the slow-wave structure is an important topic of research in this thesis, since these processes are also fundamental to the root causes of non-linearity in the terminal characteristics. This research will be covered in Chapter 4.

Efficient collection of the spent beam ensures that as much DC energy is recovered, so that it can be reused again at the DC input. The design of the multi-element collector therefore has a major effect on the overall efficiency of the tube. Its design and performance can be based solely on the spent beam distribution; such an example is given in fig 1.10. The spent beam energy is the energy remaining in the beam after its interaction with the slow-wave structure. The RF+DC beam current and voltage on entering the collector (I_1 and V_1 respectively) are normalised to their DC values (I_0 and V_0 respectively). The area within the unit square in fig 1.10 represents the initial energy in the beam, while the spent beam energy to the collector is the area under the curve. The portion of spent beam energy beyond the unity line represents the accelerated electrons, which cannot be recovered by the collector, this area should therefore be minimised. The remaining area within the unit square but outside the curve, represents the unspent beam energy, this constitutes RF energy and losses.

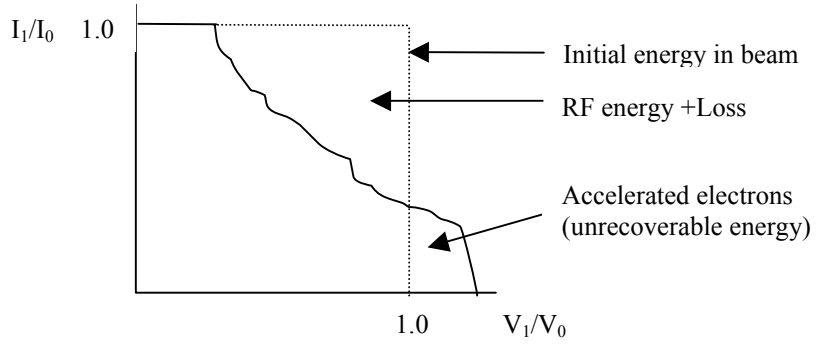

Fig. 1.10 The spent beam distribution curve

The role of the collector is to effectively recycle the useful output beam energy to re-supply the beam. A 90% efficient TWT collector increases the overall efficiency of the tube with a basic-tube efficiency of say 20%, to over 70%. It is this essential feature that gives the TWT the superior overall efficiency compared to the SSPA. The significance of the collector on the overall performance of the helix TWT will be discussed in the design limitations (in Chapter 2.3) and analysed in the TWT collector design (in Chapter 6.5).

1.5 Conclusions

Intermodulation distortion is an increasing problem in helix TWTs for satellite communications. As the flow of data traffic capacity becomes greater, the modulated waveforms carrying this data become more complex with more data nodes. Since the probability of error occurrence is greater for these higher modulation schemes, the linear performance of the TWT becomes more critical. In order to improve the C/I level, more systems are employing linearisation techniques. The drawbacks of these techniques however, are the added cost, hardware complexity and band limitations. The next chapter will discuss methods of tackling the increasingly important topic of nonlinearity, which avoids these drawbacks. The possible approaches to improve both the linearity and efficiency of Helix TWTs will be reviewed. The available tools (i.e. specialised software for simulating and analysing a generic helix TWT) to achieve this will also be covered.

Chapter 3 covers research on a TWT with uniform helix dimensions; the effect of the basic parameters on the nonlinear performance of a uniform Ku-band helix TWT is investigated. Results in this chapter reveal the nonlinearity that arises as the drive power is increased towards saturation and how this affects the TWT design parameters; this is useful as a basis for a design procedure for high linearity and efficiency.

It is very important to understand the fundamental causes of nonlinear behaviour in helix TWTs, since the knowledge gained from this can be used to find techniques for tackling the causes of non-linearity in helix TWTs. Chapter 4 discusses the non-linear processes in a TWT, especially within the electron beam and how this causes the RF transfer characteristics to become nonlinear. Chapter 5 covers the relation between harmonics and intermodulation products and discusses whether eliminating or injecting harmonics will suppress the more problematic intermodulation distortion. Research has been carried out aiming to discover the root causes of distortion in the RF signal. This is revealed in the RF beam current and voltage waveforms. This chapter shows how these non-sinusoidal waveforms relate to the growth of harmonics and intermodulation products.

The design of a practical helix TWT is covered in Chapter 6. This chapter sets out the general design procedures for a fully tapered tube. These design procedures are then modified accordingly to give the best trade-off between efficiency and linearity across the specified broad bandwidth. Finally, Chapter 7 concludes all of the results with suggestions for further work.

References

[1] S. Kirtay, “Broadband satellite system technologies for effective use of the 12-30GHz radio spectrum”, IEE Electronics. And Commun. Journal, Vol. 14, No. 2, pp.79-88, April 2002

[2] B. A. Pontano, "Satellite communications: services, systems and technologies", Microwave Theory Tech., MTT-S International Microwave Symposium, IEEE, pp.1-4, Vol.1, New York, 1998.

[3] Franchi et al., “Broadband mobile via satellite: Inmarsat BGUN”, Revue Hf. Electronique Telecommunications, No. 3, pp. 58-64, 2000, Belgium.

[4] L. Del Re E. Pierucci, “Next-generation mobile satellite networks”, IEEE Commun. Magazine, Vol. 40, No. 9, pp. 150-9, Sept. 2002.

[5] “Satellite communications - a continuing revolution”, IEEE Aerospace & Electronic systems magazine, Vol. 15, No. 10, pp. 95-107, Oct, 2000.

[6] http://www.intelsat.int/

[7] B. Sklar, “Digital Communications”, Prentice-Hall International, Inc., New Jersey, 1988

[8] D. M. Goebel and W. L. Menninger, “Design and performance of vacuum electron devices for digital communications”, Abstracts Proc. Conf. Intl. Vacuum Electronics, Monterey, USA, April 2002.

[9] G. Santella, F Mazzenga, "A hybrid analytical-simulation procedure for performance evaluation in M-QAM-OFDM schemes in presence of nonlinear distortions", IEEE Trans. on Vehicular Tech., Vol. 47, No.1, pp.142-151, February 1998.

[10] Satellites 101 Uplink, Issue 2, 1998.

[11] R. Strauss, "Reliability of SSPAs and TWTAs", IEEE Trans. on Electron Devices, Vol. 41, No. 4, pp. 625-626, April 1994.

[12] P. Ehret, A. Jager and E. Seppelfeld, “Low frequency travelling wave tubes for satellite applications”, ITG-Conf. On Displays and Vacuum Electronics, Garmisch-Partenkirchen, Germany, May 2001.

[13] A. Katz, "SSPA Linearisation", Microwave Journal, pp.22-44, April 1999.

[14] Wolfgang Boesch, Private Communications, ESTEC, Netherlands, January 1994.

[15] J. S. Kenney and A. Leke, "Design considerations for multicarrier CDMA base stations power amplifiers", Microwave Journal, Vol. 42, No.2, pp.76-86, February 1999.

[16] M. Kumar, J. C. Whartenby and H. J. Wolkstein, “Predistortion Linearizer using GaAs Dual-Gate MESFET for TWTA and SSPA used in Satellite Transponders”, IEEE. Trans. Microwave Theory Tech., Vol. MTT-33, No. 12, December 1985.

[17] A. Katz, “Increasing multi-tone power near saturation”, Microwave Journal, pp 128-134, April 2000.

[18] A. S. Gilmour, Jr, "Principles of Travelling Wave Tubes", Artech House Inc., 1994.

[19] J.Wallander, “Large signal computer analysis of distortion in TWTs”, Chalmers University of Technology

[20] S. F. Paik, “Design formulas for helix dispersion shaping”, IEEE Trans. on Electron Devices, Vol. ED-16, p.1010, 1969.

[21] S. D'Agostino, F. Emma and C. Paoloni, "Accurate analysis of helix slow-wave structures", IEEE Trans. on Electron Devices, Vol. 45, No. 7, pp. 1605-1613, July 1998.

[22] S. A. Naqvi, J. A. Nation, L. Schachter and Q. Wang, “High-efficiency TWT design using traveling-wave bunch compression”, IEEE on Plasma Science, Vol. 26, No. 3, June 1998.

Chapter Two: Methodology

2.1 Introduction

This chapter discusses the methods and strategies with which to approach the problems and issues laid out in Chapter 1. An overview of the systems requirements will first be given. This will be followed by a description of the performance limitations i.e. what is the best total efficiency that can be achieved for an acceptable linearity. The procedures for the design of broadband and high linearity will be discussed in addition to a tapered helix pitch design (required for practical tubes). A detailed description on the proposed tools for modelling and analysis of helix TWTs will also be provided.

2.2 Systems Criteria and Main Objectives

Future communications systems demand multi-channel power amplifiers that can process data packages with greater capacity and streaming at higher rates than present systems. For this greater handling capacity, the data streams will become broader band and be specifically modulated. Whilst maintaining low noise, the high power amplifier would need to produce greater output RF powers than present systems [1]. Solid-state power amplifiers are limited by their overall output efficiency at both high output powers and frequencies. The applications of SSPAs are therefore in, for instance, cellular networks (with frequencies 0.8 to 0.96GHz) and personnel communications systems (1.5 to 2GHz) [2]. For the transmission of satellite broadband digital signals at frequencies in the C-band or above, helix TWTs are required. These are capable of producing greater than say 50W of RF power across a wide band (of more than say 1GHz) with acceptable carrier-to-noise ratios.

At present, many of these systems are simply designed for maximum saturation efficiency with an added pre-distortion lineariser to improve the linearity. Because the amplifier requires some level of output backoff, the TWT design should be targeted for operation this reduced power level. The design approach should be aimed to maximise the conversion efficiency at a backoff level where the nonlinear distortion is acceptable. In addition to this, optimum linearity must be considered in the design methodology so that the output backoff required is minimised. This level of performance should be maintained across the widest possible frequency range: for this project, this range is specified in the Ku-band from 10.7 to 12.75GHz. Ways of maintaining consistency in the output performance across the frequency band of interest are discussed in Section 2.4.

Optimisation of both linearity and conversion efficiency can be achieved by the pitch profile design of the slow-wave structure. This is a very effective way of controlling the beam-wave interaction so that any possible trade-off between linearity and efficiency can be best reached. Section 2.8 will further cover the methodology for the helix pitch design.

In order to optimise the linear performance of the TWT, it is essential to understand how it arises. Knowing more about the nonlinear physical mechanisms in a helix TWT can help in the design process to minimise the root causes of nonlinearity that generate output signal distortion. The interaction processes between the electron beam and the RF wave that cause electron bunches to be formed and decelerated may need to be optimised to minimise nonlinear distortion. The parameters of the TWT that have the greatest influence on its nonlinear performance need to be identified. This can be achieved by varying one parameter at a time and observing the effect this has on the nonlinear output. This will enable an effective design method for high linearity to then be established. Design methodology for high linearity is further discussed in Section 2.5.

Efficiency, linearity, gain and broadband are the most desirable conditions to be met in a helix TWT. In order to meet these criteria in a single TWT design, it is necessary to determine the optimum design for each of there conditions. A helix with uniform dimensions will be used to identify where these conditions lie. The results of this

analysis in a uniform helix TWT will be described in Chapter 3. The task is to then establish an overall design which encompass these desirable conditions.

The multistage depressed collector has a major impact on the overall TWT efficiency; its function is to recover the power from the beam after it has been modulated by the slow-wave structure. A collector can be designed based on the distribution of the spent-beam from the output of the slow-wave structure. It is therefore preferred to first optimise the fundamental interactions in the tube for the desired criteria, then to consider the collector design based on the output spent-beam curve. At backed-off drive levels, there tends to be less energy spread in the beam, enabling better recovery of the spent beam power. The design of the multistage collector based on the spent-beam distribution for maximum overall TWT efficiency is covered in Chapter 6.5.

The main tool for the design procedure and analysis is a Large Signal computer simulation program (LSM), as discussed in Section 2.7.1. This software provides a means of quantifying the effect of adjusting TWT dimensions within the manufacturing tolerances, which is almost impossible to do experimentally without building a large number of expensive tubes and controlling several parameters at the same time.

2.3 Design Limitations

It is impossible to design a helix TWT amplifier such that the total efficiency is 100%. This is because there are always limitations in the transfer of energy from the beam to the helix and from the spent-beam to the collector electrodes. The processes in a helix TWT can be optimised however, so that the tube will operate more efficiently. These processes include the electron beam bunching, transfer of RF power from the beam to the circuit, collection of the spent-beam and the generation of a non-linear output RF signal. The practical limitations will always exist regardless of how good the design is. The following discussion will quantify these practical limitations in terms of the efficiency.

For maximum conversion efficiency, it is required to optimise the transfer of RF energy from the beam to the helix. For this to take place, the circuit field must capture all of the electrons, causing the electron velocities u_0 to become synchronous with that of the wave v_p. Then the electrons must be further decelerated, and become reflected by the circuit field, reducing their velocities to v_p-(u_0-v_p). The maximum basic tube efficiency η_0 can be expressed as the change in beam kinetic energy as a fraction of the initial beam energy. The maximum possible limit of the basic tube efficiency assumes all electrons are captured and then reflected by the circuit field. The maximum efficiency can then be expressed as in equation (2.1). This is the upper limit because all electrons are not normally captured. After the electrons are captured, they have different velocities, because their captured velocities vary with initial phase.

$$\eta_0(\max) = \frac{u_0^{\,2} - \left[(v_p - (u_0 - v_p)\right]^2}{u_0^{\,2}} = \frac{4v_p}{u_0}\left(1 - \frac{v_p}{u_0}\right) \tag{2.1}$$

where $v_p = \omega/\beta$ and $u_0 = (\omega+\omega_q)/\beta$.

and ω = angular frequency,

β = axial propagation constant,

ω_q = effective plasma frequency.

Equation 2.1 can be then rewritten in the following form:-

$$\eta_0(\max) = 4 \times \left(\frac{\omega}{(\omega+\omega_q)}\right) \times \left(1 - \frac{\omega}{(\omega+\omega_q)}\right) \tag{2.2}$$

where the ratio ω/ω_q is estimated to be 0.1. Thus $\omega/(\omega+\omega_q) \approx 1/(1.1) \approx 0.9$

$$\therefore \eta_0(\max) \approx 4 \times 0.9 \times 0.1 \approx 0.36 = 36\%$$

The best slow-wave structure that could possibly be designed and manufactured would have a performance limited to around $\eta = 36\%$, without collection of the spent-beam. This amplifier however, would produce harmonics and intermodulation noise. In many telecommunications systems, a nonlinear performance of –21dBc or better is required for a signal with a large number of discrete carriers. This requires a minimum output backoff of around 4dB to reduce the nonlinear distortion to a tolerable level. The power output (in dB) at 4dB output backoff is: -

$$P_{(dB)} = P_{sat\,(dB)} - 4$$

Converting dB into Watts gives: $P_{(W)} = P_{sat\,(W)} \times 10^{-0.4}$

The maximum efficiency that can possibly be achieved in practice with an acceptable nonlinear performance is therefore estimated to be: -

$$\eta_0\,(\max) = 36\% \times 10^{-0.4} = 14.3\%$$

An output backoff of 4dB actually reduces the conversion efficiency by more than half. This stresses the importance of design for high linearity. Even though the overall efficiency is reduced by backing-off the RF signal level, this could be compensated by the design of the helix circuit and multi-stage collector.

The collection of the spent-beam has a major effect on the overall efficiency. A 3-stage collector made of copper can produce 75% collector efficiency. This can be increased to 90% if more electrodes made of graphite are used, since graphite minimises secondary electron emission [2]. For a state-of-the-art multi-stage depressed collector, a maximum collector efficiency η_c of 90% can be assumed. The overall efficiency of the TWT would then be: -

$$\eta(\max) = \frac{\eta_0}{1-\eta_c(1-\eta_0)} = 62.6\%$$

This assumes a very efficient collector, which depends on the distribution of the spent-beam energy. More RF power extraction from the beam gives higher basic tube efficiency. But this also tends to produce a greater spread in the electron velocities, thus enabling less RF power to be recovered by the collector. The trade-off between the basic tube and the collector efficiency is clearly seen in fig 2.1.

In modern communications where the RF drive level is varying dynamically, the electron velocities in the beam are also adjusting accordingly. For a lower drive level, which occurs 50% of the time (as illustrated in fig 1.4), the electrons will become accelerated. The electrode potentials of the collision will therefore have to be set slightly lower for the most efficient collection.

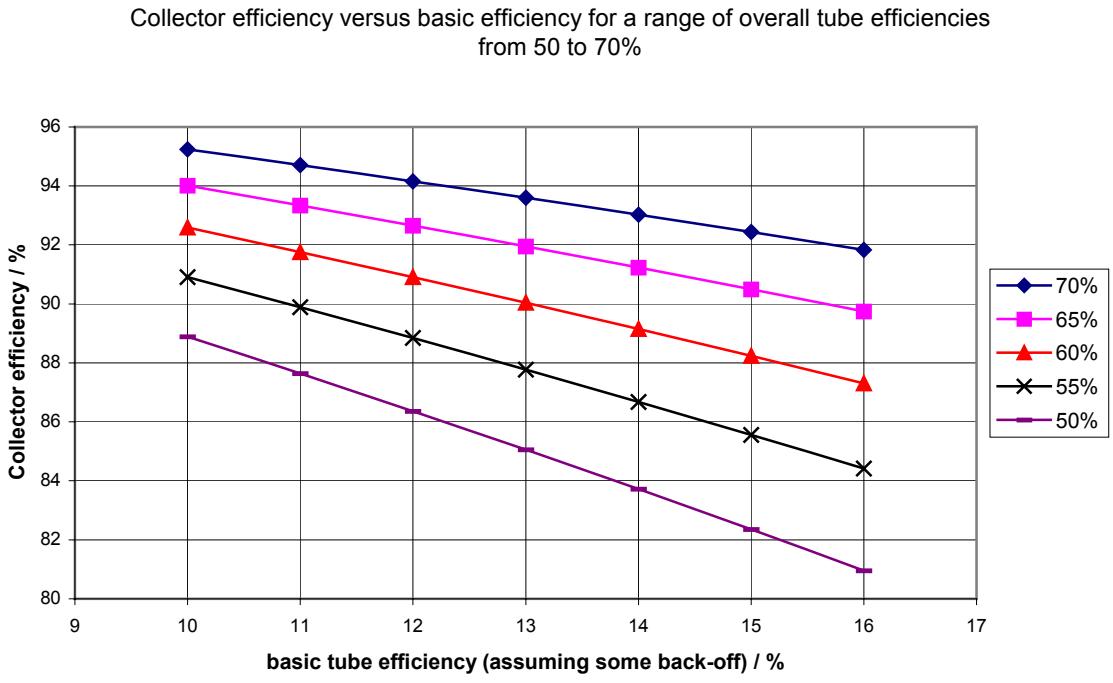

Fig. 2.1 The collector efficiency versus the basic tube efficiency for a given range of overall efficiencies.

2.4 Design for Broadband Applications

Providing a consistent level of RF output across a broad band is increasingly desirable in modern communications systems, as discussed in Chapter 1.1. Helix TWTs have a major advantage over other microwave devices in that the helix circuit properties are less dispersive. These properties which are low dispersive include the beam-wave coupling impedance and the circuit phase velocity. The selection of dielectric material in the support rods as well as anisotropic loading, i.e. vanes, can reduce the frequency dependence on the electrical properties. The purpose of anisotropic loading is to reduce the inductive coupling effects from circumferential currents flowing around the metallic shield. Fig 2.2a shows the cross-section view of the tube without any loading elements attached to the shield, fig 2.2b shows the case with vanes attached and a solid configuration is in fig 2.2c. The effect of these two types of loading on the phase velocity dispersion of the circuit in comparison with case (a) was performed with identical tubes [3]. The results in fig 2.3 show how vanes, in particular, control the frequency variation of the phase velocity of the structure. Anisotropic loading elements are therefore commonly employed for multi-octave tubes, but are capable of being used in communication applications, where broadband operation is required [4].

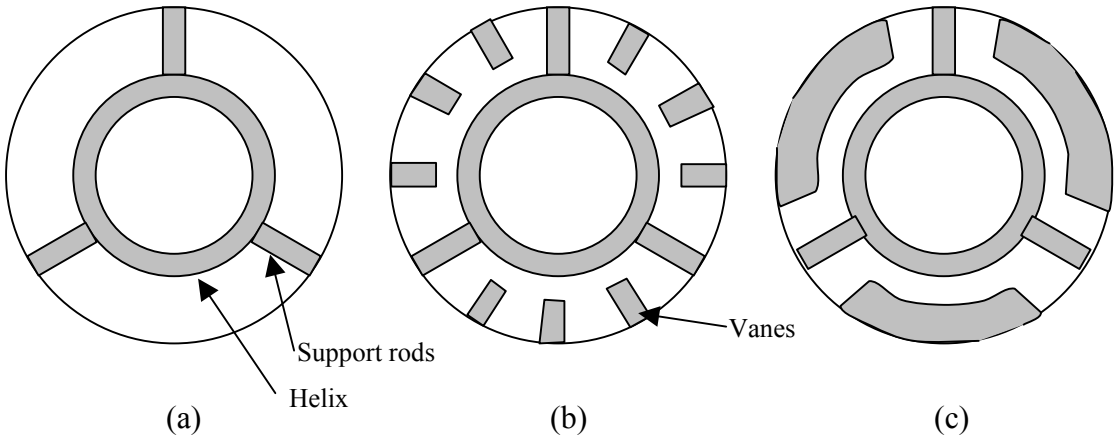

Fig 2.2 Different helix loading techniques for dispersion control: (a) unloaded (b) vanes and (c) solid

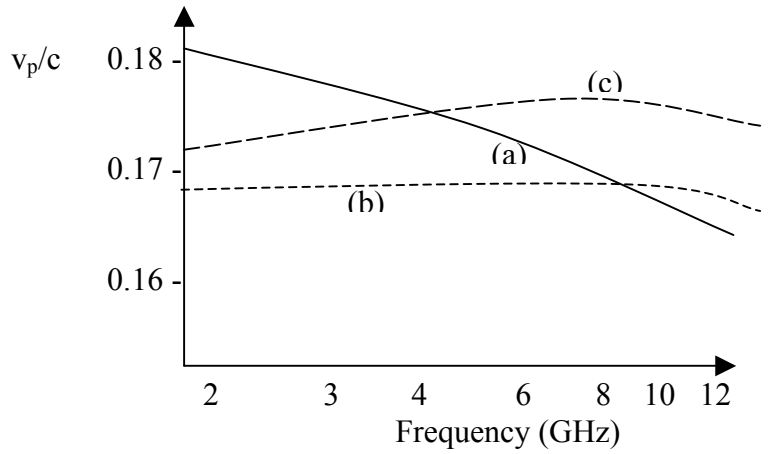

Fig 2.3 Normalised phase velocity as a function of frequency for different types of loading for dispersion control [3]

Alternative design methods of the slow-wave structure (e.g. tapering strategies) and/or the electron beam for a consistent broadband performance have rarely been documented in past literature. A design strategy for a broadband TWT becomes more difficult when considering the other criteria that are required in which a trade-off maybe necessary. For example, it is known that for a given linearity, a broadband TWT produces less output power than a narrow-band TWT [5].

It is possible to reduce the dispersion of the RF wave by adjustment of the electron beam and forward-wave phase velocities so that coupling is achieved across a broad band. A design strategy for achieving maximum coupling or maximum gain is to compute the propagation constants of the slow-space charge wave β_- and the forward circuit wave β_0, then to determine the TWT parameters where $\beta_- = \beta_0$. Figure 2.4 shows dispersion (or ω–β) diagrams where fig 2.4b represents the case where the forward-wave on the helix is optimised for broadband. The forward-wave phase velocity can be controlled most effectively by adjusting the helix pitch.

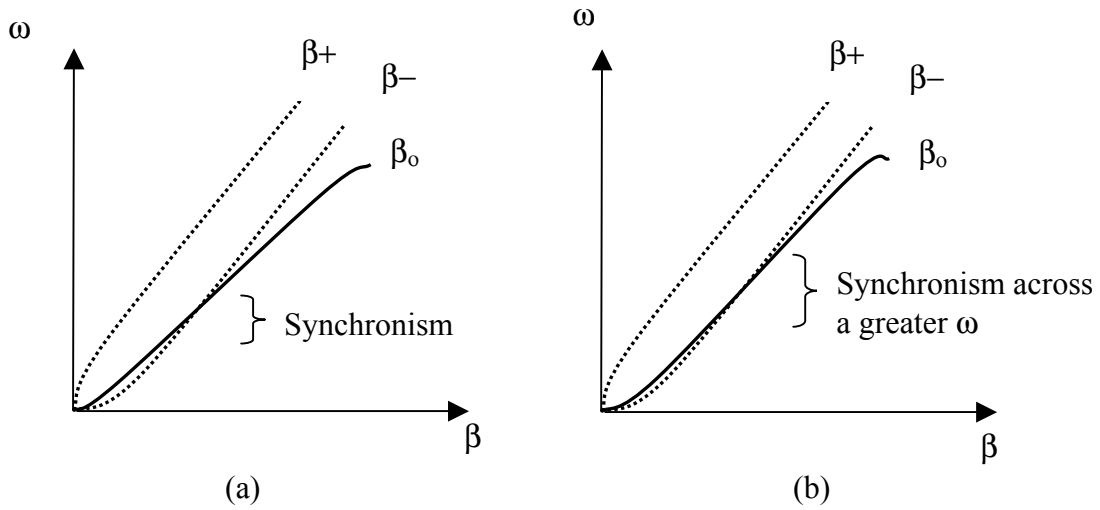

Fig 2.4 Dispersion diagrams for (a) a uniform helix and (b) a tapered pitch profile

For investigations which involve adjusting systems parameters, it is desirable to maintain consistency throughout the rest of the system i.e. keep the rest of the parameters constant. For investigations with which it is necessary to maintain beam-wave synchronism, there may be a slight restriction in that more than one parameter would have to be varied at a time. For example, if the beam-to-helix radius (filling factor) were adjusted for optimum efficiency and linearity, the beam voltage would have to be adjusted accordingly to maintain synchronism. This may pose a problem for the analysis and understanding of the effect of parameter sensitivity on performance. But it is necessary if a condition can only be met by this procedure. A final design can then be achieved for situations where the broadband criterion is essential.

2.5 Design for High Linearity

There is a lot that is unknown about how nonlinearity arises in TWTs. By understanding more about the fundamental nonlinear processes in the tube, use of this knowledge can then be implemented in the design stage. One way of gaining understanding is to investigate how adjustments made to the fundamental TWT parameters affect its nonlinear performance. This approach would then lead to a final TWT design that has the best linearity.

For a given modulation scheme, the nonlinear performance of quasi-memoryless[1] multi-carrier power amplifiers is solely determined by their transfer characteristics [6]. Research undertaken prior to this project [7,8] modelled the amplitude characteristics in terms of the radius of curvature R of the curve in the non-linear region and the gradient of the curve α in overdrive, as shown in fig. 2.2. The work demonstrated that minimum generation of intermodulation distortion occurs when the AM/AM transfer curve cuts-off immediately from the linear (45°-slope) curve at saturation then remains at this limit in overdrive. This ideal limiter characteristic is impossible to achieve in practice. However, a design can be achieved in which the curvature of the AM/AM transfer curve from the 45°-slope to the saturation point (0°-slope) occurs within the minimum drive range. Provided that R is not very small, the angle beyond saturation is not significant [8].

Phase conversion Kp is the other contributing factor to non-linear distortion in a power amplifier. The phase transfer curves in [7] were approximated by a piece-wise linear model: a constant phase response within the linear AM/AM region and a linearly decreasing phase shift within the non-linear region, as in fig. 2.5. The research revealed that as the magnitude of Kp increases, the non-linear performance deteriorates. Since R, α and Kp can predict the generation of nonlinear distortion (in multi-carrier quasi-memoryless systems), designs techniques for high linearity can be implemented based on inspection of the shapes of these transfer curves alone. This is valid for any modulation scheme used.

[1] Quasi-memoryless approximations are discussed in Section 2.7.3

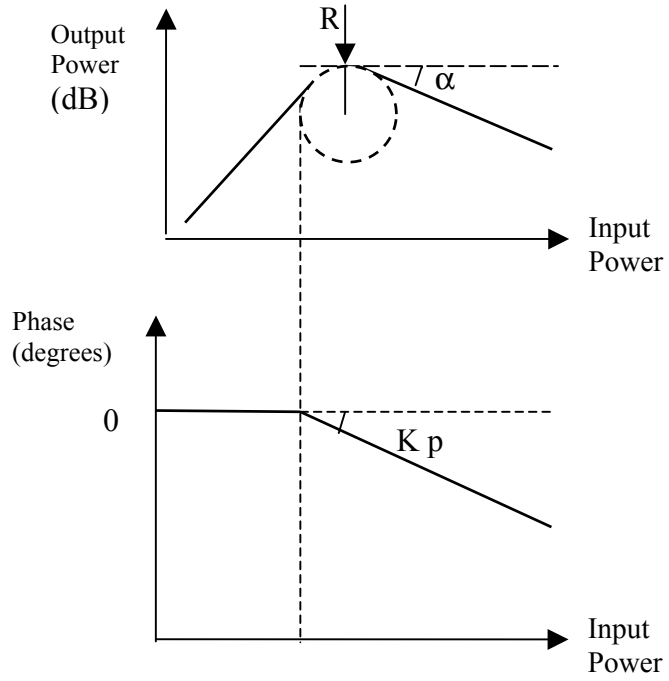

Fig. 2.5 Modelled AM/AM and AM/PM transfer curves.

Present and future satellite systems process a signal waveform carrying hundreds of signals. Such a signal can be accurately represented by using band-limited white noise. A noise-power ratio (NPR) measurement quantifies the nonlinear performance of a power amplifier [9]. An NPR represents the input signal by a finite number of signals (e.g. 12-carriers) with equal amplitudes and random phases confined by the amplifier's bandwidth. The nonlinearity in the amplifier results in the centre and edge notches being filled with intermodulation products. The NPR measurement is normally made by determining the difference in signal power (in dB) between the centre notch and the average carrier power, as shown in fig 2.6b. This is compared to the carrier-to-IM3 measurement for a 2-carrer signal in fig 2.6a.

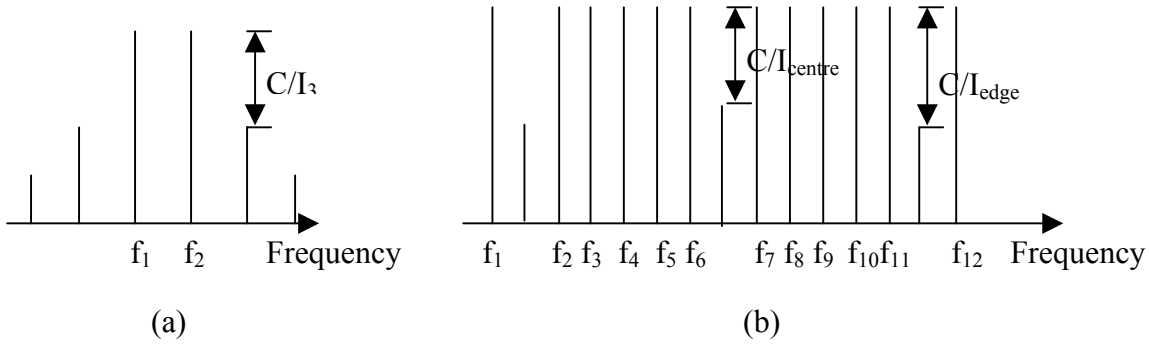

(a) (b)

Fig 2.6 Measurement of intermodulation distortion from (a) a 2-carrier signal and (b) band limited white noise

Previous research [7] has shown that for a range of different transfer curves, the carrier-to-third order IM ratio for 2-carrier input signal follows a similar trend to that used in an NPR measurement. An example of this trend is shown in fig 2.7, which compares the carrier-to-IM ratio from a 2-carrier signal with that from an NPR measurement. Correct conclusions can therefore be drawn on the linearity of a TWT design based on a 2-carrier input signal. A C/I3 value of -21dBc is generally a tolerable level of IM distortion in satellite communications applications [10]. The power level of interest in this research is therefore the backed-off level where C/I3 = -21dBc.

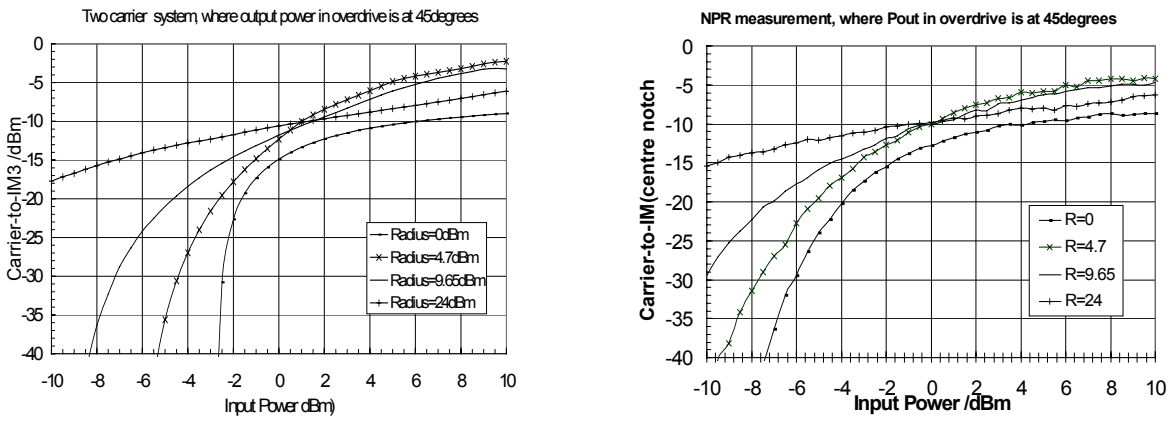

(a) (b)

Fig 2.7 Comparison of carrier-to-IM ratios generated from a (a) 2-carrier and an (b) NPR measurement

2.6 Design of the Helix Pitch Profile

The interaction processes in a helix TWT result in the conversion of kinetic energy from the electrons in the beam into RF power amplification in the slow-wave structure. Consequently, the electrons slow down towards the output end of the tube. Reducing (or tapering) the phase velocity of the forward circuit wave is a well known technique that ensures a synchronous phase relationship between the beam and circuit waves. The conventional method of tapering the pitch is to extract the maximum amount of energy from the electron bunches once they are trapped by the circuit field. By holding the electron bunch in the decelerating phase for as long as possible, the maximum amount of power is extracted from the bunch [11-13], thus maximising the basic tube efficiency. This technique also prevents any electrons in the beam from becoming accelerated which may occur towards power saturation, thus preventing energy being transferred from the circuit back into the beam. Phase velocity tapering can also be used to suppress backward-wave oscillations by adjusting the gain and phase characteristics of the TWT [17].

Review of Methodology of Velocity Taper Designs

The ideas of tapering were originally discussed in the mid 1950s [14]. Since then, there have been a number of different analytical approaches to the design of velocity tapers for efficiency enhancement. An early analytical approach, which is still used today, is the 'hard-kernel bunch' theory [15,16]. This approach is based on the bunching formation of the electron beam, where the centre of the bunch is assumed to contain all of the charge per beam wavelength. The hard-kernel bunch is then kept at the maximum decelerating phase of the circuit field. This theory, which does not involve any optimisation routines, has achieved designs with linearly decreasing velocity tapers that have been successful in improving efficiency [12,17].

A different and more recent approach is the 'dynamic velocity taper'. Computer software for helix TWTs is used to operate an optimisation routine to determine the parameters resulting in the highest efficiency for a fixed frequency [18]. The pitch profile decreases as an exponential function of distance towards the end of the tube. As well as improving the conversion efficiency, this approach has also been shown to

improve the linearity of the transfer characteristics compared with a uniform structure [19]. Experimental results have shown that tapering can give up to 4% improvement in conversion efficiency and a reduction in phase lag of up to 2 °/dB as well as a suppressed saturated harmonic power output [17].

More recent approaches have readopted the hard-kernel bunch theory, which is useful for producing a strong and tight electron bunch maintained throughout the deceleration RF electric field. The theory is then incorporated in modern computer software for helix TWT design to model the interaction processes between the helix and the beam, ensuring that synchronism is maintained for a certain frequency. This technique (Phase–Adjusted Tapers P.A.T.) has resulted in TWT designs with high overall efficiencies [20].

Careful tailoring of the pitch profile is required to suit the needs of the different performance specifications. The aim is to achieve all of the optimum conditions in a single design of the slow-wave structure. The three conditions of particular interest are high efficiency, high linearity and broad-bandwidth. These three conditions should be optimised or traded-off in the most effective way in a single design to suit the system's requirements. The performance of this final design can then be compared to those produced by optimised uniform helices.

2.7 Computer Modelling of Helix TWTs

The tools for the analysis and design of a helix TWT which are available for this research are now described.

1. The Large Signal Model (LSM-1D and 2.5D) is a specialised program which uses physical equations to simulate the processes within a helix TWT. This software is the most useful tool in this project to model the non-linear performance of a helix TWT. This is described in Section 2.7.1

2. The Helix SWS Model (HELIX code) uses the accurate and reliable tape model to determine the forward-wave propagation and impedance characteristics of a helix TWT. This is described in Section 2.7.2

3. Intermodulation Analysis Model (IMAL 2.0) determines the carrier-to-IM ratio of a quasi-memoryless power amplifier based on its transfer characteristics. This is described in Section 2.7.3

2.7.1 The Large Signal Model (LSM)

The LSM software models the helix circuit in the TWT as a generalised transmission line, which interacts with a DC electron beam. The electrostatic influence of the RF circuit fields causes modulation of the electron beam. An RF voltage is then induced on the circuit from the beam-wave interaction resulting in amplification of the RF forward wave and a reduction in the electron beam velocity. Physical equations in the model governing the beam-wave interaction, are therefore defined in terms of the RF current induced in the beam by the RF fields and the RF voltage induced on the circuit by the modulated beam [21].

A transmission line is a useful and convenient way of representing the helix slow-wave structure. The transmission line equation is defined in terms of the cold propagation constant and characteristic impedance. This is used to deduce the RF interaction field and the cold loss of the helix. The RF field is modelled as the sum of the forward and backward waves. By assuming the circuit field is axially symmetric, the wave equation can be solved in cylindrical co-ordinates to provide the expression for its longitudinal component.

Since the beam-wave interaction is continuous, the coupling effects must be calculated at each integration step. The Fourier harmonic components of the RF beam current and the induced forward and backward circuit voltages are also calculated at each integration step. This is necessary to provide a complete description of the beam-

wave interaction processes. The whole operation is iterated for all the planes in a section of the tube.

At the large-signal levels, the equations governing the behaviour of the TWT contain non-linear terms which become significant. These nonlinear terms arise in the Lorentz force and the charge-continuity equations. The electron beam is modelled using the Langrangian formulation; the motion of well-defined charge groups is tracked in small steps down the tube influenced by the RF fields and the beam-wave coupling effects.

In the one-dimensional analysis, a disc model of the electron beam is used. A single wavelength segment of the beam is sliced into a number of discs, as illustrated in fig. 2.8. Each disc has a finite thickness d, fixed radius b, charge and mass and its motion is restricted to the axial direction. An initial velocity is assigned to each disc and the discs are then allowed to pass through each other. The relative motion of charged discs produces the RF space-charge potential. For each disc, the axial electric field is calculated, then these values are integrated across half the beam wavelength to give the electric potential. When this is averaged over the disc's volume, the space-charge force between two identical discs is obtained [21].

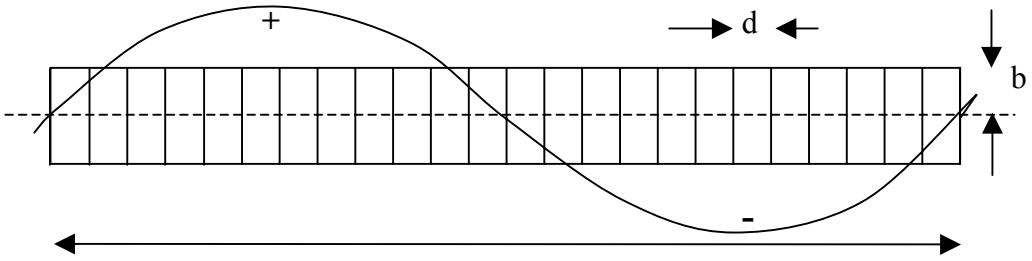

Fig. 2.8 Disc model of the electron beam in one RF cycle

A 2.5-dimensional model for the entire interaction process considers the transverse motions of the electrons. This model becomes very complicated due to involvement of the second order transverse effects and for the consideration of the axial magnetic field. The 1-D representation, which assumes a confined flow of the electron beam,

provides a fairly accurate model for the analysis for the overall tube performance. For convenience and reliable output results, the research described in this thesis has therefore used the 1-D model to carry out many of the simulations.

In addition to the LSM-1D and 2.5D processor, the software comprises of a pre-processor (INPUT) and a post-processor (VPDATA). These are now explained.

2.7.1.1 Pre-Processor (INPUT)

The LSM processor requires input information which includes the initial properties of the DC electron beam and the slow-wave structure dimensions and properties. The input powers of the RF signal and frequency values are also required. An interactive INPUT interface allows the user to choose the required input parameters. A file is then created in a suitable format to be processed by LSM. The complete set of input parameters is divided into 12 groups which are handled by 12 subroutines. The input parameters that are of interest to the design of the TWT are as follows: -

1. The number of input carrier signals and their frequencies - including the base frequency
2. Cathode voltage and DC current, the helix and beam radius
3. Cathode flux and axial magnetic field
4. Number of sections and subsections.
5. For each section: length, helix radius and pitch, tape width, pitch angle ϕ, type of circuit attenuation and phase velocity variation, cold loss α, axial propagation constant β and interaction impedance K_o.
6. Peak axial and magnetic field and number of harmonics
7. Reflection coefficients (set to 0)
8. Phase of reflection coefficients (set to 0)
9. Number of space harmonics and switches for data storage and writing
10. Drive power levels
11. Phases for the corresponding drive levels (set to 0)
12. Output file names.

Note that for more than one section (i.e. a non-uniform structure), the input data in group 5 is re-entered for each section.

The other input settings control the iteration processes. 24 disks per RF cycle of the base frequency (as represented in fig. 2.8) gives a good compromise between computational speed and accuracy. This parameter must be increased quite considerably when simulating a multicarrier system as the base frequency f_b is much smaller[2]. The computation time is therefore much greater for multicarrier simulation. For example, 2 carriers at 11.6 and 11.8GHz takes 58 times longer to run than a single carrier, since the base frequency for 2-carriers is 0.2GHz - requiring 1392 disks/RF cycle[3]. Data describing the space charge calculations is also required in LSM, including 48 axial points and 40 radial points in look up-table. Other data include 8 integration steps per RF cycle, 1 ring per disk and 5 iterations (number of passes) for the backward and reflected waves. This number of passes may need to be increased if the backward wave effect is significant, since the system becomes less stable.

2.7.1.2 Post-Processor (VPDATA)

The files generated by the processor for plotting the output results need to be re-structured so that they can be read by MATLAB. A set of programs therefore post-process the data allowing the following information to be plotted versus axial distance: the Applegate diagram, RF/DC beam current, RF phase of the voltage relative to the current, circuit gain, cold loss, beam velocity, circuit phase velocity and the forward circuit power. The Applegate diagram is a plot of the individual phases of a sample number of electrons relative to the forward wave on the helix. The code has been modified to include an option to plot the phase of the electrons relative the initial beam velocity. A data file to plot the spent beam distribution is also generated.

[2] f_b = the general common factor of the carrier frequencies
[3] Number of discs ND for multicarrier simulation = (carrier frequency/base frequency)*(standard ND=24)

2.7.1.3 Graphics Interface (PREP)

The MATLAB code reads the data from the output of the pre-processor and plots the output graphics. This code was modified at the initial stage of this project from plotting in an old DOS-based interface to the latest WINDOWS based version of MATLAB.

2.7.1.4 Code Modifications During This Project

To carry out this research, The LSM software was modified so that it could be loaded onto a machine using a fast operating UNIX system. The code was modified from the DOS based FORTRAN and UNIX Script was written to allow the user to select a wide range of options. These options include: run input interface, view or edit data files, run LSM-1D or 2.5D and run the post-processor. There is also an option to run LSM in the background mode, which may be more convenient for the longer simulations, such as multi-carrier simulations covering a range of drive levels and frequencies. In order to carry out the pitch profile design, the LSM-1D software was extensively re-structured to allow it to simulate a slow-wave structure comprising a linearly phase velocity transition. All of the calculations are now made along each plane of the tube instead of each section.

The LSM code was also modified to generate two files containing the following: -

1. output characteristics of interest to be transferred into Excel for graphical viewing, these include output power, phase, conversion efficiency and gain.

2. transfer characteristics and tube efficiency in a compatible format with IMAL, so that the intermodulation output can be quantified (Section 2.7.3).

2.7.2 Helix SWS Model – 'HELIX'

ESTEC 6 is the latest version of a code which uses the tape model [22] to calculate the axial propagation constant β_0 and interaction impedance K_0 of a helix slow-wave structure. In order to determine β_0 and K_0, for a given frequency, the helix dimensions and properties are required. A helix slow-wave structure may contain inhomogeneous loading (dielectric loading with a varying dielectric constant [23]) and/or anisotropic loading (vanes) [24,25]. Since these affect β_0 and K_0, information about the dielectric loading is included in the calculations. The input parameters of the model are listed in table 2.1. Note that $|a_2-a_1|$ equals the tape thickness δ_t. The helix dimensions are represented on a schematic of the slow-wave structure in fig. 2.9. Space harmonics can also be considered in the tape model.

Table2.1

Input parameters for the tape model	symbol
carrier frequency	f_0
helix pitch	p
inner helix radius	a_1
outer helix radius	a_2
shield radius	c
tape-width	δ
radial distance of the vanes	
total number of rods	N
type of dielectric loading (six variations)	
dimensions of support rods	
relative permeability of the homogenous dielectric loading	ε_r

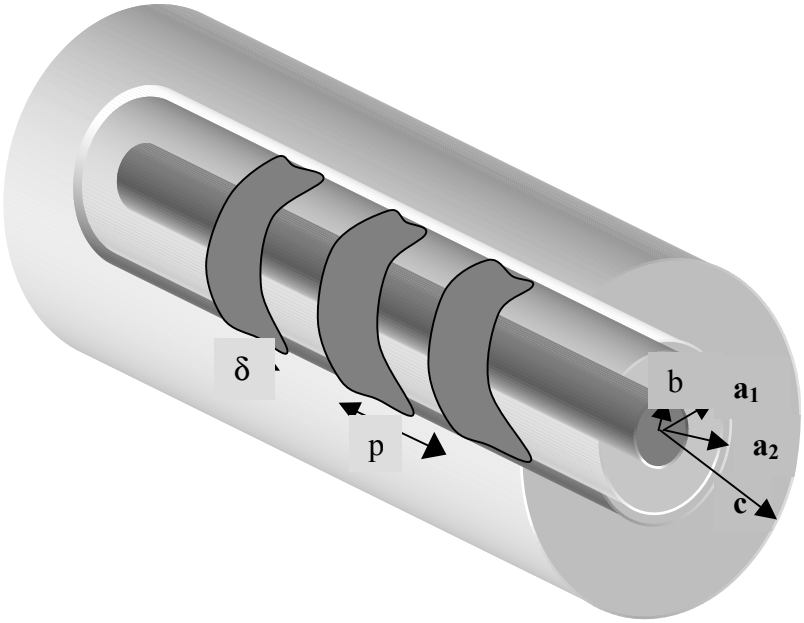

Fig. 2.9 3-D representation of the helix SWS (excluding the support rods and vanes)

Generally, use of this model provides a good description of the dispersion characteristics for a particular design; it is certainly more accurate and complex than the simpler sheath helix model. When the results are compared with experiment, the agreement is within 3% for the propagation constant and 10 to 15% for the interaction impedance [22].

2.7.3 Intermodulation Analysis Software (IMAL 2.0)

IMAL quantifies the intermodulation products which are generated from a quasi-memoryless multi-carrier amplifier. The amplitudes of the intermodulation products and the carrier powers are computed based on the amplifier's single-tone transfer characteristics and a given modulation scheme.

The main assumption made by IMAL for this purpose is that it uses a quasi-memoryless model. This means that the transfer curves are independent of frequency across the bandwidth [26]. The effect of memory in digital systems is to increase the probability of symbol error occurrence. Points in the I/Q diagrams corresponding to the output signal show more uneven movements relative to memoryless constellations [26]. Therefore memory enhances spectral spreading of the recovered signal.

Modelling a power amplifier by its instantaneous single-carrier amplitude and phase transfer functions is common practice. The use of a memoryless model is an accurate enough assumption for a single-tone or a narrow-band signal (up to a few 100MHz). The approximation becomes less accurate in the case of wider band systems however, where the amplitude and phase transfer curves may vary significantly across the band. Tests have been carried out to compare simulations from IMAL (based on the single transfer characteristics) and LSM using a variety of input correlated carriers [27]. The comparison of results between the two methods did show good agreement.

For this research, the nonlinear performances of different TWT designs can simply be compared from inspection of the transfer curves. Quantifying the intermodulation distortion is necessary however for determining the specifications of the tube. The alternative approach to the memoryless approximation (with IMAL) is multi-carrier simulation using LSM. But the latter approach is far more time consuming due to the large number of disks required in the model. Quantification of nonlinearity using IMAL is therefore the most appropriate method for this project.

When modelling the interaction and the nonlinear behaviour of a helix TWT, it is essential to use reliable and tested software. There are often discrepancies in the results between helix interaction codes and experiment. Inaccuracies in a simulation model limit the achievable efficiency of the practical TWT designed from this model. This is because optimised parameters from simulation would differ to those in practice. For example, an inaccurate spent beam distribution from the LSM simulation will result in an inaccurate design of the collector.

The Large Signal Model is the main software used for generating the results for this project. Validation of this software showed that the results were in good agreement with that of experiment [28]. The 1D-model showed particularly close agreement, more so than that of the 2.5D model, which may be due to the inaccuracies in the more complex ring configurations of the 2.5D model.

2.8 Practical Constraints on the TWT's Parameters

All parameters in any practical system have certain minimum and maximum limits, which are the manufacturing constraints. It is necessary to know what these practical limits are for the design of helix TWTs, because these determine the range with which to investigate each parameter.

All of the parameters of interest (or variables) can be divided into two groups: those that control the forward propagation of the wave on the helix (i.e. circuit parameters) and those that affect the slow-space charge wave (beam parameters). The practical constraints of the parameters will now be discussed in turn for each group.

The first group include: the helix pitch and the tape width. Note that the tape-width can be made dimensionless by redefining it as a ratio to the pitch. Quantifying the tape width δ is normally done with respect to the helix pitch p. The practical range of δ/p is from 0.4 to 0.8. The narrowest practical tape width limit is 0.4, otherwise RF losses become excessive, since the RF losses increase exponentially with decreasing δ/p [29]. As the tape width is increased, the coupling impedance also becomes greater. Therefore, the practical maximum limit of δ/p is 0.8 to prevent excessive coupling impedance with the beam. Wider tapes are preferred however, in high power devices, due to their better thermal properties [29]. The value of δ/p is therefore chosen to give a good compromise between the electrical and thermal properties of the helix.

The Electron Beam Parameters:

The beam parameters of interest are determined from the electron gun design. These are: the beam perveance or cathode voltage (under constant DC power) and the filling factor (beam-to-helix radius). Note that the 2.5D model may be needed for investigations in the radial direction (i.e. the filling factor and the tape thickness) in order to fully model the effects of radial variations on the performance.

The beam perveance is the most common parameter for the electron gun design. It is specified by the gun's geometry, but can also be written in terms of the beam voltage V_0 and beam current I_0 as in equation 2.3. This relationship is also plotted in fig. 2.10

for a constant DC power of 800W. As the beam voltage V_{DC} is increased, the DC current decreases with $(800/V_0)$; the perveance therefore decreases as $(800/V_0^{5/2})$.

$$\text{Beam Perveance} = I_0 V_0^{-3/2} \tag{2.3}$$

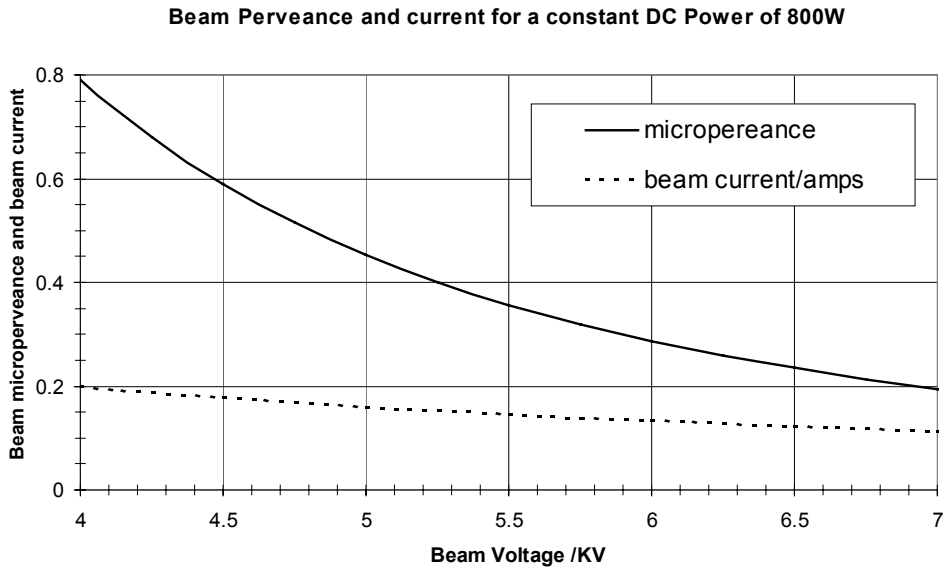

Fig 2.10 Beam micro-perveance and DC beam current as a function of beam voltage with a DC beam power of 800W.

The practical limitations of the beam perveance must be within the range of 0.2 to 0.8μ. For a gun design of which the perveance is made too low, a high beam voltage would be required, resulting in excessive size of the gun's geometry [30] and the helix, the coupling impedance is also reduced [31]. If the perveance were made too high however, the cathode life would be reduced due to the high current density required in the cathode [30]. In space applications, a trade-off with the choice of perveance is required between two important factors: the size and therefore the total weight of the components and the lifetime of the tube.

The filling factor is the amount of radial space with which the helix is filled by the beam - given as (beam radius b)/(helix radius a). This is normally about 0.5. The suitable range for investigation for b/a ranges from 0.4 to 0.6. The minimum limit enables enough beam-wave coupling to be achieved, but a maximum limit is also required to prevent any danger of the beam from getting too close to the delicate

slow-wave structure. The beam is usually kept focussed in the slow-wave structure with periodic permanent magnets (PPM). With this type of focussing, there is always some degree of scalloping due to the varying magnetic field. The shape of the beam is therefore never that of a perfectly straight cylinder.

Circuit loss and other fixed parameters:

The rest of the TWT parameters remain fixed throughout the investigation, but these are set to values that are typical in practical applications. For example, the value of the relative dielectric constant ε_r of the support rods is taken for the type of suitable materials chosen for an optimum performance. The ceramic material of Beryllia (with $\varepsilon_r = 6.6$) is therefore the choice for this project due to its high thermal conductivity. Alternatively APBN ($\varepsilon_r = 5.1$) may be used as the ceramic material to support the helix structure.

The amount of RF loss in the helix is chosen to be within practical limits; if the attenuation is too low, there is a possibility of severe variations in gain as a function of frequency. Gain oscillations will occur when the condition stated in (2.4) is satisfied [30].

$$G - L - \rho_o - \rho_\iota > 0 \qquad (2.4)$$

where G = gain /dB

L = loss /dB

ρ_o = reflection coefficient at output in dB

ρ_ι = reflection coefficient at input in dB

Circuit attenuation increases with a greater helix radius and a smaller helix pitch, due to the longer path for the current to take. The increase in length of the helix itself will therefore result in higher attenuation. Loss also increases with a higher dielectric constant of the support rods ε_r, as a result of the reduced circuit impedance.

The total circuit loss is also dependant on the electrical resistance of the helix [30]. This effect is quantified in equation 2.5

$$\text{Total Loss} \propto \sqrt{\text{Helix resistance}} \tag{2.5}$$

Figure 2.11 shows how the total loss for a selection of helix resistivities varies with frequency. Copper is normally coated on the helix with a skin depth of a few μm to increase the thermal and electrical conductivity of the structure [30]. This copper surface gives the helix a low electrical resistance of around 4×10^{-6} Ωcm. For a signal with a frequency of 11.7GHz travelling through copper, the total circuit loss is around 10dB/m, where over half of this is contributed by the cold loss.

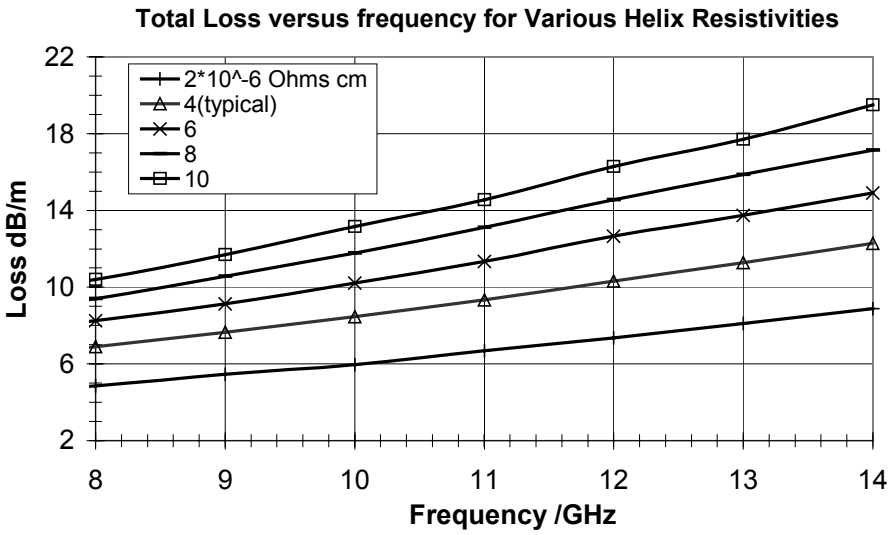

Fig. 2.11 Total loss dependence on frequency for different resistivities [30]

When simulating a helix TWT, the effect of the attenuation profile must be incorporated into the model. In a practical severed TWT, the attenuation is made to be non-uniform along the slow-wave structure for good impedance matching across the bandwidth and to reduce signal reflections.

For a uniform slow-wave structure analysis, the attenuation α is considered to be constant without severs. A suitable factor for this loss needs to be determined, since it is dependent on the frequency and other helix properties. Gilmour [30] shows loss

calculations based on Pierce's circuit loss parameter, but for the purpose of this project, we can use the relationship as shown in fig.2.11. The loss is specified in LSM as dB of power loss per axial metre length of the helix. If this value is made too small (below say 5dB/m), the excessive gain will generate backward-wave oscillations (due to the beating effects with the input signal). As a result, the simulation will fail to converge properly. A loss greater than say 5dB/m should achieve convergence after about 3 iterations for a 1-metre tube. A longer tube will have a higher gain i.e. increased likelihood of backward-wave oscillations. A cold loss of 5dB/m is appropriate for a uniform 1-metre length helix. For a tapered pitch profile with severs, an attenuation profile that is typical in practical TWTs will be employed.

2.9 Conclusions

Future satellite communications demand the design of helix TWTs with reduced non-linear distortion whilst maintaining maximum efficiency consistently across a broad band. Linearity is important, because the backoff required for an acceptable C/I of –21dBc reduces the conversion efficiency by more than half, to a value no more than 16%. The overall efficiency of a TWT therefore does not exceed 65%. The objectives for this project are thus stated as follows: -

1. To understand nonlinearity in a helix TWT
2. To recognise the optimum conditions in a helix TWT and the designs that achieve them.
3. To design of a helix TWT for high linearity whilst maintaining high efficiency consistently across the specified bandwidth.

a) To design for maximum conversion efficiency at an output backoff which gives an acceptable nonlinear performance (say 5dB).
b) To design for a broad-band performance (10.7 to 12.75GHz)
c) To design of a multistage collector from the spent-beam distribution in order to determine the overall TWT efficiency.

The outcome of this project is to achieve a final design which meets the systems requirements and improve understanding of nonlinear behaviour in helix TWTs.

It is useful to develop a design model, for example the Sheath Helix Model, so that the propagation constants for the forward wave β_0 and the slow-space charge wave β_- can be determined in a uniform structure. The TWT parameters can then be solved for a synchronous beam-wave interaction ($\beta_- = \beta_0$) where the coupling is the strongest.

The parameters that affect the performance of a helix TWT will be investigated across a range of input RF powers for a nonlinear analysis and across the frequency band for a broadband analysis. The aim of this is to determine the slow-wave structure designs that achieve the optimum desirable conditions. All of these conditions can then be best incorporated into a single helix with a varying pitch profile, or a best trade-off achieved.

It is proposed to use LSM to model the nonlinear interaction in the tube. Its nonlinear behaviour will be quantified with a quasi-memoryless model based on the single transfer characteristics of the TWT, since the results agree well with the LSM multi-carrier simulations.

References

[1] D. M. Goebel and W. L. Menninger, "Design and Performance of Vacuum Electron Devices for Digital Communications", IEEE International Vacuum Electronics Conf., Monterey, CA, USA, 23-25 April, 2002

[2] D. M. Goebel et al., "Development of Linear Traveling Wave Tubes for Telecommunications Applications", IEEE Trans. on Electron Devices, Vol. ED-48, No. 1, January 2001.

[3] J. L. Putz and M. J. Cascone, Technical Digest, IEDM, IEEE, 1979

[4] M. Agrawal, G. Singh, P.K. Jain and B. N. Basu, “Analysis of a Tapered Vane Loaded Broad-Band Gyro-TWT”, IEEE Trans. on Plasma Science, Vol. PS-29, No. 3, pp.439-443, June 2001.

[5] S. Wallander, “Large Signal Computer Analysis of Distortion in Traveling Wave Tubes”, Chalmers Univ. Technol, Goteborg, Sweden, April 1969

[6] R. G. Carter, W. Bosch, V. Srivastava and G. Gatti, “Computer Simulation of Intermodulation Distortion in Broad-Band Multi-Carrier Travelling Wave Tube Amplifiers”, Proc. Conf. Displays and Vacuum Electronics, Garmisch-Partenkirchen, Germany, April 29-30, 1998.

[7] R. O. Jenkins and R. G. Carter, “Non-linear Power Amplifiers for Telecommunications”, MSc Thesis, Communications Research Centre, Lancaster University, Lancaster UK, September 1998.

[8] R. O. Jenkins and R. G. Carter, “Optimisation of the Transfer Curves of Multi-Carrier Power Amplifiers for Low Intermodulation Distortion”, in Proc. EPSRC-PREP 2001, April 9-11, 2001.

[9] K. F. Sander, “Microwave Components and Systems”, Addison-Wesley Publishing Company Inc., 1987.

[10] Short Form Equipment Specifications for Ka-Band TWTA, Astrium Ltd, 2001

[11] J. E. Rowe and C. A. Brackett, “Efficiency, Phase Shift, and Power Limiting in Variable-Pitch Traveling-Wave Amplifiers”, Proc. National Electronics Conference, Chicago, Vol. 18, 1962.

[12] N. H. Pond and R. J. Twiggs, “Improvement of Travelling-Wave Tube Efficiency through Period Tapering”, IEEE Trans. Electron Devices, Vol. ED-13, pp. 956-961, Dec. 1966.

[13] V. Strivastava, R. G. Carter, “Design of Phase Velocity Tapers in Coupled-Cavity TWTs”, IEE Proc., Vol. 138, No. 5, October 1991.

[14] D. V. Geppert, Proceedings of the IRE, pp.1658-1664, 1958.

[15] J. G. Meeker and J. E. Rowe, “Phase Focusing in Linear-Beam Devices”, IRE Trans. Electron Devices, Vol. ED-9, pp 257-266, May 1962.

[16] J. E. Rowe and C. A. Brackett, “Velocity Tapering in Microwave Amplifiers”, IRE Trans. Electron Devices, Vol. ED-12, pp. 441-447, Aug. 1965.

[17] L. Dombro, J. Long, and L. Roberts, “The Velocity Tapered Helix in Travelling Wave Tubes for Satellite Communications”, presented at the Conf. Microwave Tubes in Systems, London, Oct. 22-23, 1984.

[18] H. G. Kosmahl and J. C. Peterson, “A TWT Amplifier with a Linear Power Transfer Characteristic and Improved Efficiency”, NASA, TM-83590, 1984.

[19] “Studies of the Effect of Circuit Tapering on TWT Performance”, Technical Documentary Report, Rome Air Development Centre, Research and Technical Division, Air Force Systems Command, Griffiss Air Force Base, New York, September 1964.

[20] J. D. Wilson, “Computationally Generated Velocity Taper for Efficiency Enhancement in a Coupled-Cavity Traveling-Wave Tube”, IEEE Trans. on Electron Devices, Vol. 36, No. 4, April 1989.

[21] V. Srivastava, S. N. Joshi, "One-Dimensional Nonlinear Model for Helix TWTs", IETE Tech. Review, Vol. 6, No. 6, 1989.

[22] P. Wang and R. G. Carter, "Modelling of Helix SWS", MRG/93/1, Engineering Department, Lancaster University, January 1993.

[23] P. K. Jain, B. N. Basu, “The inhomogeneous loading effects of practical dielectric supports for the helical slow-wave structure of a TWT”, IEEE Trans. on Electron Devices, Vol.ED-34, No.12, pt.2, pp.2643-8, December 1987.

[24] B. N. Basu, B. B. Pal, V. N. Singh and N. C. Vaidya, “Optimum design of a potentially dispersion-free helical slow-wave circuit of a broadband TWT”, IEEE Trans. Microwave Theory Tech., Vol. MTT-32, pp. 461-463, April 1985.

[25] L. Kumar et al. “Modeling of a Vane-Loaded Helical Slow-Wave Structure for Broad-Band Traveling-Wave Tubes”, IEEE, Trans. Electron Devices, Vol. Ed-36, No. 9, September 1989.

[26] J. Qiu et al., “Testing of Traveling-Wave Tubes Using Broadband Signals”, Naval Research Laboratory, Washington, USA.

[27] R. G. Carter, W. Bosch, V. Strivastava and G. Gatti, “Computer Simulation of Intermodulation Distortion in Traveling Wave Tube Amplifiers”, IEEE Trans. on Electron Devices, Vol. 48, No. 1, pp178-182, January 2001.

[28] R. G. Carter, “Highly Efficient Multi-carrier TWTA”, Report to ESTEC, 10485/93/NL/NB, Lancaster University 1993.

[29] K. Tsuaki, Y. Yuasa and Y. Morizumi, “Numerical Analysis and Design for High-Performance Helix Traveling-Wave Tubes”, IEEE Trans. on Electron Devices, Vol. ED-32, No. 9, pp1842-1849, September 1985.

[30] A. S. Gilmour, Jr, "Principles of Travelling Wave Tubes", Artech House Inc., 1994.

[31] V. Srivastava et al. “Design and Development of Electron Gun for Space Helix Travelling Wave Tube”, IEEE International Vacuum Elect. Conf., Monterey, CA, USA, 2-4 May, 2000.

Chapter Three: Uniform Helix TWT Analysis

3.1 Introduction

The effect of the basic parameters of a uniform Ku-band helix TWT on its nonlinear performance will be investigated in this chapter. A set of design procedures is described in section 3.2, which ensure that the TWT is operating at the synchronous point. Synchronism in this respect is when the slow-space charge phase velocity matches that of the forward wave on the helix. A spreadsheet in EXCEL is used for this purpose to determine the TWT parameters; these are then input into the LSM model. An intermodulation analysis software (IMAL) determines the carrier-to-intermodulation ratio for a multi-carrier signal.

The procedure in Section 3.4 involves adjusting a single parameter at a time and analysing the effect this has on the TWT performance. This will enable conditions of particular interest to be identified, these conditions are: maximum efficiency, maximum bunching intensity, maximum small-signal gain, maximum and minimum phase and amplitude linearity. The helix pitches corresponding to these conditions will be shown. The way in which these results are represented uniquely reveals how the design parameters corresponding to these optimum conditions change as power saturation is approached. These results therefore contribute to our understanding of nonlinear development in a helix TWT.

3.2 Nonlinear Analysis under a Beam-Wave Synchronous Condition

This section determines how the basic parameters of a TWT affect its nonlinear performance whilst maintaining beam-wave synchronism. Synchronism ensures active coupling between the slow space-charge wave and the forward wave on the helix. This results in maximum gain, which is the maximum basic tube efficiency at small-signal levels (or well backed-off levels) as revealed later in section 3.4. A dispersion diagram, as shown in fig 3.1, illustrates this interaction. The figure shows the angular frequencies of the transmission waves of interest in a TWT as a function of their axial propagation constants (β = angular velocity / phase velocity). The gradients of the curves represent the group velocities of the waves. The beam and the helix parameters influence the slow-space charge wave and the forward wave respectively. If the synchronism point is too high, such that it interacts with the backward wave $-\beta_0$, there may be backward wave oscillations. As the synchronism point decreases, the helix becomes more dispersive - reducing the bandwidth of the tube. The typical value of β at synchronism is 0.5π.

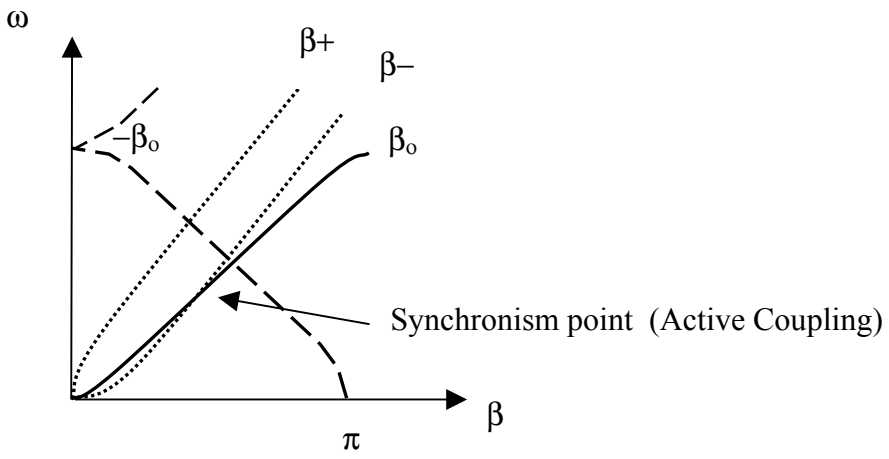

key:-
β+ = fast space-charge wave
β– = slow space-charge wave
β_o = forward wave on the helix
$-\beta_o$ = backward wave on the helix

Fig 3.1 Dispersion diagram of a helix TWT

3.2.1 Achieving Synchronism using a Design Spreadsheet

Design calculations for a helix TWT have been written in three different EXCEL spreadsheets interacting with each other. Each spreadsheet allows the user to input values and perform a series of calculations, based on the Sheath Helix Model [1] (as discussed in Chapter 1.4.4). One spreadsheet computes β-, whilst another spreadsheet computes β_o. The input parameters and calculated output values are given in table A.1 in Appendix A. The Appendix also shows a Brewer diagram [2], which is required to determine the effective plasma frequency ω_q. For these curves, a polynomial expression is obtained for the plasma frequency reduction factor as a function of [angular frequency (ω) × beam radius (b)] / beam phase velocity (v_0) for a specified fill factor. EXCEL includes a solver, which effectively re-adjusts specified design parameters (e.g. helix and beam dimensions) to ensure that synchronism is maintained. This is subject to the condition of a constant centre frequency of 11.7 GHz.

Figures 3.2a-b show the dependence of β_o and β- on the helix pitch p and radius a. It is shown that β_o is strongly dependent on the helix pitch and radius, while β- is independent on these helix parameters. Figure 3.2a shows the case when the helix radius is 0.68mm; here the pitch at synchronism is around 0.74mm. For a pitch of 0.76mm, the helix radius at synchronism is 0.7mm (see fig 3.2b), while β- stays approximately constant at 1700 for a DC supply of 6KV (800W).

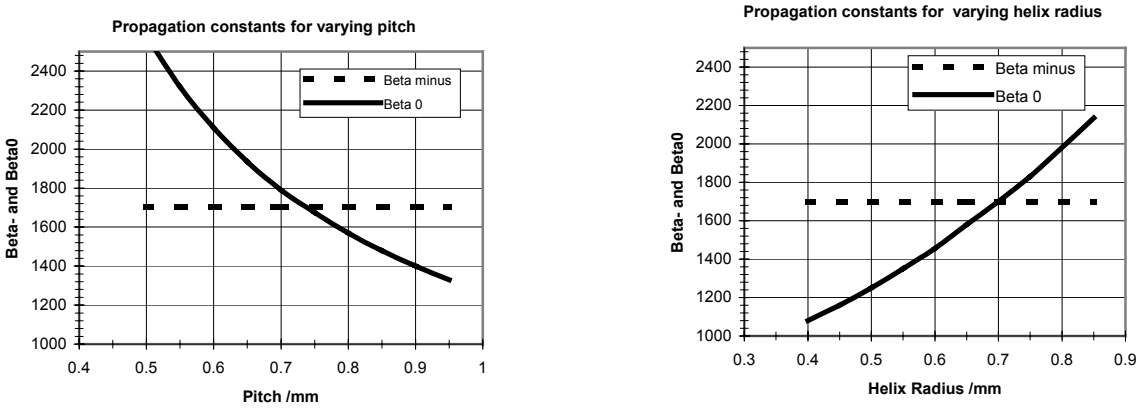

(a) (b)

Fig. 3.2 β- and β_0 as a function of the (a) helix pitch and (b) helix radius

The effect of the beam voltage (at constant DC power) on the propagation constants β_o and β- is shown in fig 3.3a. Here, the beam voltage has a strong influence on β- and not on β_o, where β- is shown to decrease more rapidly with a reduced beam voltage. Note that this is a basic model which is not multi-dimensional, thus the effect of the beam radius on β_o and β-, for instance, is relatively minor.

When the synchronous condition is fully satisfied i.e. $\beta_o = \beta$-, the computed values for a and p are shown as a function of beam voltage (in fig 3.3b). As the beam voltage is increased, the helix diameter should be made bigger and longer pitch used. Synchronism will be achieved for instance when a 6KV cathode voltage is used and the helix has a pitch of 0.636mm and a radius of 0.593mm.

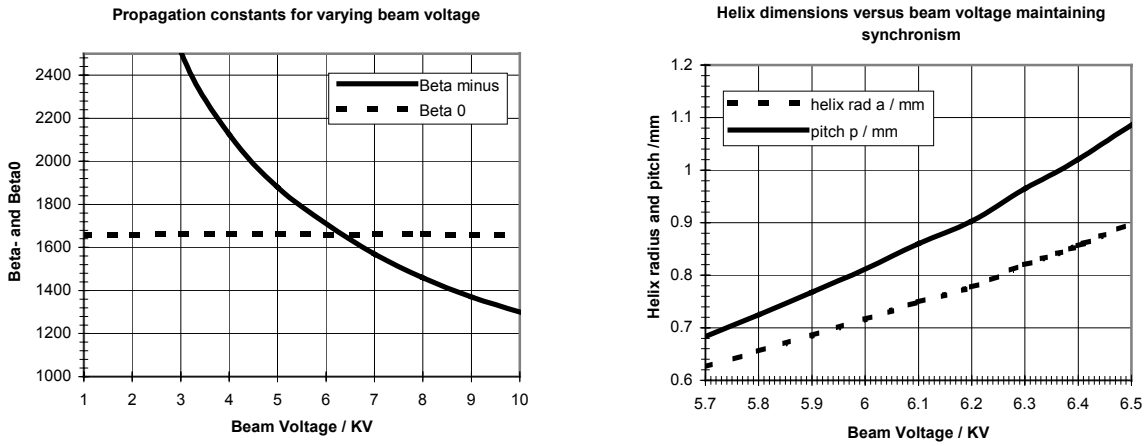

(a) (b)

Fig. 3.3 (a) β- and β_0 versus beam voltage; (b) helix pitch and radius versus beam voltage under synchronism.

Methodology

The spreadsheet design enables all of the necessary parameters to be determined. The parameters of interest for this investigation are: (1) the beam voltage or beam perveance under constant DC power, (2) the beam to helix radius (fill factor) and (3) the tape width to pitch ratio. When these parameters are not varied, they are set to default values, as listed in table 3.1. The table also gives chosen values of other parameters which constitute the TWT design.

Table 3.1

Default TWT Design Parameters	
Centre frequency	11.7GHz
DC power P_{DC}	800W
Cathode Voltage V_0	6KV
Fill factor b/a	0.5
Tape width to pitch δ/p	0.6
Beam stiffness factor m	2
Dielectric loading ε_r (Beryllia)	6.6
θN = wedge angle of support rod $\times$ number of support rods	$30° * 3 = 90°$

These design values are then input into the input data file of the Large-Signal (LSM) program. A TWT with a single section of 100mm (i.e. uniform dimensions throughout the structure) was simulated, with a cold loss of 5dB. The HELIX code (in Chapter 2.7.2) was used to obtain the final values of the axial propagation constant and the interaction impedance. This is because the sheath helix model predictions from the spreadsheet design are not very accurate for the calculation of coupling impedance. This HELIX code is based on the more sophisticated and accurate tape model. An intermodulation analysis software (IMAL) then computed the carrier-to-intermodulation ratio for a multi-carrier system, based on the transfer characteristics from the output of LSM. A broadband analysis has also been carried out and is given in section 3.2.4.

3.2.2 Effect of the Beam Voltage on the Nonlinear Performance

For this investigation, the beam voltage was varied from 5.7 to 6.4KV, at a constant DC power of 800W. This corresponds to a change in beam perveance from 0.326 to 0.244μPerv, which is within the practical geometrical limits of a space TWT electron gun.

Because the beam voltage strongly affects the slow space-charge wave β- and has very little effect on the axial propagation constant β_o, β- was synchronised to the approximately constant β_o. The result of this was to vary the helix pitch p subject to a constant frequency of 11.7 GHz. The flowchart in fig. 3.4 is a simplified illustration of the design process for the variation of DC voltage under constant power, where the rectangles represent the input parameters. The solver is used to set β_o to synchronise with β- determined by the beam settings and frequency. This then alters the circuit capacitance and inductance, subject to the constant frequency condition. These adjust both the helix radius a and the pitch angle ϕ, which in turn change the pitch. These modified values are then reiterated through the sequence of calculations, by modifying β-. This process should actually achieve convergence in just two iterations.

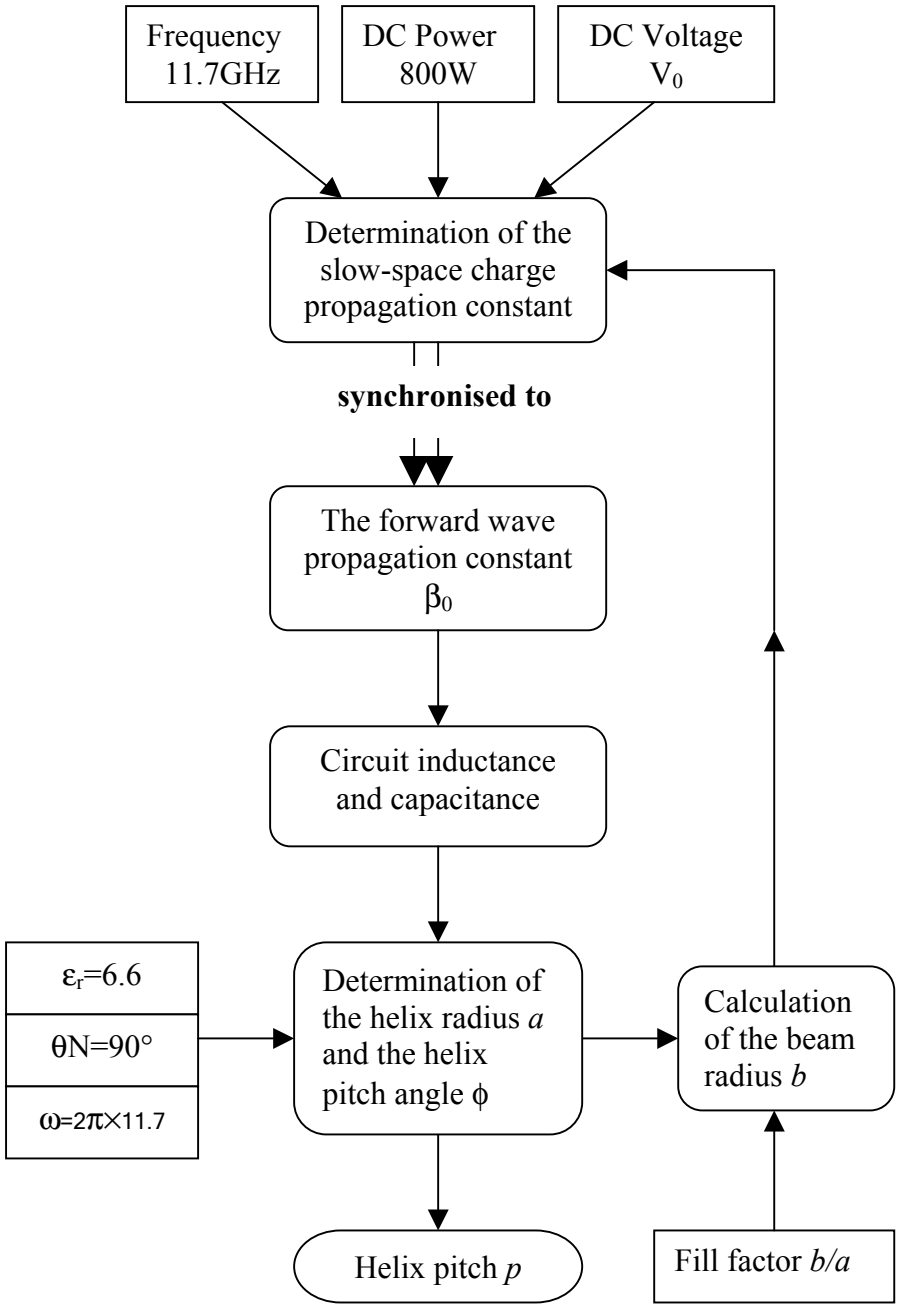

Fig. 3.4 Basic flow chart for the design of a synchronous helix TWT when the beam voltage is adjusted.

Analysis

Figure 3.5 shows the RF output power versus RF input power for the selected DC voltages of 5.7 to 6.4KV(0.326 to 0.244μPerv). The curvatures of the various AM/AM curves appear to be similar, however the 5.7 and 6KV beams give a slightly larger radial curvature than the higher voltage beams. The gradients at which AM/AM curves decrease in overdrive appear similar, apart from the 6KV beam which loses slightly more power than the rest. Note that these angles at overdrive should not affect the nonlinear distortion from the multi-carrier TWT. This is because the radii of curvature are not small enough for the IM performance to have any dependence on these angles of overdrive [3], as discussed in Chapter 2.5.

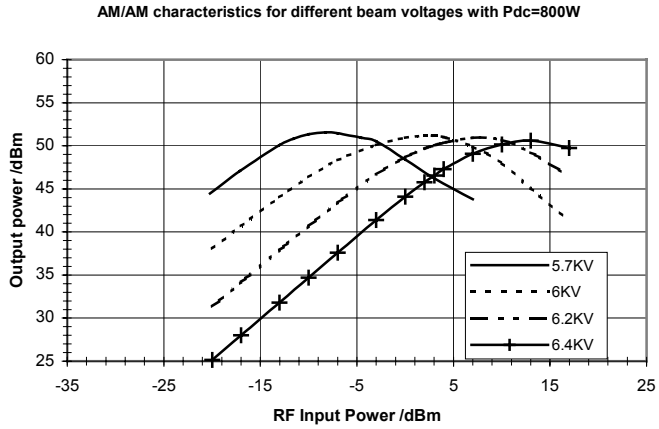

Fig. 3.5 AM/AM transfer curves for different beam voltages from 5.7 to 6.4KV

The AM/PM characteristics are shown in fig 3.6. The phase conversion (i.e. the phase shift per dB increase in drive power) is far greatest for a 5.7KV beam, compared to the other voltages. The case with the higher phase shift also produces the greater saturated conversion efficiency, as shown in fig. 3.7. This figure shows that the maximum efficiency decreases with increasing beam voltage.

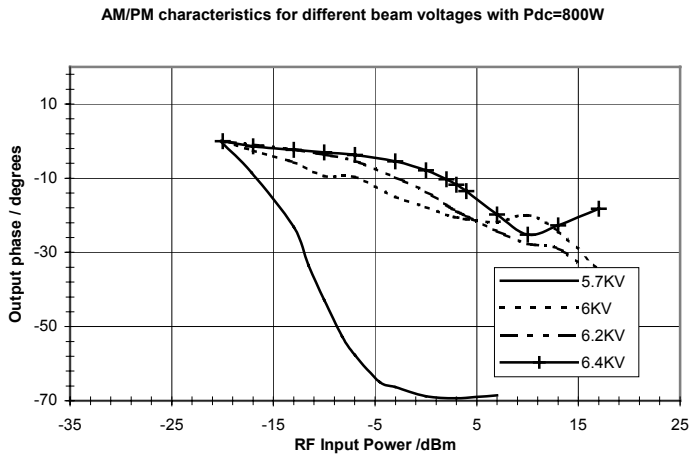

Fig. 3.6 AM/PM transfer curves for different beam voltages from 5.7 to 6.4KV

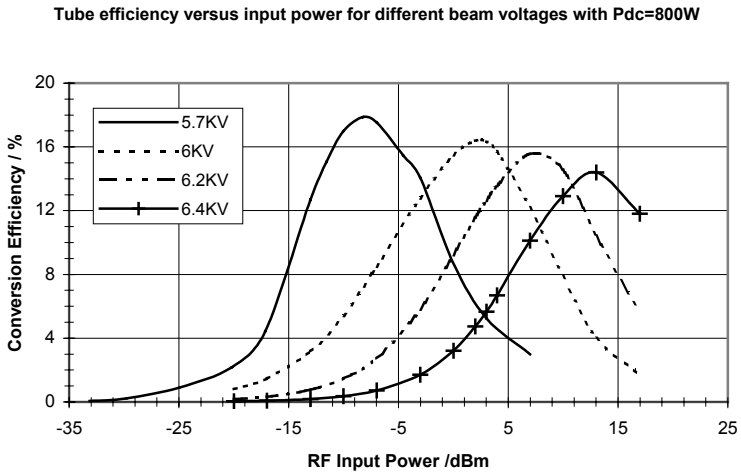

Fig. 3.7 Conversion efficiencies versus input power for different beam voltages

The carrier-to-third order intermodulation ratios (C/I3) computed by IMAL are displayed in fig. 3.8. When the IM3 amplitudes are more than 24dB below the carrier, the nonlinear performance deteriorates with decreasing beam voltage or increasing beam perveance. For an acceptable level of C/I3 of say 21dBc as specified in Chapter 2.5, the output backoffs (OBO) required for the 5.7, 6.0, 6.2 and 6.4KV beams are 8.5, 6.0, 3.93 and 4.64 dB respectively. For 5.7KV, the output backoff becomes exceptionally large when C/I3<–21dBc. This is mainly due to the large phase shift of up to - 6°/dB (fig 3.6). The large output backoff requirement for C/I3=–21dBc reduces the tube efficiency from 18% at saturation to 1.6%. The other cases, with

their flatter phase responses and more desirable AM/AM characteristics, have improved backoff efficiencies. Figure 3.9 shows the tube efficiencies versus beam voltage for a C/I3 requirement of –21dBc. As shown in the figure, the best beam voltage is 6.2KV giving a tube efficiency of 6.5%, this is followed by V_0=6.0 and 6.4KV with efficiencies of 4.5 and 4.2% respectively.

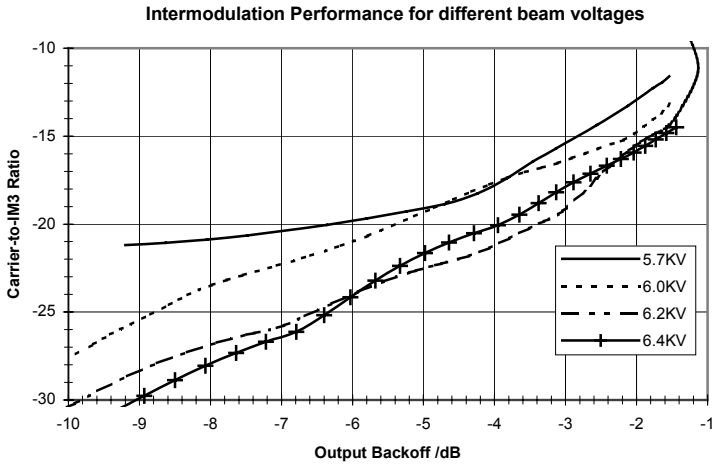

Fig. 3.8 Intermodulation performance versus output backoff for different beam voltages

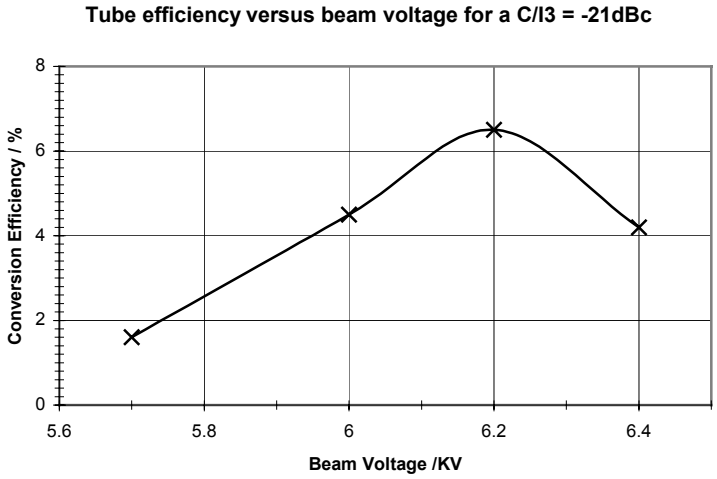

Fig. 3.9 Conversion efficiency versus beam voltage for a C/I3=-21dBc

3.2.3 Effect of the Fill Factor on the Nonlinear Performance

In the design procedure for the fill factor variation, the beam voltage is fixed at 6KV while the ratio of the beam to helix radius is varied from 0.4 to 0.6. The helix radius is set at 0.7159mm, while the beam radius is adjusted according to the desired b/a ratio. Since β- depends strongly on the beam radius, β_o is made to synchronise with β-. The helix radius a and pitch angle ϕ are therefore adjusted to maintain synchronism, as in the previous case. The added complication however is that the Brewer relationships are also dependent on the fill factor (see fig. A.1 in Appendix A), so the quantitative effect these have on β- need to be incorporated in the design. The design algorithm follows the same routine as given in fig 3.4. Note that the fill factor is a parameter in the radial direction, a 2.5 or 3D model will produce a more accurate representation. The following results may differ to those found in practice, but the general trends should be the same.

Analysis

The practical limitation of the beam-to-helix radius is from 0.4 to 0.6 as discussed in Chapter 2.8. The AM/AM curves in fig 3.10 appear to be similar, however when the b/a ratio is increased to its practical maximum the gradient of the curve becomes slightly greater than 45° just before the curve becomes nonlinear (at ~4dB OBO). This behaviour results in deterioration in the intermodulation performance of the TWT. The AM/PM curves (fig. 3.11) show more phase lag across the drive power range for a greater beam-to-helix radius (to some 4°/dB of phase conversion when b/a=0.6). The result of this is greater intermodulation distortion, as shown in fig 3.13. The output backoff required for a two-carrier input signal to achieve -21dBc increases from 4.8 to 6.6dB as b/a is increased from 0.4 to 0.6 respectively. The drawback however, is reduced basic saturation efficiency, as shown in fig 3.12 (roughly 1% efficiency reduction for a decrease in b/a of 1). Figure 3.14 shows the conversion efficiencies for a C/I3 of –21dBc versus b/a; these are 3.6, 5 and 4% for b/a = 0.4, 0.48 and 0.6 respectively. Meeting the stringent linearity requirements has cut the conversion efficiencies by more than third. From the results so, far, it does appear to be a general rule that when the conversion efficiency is greater, there is more phase lag and more intermodulation distortion is generated from the tube. This will be

verified further in Section 3.4, where the nonlinear performance will be investigated for a wide range of helix and beam parameters.

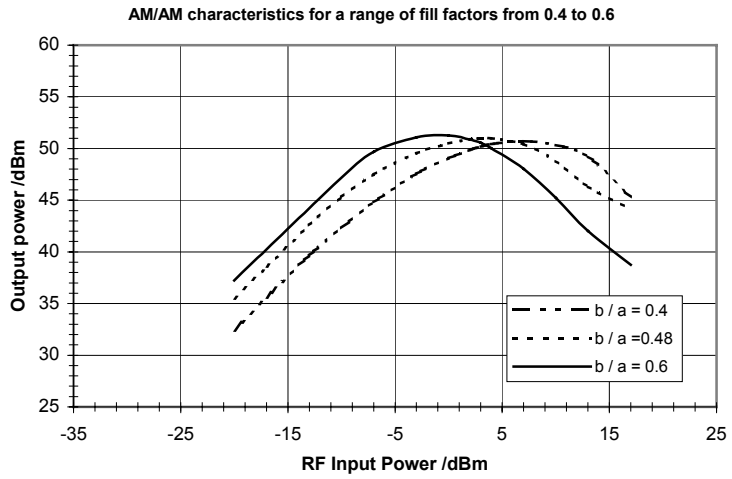

Fig. 3.10 AM/AM transfer curves for different ratios of beam to helix radius

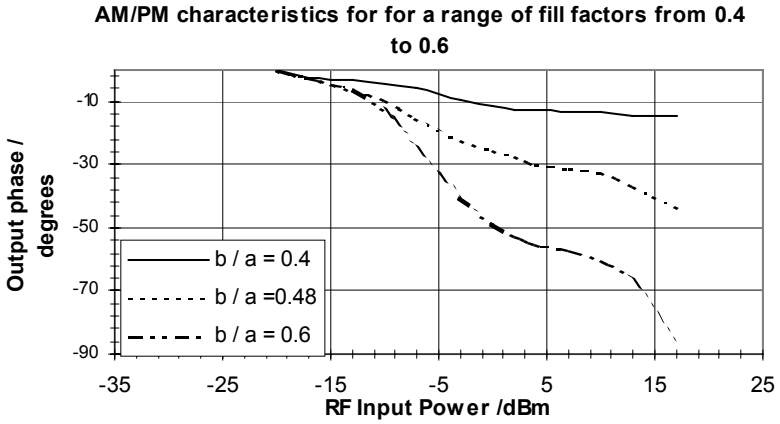

Fig. 3.11 AM/PM transfer curves for different ratios of beam to helix radius

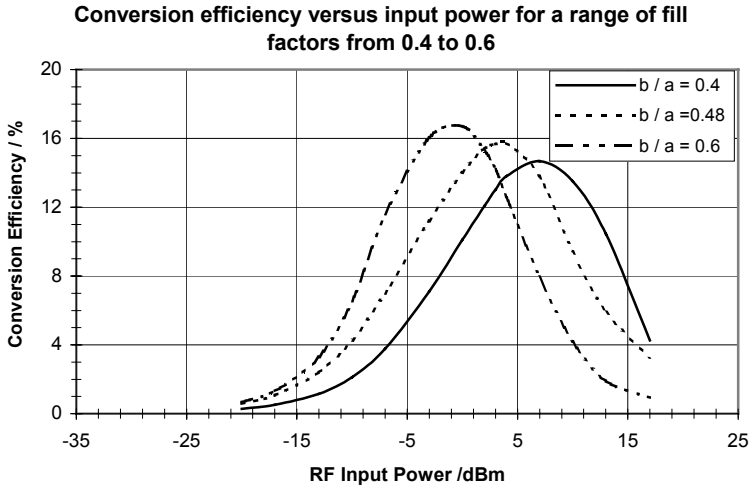

Fig. 3.12 Conversion efficiencies versus input power for different fill factors

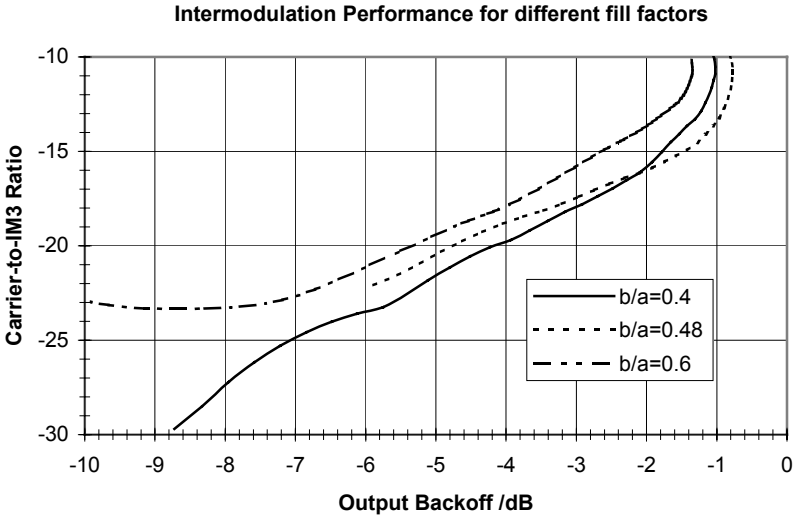

Fig. 3.13 Intermodulation performance versus output backoff for different fill factors

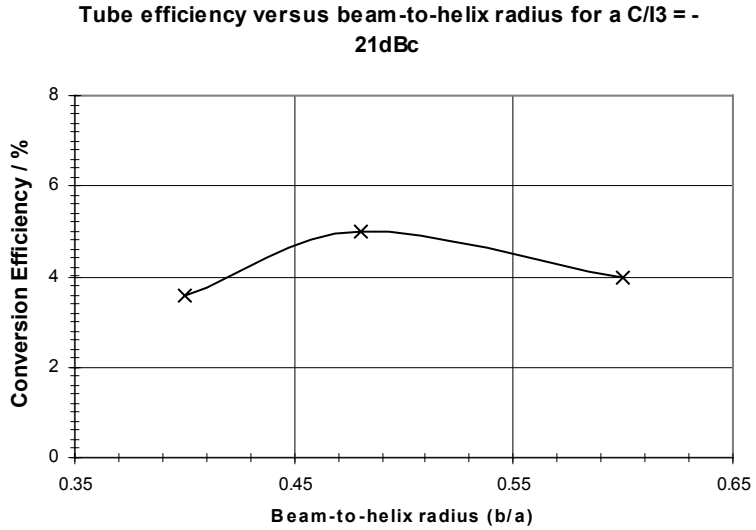

Fig. 3.14 Conversion efficiency versus fill factor for a C/I3=-21dBc

3.2.4 The Broad-Band Performance

The bandwidth target set out for this project is an ambitious one for a communications helix TWT: 10.7 to 12.7GHz (a 2GHz bandwidth). The design strategy employed of ensuring a beam-wave synchronous condition at the band centre guarantees a consistent broad-band performance. This is therefore a good approach to use where broadband is essential. In the design procedure, the system was made to be synchronous at a fixed centre frequency of 11.7GHz, ensuring a peak small-signal performance at or near to the centre frequency.

Figures 3.15 to 3.17 show the output performance across the specified bandwidth for selected design parameters: V_0 = 6KV, b/a=0.5. The figures give the output RF power, phase and gain as a function of frequency (in GHz). Saturation occurs when the drive power is 2dBm as in fig 3.15. Here, the saturated output power remains over 50dBm with minor variations across the band. The broadband performance at drive levels backed-off from saturation is also revealed, where the output power and therefore the efficiency is reduced at the lower band-edge. For higher frequency components in the signal envelope reaching the upper band, there is a wider dynamic phase variation than at the lower band-edge as shown in fig. 3.16. The small-signal gain of the TWT (see fig 3.17) increases with frequency across the band by about 5dB. At saturation however, the gain is roughly constant at around 49dB. For a C/I3 of –21dBc, the output backoffs for 10.7, 11.7 and 12.75GHz are 4.3, 4.5 and 5.7dB respectively reducing the conversion efficiencies to 4.1, 5.8 and 6.0dB as shown in fig 3.18 .

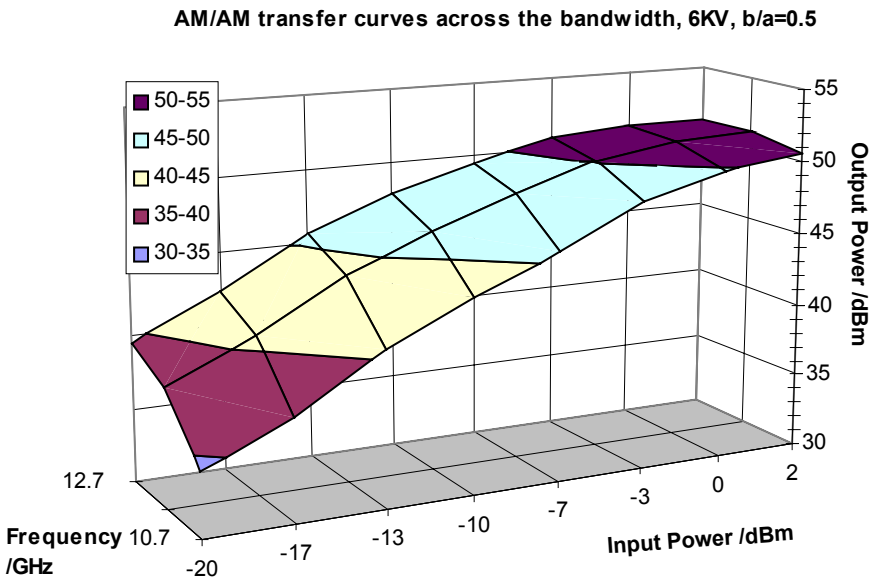

Fig. 3.15 AM/AM transfer curves across the band for 6KV, b/a=0.5

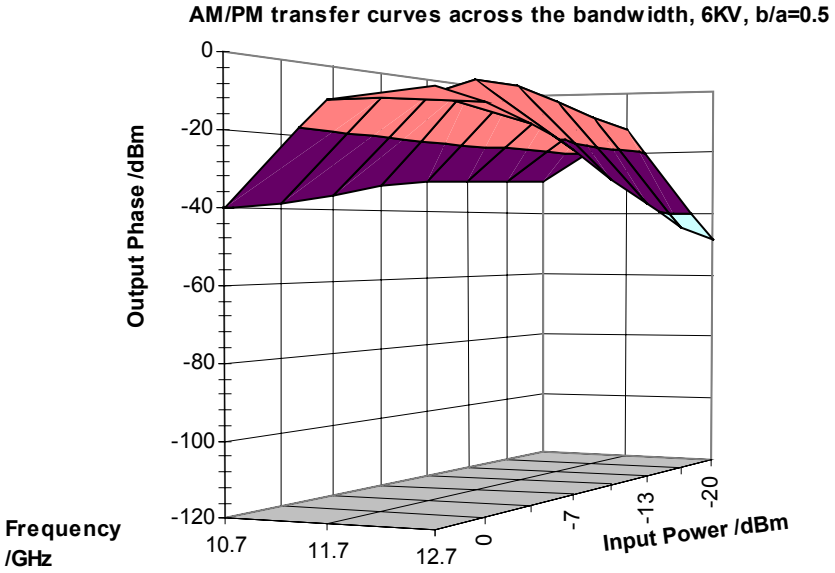

Fig. 3.16 AM/PM transfer curves across the band for 6KV, b/a=0.5

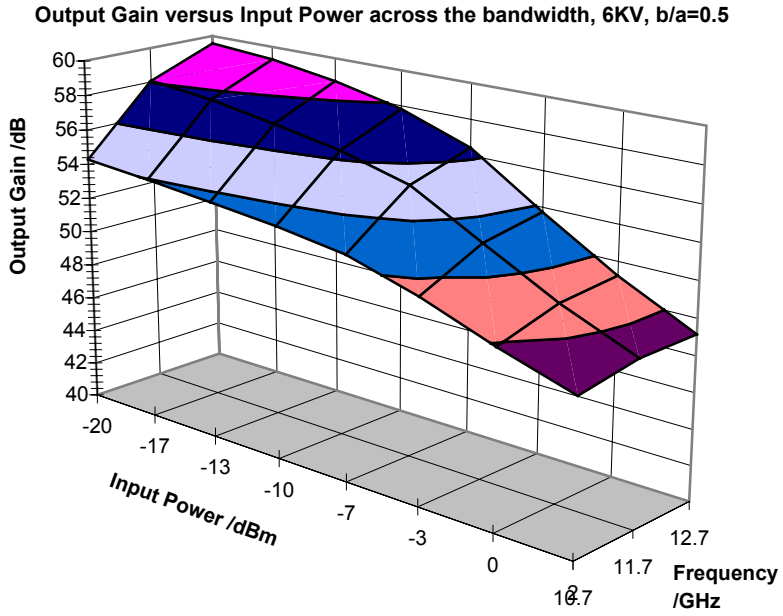

Fig. 3.17 Output gain across the band for 6KV, b/a=0.5

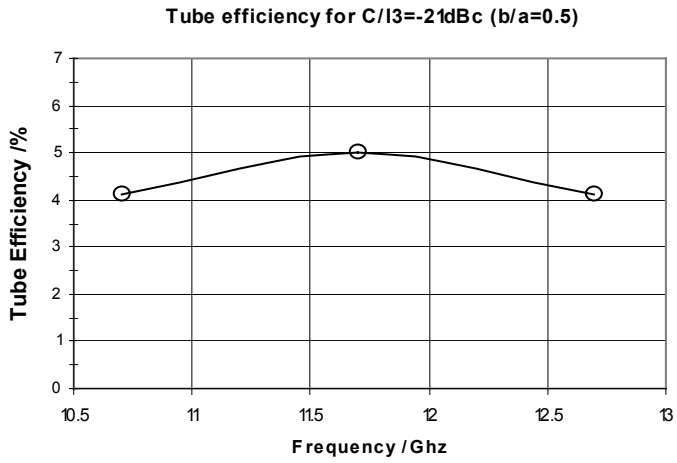

Fig. 3.18 Conversion efficiency at frequencies 10.7, 11.7 and 12.75GHz for a C/I3=-21dBc

Figures 3.19 to 3.21 show the broadband performance for the case when the beam fill factor is at its practical maximum i.e. b/a = 0.6. Here, power saturation occurs at a drive power of 0dBm (fig. 3.19). At this saturated power, the results are fairly similar to those with b/a=0.5, in that both the output power and gain are approximately constant at 51dBm (in fig's 3.19 and 3.21). The saturated tube efficiency is therefore constant (at 16%) at the three frequency points 10.7, 11.7 and 12.75GHz. The variations of phase with frequency are greater however for a higher fill factor: the phase shift across the band and the dynamic phase shift at each frequency are both considerably greater than when b/a=0.5. This greater dynamic phase shift is expected from the results in fig. 3.11, as the phase shift increases with fill factor.

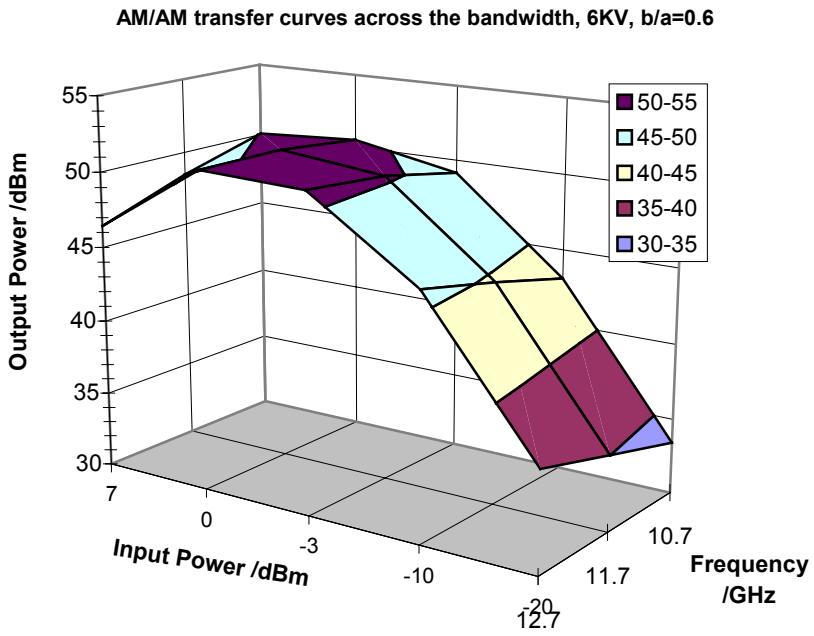

Fig. 3.19 AM/AM transfer curves across the band for 6KV, b/a=0.6

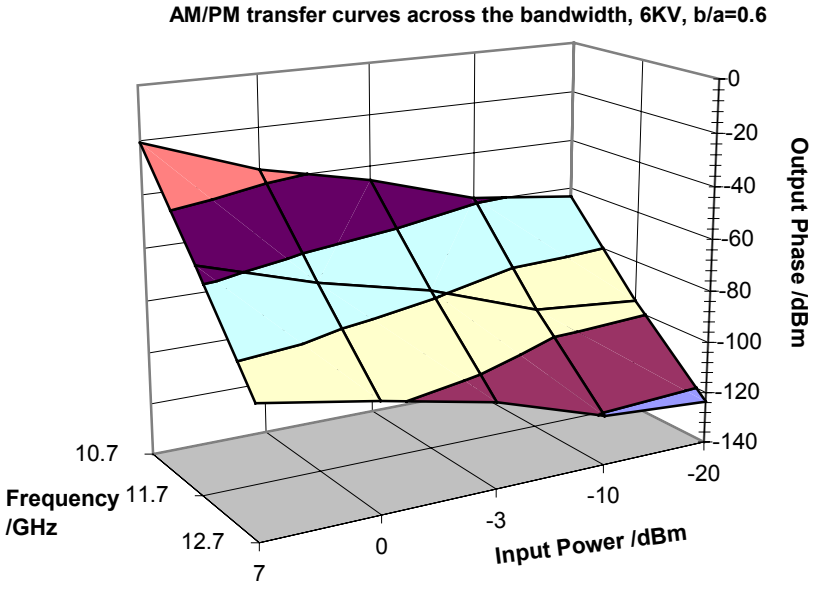

Fig. 3.20 AM/PM transfer curves across the band for 6KV, b/a=0.6

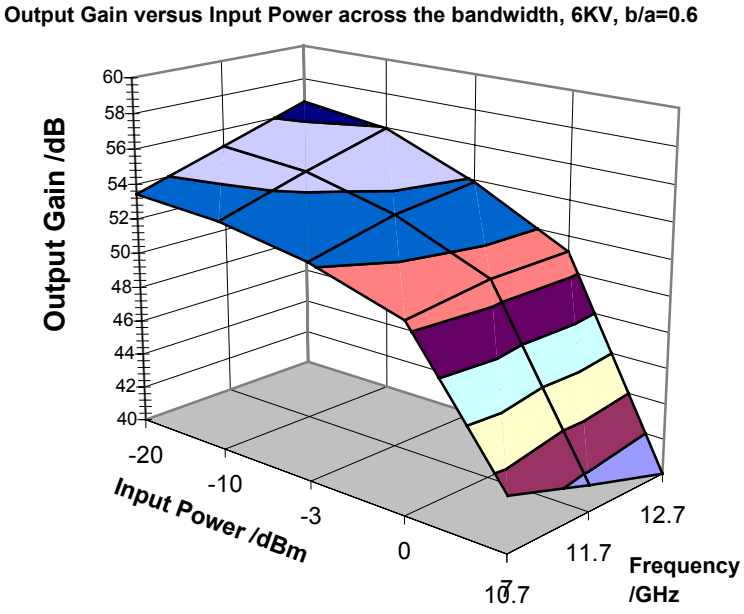

Fig. 3.21 Output gain across the band for 6KV, b/a=0.6

Further investigations have been carried out on the effect of other parameters on the nonlinear performance [4]. One such case was the tape width-to pitch (δ/p) variation within the practical range of 0.4 to 0.8. The results have not been presented here since δ/p was shown to have a negligible effect on the transfer curves and the efficiency.

3.3 Determination of the Location of the Optimum Conditions on a Dispersion Diagram

The interaction in a TWT can be understood in terms of the synchronism between the slow space-charge wave on the electron beam and the wave on the helix. Figure 3.22 shows a typical dispersion diagram of the interaction between the slow-space charge wave and the forward wave on the helix, for different beam voltages or perveances (with constant beam power). The frequencies of the interacting waves are plotted versus their propagation constants. Here, the pitches controlling the helix phase velocities had to be adjusted to centre the beam-wave interaction at the same frequency (11.7GHz).

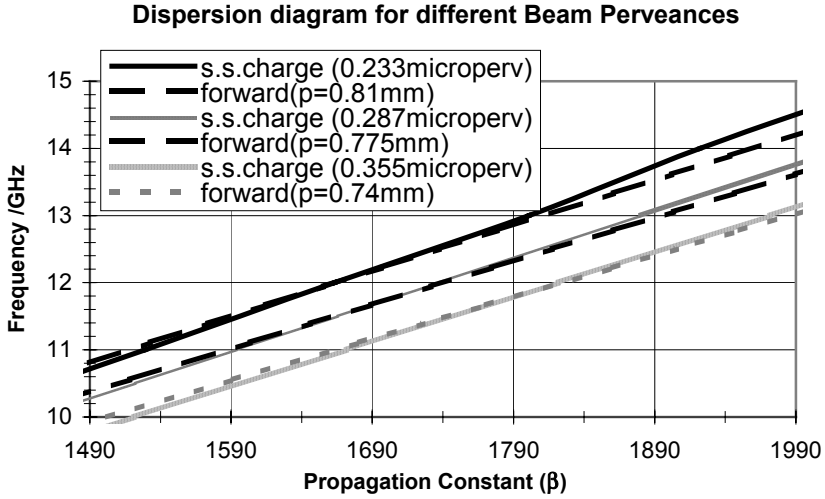

Fig. 3.22 Beam-wave interaction region on a dispersion diagram for different beam perveances

The desirable conditions in a helix TWT depend on separation between β_0 and β_-. Figure 3.23 shows the power transfer curves for a range of $\beta_0 - \beta_-$ values; a uniform helix is simulated with the tube data as in table 3.1. The most favourable condition for AM/AM linearity is shown to lie below the synchronous point at $\beta_0 - \beta_- = -10$. The synchronous condition actually results in the largest AM/AM curvature, but the gain is the highest and the saturation efficiency is close to maximum. At the synchronous point, the RF energy removed by the beam is also maximum as shown in the spent-beam distribution in fig 3.24 (taken at an input power of −1dBm), but the

unrecoverable energy is also highest. Both the spent-beam energy and the unrecoverable energy decrease as the system is operated further away from synchronism.

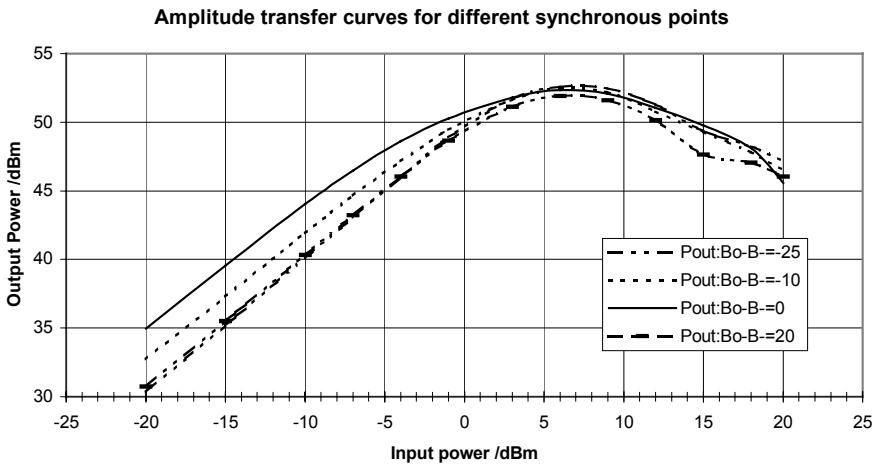

Fig 3.23 AM/AM curves for different synchronous positions

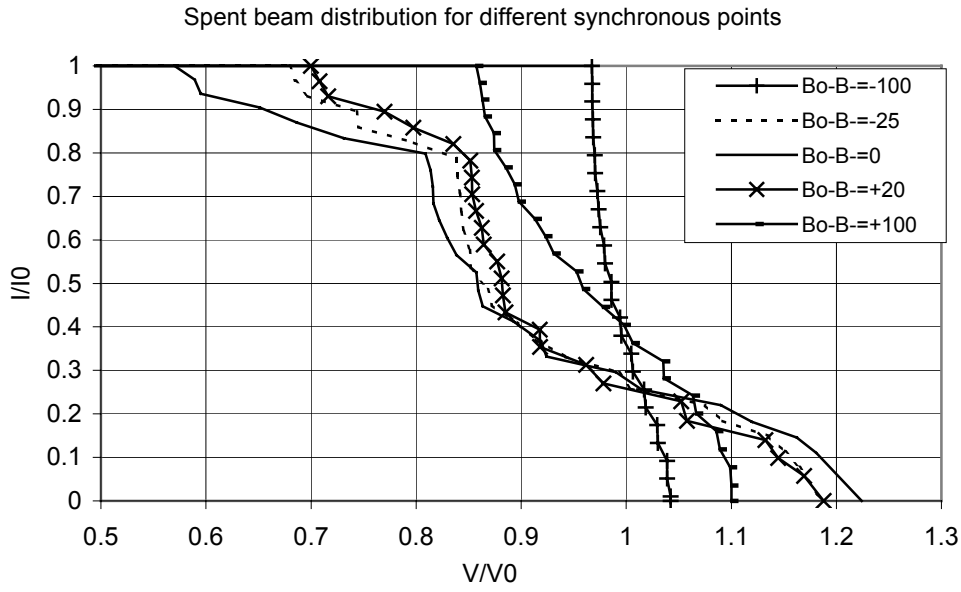

Fig 3.24 The spent-beam distribution for different synchronous positions

Figure 3.25 summarises the locations of the desirable conditions. These positions on the ω–β diagram may vary according to the type of design employed. It may be possible to design the TWT (e.g. the perveance of the electron gun) so that these different optimum conditions lie in closer proximity; the effect of the beam perveance on the nonlinear performance is covered in Section 3.4.2.

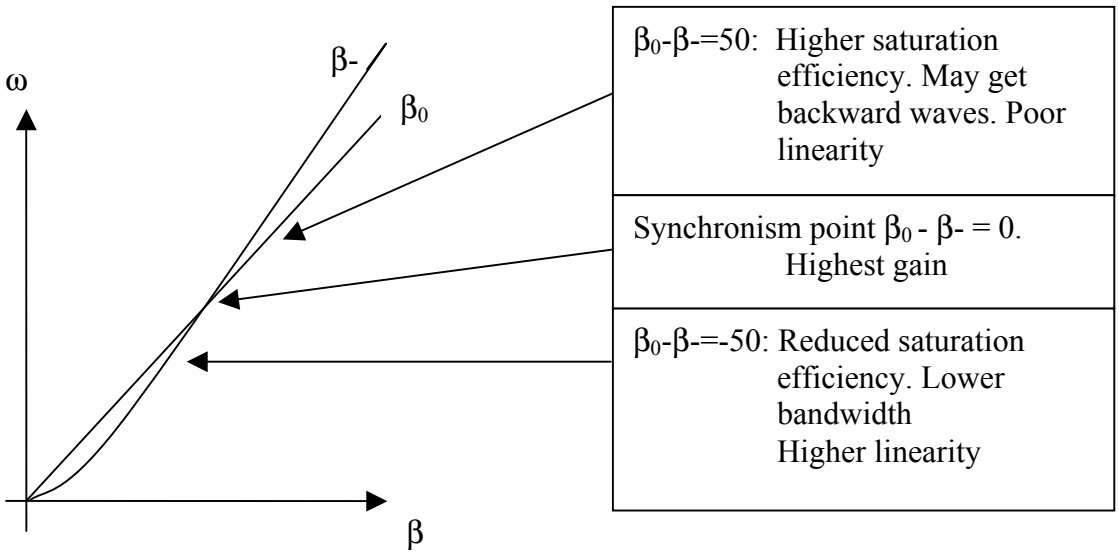

Fig 3.25 Dispersion curve indicating where the optimum conditions lie

3.4 Nonlinear Uniform Analysis of the Helix and Beam Parameters on the Nonlinear Performance

Research has been carried out to understand the effect individual parameters have on the nonlinear performance in a TWT. This investigation is quite different to that in Section 3.2, in that only one parameter is varied at one time; the parameters which are not investigated are set to a constant default value. Because there was no requirement for a synchronous condition, a design spreadsheet was not necessary. Exactly the same parameters were used as in table 3.1, but a 60mm length of tube was used to minimise occurrence of backward-wave oscillations. The helix pitch and voltage were the two variables used in the investigations, since these were found to be most influential on the forward wave and the slow space-charge wave respectively.

The helix pitch was varied in steps across a predefined range in a uniform helix structure. For each successive increment of the helix pitch, output data describing the TWT performance was produced. The LSM code was modified to perform this operation. The output TWT performance could then be accurately represented across the required helix pitch range. This approach enables the conditions of particular interest to be identified. These conditions are: maximum efficiency, maximum bunching intensity, maximum small-signal gain, maximum and minimum phase and amplitude linearity.

3.4.1 Effect of the Helix Pitch on the Performance

The results shown in fig. 3.26a-c reveal the development of nonlinearity in the output RF power, output phase and peak RF beam current respectively as a function of helix pitch. The peak RF current corresponds to the condition of maximum bunching intensity in the helix [5]. The physical significance of this will be explored further in Chapter 4. The contour lines in the figures represent 2dB increments of RF drive power up to the saturation region. In the linear region the figures show that a helix pitch of 0.82mm produces maximum RF output power, output phase and peak RF beam current. As power saturation is approached, the nonlinearity in the device causes the helix pitches corresponding to these maximum conditions to change.

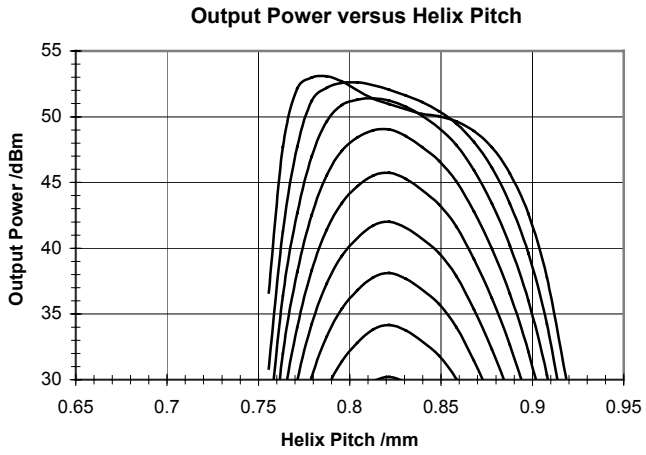

(a)

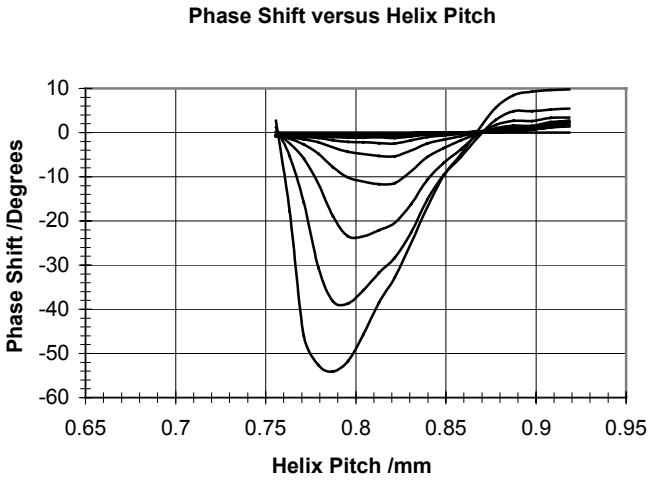

(b)

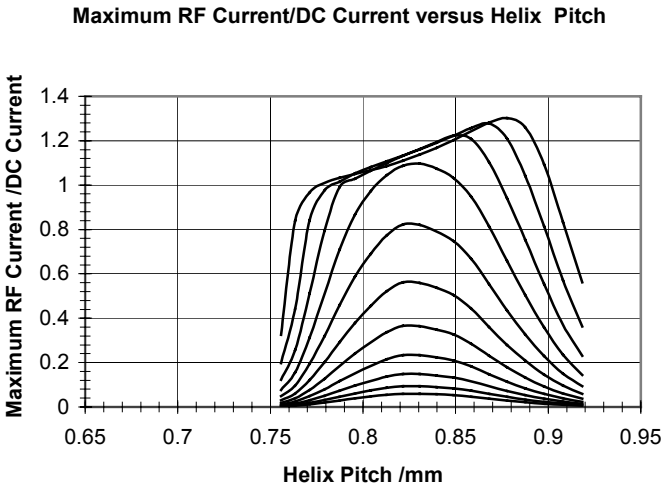

(c)

Fig. 3.26 Output power, Output phase and peak RF current as a function of helix pitch for different drive levels with a 0.235μPerv (6.5KV) beam

Figure 3.26c shows how the nonlinearity in the amplifier causes limiting in the peak RF beam current. This figure is particularly useful in the design stage by indicating where the helix pitch lies which corresponds to the maximum electron bunch intensity. This will be discussed in more depth in Chapter 6.

In order to maximise the intensity of the bunch at an input power backoff of say 4dB, a pitch of 0.85mm would therefore be used. Because the phase lag corresponding to this pitch is low (see fig 3.26b), the phase linearity of the device would also be improved.

Figure 3.26a shows how the power compression at saturation varies with helix pitch. The optimum amplitude linearity occurs where the AM/AM curve saturates over the smallest input power range [3]. It can therefore be shown that the optimum AM/AM linearity occurs at a pitch of 0.855mm. With this choice of helix pitch however, the saturated output power is 3dB below the highest that can be achieved. The pitch corresponding to maximum power and therefore maximum conversion efficiency is 0.785mm. But this also coincides with the maximum condition for phase nonlinearity. A helix design that corresponds to maximum linearity is clearly different from that corresponding to maximum efficiency. It is next revealed how this difference can be reduced by selection of the beam parameters.

3.4.2 Effect of the Beam Perveance on the Nonlinear Performance

The properties of the electron beam influence the synchronisation between the electron beam and the helix, affecting the non-linear properties of the TWT. The most effective beam parameter to influence the beam-wave synchronism, and therefore the nonlinear properties, is the beam voltage or gun perveance [6,7]. This section will refer to the perveance instead of the voltage since this is specified by the geometry of the electron gun and is therefore more appropriate from the design perspective.

Figures 3.27 and 3.28 show results when the micro-perveance is increased from 0.233μPerv to 0.287 and 0.355μPerv respectively. Figure 3.27a shows that with a

higher beam perveance, the AM/AM curves are flatter in overdrive, indicating that the power in the circuit is maintained better beyond saturation, and not lost to the beam. Here, the condition for maximum AM/AM linearity occurs with an increased pitch of 0.81mm. This lies closer to the maximum efficiency condition, thus providing increased output RF power (2dB below the highest that can be achieved). The non-linear phase shift at this optimum AM/AM condition however is increased (from 5° to 16°), as shown in fig. 3.27b.

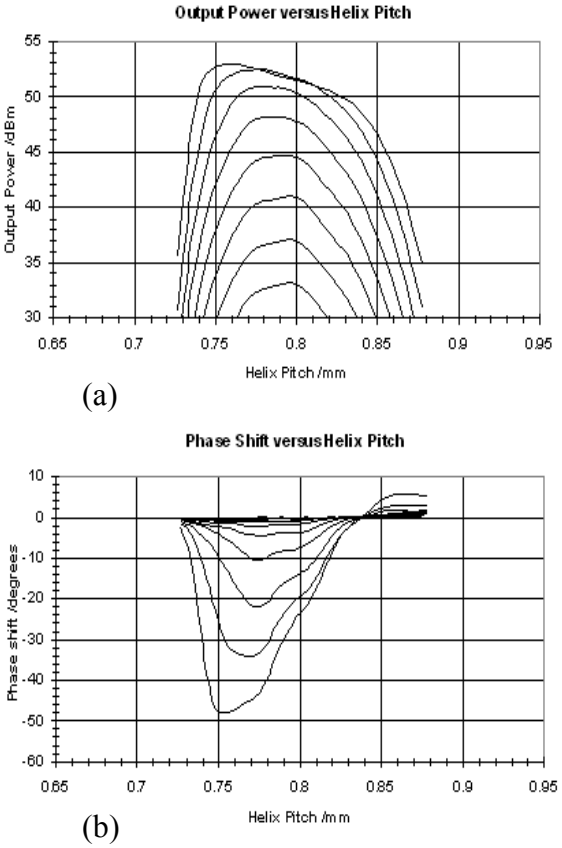

Fig. 3.27 Output power and phase versus helix pitch for different drive levels with a 0.287μPerv (6KV) beam

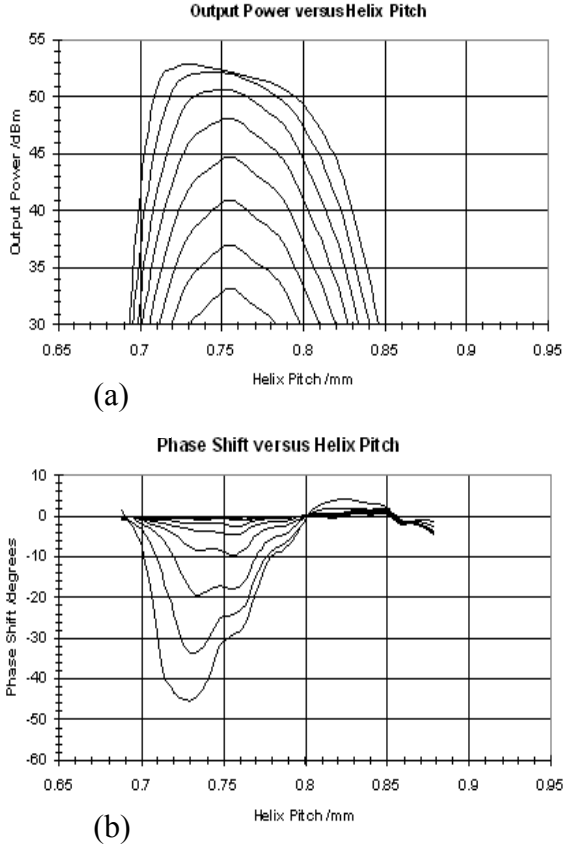

Fig. 3.28 Output power and phase versus helix pitch for different drive levels with a 0.355μPerv (5.5KV) beam

When a higher gun perveance of 0.355μPerv is used, as in fig. 3.28a, the optimum amplitude linearity occurs with a reduced pitch of 0.755mm. The difference between the conditions of optimum linearity and efficiency is therefore reduced further, but the trade-off again is increased phase nonlinearity.

3.5 Conclusions

In this chapter, research has been carried out on how the fundamental parameters of a helix TWT affect its nonlinear performance. The transfer curves of each design were generated, since these determine the nonlinear performance of any quasi-memoryless power amplifier. The carrier-to-intermodulation ratio was also computed.

The initial criterion (in Section 3.2) was to ensure beam-wave synchronism. It was found that the space-charge waves is particularly sensitive to voltage adjustment, while the forward wave is very sensitive to the helix pitch. Therefore any variation of the beam voltage required a pitch adjustment to re-align the forward wave to intersect with the slow space-charge wave.

Basically, the aim is to maximise the operating efficiency at a backed-off power level that gives an acceptable level of carrier-to-IM ratio. The results from this section have found that the basic parameters resulting in an optimum backed-off operating efficiency with C/I3=-21dBc is as follows: -

1. A 6.2KV(or a 0.244μPerv) beam with DC Power of 800W
2. A corresponding helix radius of 0.778mm and a pitch of p=0.902mm to ensure $\beta_o = \beta$-
3. A beam filling factor of 0.6
4. The tape width (within the realistic range $0.4<\delta/p<0.6$) has a negligible effect on the nonlinear performance.

The design strategy for this case is favourable where broadband is essential; this is shown by the consistency of the results across the bandwidth. The condition where the beam-wave synchronism applies may not include the optimum linearity condition

In Section 3.4, the work involved adjusting one design parameter at a time in order to determine the design which corresponds to the most favorable conditions. The helix pitch and beam perveance are the two most effective design parameters for controlling

the forward wave on the helix and the slow space-charge wave respectively. The results reveal how these parameters affect the efficiency and linearity of a helix TWT.

Towards power saturation, the non-linearity in the TWT causes a substantial amount of peak RF beam current to be lost at that frequency. It is also shown how the amplitude and phase curves vary across the range of helix pitches as power saturation is approached. The nonlinear TWT processes result in (1) an increased helix pitch for optimum electron bunch intensity and (2) a reduced pitch for maximum conversion efficiency. The results also reveal that the helix design corresponding to the minimum phase shift is independent of drive power up to power saturation.

A major goal in the design of high power TWT amplifying systems is achieving maximum efficiency for an acceptable linearity. This chapter concludes a number of trade-offs: if the helix pitch is designed to correspond to optimum AM/AM linearity, then increasing the beam perveance increases the output power, at the expense of increased phase conversion. If a helix pitch corresponding to optimum AM/PM linearity is selected however, then the output power remains constant at 49dBm as the beam perveance increases, but at the expense of AM/AM linearity.

Single, un-severed uniform structures are not used in practice, because the saturated output gain is at such a level that is too high for stable operation. The design of a practical helix TWT will therefore be covered in Chapter 6. This Chapter however, has explored how the fundamental parameters affect its nonlinearity in a uniform structure. The results provides a basis on which to fully optimise the design of a helix by identifying the design parameters which correspond to the desirable high linearity and high efficiency required in modern communications systems. The work has also contributed to our understanding on the development of nonlinearity in helix TWTs across a range of helix and beam designs. Further research in the next chapter will attempt to uncover the fundamental mechanisms that produce nonlinearity in a TWT.

References

[1] S. F. Paik, “Design Formulas for Helix Dispersion Shaping”, IEEE Trans. on Electron Devices, Vol. ED-16, p.1010, 1969.

[2] A. S. Gilmour, Jr, "Principles of Travelling Wave Tubes", Artech House Inc., p. 259, 1994.

[3] R. O. Jenkins and R. G. Carter, “Optimisation of the Transfer Curves of Multi-Carrier Power Amplifiers for Low Intermodulation Distortion”, in Proc. EPSRC-PREP 2001, April 9-11, 2001.

[4] R. O. Jenkins and R. G. Carter, “High Linearity Broad-band TWT Amplifiers for Satellite Communications Systems”, MRG/2000/1: Report One, Lancaster University, January 2001.

[5] V. Strivastava et. al., “Design of Helix Slow-wave Structures for High Efficiency TWTs”, IEEE Trans. on Electron Devices, Vol. 47, No. 12, December 2000.

[6] R. O. Jenkins and R. G. Carter, “Effect of the Beam Parameters on the Non-linear Performance in Helix TWTs”, in Proc. Conf. Intl. Vacuum Electronics, Monterey, USA, April 2002.

[7] R. O. Jenkins and R. G. Carter, “Design of Helix TWTs for Optimum Linearity”, in Proc. 7th IEEE Freq. Postgraduate Student Colloq., London, 9th Sept 2002.

Chapter Four: The Development of Non-Linearity in Helix TWTs

4.1 Introduction

Nonlinearity is a phenomenon that exists in all power amplifiers. Intermodulation distortion, which arises as a result of this, can result in severe degradation of the amplifier's performance. Since the nonlinear performance of a quasi-memoryless power amplifier can be determined by its AM/AM and AM/PM transfer curves [1], it can be separated into two types: phase and amplitude nonlinearity.

Amplitude nonlinearity occurs whenever there is a limiting of RF power generation at the operating frequency. This power becomes distributed across discrete frequency values. For a single carrier, regrowth occurs at multiple frequencies of the carrier (as harmonics), for a multicarrier signal regrowth also occurs at frequencies spaced by the difference between the carrier frequencies. Across the complete range of helix pitches, the power transfer characteristics are never completely linear i.e. there is always some degree of curvature from a slope of 45° to 0° (saturation point). Therefore, the helix TWT is never a completely linear device: there is always some generation of harmonics and IM products (for multi-tone signals).

Whenever there is a phase delay in the output RF signal, the spectral regrowth of the output signal is increased. Phase delay has traditionally been known to develop naturally from the deceleration of the beam as RF energy is transferred to the circuit [2]. The relationship between the beam velocity and the resulting phase conversion in the helix will be investigated in Section 4.4.4. However, it was shown in Chapter 3.4 that, for a certain helix pitch, a condition occurs where there is a phase shift transition between positive and negative. At this point, the phase shift is zero. It was also shown in fig 3.26 that the helix pitch for minimum phase lag corresponds roughly to a high intensity of electron beam bunching. The manner in which electrons are formed and captured and decelerated by the RF electric field is fundamental to the overall nonlinear performance of the helix TWT. All of this is covered in Section 4.4. which

uses Applegate diagrams to compare results (simulated from the Large-Signal Model) that correspond to conditions of interest e.g. minimum phase lag and high efficiency. This chapter will first introduce the basic models of nonlinearity in TWTs and SSPAs.

4.2 Modelling Non-Linearity in Power Amplifiers

Spectral regrowth can be modelled using a memoryless, bandpass, nonlinear model. [3] A single-tone amplitude and phase modulated input signal can be expressed as:

$$x(t) = a(t) \cos [2\pi f_c t + \phi(t)] \tag{4.1}$$

where a(t) represents the amplitude modulation

$\phi(t)$ represents the phase modulation

f_c is the carrier frequency of the signal.

When this is fed into a bandpass non-linear device, the instantaneous output voltage y[x(t)] can be represented as a Volterra expansion as in equation (4.2).

$$y[x(t)] = \sum_{n=0}^{\infty} c_n x^n(t) \tag{4.2}$$

The output signal will contain distortion products due to the non-linear processes. They are centered at integer multiples of the carrier frequency f_c. This model only considers the signal content within the system bandwidth i.e. the in-band products. It is assumed that the out-of-band signals are removed by a band-pass filter. Substituting the modulated input signal (4.1) into (4.2), the fundamental component of the output signal [3] is:-

$$f[a(t)] = \sum_{n=1,3,..} c_n a^n(t) \frac{n!}{2^{n-1}\left(\frac{n-1}{2}\right)!\left(\frac{n+1}{2}\right)!} \tag{4.3}$$

The function f [a(t)] represents the AM/AM distortion. The AM/PM characteristic is also a function of the input amplitude a(t). Considering the amplitude-to-phase modulation, the output signal can be expressed [3] as

$$y_o(t) = f[a(t)] \cos(2\pi f_c t + \phi(t) + \theta[a(t)]) \tag{4.4}$$

where $\theta[a(t)]$ is the AM/PM characteristic.

Equation (4.4) provides a basis on which to further represent nonlinear power amplifier models for both the TWTA containing AM/PM conversion and an SSPA without AM/PM conversion. The TWTA representation is obtained from the memoryless Saleh model [4] as follows:

$$f[a(t)] = A_{sat}^{\ 2} \frac{a(t)}{a^2(t) + A_{sat}^{\ 2}}$$

$$\theta[a(t)] = \frac{\pi}{3} \cdot \frac{a^2(t)}{a^2(t) + A_{sat}^2} \tag{4.5}$$

where A_{sat} represents the amplifier's input saturation voltage.

The equivalent AM/AM and AM/PM characteristics for an SSPA [5, 6] can be approximated as:

$$f[a(t)] = \frac{a}{\left[1 + \left(\frac{a}{A_0}\right)^{2p}\right]^{1/2p}}$$

$$\theta[a(t)] = 0 \tag{4.6}$$

Here, A_0 is the maximum output amplitude and the parameter p controls the smoothness of the transition from the AM/AM linear region to the saturation point. Since this project is concerned with the nonlinearity in TWTs, equation 4.5 is of particular interest, because it provides a basic mathematical representation of the nonlinear amplitude and phase of the output signal as a function of drive power. Figure 4.1 illustrates the case when $A_{sat} = 10$ for a TWTA and when $A_0 = 10$ and $p = 1.5$ for a SSPA. The additional parameter with the SSPA model means that more variations in shape are possible. The curves show that power saturation occurs with the TWTA, then for this case, the output power is reduced in overdrive; whereas in the SSPA, no reduction of RF power is modeled. The output phase is shown to grow with input power from where the input amplitude is zero; this growth then becomes greater as the output signal amplitude approaches saturation. The processes that result in power saturation in a helix TWT will now be investigated.

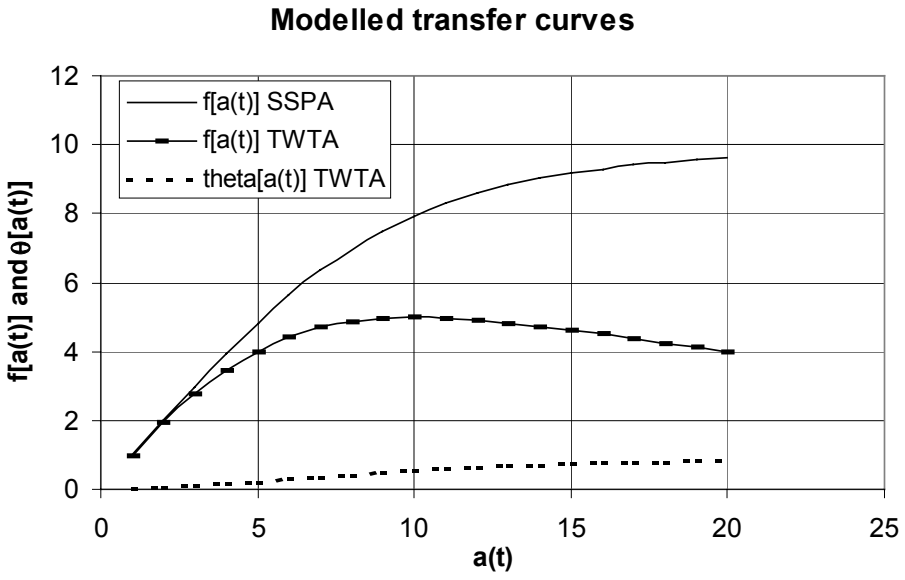

Fig 4.1 Modeled transfer curves for a TWTA and SSPA

4.3 The Processes of Power Saturation

The output RF power becomes saturated due to a limited generation of output RF power at that particular frequency. This limited output RF power must be as a result of the interaction processes between the electron beam and the circuit wave in the tube. Observing the RF power growth in the circuit provides an insight into how saturation arises. It is also necessary to observe the change in behaviour between successive drive levels in order to analyse the development of nonlinearity. This is because the drive power is the only parameter of the AM/AM and AM/PM transfer curves which determine the nonlinear performance. Figure 4.2a shows the RF power versus axial distance for equal increments of drive level.

At Pin = 0 and 2dBm, the output power growth in the tube is linear. AM/AM nonlinearity begins as the input power is increased to 4dBm. This is confirmed in the corresponding AM/AM curve in fig 4.2b. When Pin = 8dBm, the maximum signal growth occurs at the output end of the tube, this is therefore the point of maximum output power or tube efficiency. For higher drive levels, the RF signal does actually reach that maximum point but at positions nearer to the tube input, thereafter the amplitude drops. This reduction of power in beyond saturation is when some of the RF power is being transferred back into the beam, thus reaccelerating the electrons.

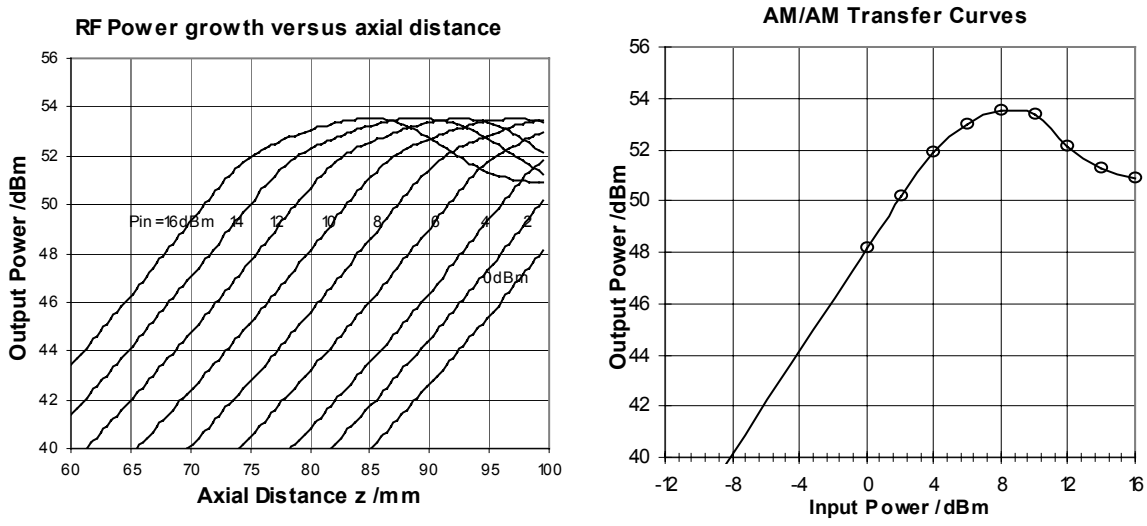

(a) (b)

Fig. 4.2 (a) RF power growth as a function of axial distance for different drive levels in a uniform helix and (b) the corresponding AM/AM curve.

Power saturation cannot be avoided, since the tube efficiency is limited. A practical design must therefore be aimed to produce characteristics resembling those of a hard power limiter, as in fig 4.3b. In order to achieve this, the RF power growth in the slow-wave structure would have to be linear with axial distance up to saturation (point D in fig 4.3a). Thereafter, (for higher drive powers,) every power growth curve must also reach its maximum at the tube output.

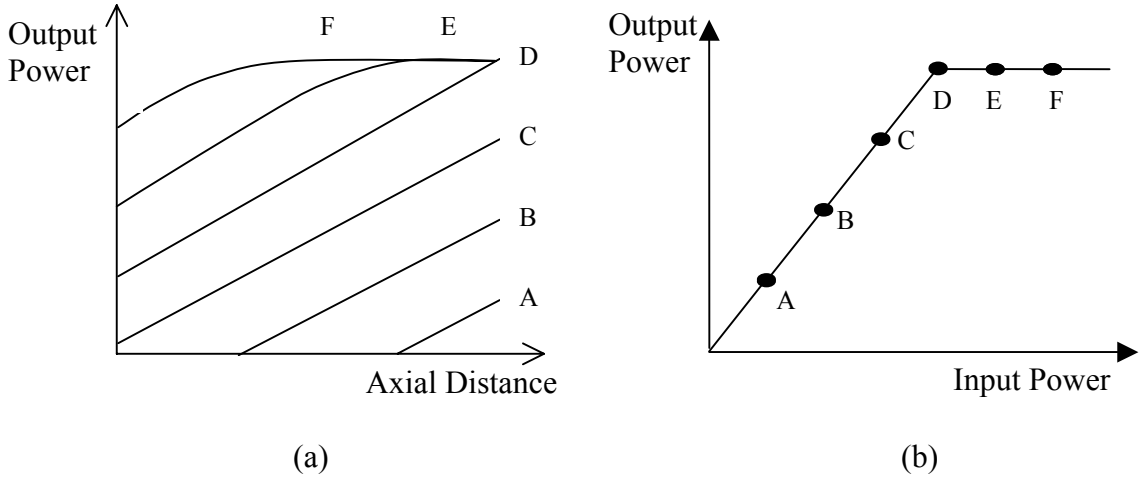

Fig. 4.3 (a) RF power growth versus axial distance for different drive levels corresponding to (b) the AM/AM curve of a hard power limiter.

A hard power limiter may be theoretically possible in a helix TWT. But in practice, there always seems to be some curvature towards saturation, when the output power curves are viewed across the whole range of helix pitches (e.g. fig 3.26 in Chapter 3.4). Even if the TWT's characteristics were hard limited, the output signal would still contain IM products, since saturation itself involves nonlinear signal growth in the tube, as shown by the curves E and F in fig 4.3a.

The results of power saturation that have been shown so far, is the result of the complex interaction processes which become limited in the tube. Electron beam analysis provides a means of in which to understand the physical processes that cause nonlinear signal amplification. The significance of electron beam bunching with the operation of a TWT will now be discussed.

4.4 Nonlinear Processes in the Electron Beam Bunching

When the amplifier is driven beyond the small-signal levels towards the non-linear region, the RF electric fields imposed on the electron beam causes the electron density to become non-sinusoidal as a function of axial distance [7]. The initial indication of non-linearity is shifting of phase which, from the LSM results (e.g. fig 3.11), is shown to occur at very small-signal levels. This phase shift is probably related to the net decrease in the electron velocities as RF energy is continuously being transferred to the helix.

When the amplifier is driven towards power saturation, electrons become trapped by the circuit field. This results in many of these electrons to be decelerated while the remaining electrons become reaccelerated. Regions of high and low space charge density regions exist, where the effects of space-charge are significant. At the tube output, the dynamic range of electron velocities increases with drive level. Spectral spreading (where the output power spreads across the frequency spectrum) also results. This section will now discuss how electron bunches are formed by the RF electric fields before they become trapped, which is significant to the development of nonlinearity in a helix TWT.

4.4.1 Formation of Electron Bunches

The sinusoidal input RF wave on the helix produces regions of alternating high and low electron densities in the beam as shown in fig 4.4. When the electrons are influenced by a positive axial electric field, this repulsive force acting against their direction of motion, causing them to slow down. When E_z is zero, and where dE_z/dz is a positive maximum, the decelerating field acting on the electrons meet with and push against the accelerating field, causing bunch compression. In this high electron density region, the space-charge forces repelling the electrons are at their greatest. This also corresponds to an approximately linear phase response [7]. A rarefaction occurs in the adjacent regions (where $E_z = 0$ and dE_z/dz is a negative maximum) due to the absence of electrons.

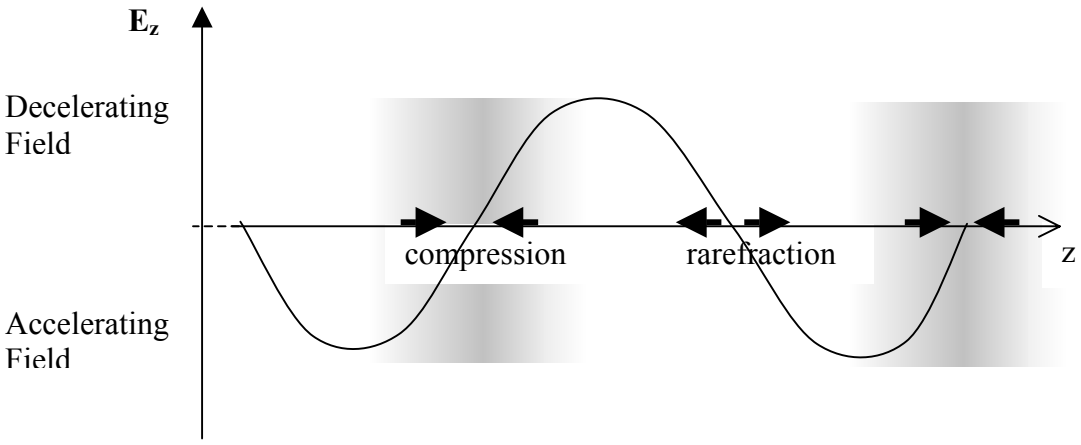

Fig 4.4 Axial electric field as a function of axial distance z, where regions of electron compression and rarefaction are formed

The bunching profile of a system is determined by the space-charge forces within the bunch and the velocity distribution of the electrons. Space-charge is caused by an underlying physical force in the system whose magnitude depends on the distance between the electrons. The velocity distribution of the electrons however, is influenced by the gradient of the electromagnetic field across the bunch. It is often difficult for an electron bunch to be sustained and it may therefore oscillate if allowed to drift towards the output end of the tube.

To achieve a tighter bunch, it is always necessary to keep the electrons in the positive slope of the electric field, so that the head of the bunch will slow down more than the tail of the bunch. This results in narrower bunches and a substantial momentum gradient along each bunch - sustaining the length of the bunch for a long distance [7]. If the bunch lies in the negative slope of the decelerating field, the particles at the head of the bunch will tend to travel faster than those at the tail of the bunch, causing the bunch to spread out. But this allows the bunch to spend a longer time in the positive E_z region, so that the bunch loses more energy to the electromagnetic field [7].

If the phase velocity of the RF wave is reduced, a trapped electron bunch moves into the decelerating phase. This reduces the beam velocity, effectively extracting more RF power from the beam. When this happens, the centre of the bunch tends to move backwards with respect to the maximum decelerating electric field.

If the amplifier is driven beyond power saturation, the electron bunches move from the retarding field into the accelerating field. The average electron velocity is then increased towards the output end of the tube, indicating energy transfer from the helix back onto the beam. Design of the slow-wave structure can prevent this by maintaining the electrons in the decelerating phase for as long as possible. The two fundamental processes that determine the overall performance of a TWT are the bunching of the beam and the deceleration of the bunch. The TWT must therefore be designed to be an efficient beam "buncher" as well as an efficient beam decelerator (RF conversion); design of practical helix TWTs will be covered in Chapter 6. The next discussion will compare the beam bunching between two helix designs in order to determine an optimum bunch formation.

4.4.2 Analysis of Electron Beam Bunching

For a highly efficient TWT design, the formation of a trapped electron bunch must be such that a maximum amount of RF power can be extracted from it. The exact form of such a bunch is not fully known. This section will therefore discuss the factors which determine this optimum bunch formation by comparing two sets of results from uniform tubes with different pitches: 0.660 and 0.664mm and how these relate to the nonlinear performance of the TWT. The tube-data for this analysis is from that determined in Chapter 6.2.2,

Figure 4.5a shows the normalised RF beam current for a helix pitch of 0.660mm with a range of drive levels from –24dBm to –3dBm. It is shown that the input power does not affect the peak current; the curves of current towards saturation also appear similar. The differences lie in the magnitude of the RF current after the peak. When these results are compared with those of a tube with a slightly increased helix pitch (by 0.004mm) to 0.664mm, the current peaks are slightly increased (fig. 4.5b).

However, this observation is insignificant when the behaviour of the current curves beyond their maximum points is compared. When p = 0.660mm, a secondary current peak is more likely to occur, as shown for the drive levels of –10dBm and –3dBm. This corresponds to a second region of electron bunching nearer the end of the tube.

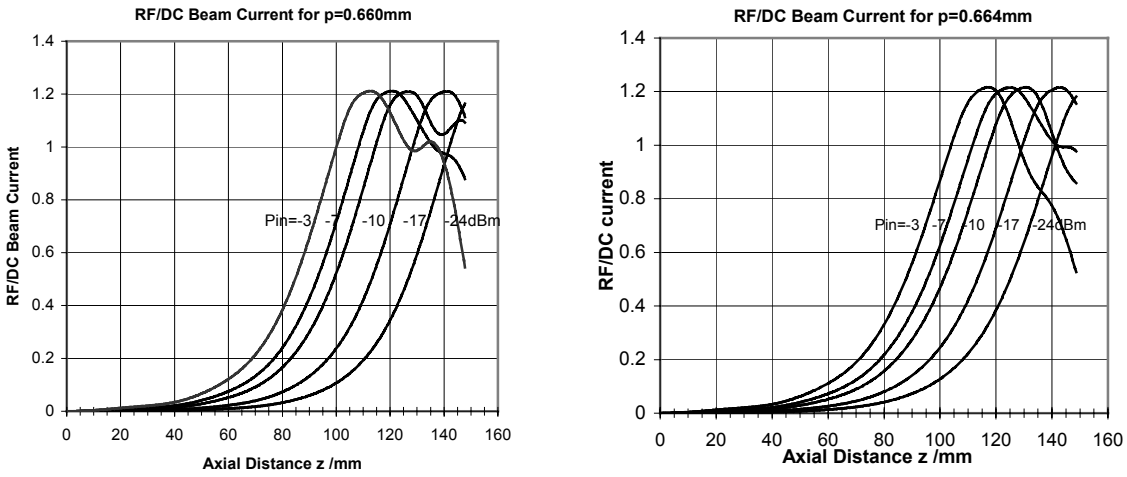

(a) (b)

Fig 4.5 RF beam current for pitch = (a) 0.660mm and (b) 0.664mm as a function of axial distance

The Applegate diagrams for the same cases with drive levels of –7 and –3dBm are shown in fig. 4.6 for p=0.660mm and fig 4.7 for p=0.664mm. The Applegate diagram gives a clear representation of the bunching profile of a system. By plotting the electron phases relative to the circuit phase, it reveals the velocity distribution of the electrons, which is strongly influenced by the space charge spreading in the bunch. Both plots show that the design that closely corresponds to maximum RF current or maximum bunching intensity is well sustained, particularly in fig. 4.6b. When p=0.660mm at Pin=-7dBm, the electron beam phase increases until maximum bunching occurs at around z=100mm. Thereafter for a further 35mm, the space-charge forces which forces the electrons apart are well controlled by the dominance of the RF field. The electrons therefore remain bunched and their total average velocity is reduced as energy is transferred to the circuit wave. When p=0.660mm (Pin=-3dBm) however, the electrons gain energy back from the circuit beyond z=135mm

(power saturation) and are thus re-accelerated. This behaviour causes a sharp drop in RF current induction in the beam (in fig 4.5a). But at –3dBm, the bunching does remain favourably tighter over a longer axial distance when p=0.660mm, compared to p=0.664mm. A more optimum bunch is thus formed continuously along the TWT. This is indicated as a greater area under the RF current curve (fig 4.5a). This continuous bunch formation allows more RF power to be extracted from the beam over a longer axial distance. The result of this is greater RF output power in the helix.

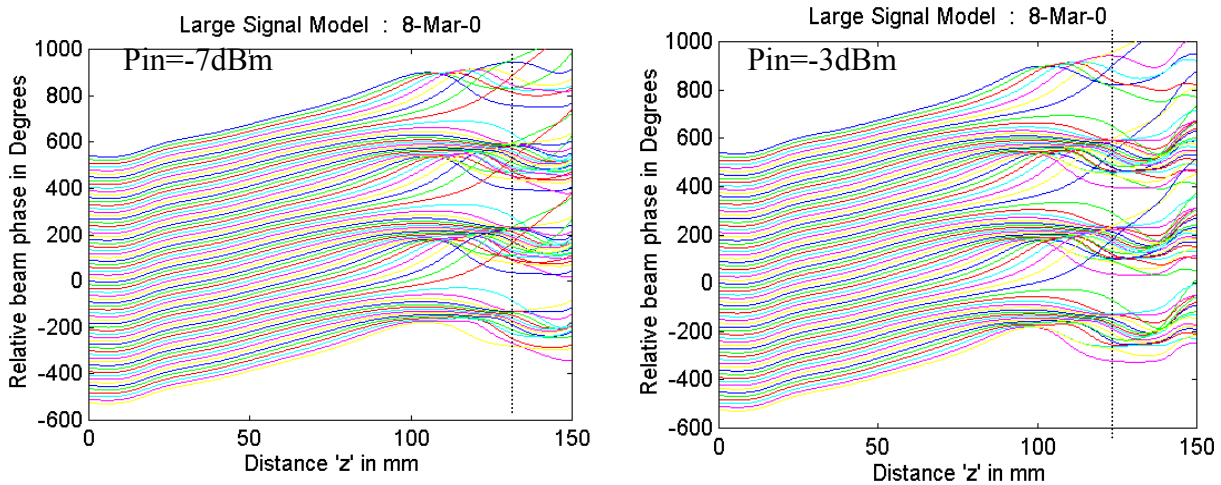

(a) (b)

Fig 4.6 Applegate diagrams for a pitch = 0.660mm for drive levels of (a) -7 and (b)–3 dBm. (The dotted lines indicate where the output power is maximum.)

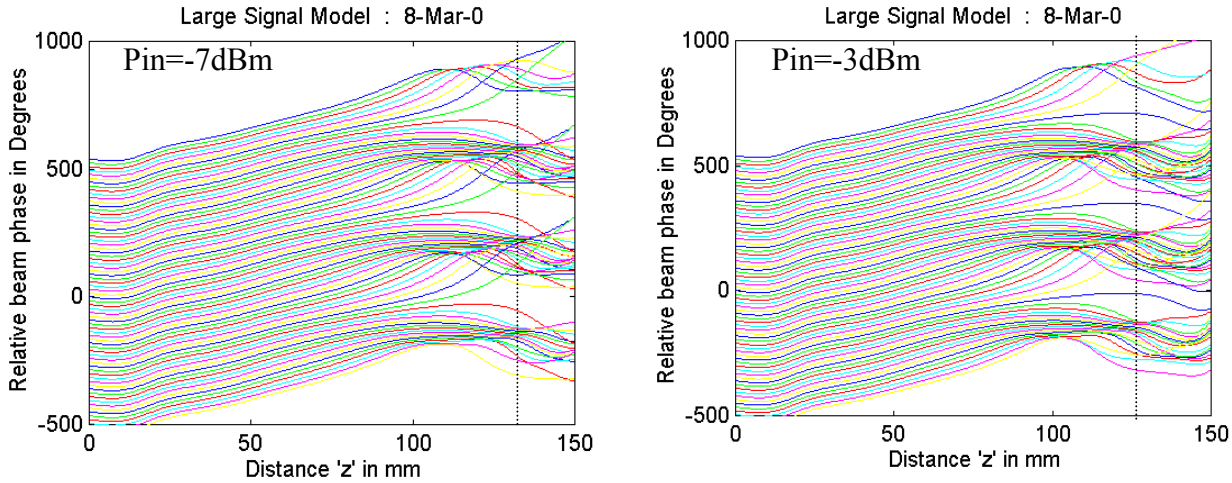

(a) (b)

Fig 4.7 Applegate diagrams for a pitch = 0.664mm for drive levels of (a)–7 and (b)–3 dBm. (The dotted lines indicate where the output power is maximum.)

The corresponding AM/AM and AM/PM transfer curves are shown in figs. 4.8a and 4.8b respectively. The helix with a pitch of 0.664mm generates greater RF output power than p=0.66mm when driven up to 12dB beyond saturation; there is therefore reduced dynamic variation of the output signal amplitude, which is favourable in addition to a better nonlinear performance (for a small AM/AM curvature) [8]. In the bunching analysis however, we have been focusing on an input power of -3dBm, where a 0.66mm pitch produces the greater output power. The AM/PM curves (in fig 4.8b) show that, the phase shift in the linear power region is as significant as the nonlinear power region. The next section will further investigate the development of phase nonlinearity in the tube.

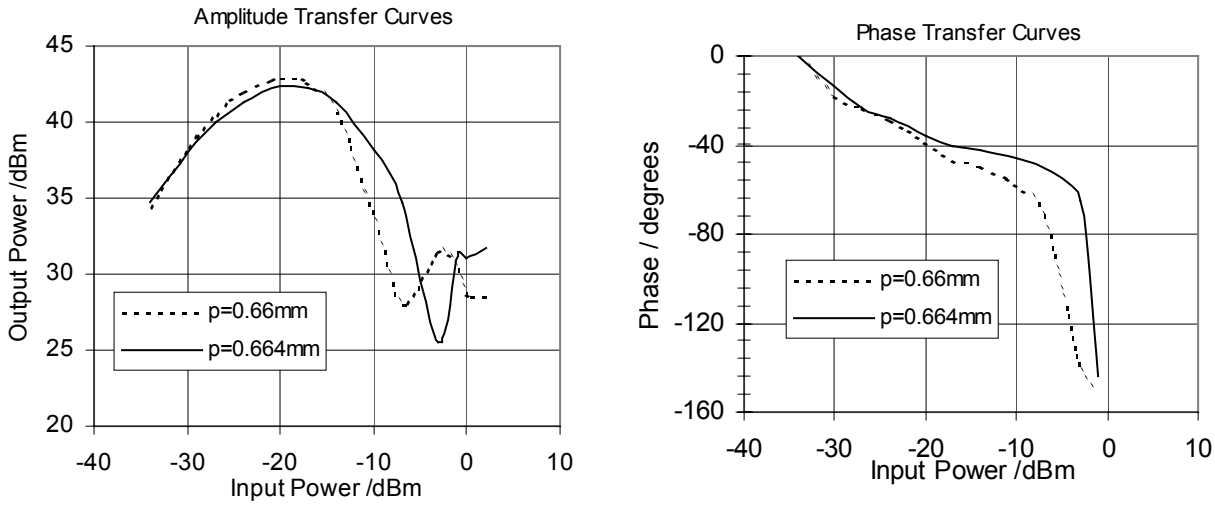

(a) (b)

Fig 4.8 (a)AM/AM and (b)AM/PM transfer curves for pitch values of 0.66mm and 0.664 mm

4.4.3 Analysis of Phase Nonlinearity in the Electron Beam

As mentioned in Section 4.3, in order to determine the nonlinear performance of a power amplifier it is necessary to analyse the change in behaviour between consecutive drive powers. For example, there is a very large phase lag between –7 and –3dBm for p=0.660mm. The difference in the relative beam phase of the bunches between these two drive levels (fig. 4.6 a and b) is shown to be greater than when the pitch is 0.664mm. This section shows how it is possible to represent phase nonlinearity in the beam by observing the change in the behaviour of the bunching as the drive level is increased.

Figure 4.9 shows the amplitude and phase transfer curves of an 11.7GHz uniform TWT with 6KV beam voltage and tube data as given in table 3.1, harmonic interaction is included however and the tube is 140mm long. The figure shows gain compression from around –14dBm of input drive. This is also where the phase conversion becomes the greatest. A way of representing the phase nonlinearity in the beam is to subtract the data of the Applegate diagram of one drive level from that of another drive level. A program has therefore been written to subtract the phases of the electrons at each axial position between any two specified drive levels. This routine is repeated for all positions along the TWT. A typical result is shown in fig. 4.10a, effectively revealing the phase nonlinearity of the electrons in the beam between the two drive levels of –24 and –20dBm. The curves in the plot are shown to spread asymmetrically; at the tube output, the phase lag is shown to spread from –8 to 16°, thus there is a net shift of phase of the electrons, which directly results in AM/PM conversion.

Between higher RF power levels of –14 and –10dBm, where there is some AM/AM conversion (in fig. 4.9), the corresponding change in the electron phases is shown to be much greater (in fig. 4.10b). Here the curves become distorted beyond 125mm and the maximum phase change of one sample electron becomes 110°. On the verge of power saturation (Pin = -7 to -4dBm; fig 4.10c), the curves in the chart show greater distortion where there is no order of their paths beyond 125mm.

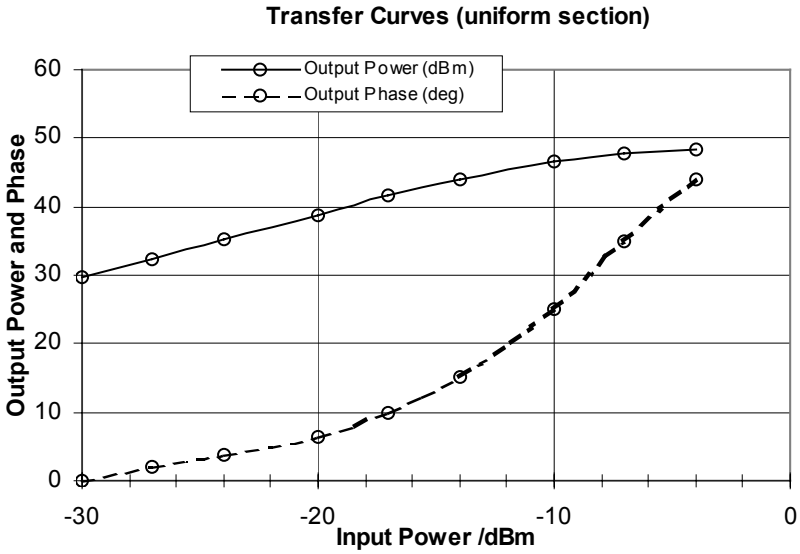

Fig 4.9 AM/AM and AM/PM transfer curves for a uniform Ku-band TWT with 800W of DC beam power.

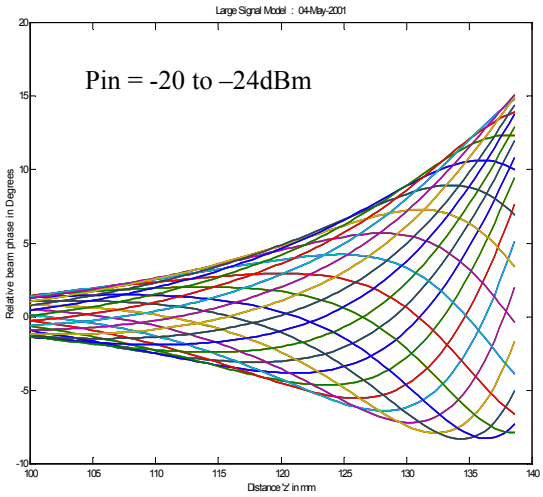

(a)

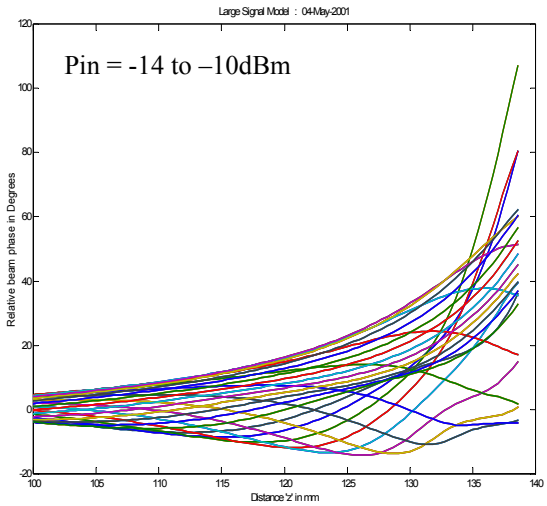

(b)

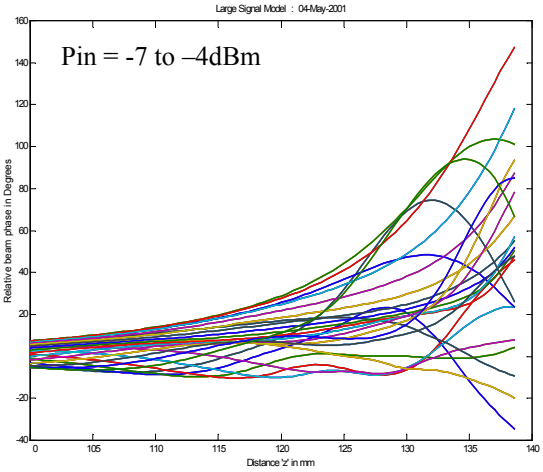

(c)

Fig 4.10 Plots showing the change of electron phases during (a) Pin = (a) -20 to –24dBm, (b) –14 to –10dBm, (c) –7 to –4dBm versus axial distance

The next aim was to determine whether the phase change of the sample electrons (as revealed in figs 4.10a-c) is wholly responsible for the phase conversion in the RF output as given in fig. 4.9. The answer to this was found by plotting the mean value of the phase change of all sample electrons at the tube output as a function of the phase lag. The former was computed by integrating the phase change at the tube output for all of the sample electrons N_s (which is normally 24 discs) between the two drive levels and dividing this by N. The results are given in fig. 4.11, where three of the points on the "6KV with harmonics" curve in fig 4.11a correspond to figs. 4.10a-c. The other curves correspond to the results of similar simulations, but with the beam voltages set to 6.0 and 6.1KV without any harmonic interaction.

This proportionality between the RF phase shift and the mean electron phase shift is not shown to be continuous for all RF amplitudes. This is because the change in beam phase continues to grow between higher drive levels (as shown in figs 4.10), whereas the corresponding output RF phase shift in the circuit (in fig 4.9) reaches a maximum before saturation is reached. This behaviour is shown in fig 4.11; the beam phase distortion is ever increasing as the drive level is increased, while the shift in RF phase becomes constant or is reduced. Based on this observation, it could be suggested that the nonlinearity within the beam phase results in harmonics and other forms of spectral regrowth, while the phase lag of the RF fundamental signal is partially responsible for the generation of spurious spectral noise. Thus this increased distortion within the electron beam also contributes to AM/AM distortion as power saturation is approached.

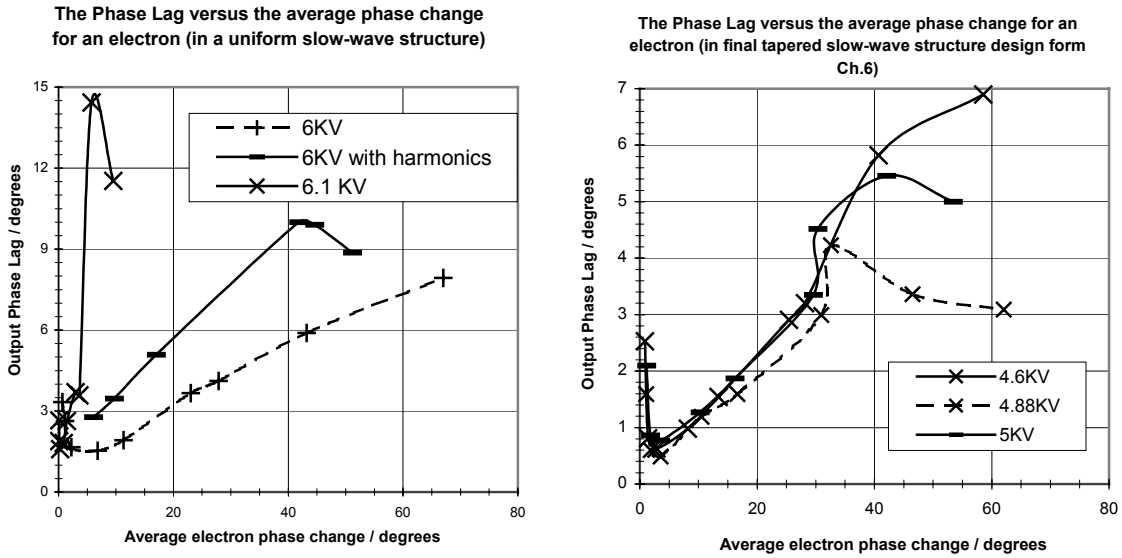

(a) (b)

Fig. 4.11 The phase lag versus the total change in the electron phases at the tube output between specified drive levels, simulated with (a) uniform and (b) tapered helices.

4.4.4 The Relationship between the Phase Conversion and the Beam Velocity

Results from Chapter 3 showed that, even though a zero phase lag condition exists, the phase conversion is generally greater when there is more output RF power. In order to supply more power to the slow-wave circuit, a greater amount of RF power must be extracted from the beam (from the basic law of energy conservation), thus effectively reducing the beam velocity. This section will investigate the relationship between the phase conversion K_p and the beam velocity.

As the velocity of an electron in the beam is reduced, the average time it takes to travel through the tube is increased. This average time taken (or the time delay) Δt for an electron travelling a distance L along the axial length of the tube can be represented as an integral of the beam velocity u(z), as in equation (4.7)

$$\Delta t = \int_0^L \frac{dz}{u(z)} \tag{4.7}$$

The value of Δt was determined by plotting 1/u(z) as a function of axial distance z, and the total area under the 1/u(z) curve represents Δt, as in fig. 4.12. This was simulated by LSM which plots the beam velocity (normalised to the circuit wave velocity) versus z. A trapezoidal approximation was incorporated in the LSM program to calculate $\Sigma[u(z)]^{-1}$ along the length L of the tube in order to compute Δt. Note that u_0 is the velocity of the beam when entering the helix circuit (i.e. the initial beam velocity).

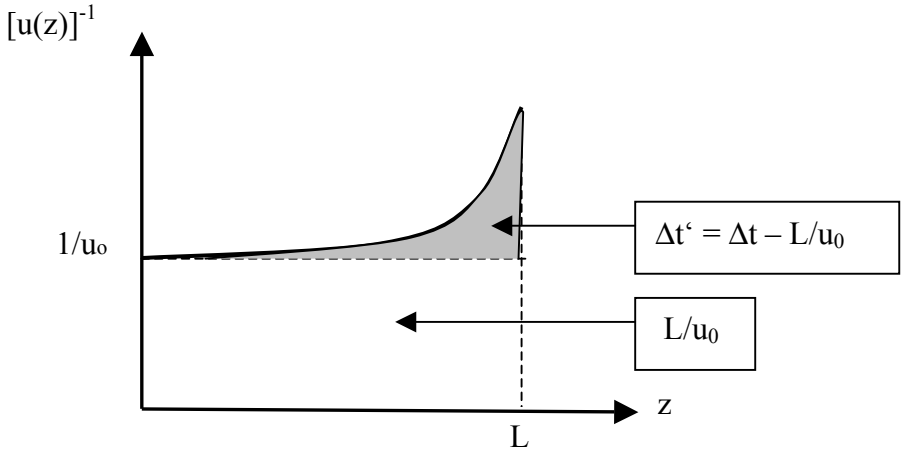

Fig 4.12 Reciprocal of the beam velocity as a function of axial distance z

Figure 4.13 shows the time delay as represented by Δt' in fig.4.12 plotted as a function of phase conversion K_p; this is given for the tube-type in table 3.1, but with a range of beam voltages (P_{DC}=800W). When the beam velocity is constant Δt' is zero, which should not occur in a helix TWT even at very small-signal levels. At these small-signal levels, the graph shows that there is more than 2×10^{-8} seconds of time delay in the beam for the range of beam voltages. It is also shown that the phase conversion does not become less than 0.5°/dB, as expected. The time delay Δt' grows roughly proportional with K_p as the drive power is increased; the rate of this increase depends on the beam voltage. In some cases, the curves in the figure actually bend back. This is where there is a decline in the output RF phase conversion even though the tube is driven harder and the beam velocity is continuing to decrease at the output. Conditions do arise therefore, where the electrons in the beam continue to decelerate, increasing the time delay of the beam and thus greater output RF power, while the phase conversion is reduced.

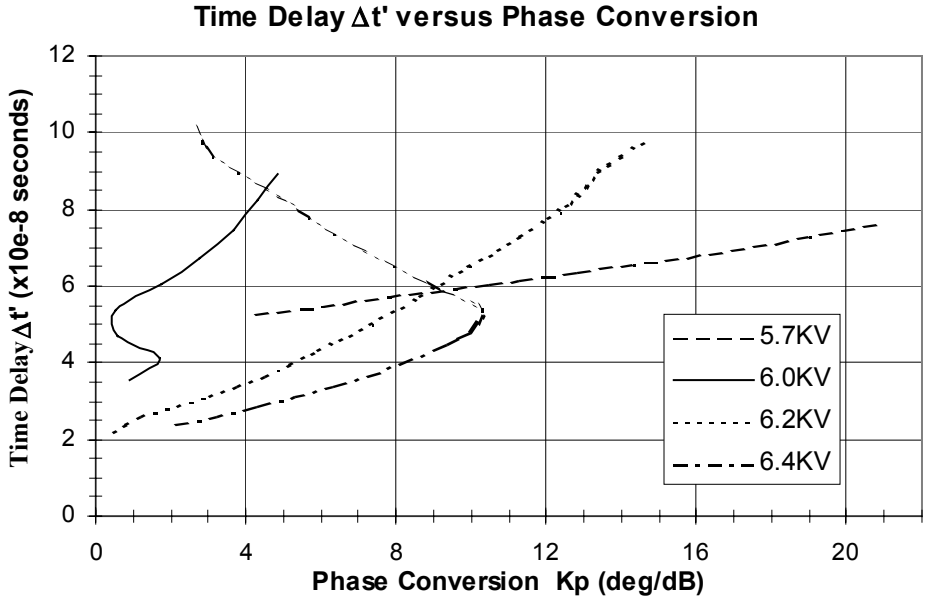

Fig 4.13 The time delay of beam Δt' versus the phase conversion K_p for a range of beam voltages

From these results, a relationship between the phase conversion and the beam velocity can be deduced, as written as equation 4.8. The phase conversion depends on both the angular frequency ω and the integral of 1/u(z) as shown, both the slope and the constant term depends on the beam parameters. The unknown factors in equation 4.8 are due to additional interaction processes that have not been considered in the model, for instance, the bunching caused by the phase difference between the bunch and the field. How this should be modelled and incorporated into equation 4.8 is unknown.

$$K_p \propto \omega \int_0^L \frac{dz}{u(z)} - \text{constant} \tag{4.8}$$

So far, we have observed phase nonlinearity within the beam which then emerges in the RF signal from the electromagnetic interaction. Generally, it has been found that his phase nonlinearity grows as the beam slows down or as power is extracted from the beam. Certain conditions do exist however when the beam decelerates while the phase does not change; this will be explored later in Section 4.4.6.

4.4.5 Effect of the Desirable Conditions on the Electron Beam Bunching

Chapter 3.3.1 demonstrated on how, by varying the pitch of a uniform helix, desirable conditions could be achieved. The conditions of particular interest are maximum efficiency, minimum intermodulation distortion and minimum phase lag. Other conditions for the interest of design (for Chapter 6) include maximum small-signal gain and maximum RF current. The helix pitches are given in fig 4.14 for the particular drive level where the optimum condition lies, since these conditions vary with drive level in the AM/AM nonlinear region. The same uniform tube design was used as that in table 3.1 (Chapter 3.2), with the length L of the tube set to 100mm. These conditions differ from those in fig 3.27 (6KV) where L=60mm due to the 40mm of longer length. Applegate diagrams have been produced for each condition as a means of understanding the behaviour of the electron bunches and what to aim for in the design stage.

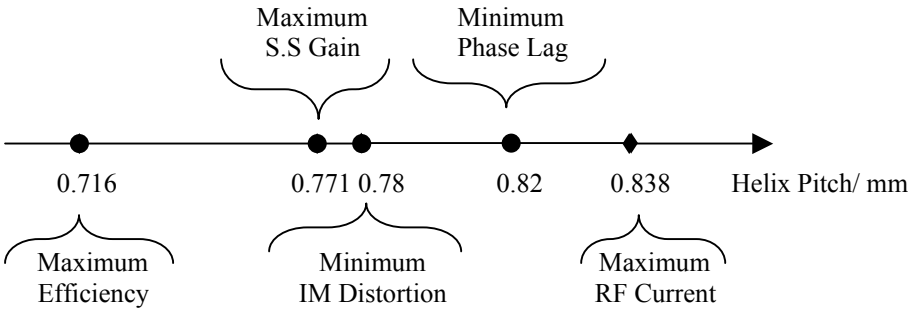

Fig 4.14 Helix pitches corresponding to each of the optimum conditions for a tube length of 100mm.

Optimum Conversion Efficiency

It is of prime interest to understand the physical interaction processes which result in optimum power transfer from the beam to the helix. The Applegate diagram for a helix pitch corresponding to the condition of maximum conversion efficiency is shown in fig. 4.15. Here, the drive power is well in overdrive (Pin=20dBm), because this gives more information on the bunching behaviour after a lot of beam-wave interaction has occurred. Similar behaviour is observed for any drive level beyond power saturation, because the peak efficiency becomes less dependant on the pitch in overdrive as shown from the results in Chapter 3.4.1. The Applegate diagram shows that for maximum transfer of RF beam-wave power, the electrons are captured by the circuit wave in an orderly and separate manner. Virtually all electrons become trapped and are strongly reflected in the potential well. This occurs continuously over a long axial distance (from 65mm to the tube output). Once trapped, the electron decelerates – reducing its relative phase by 200°. The velocity of the electron is then further reduced, kept constant or is increased (re-reflected within the potential well).

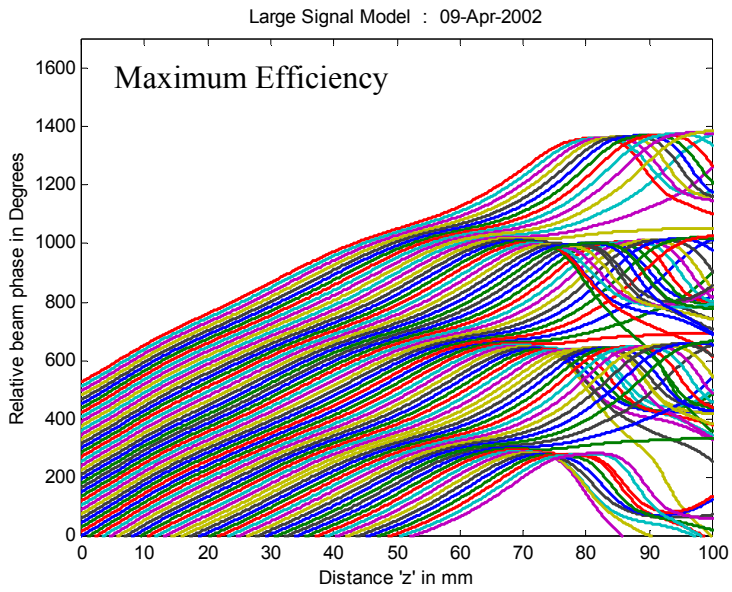

Fig 4.15 Applegate diagram for the maximum efficiency condition (pitch p= 0.716mm)

Maximum Small-Signal Gain

The results in Chapter 3.4.1 revealed that at small-signal levels, the helix pitch corresponding to optimum RF current and power coincides with that of maximum gain. Only when the signal amplitude becomes large and non-linear to the input amplitude do the design conditions for optimum efficiency and optimum RF current become separated. Therefore the maximum small-signal gain condition should be achieved in design when the input RF signal has low amplitude.

Figure 4.16 shows the Applegate diagram for maximum small-signal gain. This is a condition which is only useful when the RF signal has a low amplitude i.e. well before bunching occurs. Therefore, the analysis of the bunching at this condition is not very significant. Before bunching occurs, maximum gain is achieved when the beam phase (relative to the RF forward wave phase) increases by 5° per mm along the tube.

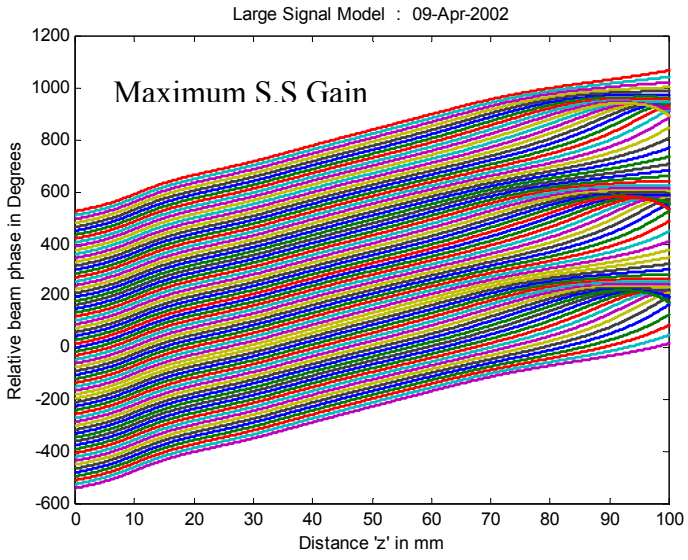

Fig 4.16 Applegate diagram for the maximum small-signal gain condition (p= 0.771mm)

Minimum Intermodulation Distortion

The condition of minimum IM distortion is specified by IMAL. Both the AM/AM and AM/PM transfer curves determine the level of IM distortion. This condition therefore requires the combination of minimum AM/AM conversion i.e. the shape closest to that of a hard-power limiter [8] and minimum AM/PM conversion. The pitch corresponding to this overall linearity condition is 0.78mm, which lies between that of maximum gain and minimum phase lag.

The Applegate diagram (in fig. 4.17) shows that most electrons become trapped into a tight bunch. All of these captured electrons are then decelerated. However, most of these electrons which are not captured continue to be accelerated, which reduces the conversion efficiency of the TWT.

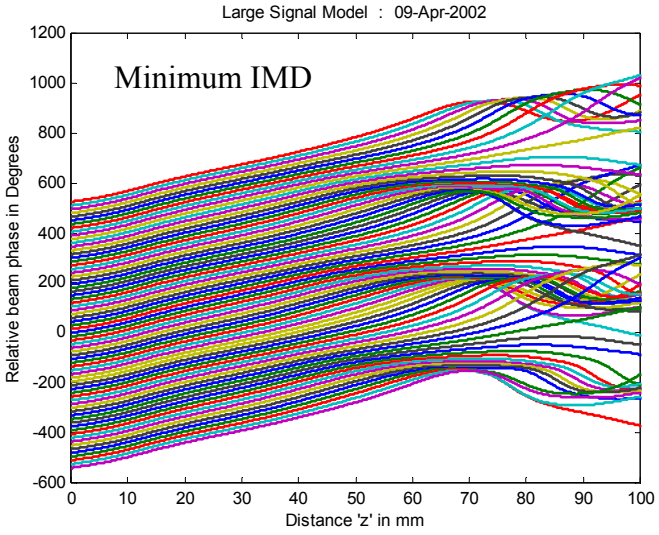

Fig 4.17 Applegate diagram for the minimum intermodulation distortion condition (p= 0.82mm)

Minimum Phase Lag (see Section 4.4.6)

Maximum RF Beam Current

If the helix pitch is increased to a condition where the RF current induction in the beam is maximum (at p=0.838mm), the bunch compression is at its most intense. When designing an efficient helix TWT, it is desirable to maximise the bunch compression prior to extracting maximum power from the beam (further discussed in Chapter 6.2).

The Applegate diagram (fig. 4.18) shows the curves to converge to produce maximum overlapping, thus the most intense bunch compression. Since the pitch values for this condition is the greatest compared to other conditions discussed in this section, the formation of the bunch is gradual and there is a reduced velocity spread of the electrons.

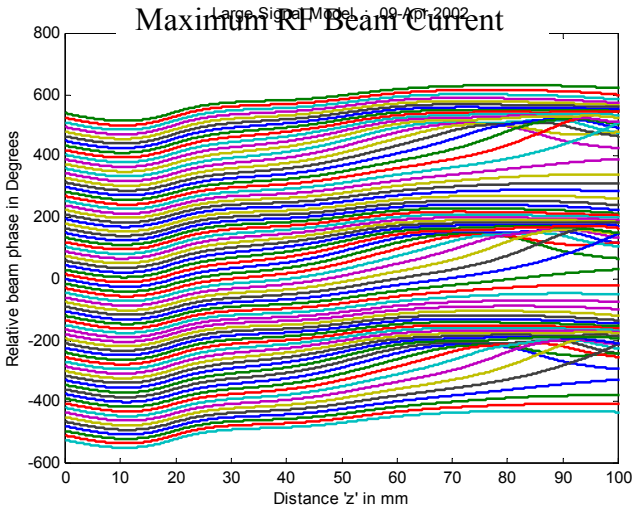

Fig 4.18 Applegate diagram for the maximum RF beam current condition (p= 0.838mm)

4.4.6 Analysis of the Minimum Phase Lag Condition (Tube Length = 60mm)

The results in Chapter 3.4.1 uniquely revealed that for a given helix pitch, the phase growth from small-signal levels to saturation falls to zero and actually reverses sign at this point. For drive levels up to saturation, the results show that this zero condition is also independent to drive level. This is a condition which is previously undiscovered in helix TWTs and could be of potential significance for a design for high linearly, for a helix TWT without any phase conversion would be highly desirable product. The growth of phase versus input power is shown in fig. 4.19 for a range of pitch values. The chosen pitch (p=0.8397mm) for minimum phase shift is indicated as the bold curve, which undulates around the 0° phase shift for a drive level of less than 25dBm. Note that the pitch value for this condition is for a 60mm long tube (as in fig 3.27b in Chapter 3.4), which differs to that of a 100mm long tube (as in fig 4.14).

The corresponding output characteristics (AM/AM, AM/PM, efficiency and gain) are given in fig. 4.20. Power saturation occurs at Pin=28dBm, where the tube efficiency is 9% and the output phase shift is 0.9° (fig. 4.20). If the TWT were driven at saturation, a slightly lower pitch of 0.8374mm would produce zero output phase shift. However, since the dynamic drive level of the signal is centered at levels well backed-off from saturation (e.g. Pin=17dBm), a pitch = 0.8397mm gives the optimum phase condition. The results reveal that for p=0.8397mm, the phase shift is independent to drive levels from small signal levels up to 1dB of output backoff. This independence of phase shift to the dynamic signal variation is an additional desirable feature of this condition.

The Applegate diagrams for Pin=28dBm and 32dBm are shown in figs. 4.21a and b respectively. The output phase in fig.4.21a is 0.9°, while in fig. 4.21b the phase shift is 4.6° since this is driven 4dB into overdrive. The bunching is observed to be tight and very consistent along the axial distance, in fact the bunching is better defined throughout the output region than the condition for maximum bunch intensity (maximum RF current). This is therefore the optimum condition for bunch formation and consistency.

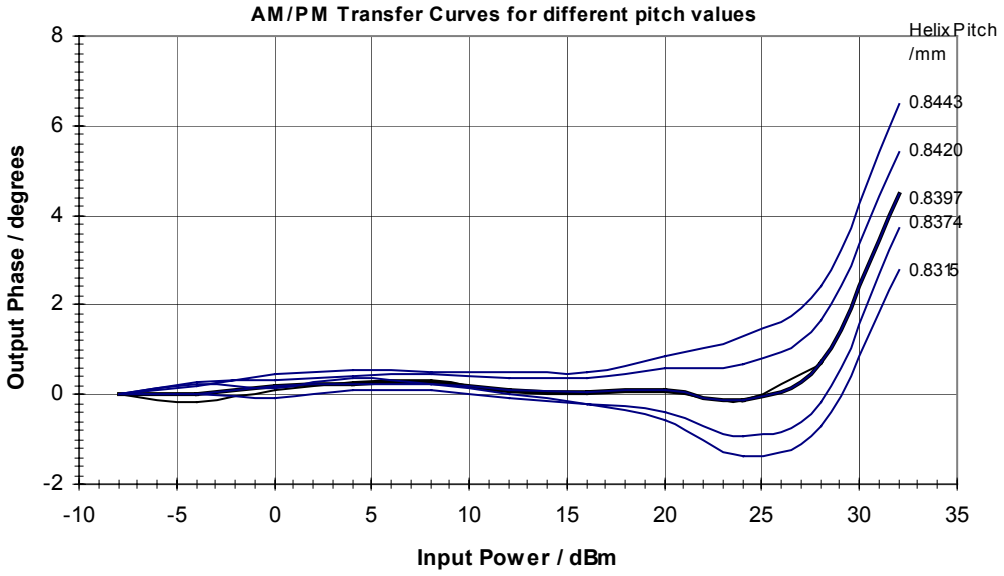

Fig 4.19 Output phase for different pitches where the minimum phase lag is minimum (L=60mm).

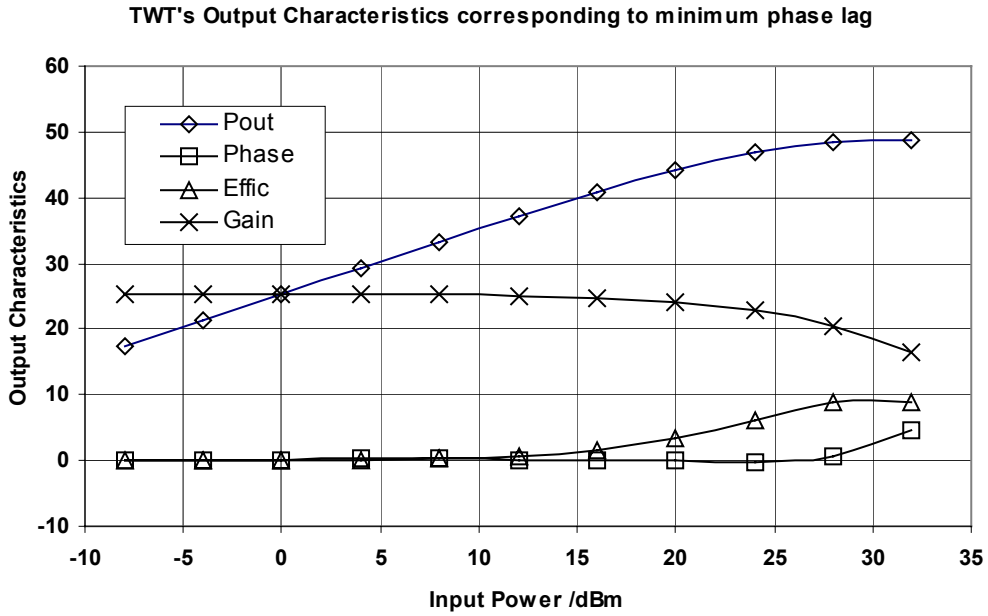

Fig 4.20 TWT Output Characteristics for the minimum phase lag condition (p=0.8397mm)

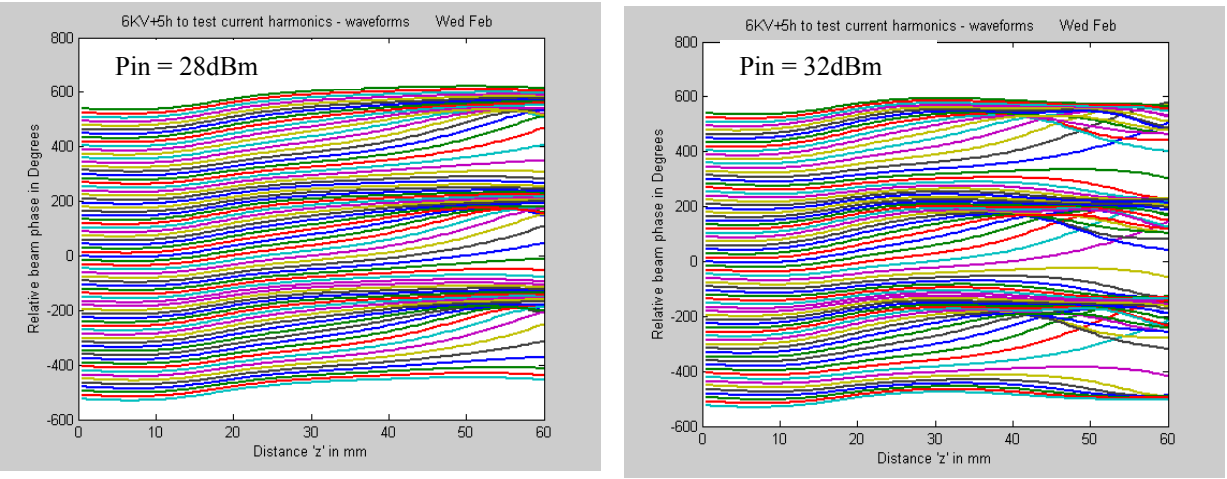

(a) (b)

Fig 4.21 Applegate diagram for the minimum phase lag condition (p= 0.8397mm) when Pin = (a) 28 and (b) 32dBm.

4.5 Conclusions

Travelling-wave tubes are inherently nonlinear devices, since the output power will always eventually saturate (producing AM/AM conversion), AM/PM conversion normally occurs as well. Both of these result in the generation of spectral distortion (i.e. harmonics and intermodulation products) in the output signal when the tube is driven hard enough. The next chapter (Chapter 5) will cover the intrinsic relationship between harmonics and intermodulation distortion.

The key to developing a design strategy for a highly linear and efficient helix TWT is to understand what causes nonlinearity to arise in the tube. This Chapter has addressed this issue by relating the amplitude and phase nonlinearity with the interaction processes in the beam. The Applegate diagram provided the best means by which to observe and understand the behaviour of the electrons and their interaction with the RF circuit field.

The bunching in the beam has been compared between two tubes with different helix pitches and different transfer curves. This has given an initial insight into how nonlinear behaviour and bunching are related. New ways of representing the development of phase nonlinearity throughout the beam have been accomplished by plotting the change in phases of the electrons. These figures were then used to show a strong relationship between the average phase change of an electron and the phase conversion. The aim of TWT design for high phase linearity, therefore, is to maintain the phase of the electrons across the dynamic signal range.

The condition of zero phase-lag has been investigated in this chapter; such a design actually gives over 40dBm of output RF power. This is because the bunch is very tight over a long axial distance of the tube and there is some energy extraction from the bunch resulting in net reduction of beam velocity. A decelerated bunch, therefore, does not necessarily result in phase shift; it is the dynamic variation of the electron velocities at the tube output.

Bunching profiles for other desirable conditions have been investigated. For example, the bunching profile for maximum efficiency revealed the maximum electron oscillation within a potential well. This formation corresponds to high phase conversion. A helix design is therefore required which achieves minimum phase conversion whilst decelerating all of the electrons without causing them to oscillate.

References

[1] R. G. Carter, W. Bosch, V. Srivastava and G. Gatti, “Computer Simulation of Intermodulation Distortion in Broad-Band Multi-Carrier Travelling Wave Tube Amplifiers”, Proc. Conf. Displays and Vacuum Electronics, Garmisch-Partenkirchen, Germany, April 29-30, 1998.

[2] A. S. Gilmour, Jr., “Principles of Microwave Tubes”, Artech House Inc., Norwood MA, USA, 1994.

[3] V. Borich, Je-Hong Jong, J. East and W. E. Stark, "Nonlinear Effects of Power Amplification on Multicarrier Spread Spectrum Systems", IEEE MTT-S International Symposium Digest, Vol. 1, 323-326, 1998.

[4] A. A. M. Seleh, "Frequency-Independent and Frequency-Dependent Non-Linear Models of TWT Amplifiers", IEEE Trans. Commun., Vol. COM-29, No. 11, pp. 1715-1720, Nov. 1981.

[5] C. Rapp, "Effects of HPA-nonlinearity on 4-DPSK-OFDM-Signal for a Digital Sound Broadcasting System, Proc. 2nd European Conf. Satellite Communications, Liege, Belgium, vol. ESA-SP-332, pp179-184, Oct. 22-24, 1991.

[6] E. Bogenfeld, R. Valentin, K. Metzger and W. Sauer-Greff, "Influence on Nonlinear HPA on Trellis-Coded OFDM for Terrestrial Broadcasting of Digital HDTV", ICC'93, pp. 1433-1438.

[7] S. A. Naqvi, J. A. Nation, L. Schachter and Q. Wang, "High-Efficiency TWT Design using Traveling-Wave Bunch Compression", IEEE on Plasma Science, Vol. 26, No. 3, June 1998.

[8] R. O. Jenkins and R. G. Carter, "Optimisation of the Transfer Curves of Multi-Carrier Power Amplifiers for Low Intermodulation Distortion", in Proc. EPSRC-PREP 2001, April 9-11, 2001.

Chapter Five: Non-linearity, Intermodulation and Harmonics

5.1 Introduction

The previous chapter revealed how the physical processes in a helix TWT result in power saturation and phase nonlinearity, both of which result in harmonic generation and intermodulation distortion. The initial signs of nonlinearity are found in the electron beam itself. The influence of the RF wave on the beam causes RF components in the beam, particularly the RF beam current, to become non-sinusoidal with time. This RF nonlinearity is then transferred back to the slow-wave structure via the RF electric field interaction, resulting in a distorted output signal. The deviations in phases and velocities of the electrons also occur as a result of the interaction processes with the slow-wave structure.

This chapter aims to uncover the initial causes of nonlinearity as it manifests and grows within the beam and also how this becomes transferred to the slow-wave structure. RF beam current waveforms for different drive levels containing harmonics will be generated and simulated. These will reveal in the time domain, how nonlinearity initially arises in the beam (in the RF beam current) and then becomes transferred to the helix circuit (in the forward-wave voltage). This will improve our understanding on how TWT nonlinearity causes harmonic signals to arise.

The other aim of this chapter is to determine the relationship between harmonics and intermodulation products, which are the two forms of spectral distortion generated from the nonlinearity within the TWT. Such answers to these problems would improve the physical understanding of nonlinear interaction processes in a TWT, which would have benefits in its design. For instance, whether a design for minimum harmonic output also achieves minimum intermodulation distortion.

5.2 The Relationship between Intermodulation Products and Harmonics

When a sinusoidal single-carrier signal is passed through the helix circuit, its interaction with the beam causes harmonics to arise in the RF signal. For example, with an input signal frequency f_1 of 11.6GHz, spurious signals arise at the output frequencies $2f_1$ (=23.2GHz), $3f_1$ (=34.8GHz) and so on. When two signals having frequencies of f_1 and f_2 are applied to the input of a helix TWT, the nonlinear processes cause the two signals to become mixed together resulting in intermodulation products to arise at $2f_1$-f_2 and $2f_2$-f_1.

Figure 5.1 shows a typical example of the harmonic and IM product amplitudes computed by LSM simulation with two-carriers (11.6 and 11.8GHz). The figure shows that IM products and harmonics are being generated at small signal levels (Pin = -10dBm or less). This spurious generation is due to the inherent nonlinear properties of the TWT, especially within the electron beam. The amplitudes of the third order IM products are shown, in the figure, to be greater than those of the harmonics; these IM amplitudes continue to grow beyond carrier saturation. More output power in the amplifier therefore result in a greater level of IM noise, whereas the harmonic output powers reduce rapidly with increasing drive level in overdrive. This drop in harmonic amplitude could be due to a beating effect between the two carriers. The effect of the harmonics on the signal output is most significant at around 3dB output backoff. However, harmonics do not generally present a major practical problem to systems, since they arise well outside of the operating band where they can therefore easily be removed with a band-pass or low-pass filter. Harmonic amplitudes also normally become weaker at frequencies further away from the fundamental.

The amplitudes of the IM products present a much greater practical problem however, which is mainly due to the close proximity of the IM products to the carriers. A typical signal comprises an envelope of many carriers in an allocated band; the IM products arise throughout the band itself and spread out on either side of it. The amplitudes of the spurious signals are also greatest at frequencies nearer to those of the carriers.

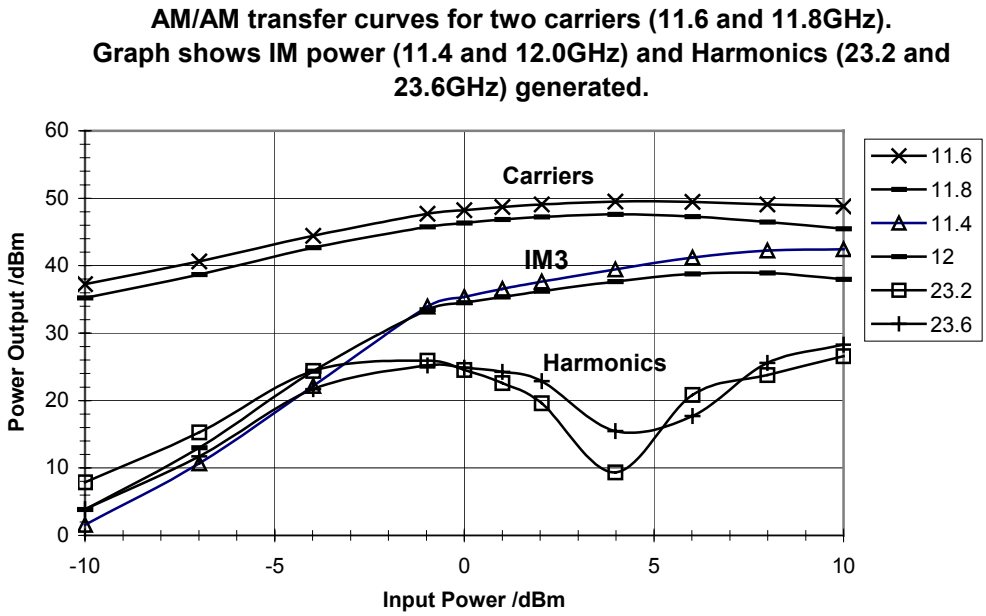

Fig 5.1: AM/AM transfer curves from a two-carrier LSM simulation. The output amplitudes of the harmonics and intermodulation products are displayed versus drive power.

Figure 5.2a shows the amplitudes of two carriers with frequencies f_1 and f_2 (11.6 and 11.8GHz) respectively. IM products arise at the frequency combinations of $2f_2$-f_1 and $2f_1$-f_2 as shown in the figure. This can be represented in an alternative form, as shown in fig. 5.2b. The frequency points f_1, f_2, $2f_1$, $2f_2$, etc. are shown vertically from top to bottom. Note that the multiples of the frequencies correspond to the harmonic values. The figure shows a third order intermodulation (I_3) product arising at the frequency corresponding to ($2f_1$-f_2), and the other I_3 product arising at ($2f_2$-f_1). The later could also be interpreted as [(the 2nd order harmonic of f_2) - f_1]. Fifth order products I_5 arise at ($3f_1$ - $2f_2$) and at (3rd order harmonic of f_2) - (2nd order harmonic of f_1). This suggests that the IM products may be formed from the carrier signal and the harmonic beating together. Otherwise, the IM products could be formed purely from the two carriers alone.

The Eulerian analysis by S. K. Datta et al. [1,2] has shown that by injecting a harmonic signal at the input with a frequency $2f_1$ and at a particular phase can reduce the 3rd order IM product (I_3) at $2f_1$-f_2. Likewise, injecting a signal with a particular phase at $2f_2$ reduces the I_3 at $2f_2$-f_1. To eliminate both 3rd order products however, the signals would need to be injected simultaneously at $2f_1$ and $2f_2$. Research by M. Wirth et al. [3] has shown experimentally with TWT amplifiers that injecting a signal at the upper harmonic ($2f_2$) with the correct phase and amplitude significantly reduces the I_3 at $2f_2$-f_1. This is also confirmed by experimental and analytical work by Wöhlbier et. al [4-6]. Moreover, Wöhlbier [7,8] has recently shown that it is the beating between the 2nd harmonic ($2f_1$) and the fundamental (f_1) which results in an intermodulation product to arise at the fundamental (f_1) itself resulting in a phase shifted output signal.

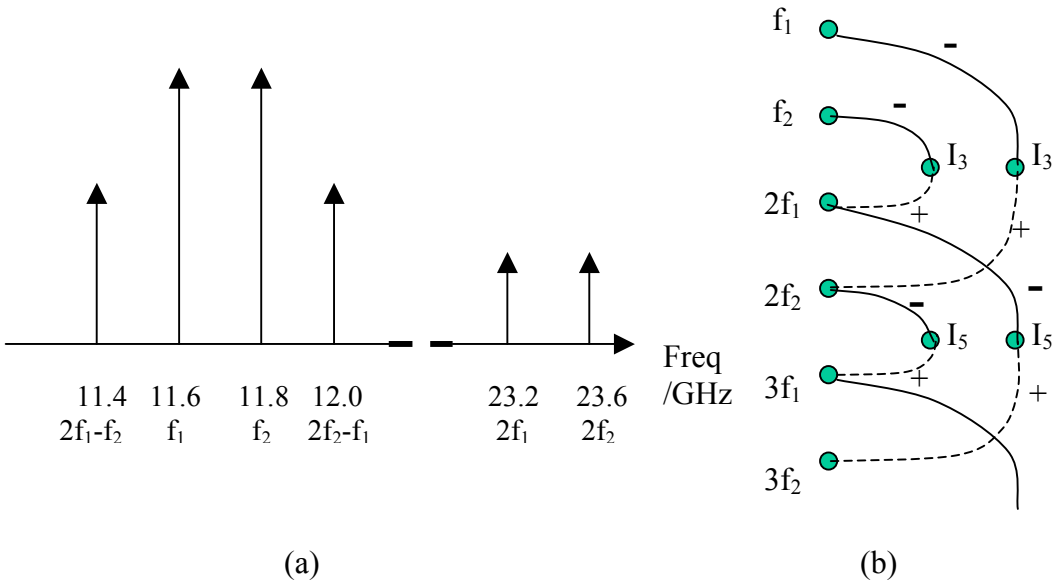

Fig. 5.2 Frequency locations of harmonics and intermodulation products arising from a nonlinear power amplifier

Multi-carrier simulations have been made with LSM to determine whether the connection between harmonic and IM generation is indeed an intrinsic one. For instance, whether the amplitudes of the harmonics in the LSM simulation directly affect the amplitudes of the IM products. Two input signals with frequencies 11.6 and 11.8GHz were made to interact with their harmonics (with frequencies 23.2 and 23.6GHz). The harmonic power levels were set at 15dB below the carrier power; this

is deliberately higher than in typical systems so that their effect on the output performance is more noticeable. The output response was taken at the frequency positions of the IM products (11.4 and 12.0 GHz) by setting these frequencies as two added input RF signals with zero drive power. The ratio of the carrier power to I_3 power (C/I3) was then computed for different input drive levels. The procedure was then repeated with the two harmonics removed from the system, i.e. zero harmonic effect in the simulation. The results, shown in fig. 5.3, reveal that removing the harmonic interactions from the system has little effect on the resulting IM distortion. The minor changes in C/I3 between the cases with and without harmonics are actually due to the deviations in the carrier output powers. These results imply that interaction of harmonics with the fundamental is not required to generate IM products; only the carriers are required.

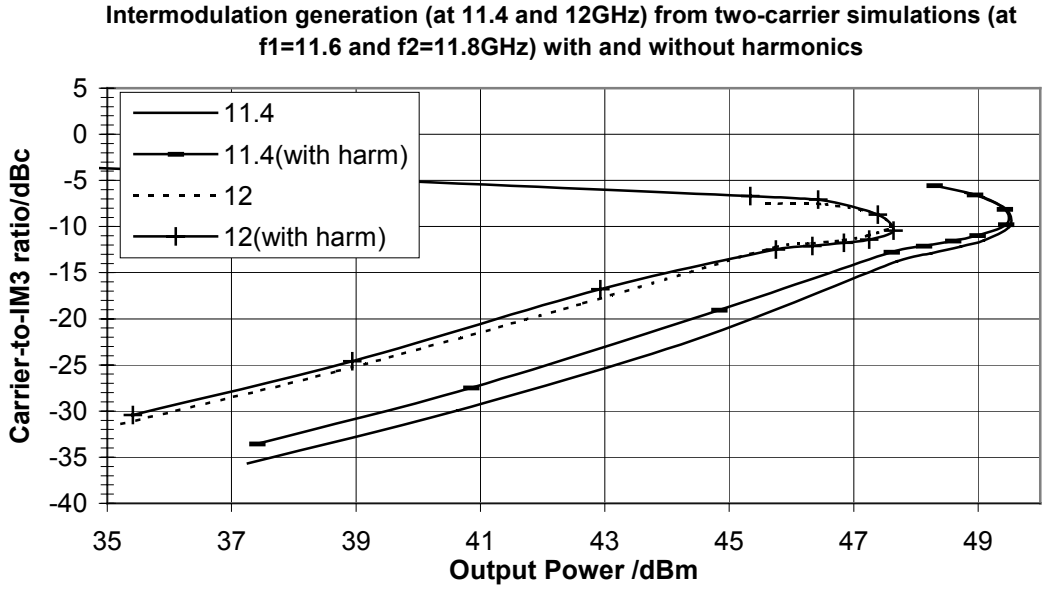

Fig 5.3 Comparison of carrier-to-IM ratio generation levels (at $2f_1$-f_2 = 11.4GHz and at $2f_2$-f_1 = 12.0GHz) from two-carriers (f_1=11.6 and f_2=11.8GHz) with and without harmonic interaction.

Further simulations were carried-out to verify these implications. Figure 5.4 shows the comparison of the Carrier-to-IM3 ratio between single-carrier simulations with harmonics and a 2-carrier simulation. Note that these results are plotted versus the sum of the carrier output powers, which is assumed to be equal to the total output power. A single carrier (at f_2=11.8GHz) was simulated with a single harmonic signal at: (1) $2f_1$=23.2GHz with an RF power equal to that of the carrier, (2) $2f_1$=23.2GHz with a power level 20dB below that of the carrier and (3) $2f_2$=23.6GHz with an RF power equal to that of the carrier. The figure reveals that substantial intermodulation power only arises when two or more carriers are simulated. It the harmonics are in-phase with the fundamental, they have a negligible effect on the generation of IM distortion. The phase of the harmonics would therefore have to be carefully selected for them to have any affect on the resulting level of intermodulation at the output. These results assume that the multicarrier interaction between harmonics and IM products is fully modelled and accounted for by the LSM program.

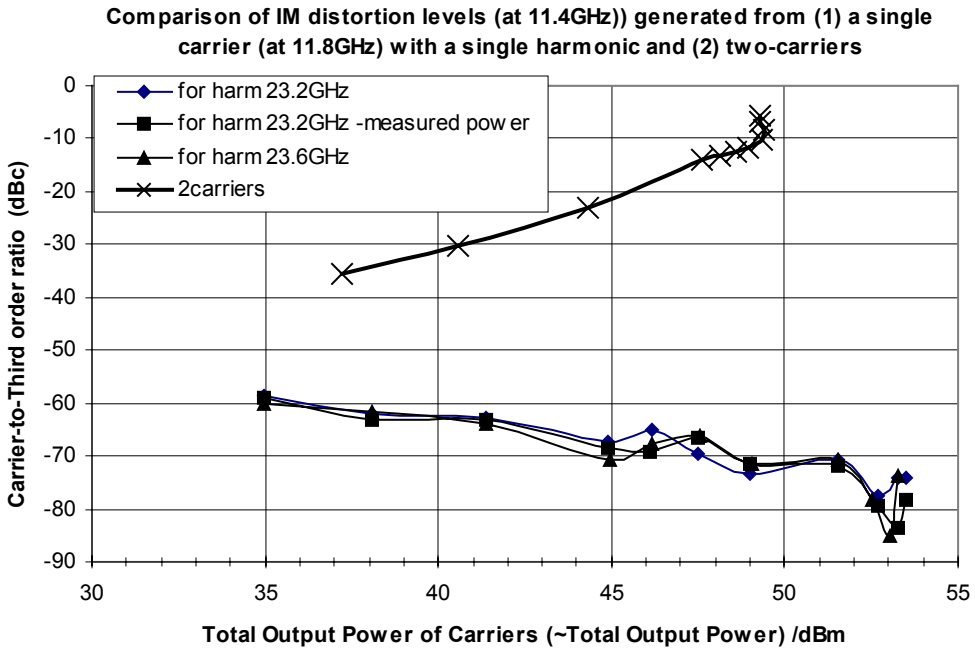

Fig 5.4 Carrier-to-3rd order IM ratio at $2f_1$-f_2=11.4GHz, generated from (1) a single carrier with a single harmonic at (a) $2f_1$=23.2GHz of varying power, (b) f_2=23.6GHz, (2) two-carriers

For a TWT designed to produce characteristics as those in fig.5.1, the harmonic power has little effect on the output signal, where the harmonic power is shown to be more than 20dB below the carrier power. Generally, including harmonic interactions in the system slightly modify the shapes of the fundamental AM/AM curves, which in-turn slightly affects the level of C/I3. This explains the deviation in the C/I3 results (for the cases with the same frequency with and without harmonics) in fig 5.3.

The research covered so far in this chapter involving the use of LSM and IMAL has not shown any direct intrinsic relation between harmonics and IM products. Past literature however proves that harmonic injection can suppress IM products. This is because suppression is possible, but under specific phase conditions. For example, two harmonics signals would have to be injected simultaneously at a specific axial position in the helix with specific phases. A greater reduction of the IM product amplitudes is possible when signals are injected at the difference frequencies i.e. $|f_2-f_1|$ instead of the harmonic frequencies. This was demonstrated by Aitchison et al. [9] using SSPA simulations, where a larger C/I3 improvement was found when injecting signals at the difference frequencies. Present and future communications systems however involve amplification of complex signal envelopes with dynamic varying amplitudes and phases. Applying such techniques of harmonic injection in these systems will prove very difficult

Harmonic and IM products are generated from the same source; it is the inherent nonlinearity found initially within the electron beam, which is responsible for the generation of all spurious signals including harmonics and IM products. Section 5.3 will investigate how the RF current becomes non-sinusoidal in the beam itself and how this becomes manifested on the forward wave on the helix circuit. The next section will however study the relationship between the integrated harmonic current and intermodulation distortion.

5.2.1 The Relationship between the Integrated Harmonic Beam Current and Intermodulation Distortion

A major factor in describing the harmonic behaviour in helix TWTs is the generation of harmonic current. W. Kim et al. [10] has shown analytically in heterojunction bipolar transistors that the third-order IM currents are dependant on the 2nd harmonic impedances. Otherwise the behaviour of harmonic currents is scarcely mentioned in any literature; yet it is the RF current at harmonic and IM frequencies which is the main indicator and carrier of nonlinearity.

Figure 5.5 shows the RF/DC fundamental and harmonic beam currents plotted as a function of axial distance in the output region of the tube for different drive levels. The behaviour of the harmonic current is shown to be unpredictable beyond its first maximum. As the drive level is increased, the total amount of harmonic current i.e. the area under the curve is also increased. Some code was therefore written in the LSM software to integrate the harmonic currents generated in each plane throughout the whole slow-wave structure. The aim was to discover a relationship between this integrated harmonic RF beam current and the RF power at the output.

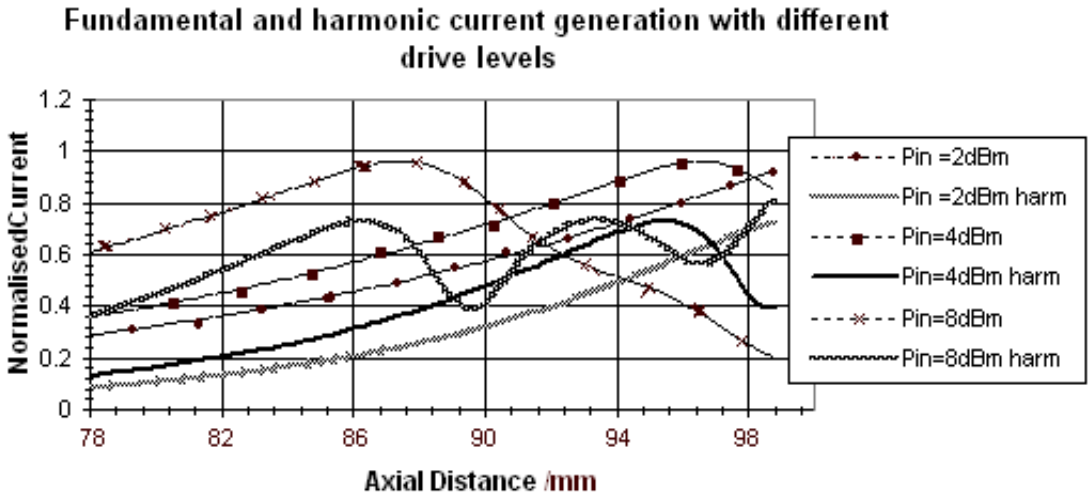

Fig. 5.5 Fundamental and harmonic RF beam current with different drive levels plotted against axial distance

The result, in fig. 5.6, shows that the output power is approximately proportional to the LOG of the integrated harmonic beam current that is continuously being induced in the helix. This relationship is shown to be valid up to a point before the output power becomes saturated. Results are shown in the figure for a range of practical beam voltages (with constant beam power or perveance). Assuming that the slopes of the curves are the same, this relationship can be analytically represented as written in equation 5.1. Here, C is the intercept on the power axis, which depends on the beam voltage. Note that when other TWT parameters are varied, this could affect the gradient of the curves.

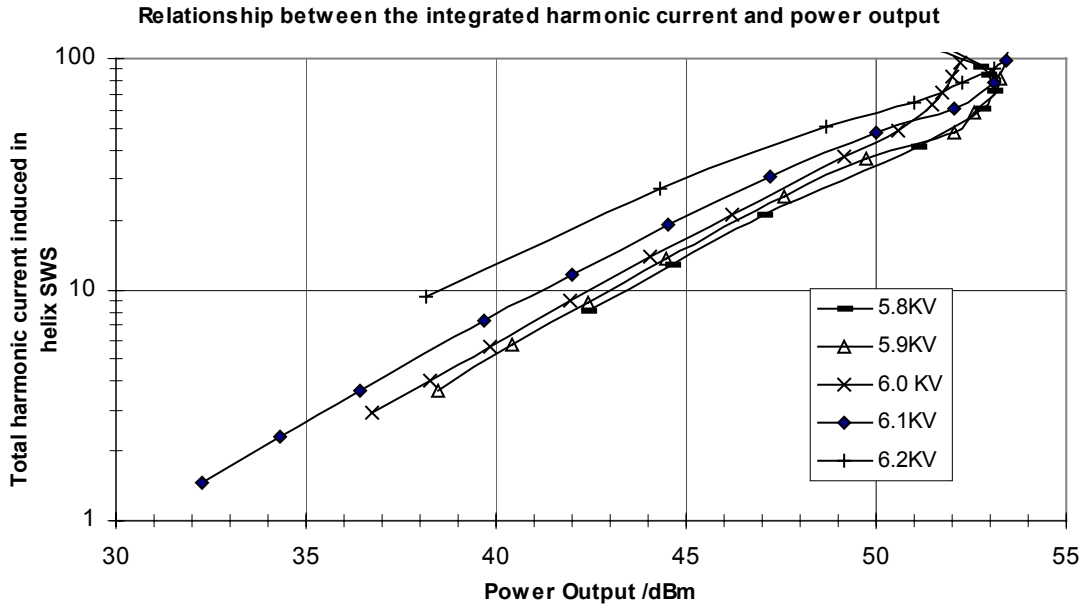

Fig. 5.6 LOG of the integrated harmonic beam current versus output power

$$P_{out}(dB) \approx 11.47(\log \sum_z I_{harm}) + C \qquad -5 \le C \le 5$$

$$\text{or} \quad P_{out}(W) \approx (\sum_z I_{harm})^{1.147} + C \qquad 0.316 \le C \le 3.16$$

} linear region (5.1)

When the results in fig. 5.6 are compared with the carrier-to-intermodulation ratio versus output power (or output back-off) for the same cases, they appear similar. The carrier to 3rd-order IM ratios for the same cases are therefore plotted against the LOG of the integrated (RF/DC) harmonic current in fig 5.7. The figure shows that

proportionality is maintained, even in well into overdriven power levels. Therefore, this relationship is valid for all drive levels. The simulations were repeated across a practical range of DC voltages as before. Additional examples are displayed in fig. 5.8 for: (1) two NPR simulations and (2) cases with the phase shift removed when transferring the data into the IMAL simulation. The number of carriers has shown to make little difference on the relationship. When the phase is removed, there is a reduction in the intermodulation distortion level. Thus the proportionality is lost because of the sharp reduction in the C/I3 ratio. This drop in the C/I3 ratio curve is less profound when the phase lag is set to 10% of the total. Therefore, for this relationship to be valid, the nonlinear effects from both the AM/AM conversion and the AM/PM conversion must be included.

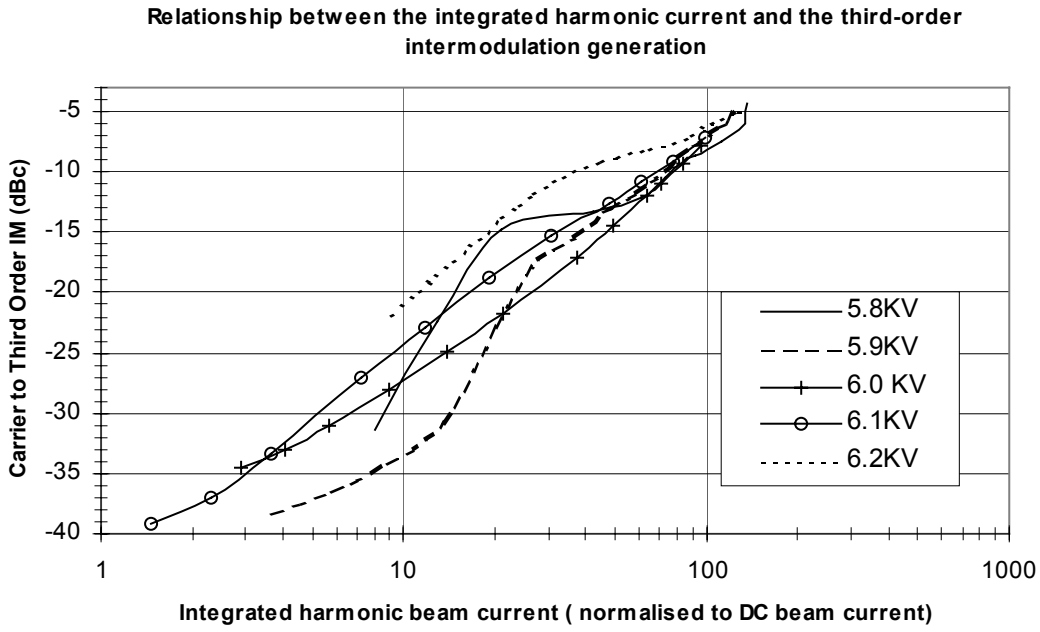

Fig 5.7 Carrier-to-IM3 ratio as a function of the integrated harmonic beam current

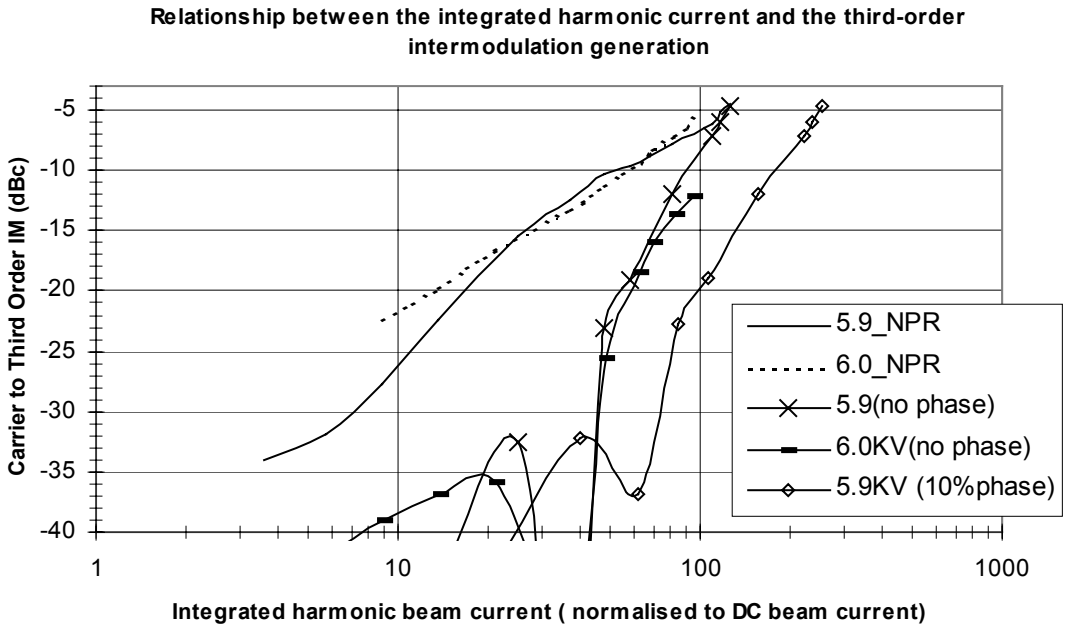

Fig 5.8 Carrier-to-IM3 ratio as a function of the integrated harmonic beam current

In this section, it has been discovered that the LOG of the integrated RF harmonic current generated in the beam increases proportionally with the power in the circuit. This relationship is only valid for up to a certain level of nonlinearity. The proportionality between the LOG of the integrated RF harmonic current and the level of intermodulation distortion however is found to be valid for all signal levels and for any number of carriers. This chapter will next reveal how nonlinearity initially arises in the beam and circuit of a TWT by the analysis of the RF beam current and circuit voltage waveforms.

5.3 Time Domain Analysis of the RF Current and Voltage with Harmonics

It is not fully understood how the nonlinear processes in TWTs cause spectral distortion to arise in the output signal, even for a single carrier. In solid-state power amplifiers, the mechanisms that cause harmonics to arise are better understood. Firstly, the voltage transfer curves of SSPAs can be determined for a particular design. Based on these voltage transfer curves, the harmonics and IM product amplitudes can then be modelled using a Volterra or power series. These nonlinear models for SSPAs can also compute how the power transfer curve is linked to the harmonic generation for a single carrier. In TWTs however, the distributive nonlinear interaction is very different, which makes the above modelling unknown for TWTs. In particular, a nonlinear TWT model that relates harmonic generation to the single carrier transfer curves needs to be determined.

To improve our understanding of nonlinear TWT interaction, it is useful to be able to determine the RF voltage of the forward wave on the helix and RF beam current for different signal amplitudes. This will enable the RF voltage and current transfer curves to be generated, which has not yet been achieved in TWTs. A Matlab program has been written that generates an RF beam current waveform (i.e. output current versus time) with harmonics for a given drive level. The real and complex amplitudes and phases of the output RF beam current are read from the LSM program for different drive levels. This is repeated for all harmonics up to say $4f_0$. Matlab also reads the fundamental frequency of the signal, which is assumed to be 11.7GHz. A Fast-Fourier Transform (FFT) is performed on the time domain signal to display its output spectrum containing its harmonics. Note that all of figures in this section correspond to the same designs where the Applegate diagrams are produced in Chapter 4.4.5.

5.3.1 Current Waveforms

Maximum RF Current

Figures 5.9a-d show the absolute (AC+DC) output RF beam current as a function of time, where the DC beam current is 0.133A. Each of the four plots are for different drive levels: 0, 7, 13 and 19.5dBm respectively, where the output signal of the TWT contains three added harmonics, i.e. $2f_0+3f_0+4f_0$.

In fig. 5.9a, the TWT is driven at a small-signal level (0dBm), the output waveform therefore shows closest resemblance to a purely linear (sinusoidal) wave. The nonlinearity in the current waveform is more noticeable when the drive level is increased to +7dBm (in fig. 5.9b), where ripples are observed. With greater drive powers, the harmonics in the TWT enhance the form of these ripples, especially when the output (AC+DC) current is less than 0.13A, as seen in fig. 5.9c. When the TWT amplifier is operated at around power saturation (19.5dBm) in fig 5.9d, the current peak actually becomes limited when the (AC+DC) current is around 0.13A. The effect of the harmonics in this nonlinear single-carrier system is broadening and clipping of the RF beam current waveform peak. Figure 5.10 shows the output spectra corresponding to the 4 drive levels. All harmonic amplitudes with an input power of 7dBm have roughly similar levels of harmonic output amplitudes. As the drive power is increased from 13 to 19.5dBm, the growth of the fundamental becomes limited, a reduction of the induced 2^{nd} ($3f_0$) harmonic current occurs, while the signal continues to grow at $4f_0$.

Figure 5.11 displays the RF beam current and voltage transfer curves. The plots to the left of this figure show the amplitude transfer curves of the fundamental and the first ($2f_0$) harmonic beam current and the phase transfer curve of the fundamental RF beam current. The two figures to the right show the equivalent voltage transfer curves. The first harmonic level is more evident in the beam current than the RF voltage. Here the output harmonic current is roughly half that of the fundamental. Limiting of both the current and voltage signal amplitudes is shown; this directly results in AM/AM distortion.

Maximum RF Current

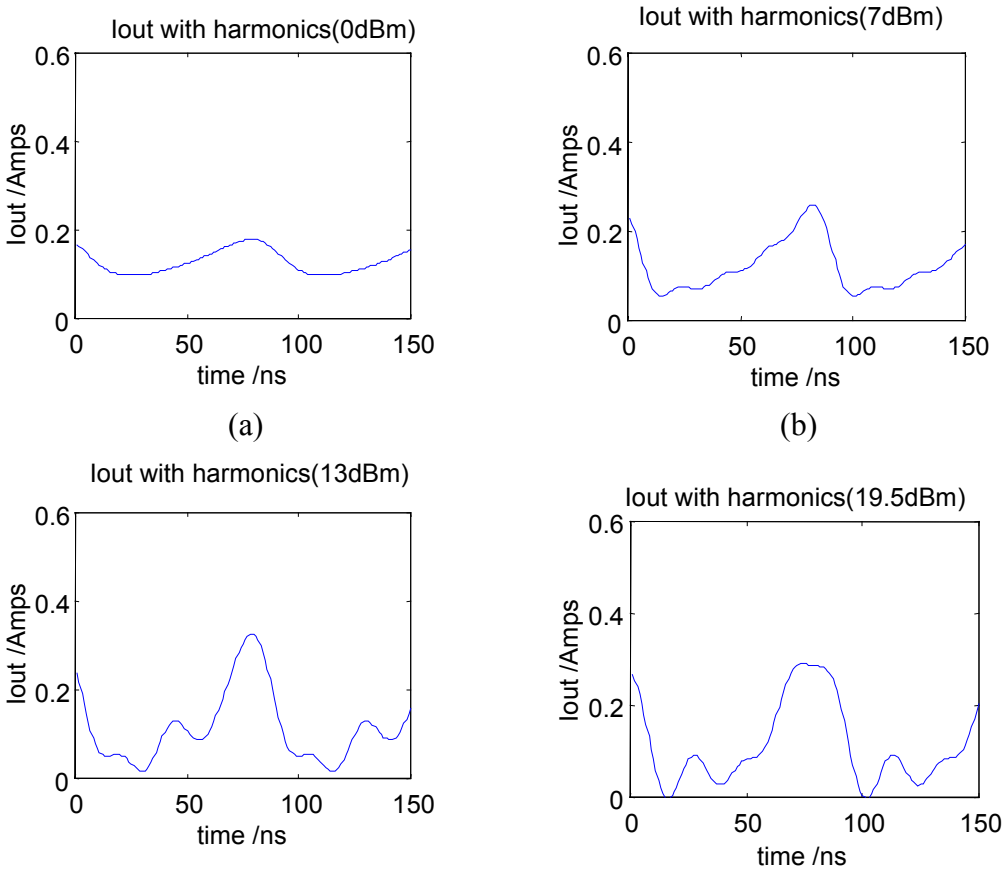

Fig. 5.9 Beam current waveforms when harmonics are added for different RF drive levels.

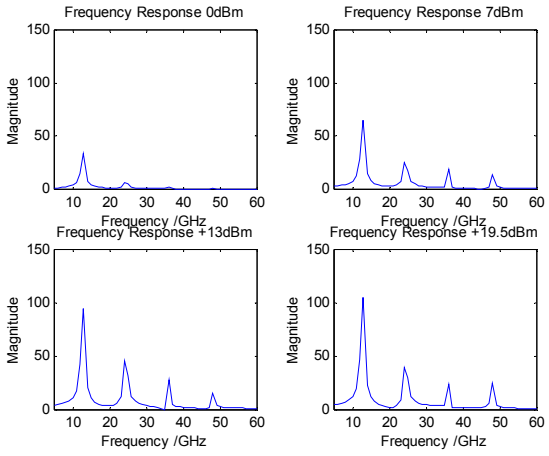

Fig. 5.10 Frequency response corresponding to the signals 5.9 (a) to (d)

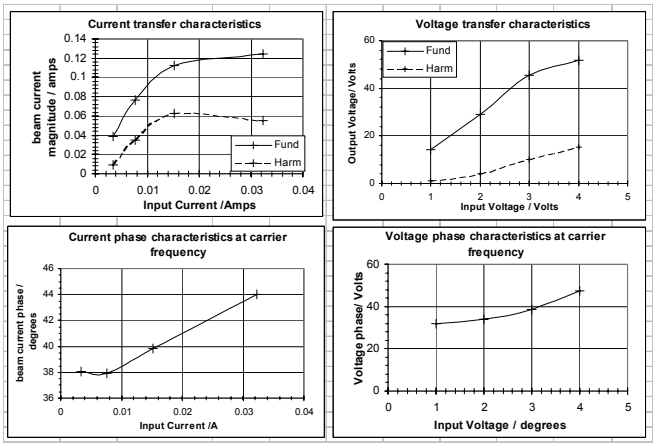

Fig. 5.11 Current and voltage transfer curves for maximum RF current

Minimum Intermodulation Distortion

The same set of results have been produced where the helix pitch is made to correspond to the minimum intermodulation distortion condition, i.e. combined optimum AM/AM and AM/PM linearity in a multi-carrier system. For this reduced helix pitch from 0.838mm to 0.780mm, the input RF power levels for these plots are set lower, at –10, 0, 7 and 13dBm, since the output gain is higher. When comparing plots corresponding to similar output backoffs, e.g. comparing fig. 5.9c with fig. 5.12b and comparing fig. 5.10 with 5.13, the harmonic output is generally increased. Figure 5.13 shows that the amplitude of the 2^{nd} harmonic ($3f_0$) nearly equals that of the fundamental at around power saturation (0dB). This causes significant distortion to the waveform, as shown in fig. 5.12b. The current and voltage phase change is also revealed to be much greater for the optimum linearity condition (see fig. 5.14). Note that the minimum phase lag condition corresponds closely to where the RF current is maximum, as shown in Chapter 3.4.1. This minimum IM distortion condition is a trade-off between an optimised AM/AM transfer curve and minimum AM/PM conversion. The phase shift is also indicated by the movement of the waveforms along the time axis as the signal level is increased in fig. 5.12.

Optimum Linearity

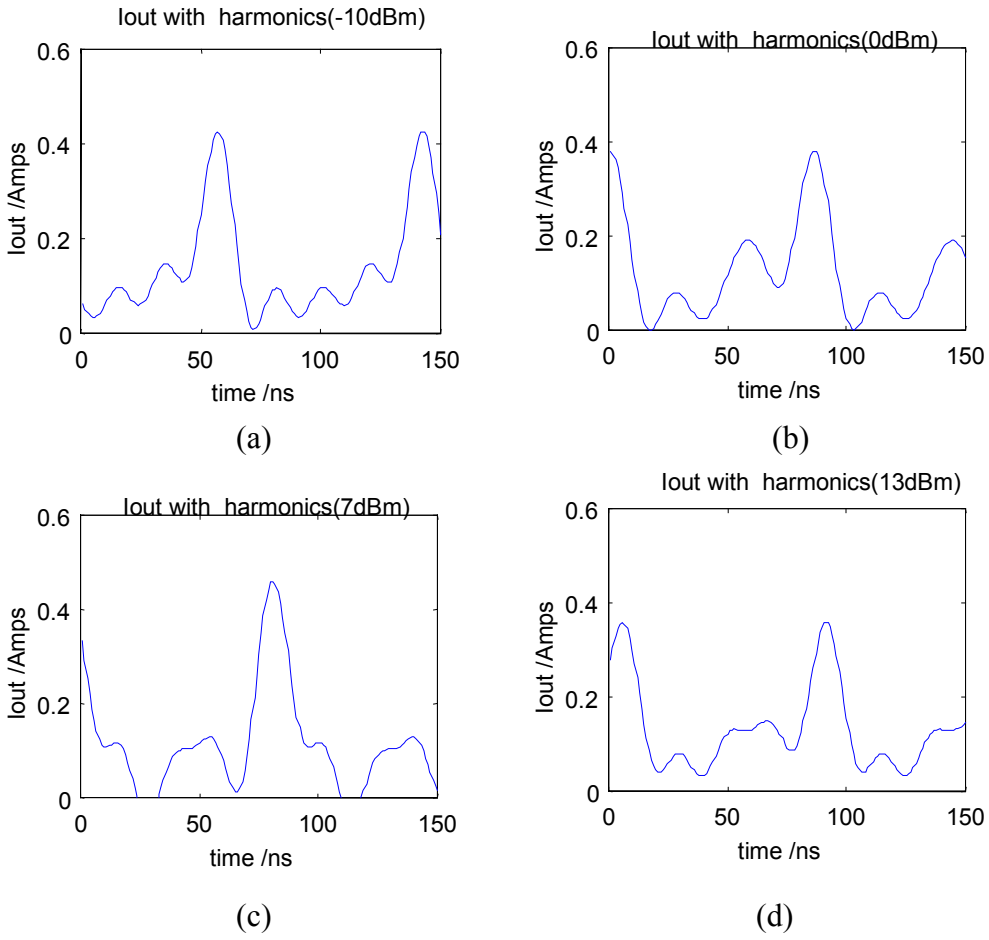

Fig. 5.12 Current waveforms when harmonics are added for different RF drive levels.

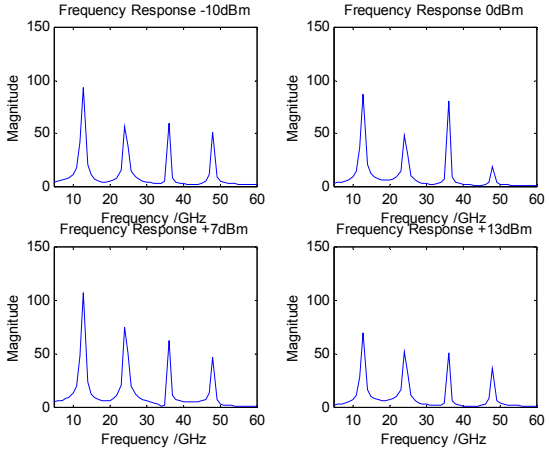

Fig. 5.13 Frequency response corresponding to the signals 14 (a) to (d)

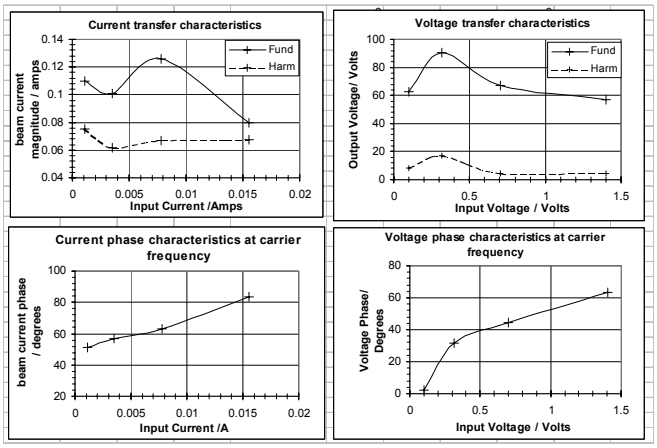

Fig. 5.14 Current and voltage transfer curves corresponding to optimum linearity

Maximum Efficiency

When the helix pitch is further reduced to a level (0.716mm) such that the conversion efficiency at the output of the TWT is maximised, the current waveforms are of the form as shown in fig. 5.15a-d. The RF input power levels for these plots are set higher, as the output gain has reduced from the minimum IM distortion condition. For an input power of 7dBm (fig. 5.15b), the effect of the harmonics causes the peak of the current waveform to become narrower with larger amplitude, while the remaining waveform becomes a consistent ripple. When the TWT amplifier is driven at around power saturation (13dBm), the current magnitudes of the 1^{st} and 2^{nd} harmonics are actually higher than that of the fundamental, as shown in fig. 5.16. A significant amount of nonlinear disturbance is therefore contained in the waveform, as shown in fig. 5.15c. In overdrive, the 1^{st} and 2^{nd} harmonic currents equal that of the fundamental and the amplitude of the 3^{rd} harmonic is small, but the total harmonic content significantly modifies the harmonic waveforms, as in fig. 5.15d. The waveforms in all four plots consist only of peaks pointing in the direction of the positive current.

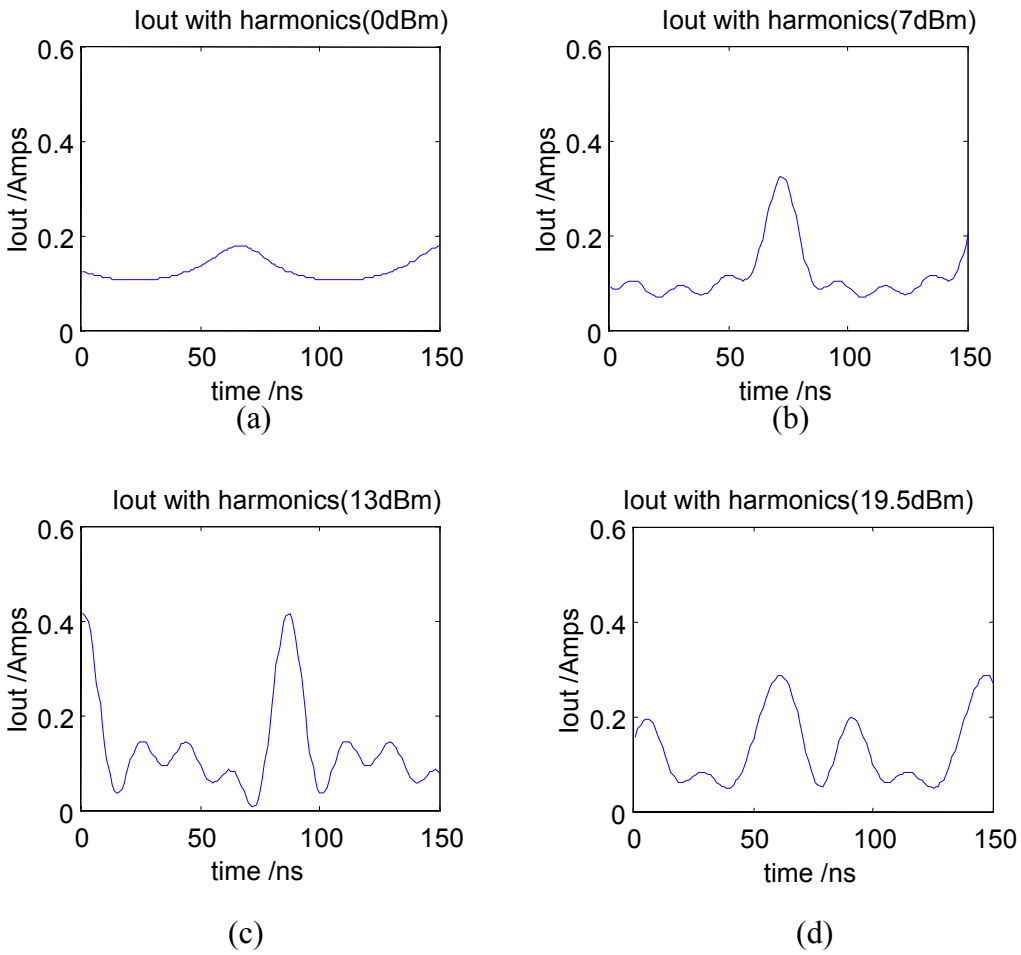

Fig. 5.15 Voltage waveforms when harmonics are added for different RF drive levels.

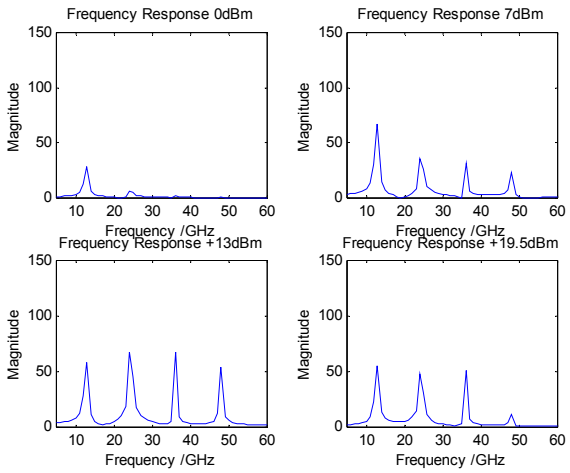

Fig. 5.16 Frequency response corresponding to the signals 17 (a) to (d)

5.3.2 Voltage Waveforms

The Matlab code was modified to repeat the same operation as in section 5.3.1 but instead with the RF voltages induced in the slow-wave structure. Plots of the AC voltage are shown for the condition of maximum efficiency in fig. 5.17 as a comparison with fig. 5.15. It is clear that the harmonics have a far less influence on the voltage induced in the circuit than the current induced in the beam. It is only when the device is driven beyond saturation (in the highly nonlinear region) where the 1st ($2f_0$) harmonic has some influence (see fig. 5.18). This 1st harmonic results in the clipping of the voltage waveform peak and further reduces the negative amplitude of the waveform peak. Figure 5.19 confirms that the harmonic amplitude of the voltage is well below that of the fundamental. However, a significant voltage phase shift is revealed in the figure (more than 80° shift across the driven range). The beam current phase shift is also large, increasing to a 70° shift at saturation, then reversing phase beyond power saturation.

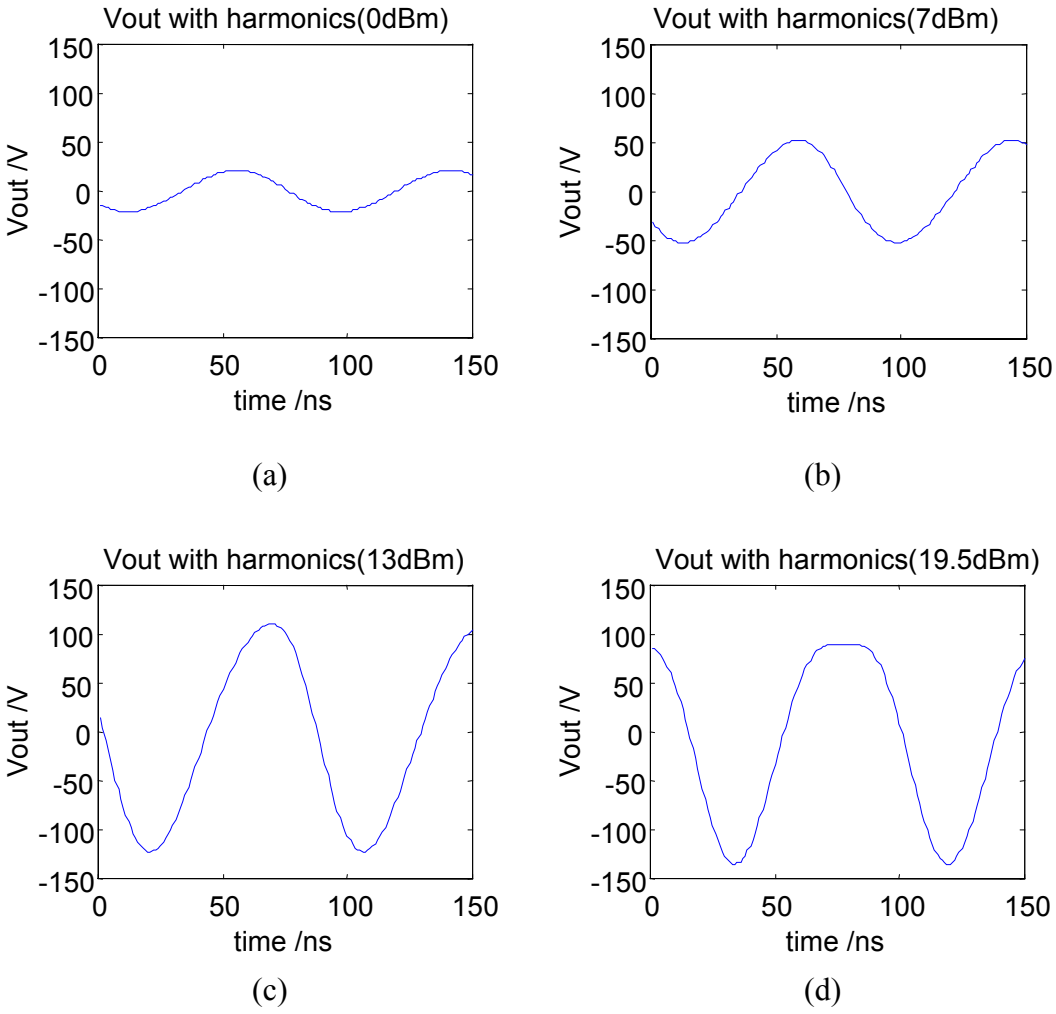

Fig. 5.17 Current waveforms when harmonics are added for different RF drive levels.

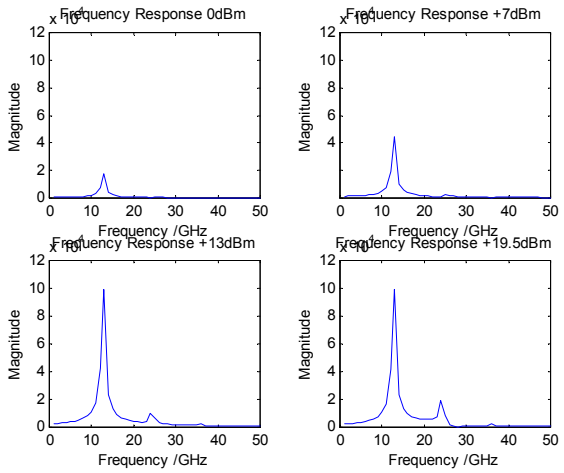

Fig. 5.18 Frequency response corresponding to the signals 19 (a) to (d)

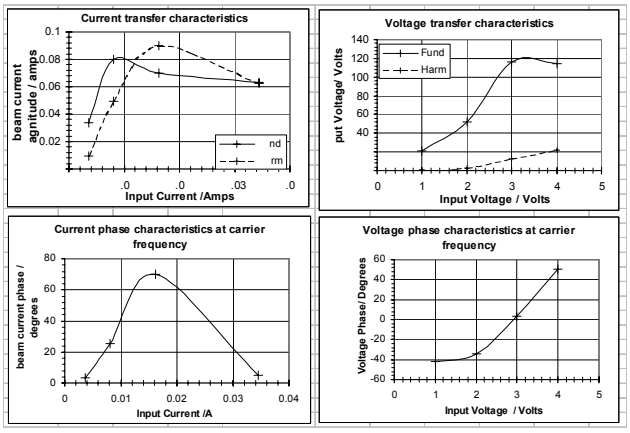

Fig. 5.19 Current and voltage transfer curves corresponding to maximum efficiency.

5.4 Conclusions

This chapter has explored the possible links between harmonics and intermodulation distortion using LSM and IMAL simulations. The initial aim was to determine whether harmonic interaction in a TWT influences the amount of intermodulation distortion. It was found that removing RF power at the harmonic frequencies did not have a significant affect on the level of intermodulation generation at the difference frequencies of the carriers. The results also confirmed that no intermodulation products were generated from a single carrier and a single harmonic. Therefore, harmonic interaction with the beam, which is modulated with a single carrier, is not sufficient as a means to produce intermodulation distortion; at least two carriers are required.

Harmonic injection may suppress intermodulation products, but only when the amplitude and phase of the harmonic is predetermined. The technique of harmonic injection would be impractical for present and future communications systems however, since these employ dynamically varying phase and amplitude multiplexing schemes.

By determining whether any intrinsic relation exists between harmonic and IM generation, it was found that as the drive power is increased, the integrated harmonic power induced in the beam is also increased. A relationship was then deduced between the total RF harmonic current and the carrier-to-intermodulation power ratio, which was found to be independent to drive level.

Current waveforms containing harmonics were generated from the LSM program for a uniform structure corresponding to desirable conditions, such as minimum C/I3, maximum RF current and maximum efficiency. This revealed how the harmonics influence the form of the RF beam current waveform for each of these conditions. When the RF current is maximum, clipping of the waveform peak is noticed at power saturation. For minimum C/I3 generation, the peak-to mean current is high (greater than three times the DC current). For maximum efficiency, the harmonic output is the greatest. This chapter has provided an insight and contributed to our understanding on

how TWT nonlinearity causes spurious spectral output to be generated. Further work is required in this particular field however, as discussed in Chapter 7, to fully relate the nonlinear processes in a TWT with the resulting distortion.

References

[1] S. K. Datta, P. K. Jain and B. N. Basu "Control of IM3 distortion in helix TWTs by harmonic injection - An Eulerian hydrodynamical study", IEEE Trans. Electron devices, Vol. 48, No. 1, January 2001.

[2] S. K. Datta et al.,"Eulerian analysis for harmonic generation and its control in a helix traveling-wave tube," International Journal of Electronics, Vol. 85, No. 3, pp. 377-395, 1998.

[3] M. Wirth et al., "Third-Order intermodulation reduction by harmonic injection in a TWT amplifier", IEEE Trans. Electron Devices, Vol. 49, No. 6, June 2002.

[4] J. G. Wöhlbier, J. H. Booske and I. Dobson, "The physics of harmonics injection in a TWT", Proc. Intl. Vacuum Electronics Conf., Monterey, USA, pp.280-281, April 2002.

[5] J. G. Wohlbier, I. Dobson and J. H. Booske, "Generation and growth rates of nonlinear distortions in a traveling wave tube, "Phys. Rev. E, Vol. 66, No.5, pp. 56504-1-5, November 2002.

[6] J. G. Wohlbier, J. H. Booske and I. Dobson, "The multifrequency spectral Eulerian (MUSE) model of a traveling wave tube", IEEE Trans. Plasma Sci., Vol. 30, No.3, pt.1, pp. 1063-75, June 2002.

[7] J. G. Wohlbier, J. H. Booske and I. Dobson, "A new view of phase distortion in a traveling wave tube", Proc. Intl. Vacuum Electronics Conf., Soul, S. Korea, May 2003.

[8] J. G. Wohlbier, J. H. Booske and I. Dobson, “On the mechanisms for phase distortion in a travelling wave tube”, to be submitted to Phys. Rev. E, March 2003.

[9] C. S. Aitchison, et. al., “Improvement of third-order intermodulation product of RF and microwave amplifiers by injection”, IEEE Trans. on Microwave theory and tech., Vol. 49, No. 6, June 2001.

[10] W. Kim et. al., “Analysis of nonlinear behaviour of power HBTs”, IEEE Trans. on Microwave theory tech., Vol. 50, No. 7, July 2002.

Chapter Six: Design of a Practical Helix TWT

6.1 Introduction

The main objective of this project is to design a helix TWT with high linearity and efficiency over a broad bandwidth. These three criteria are the most desirable properties of any power amplifier in modern communications system. But these highly sought-after properties require different helix designs as shown from the research of a uniform structure in Chapter 3.

By achieving beam-wave synchronism, Chapter 3 showed consistent output power across the 2GHz bandwidth. If the helix design were changed so that for instance, a more linear condition was achieved, the bandwidth and the efficiency of the TWT would both be reduced. Careful trade-off between these conditions is therefore required. Optimisation of the pitch profile along the length of the slow-wave structure can be done in a systematic way to best achieve the desired conditions in a single TWT design. This chapter will explain how this has been done.

The final design which aims to achieve the best trade-off between linearity and efficiency will be analysed across the frequency band of 10.75 to 12.7GHz as specified in the systems objectives in Chapter 2.2. A multistage collector will be optimised based on the spent-beam distribution curves enabling the overall efficiency to be determined.

6.2 Design of a Non-Uniform Slow-Wave Structure

The principle of designing the helix pitch profile is to optimise the interaction processes throughout the slow-wave structure. This includes achieving tight electron bunch compression followed by optimised power extraction from the beam. Tapering or reducing the phase velocity towards the outplut end of the tube allows the electron bunch to remain in the decelerating phase over a longer axial distance. More power is therefore extracted from the beam, improving the conversion efficiency.

A strategy needs to be developed which tailors the pitch profile to minimise nonlinear distortion in addition to providing enhanced efficiency. Adjusting the helix pitch affects the shapes of the transfer curves [1], which determine the level of intermodulation distortion [2]. The pitch profile can therefore be optimised for minimum intermodulation distortion by consideration of its effect on the shapes of the transfer curves. Past experiment has demonstrated that tapering the pitch can reduce the phase conversion by up to 2° / dB [3].

A Helix TWT designed for today's practical systems must also have a suitable attenuation profile with severs. Severs prevent oscillations arising at high gain levels (>50dB at saturation) from reflection of around 10% of the forward wave voltage at the input and output terminals. The position of a sever must be carefully chosen or the conversion efficiency and the operating bandwidth could be adversely affected [4]. If the sever is placed where there is some non-linearity in the beam, the efficiency is more likely to be degraded. This degradation is due to the de-bunching in the beam by space-charge forces in the region beyond the sever [5]. This can be prevented if the sever should is made as short as possible and the ratio of the gain of the output section to the input section is maximised.

6.2.1 Taper Design Procedure

The methodology used this chapter, for the helix pitch profile design, was initially based on a paper by V. Strivastava [6]. This is the most recent published work on the design of a slow-wave structure. The method is based on the fundamental processes within the tube, these are: the growth of RF wave on the helix, bunching of the electron beam and power extraction from the beam. The helix pitch should be designed to exploit these processes as they happen along the tube. This methodology is next described.

In the region where the initial growth in RF signal takes place, the helix pitch p_0 is designed for maximum signal growth. In the region where the bunching takes place, the pitch p_1 is then adjusted to maximise this process i.e. achieve the tightest bunches. Towards the end of the tube, RF power is extracted from the electrons in the beam reducing the beam velocity. The helix in this region p_2 should then be designed to optimise this power extraction process. These pitch values can be optimised using a single section with a uniform pitch.

The paper [6] states that with a positive step taper included, the input section length z_0 with pitch p_0 is designed for maximum RF current or bunch intensity. With a negative step added, z_1 is then adjusted for maximum forward RF power in the output region (with pitch p_2). The length of taper in the output region z_2 is then adjusted for maximum forward power at the output. A summary is given below:-

For a single uniform section:-

adjust p_0 for maximum small signal gain

adjust p_1 for maximum bunching (maximum RF current)

adjust p_2 for maximum output power or efficiency

Then:-

Adjust z_0 for maximum bunching in centre region (with pitch p_1)

Adjust z_1 for maximum forward power in output region (with pitch p_2)

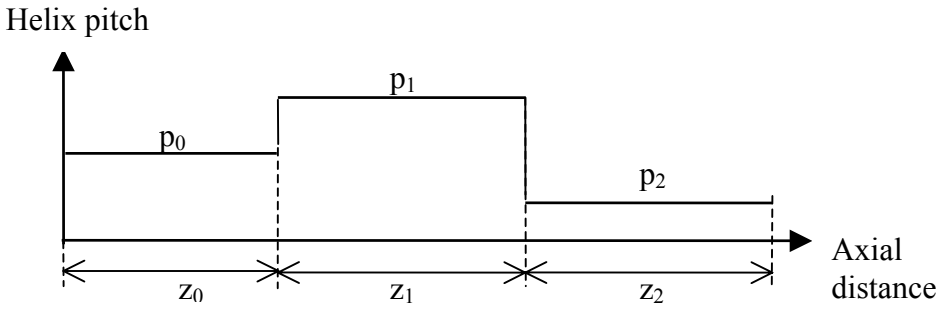

Fig 6.1 Stepped helix pitch profile for optimised performance [6]

The strategy described above effectively optimises the signal gain, development of the bunch formation, capture of the bunch and power extraction. Hence, the strategy is ideal for gain and efficiency optimisation. The drawback with this method however is no consideration for the nonlinear performance or the broadband performance. The method needs to be developed therefore, by incorporating optimisation for a linear performance and, if possible, a broadband performance. A brief description of the important interaction processes and the modified criteria for a full TWT design is next explained. For this purpose, the TWT structure is divided into the three interaction regions: linear, bunching and output.

Helix TWT Processes and Design Criteria

Linear Region

In the region nearest to the tube input, the un-modulated beam is surrounded by a sinusoidal RF wave on the helix. The electrostatic influence of the AC wave on the beam causes a sinusoidal current to become established in the beam at the same frequency (or frequencies) as the RF signal. At this small-signal level, the phase of the electrons in the beam relative to the forward-wave on the helix is almost constant, the RF characteristics are approximately linear and the tube efficiency is very low. The design criteria for this region are thus: maximum signal growth rate at the band centre and for the small-signal gain variations to be minimal across frequency. These criteria can be achieved from the design of the slow-wave structure.

Bunching Region

In this region, strong electron beam bunching occurs due to the influence of the circuit field. The bunch becomes strong where the RF current component in the beam grows until a maximum is reached. This is where mutual repulsion between the electrons, which is due to the space-charge effect, becomes an important factor on the overall behaviour. An electromotive force is induced in the helix by this AC beam current component, which becomes limited when the amplifier is driven hard enough, resulting in a limited RF output power. Phase shifting of the RF signal in the slow-wave structure also occurs as a result of its interaction with the inherently nonlinear beam (as discussed in Chapter 4).

To enhance the bunching process, an increased phase velocity is required at a position before the beam phase becomes non-linear. The aim is to optimise the convergence of the electron trajectories so that the bunch has a maximum number of electrons captured. As a result, more RF power can be extracted from the bunch enhancing the conversion efficiency. In addition, less velocity spreading in the bunch often results from the optimised bunch formation. Careful design of the positive taper is necessary to optimise the AM/AM and AM/PM conversion. The circuit phase velocity in this region must be chosen to optimise the shapes of the transfer curves without sacrificing too much conversion efficiency.

Output Region

The output region of the TWT is beyond the point of maximum bunching. The RF beam current therefore declines in this region, while the forward circuit power continues to grow until it saturates. The beam velocity decreases rapidly and the non-linear behaviour of the signal is most profound.

To optimise the power extraction from the beam, the circuit phase velocity is lowered. For the electrons to lose most of their energy in this output region, it is desirable for them to remain in their maximum retarding phase. It is also desirable to confine the spread of the beam velocity, especially to limit the number of fast electrons. This is to improve the depressed collector efficiency, enhancing the overall efficiency.

A constant output power in overdrive is significant when the curvature of the power transfer curve is small enough [2]. The nonlinear performance in this region may therefore be improved if the RF power is retained without it being lost back to the beam. The broadband operation can be optimised if the reduction of beam phase in this tapered region is made consistent across a range of frequencies in the band. Signal reflections at the output terminal should also be avoided in the practical design.

6.2.2 Determination of the Fixed TWT Design Parameters

The most practical way of adjusting the circuit phase velocity along the axial direction is by varying the pitch profile. When simulating the designs with the LSM program, the axial propagation constant β_0 and interaction impedance K_0 need to be computed separately for each pitch value using the HELIX code. Figure 6.2 shows that the interaction impedance K_0 increases with the helix pitch, while the axial propagation constant β_0 decreases.

The parameters which are being chosen specifically for the design procedures in section 6.2 are:-

1. The pitch values (p_i) for each of the interaction regions with the corresponding values for the axial propagation constant and interaction impedance.

2. The lengths (L_i) of each of the interaction regions.

The drive power and frequency are not the actual design parameters, but they provide operating conditions which are very important in the design methodology; the output characteristics of the amplifier as a function of input power and frequency should be closely monitored. The range of input powers begin from small signal levels to overdrive and the frequency band is from 10.7 to 12.75 GHz with a centre frequency of 11.7GHz, as specified in the systems criteria in Chapter 2.2.

The circuit attenuation profile was based on the design in [6], which typically represents the circuit attenuation in TWTs. The attenuation profile is not constant for a tapered helix, but varies to minimise the signal reflections at the sever position.

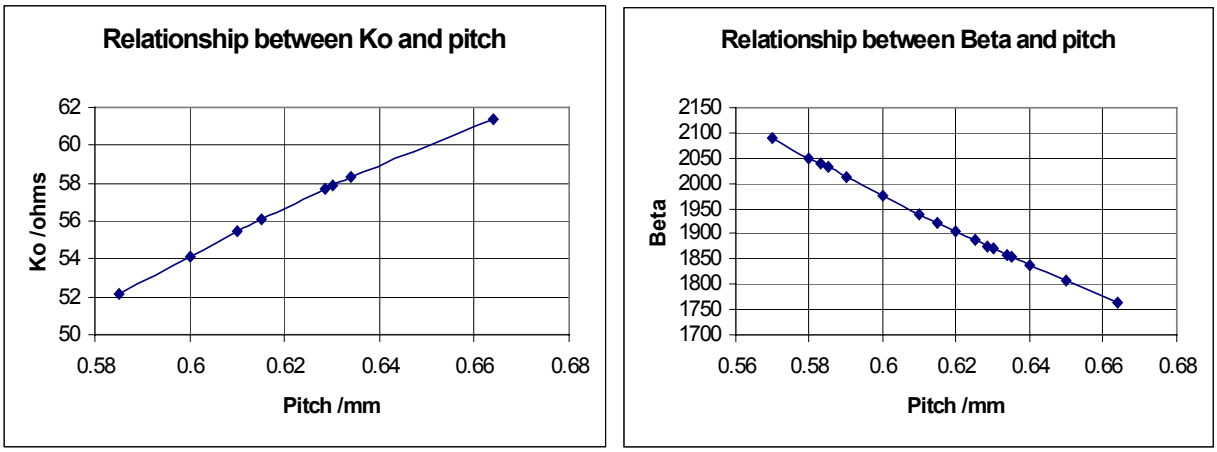

Fig 6.2 Dependence of the helix pitch on Ko and β_0.

The other parameters which remain constant throughout this investigation include the DC beam power, beam perveance, helix radius etc. The DC power can be estimated from the electronic efficiency and the required output RF power. The beam voltage and current are determined by the desired beam perveance and were thus chosen as:-

Beam Voltage	4.88KV
Beam Current	54.7mA

The helix radius a was chosen such that $(\beta_e)a \approx 1$

where $\beta_e = \omega / u_0$

(ω = signal frequency at band centre in radians per second)

(u_0 = initial velocity of electron beam in meters per second)

thus $a \approx u_0 / \omega$

If $\omega = 2\pi f = 7.351 \times 10^{10}$ radians per second and $u_0 = 5.109 \times 10^7$ m/s

then $a = 6.95 \times 10^{-4}$ m

i.e. The helix radius is 0.695mm and for a given fill factor, the beam radius = 0.275mm.

The rest of the parameters (listed below) were chosen in the conventional manner - partly from experience and what is used experimentally and is therefore reliable in practice.

Tape width	0.14mm
Cathode flux	$3.493e^{-08}$ Wb
Axial magnetic field	0.1698T
Tape thickness	0.035mm
Relative dielectric constant of support rods (Beryllia)	6.6
Number of support rods (per helix turn)	3
Wedge angle	20°

6.2.3 Determination of the Helix Pitch Values

Figures 6.3 to 6.5 show the small-signal gain, maximum RF beam current and the output power respectively as a function of helix pitch for a uniform TWT section. Note the pitch range of which these three conditions are contained is just 0.1mm. The small-signal gain is shown at a very low RF drive power of -50dBm. The other two conditions are shown at around power saturation and backed-off drive levels. The optimum conditions were selected as follows:

Maximum small signal gain at $p_0 = 0.634$mm
Maximum beam RF current (bunching intensity) at $p_1 = 0.664$mm
Maximum power output / efficiency at $p_2 = 0.585$mm.

These chosen pitch values are given to the nearest micron. When manufacturing the helix pitch variations may occur that are greater than 1μm, thermal vibrations can also cause fluctuations to the helix pitch of this order. The preciseness of these pitch estimations for the three conditions emphasise the importance of accuracy in manufacturing the slow-wave structure.

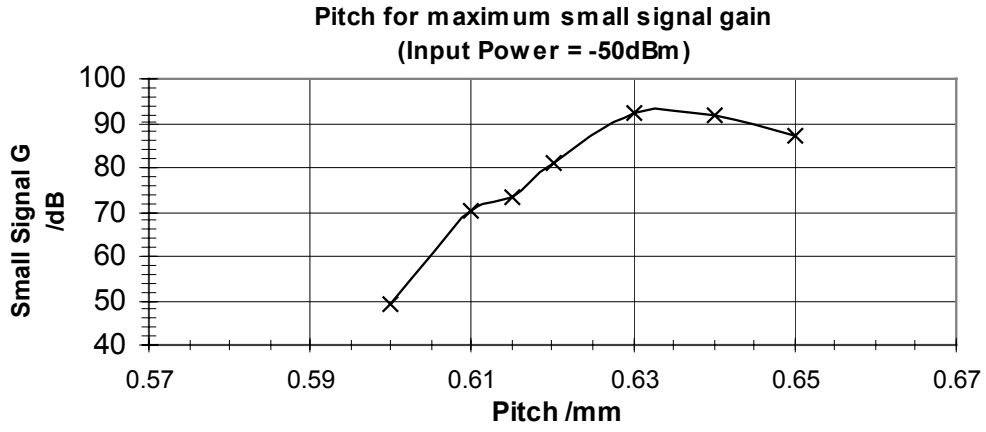

Fig 6.3 Optimisation of pitch for maximum small-signal gain in a uniform helix TWT

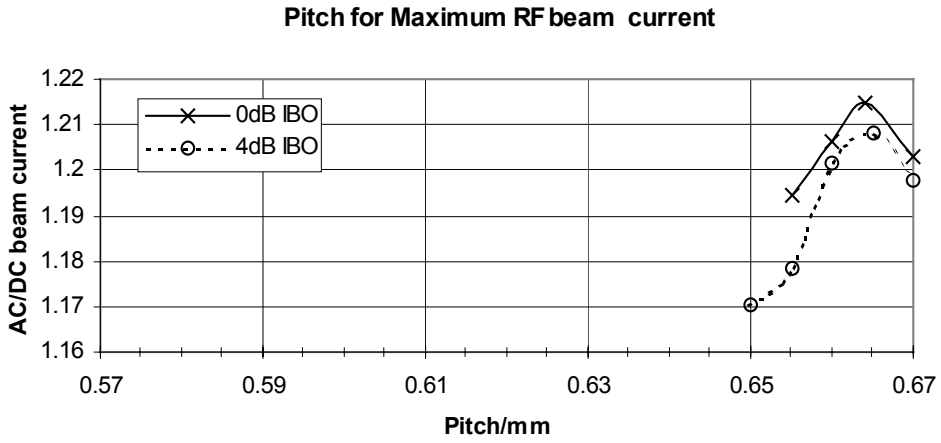

Fig 6.4 Optimisation of pitch for maximum RF beam current in a uniform helix TWT

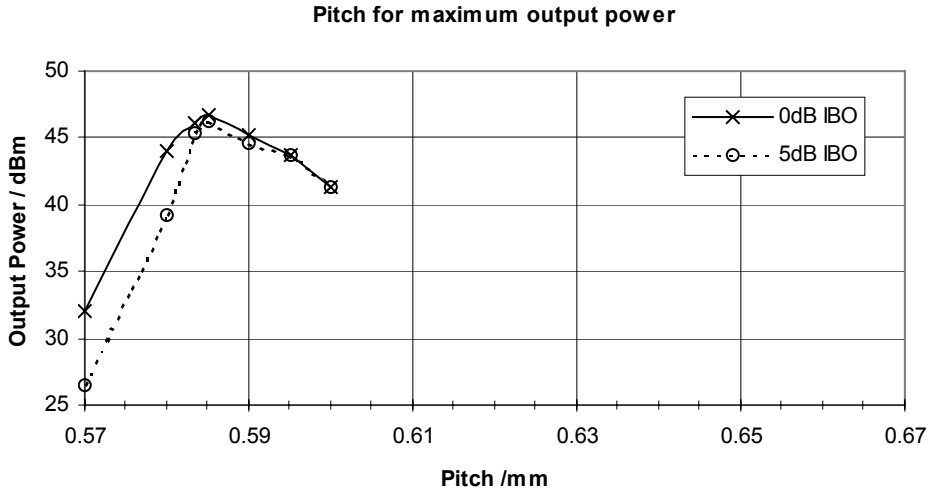

Fig 6.5 Optimisation of pitch for maximum power output in a uniform helix TWT

6.2.4 Design of a Positive/Negative Double Step Taper

Using the pitch values from the single section results (p_0, p_1 and p_2) and incorporating an attenuation profile with sever in the design, the set up of the structure is shown in fig 6.6.

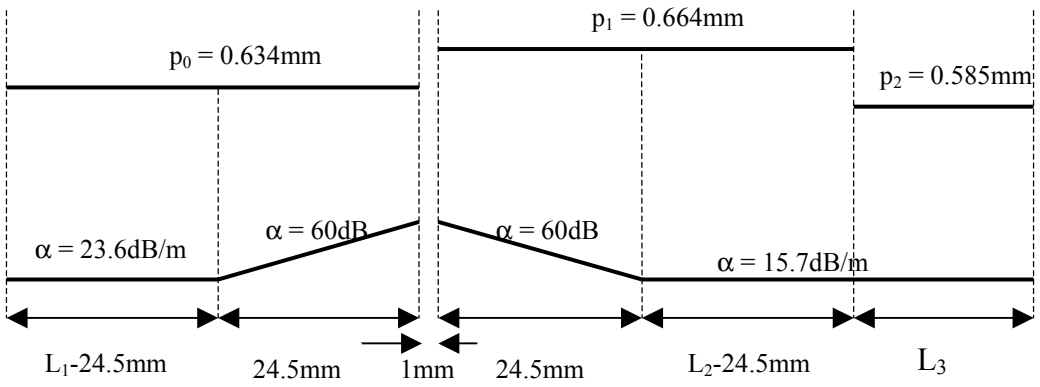

Fig 6.6 Representation of the pitch and loss profiles for a double step taper

6.2.4.1 Design of the Input Section Length

To determine the length L_1 of a positive/negative step taper, the approach by [6] is to simulate a single positive step taper with two sections. The first section consists of a pitch p_0 and the second section has an arbitrary length L_2 with a pitch p_1. L_1 is then varied for maximum RF current for a given drive level. This approach was carried out and is shown in Appendix B. The Appendix also gives an insight into how L_1 affects the bunching in a single negative step taper. Figure 6.7 shows that when the input drive level is varied the RF current peaks at different power levels. To determine the maximum current, it is therefore necessary to scan across the input power range. The figure also shows that all of the maximum current values are fairly similar. An alternative method for the determination of L_1 is therefore required.

From the sensitivity analysis shown in Chapter 6.3.2, the variation of L_1 within a full helix structure only affects the small signal gain. The results (in fig. 6.25b) show that the small signal gain is reduced by 5/8 dB for every mm reduction in length. Neither the AM/AM or AM/PM conversion nor the saturation efficiency is affected by L_1. This parameter should therefore be used to achieve maximum signal gain in this region. Since the gain grows with L_1, the longest input length is favourable. However, since too much gain in the input region will cause it to oscillate with frequency, a length of say 70mm which gives maximum gain without these oscillations is selected.

The other parameters to be optimised specifically for a double-step taper design are the lengths L_2 and L_3. For the optimisation of these parameters, the full structure as shown in fig. 6.6 is used

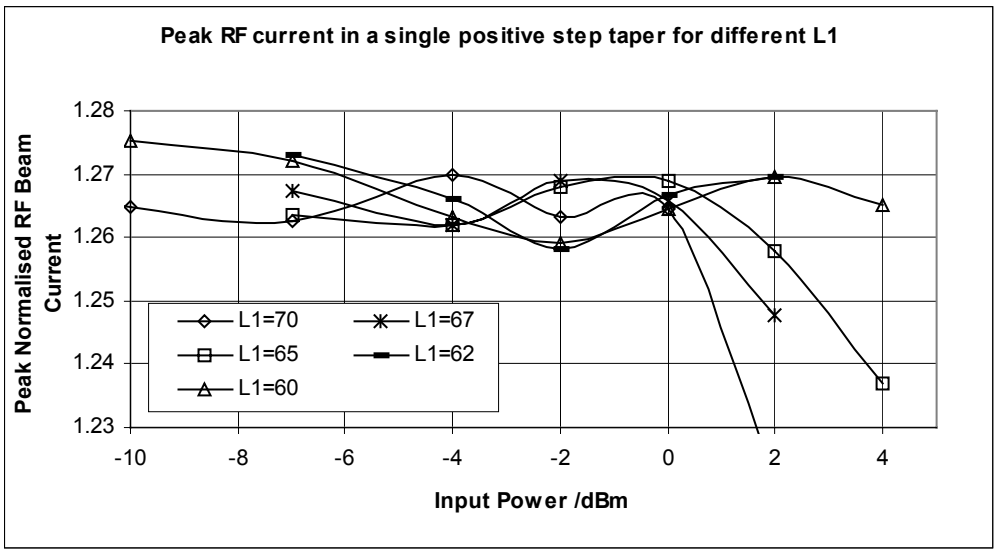

Fig 6.7 Maximum RF/DC beam current versus input power for a given range of input section lengths

6.2.4.2 Design of the Centre Section Length

For the determination of L_2, the output section length L_3 was set to an arbitrary length of say 30mm, and L_1 was set to 70mm for maximum small-signal gain.

The previous approach [6] was to adjust the centre section length for maximum forward power in the circuit for a particular drive level. Fig 6.8 shows that this occurs when L_2 = 63mm for a drive power –12dBm. The AM/AM curves (in fig 6.9) show however that the power peaks of the various lengths L_2 occur at different drive levels. The saturated output powers are also similar across the L_2 range of 58mm to 68mm. An alternative strategy is therefore required for the selection of the centre length region L_2.

By observing the nonlinear performance at the output, L_2 has a minor influence on the shapes of the AM/AM shapes: they appear fairly similar except for a slight increase in radial curvature for higher L_2 values. At the initial point of gain compression, a slight increase in the slope above 45° is observed on all of the AM/AM curves. This has detrimental impact on the linear performance and is due to the length L_3 set too long. The slight oscillations of the output power in overdrive are probably due to the oscillations of the bunch within the potential well of the circuit field. The phase conversion (fig 6.10) also shows to be similar for the various lengths of L_2: a poor Kp of 5°/dB. This is because L_3 and other helix parameters have not yet been optimised for a linear performance. The conversion efficiencies at saturation (in fig. 6.11) show minor variations: a slight decrease for shorter lengths.

Since this centre region is where electron bunches are formed, L_2 should be adjusted to optimise this. The sensitivity analysis in Chapter 6.3 confirms this suggestion by showing that the electron bunch intensity is indeed influenced by L_2.

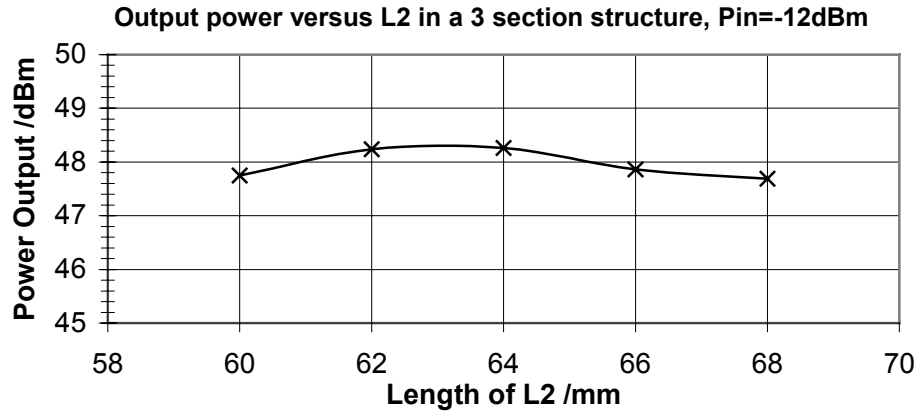

Fig 6.8 Output power as a function of centre region lengths for an arbitrary output section length and a drive level of –12dBm.

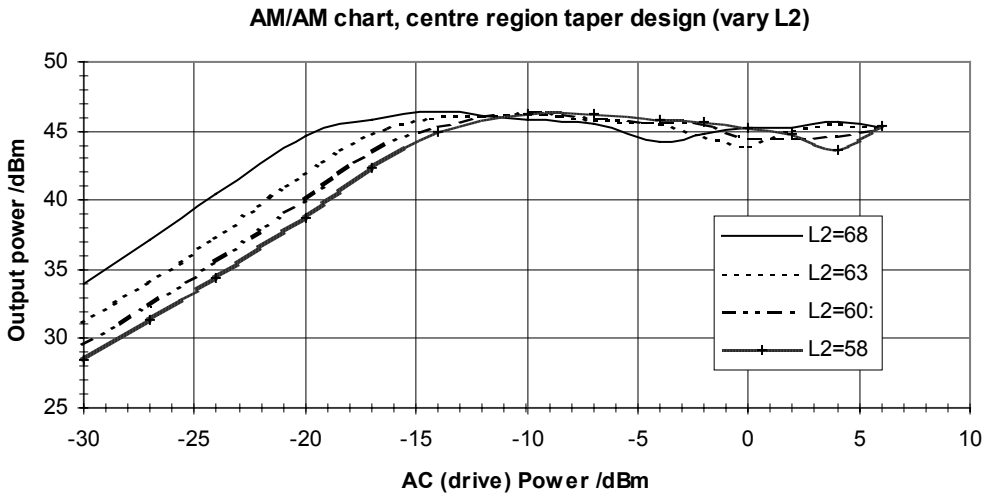

Fig 6.9 AM/AM curves for a range of centre region length values

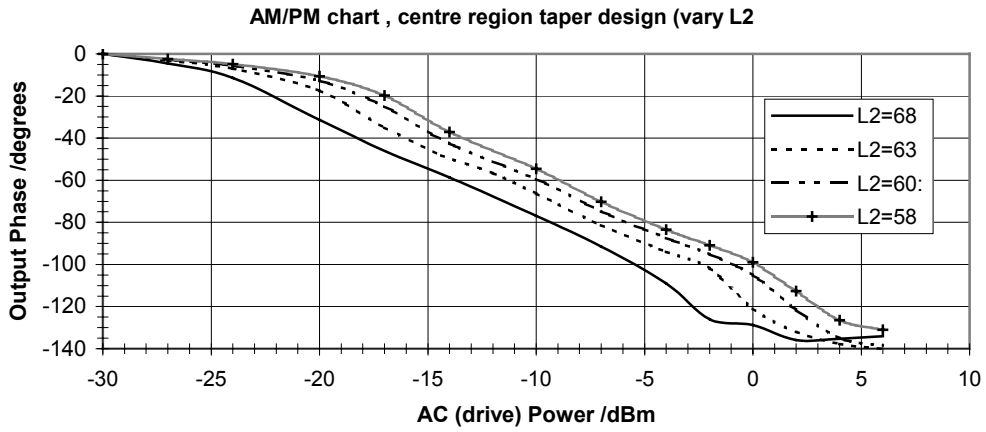

Fig 6.10 AM/PM curves for a range of centre region length values

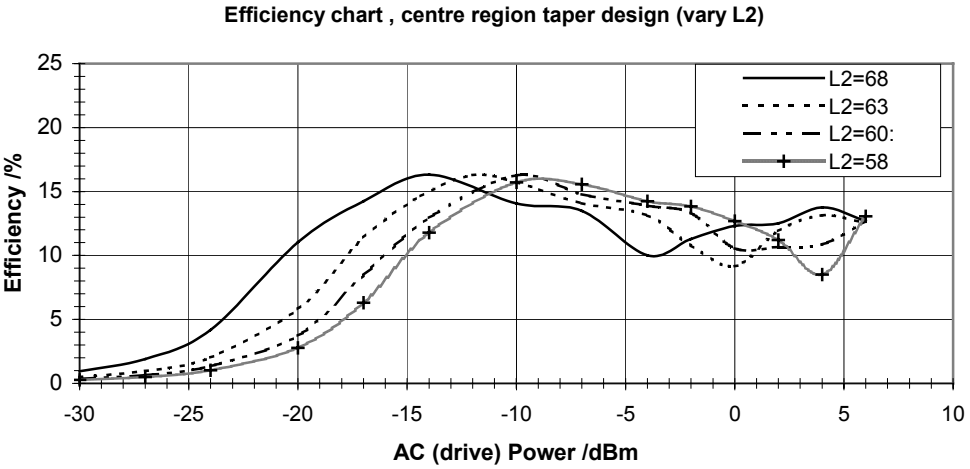

Fig 6.11 Conversion efficiencies for a range of centre region length values

6.2.4.3 Design of the Output Section Length

The output section length L_3 has a major impact on all of the properties of the tube as seen in figures 6.12 to 6.14 for a range of L_3 from 10 to 35mm. Fig. 6.12 shows that a longer output section requires less RF drive power to reach output saturation, this is because the small signal gain increases for longer tubes.

The shortest output section of 10mm has a well-behaved curve reaching saturation at 47dBm. As the length is increased from 10 to 17mm, the saturated output power is 1.1dB higher for the same drive power of 2dBm and the power curve is flatter in overdrive. As L_3 is increased beyond 20mm, the saturated power decreases. The shape of the AM/AM curves also becomes undesirable beyond L_3=25mm, this is because the curves are nonlinear at a large output backoff as their slopes become greater than 45°. An optimum output section length for maximum power extraction exists which results in maximum efficiency. This optimum length was chosen to be L_3 = 17mm. The reason for this can be seen more clearly in the efficiency curve (fig 6.14), where the maximum is around 23.5%. The phase lag (fig 6.13) increases for a longer output section. The rate of this increase per mm increase in L_3 is around +0.15°/dB.

The increase in phase lag when the output section is made longer is probably related to the greater reduction in the beam velocity, as discussed in Chapter 4.4.4. Because the beam is remaining in a decelerating phase in overdrive is minor, a longer output section continues to reduce the beam velocity, resulting in higher phase conversion. The final design for a double-step taper is shown in fig 6.15.

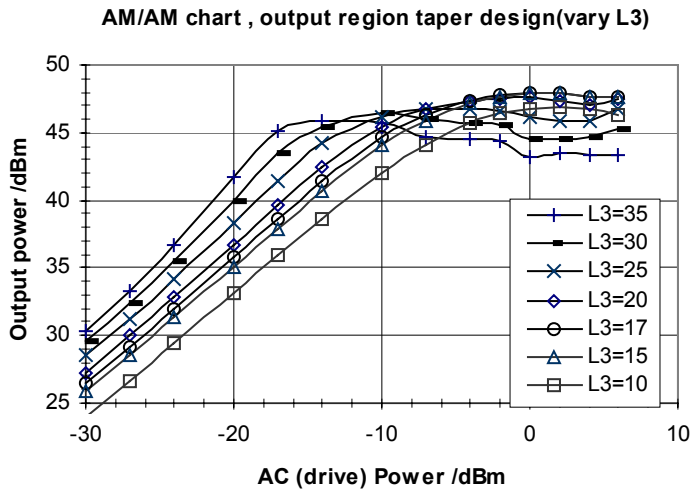

Fig 6.12 AM/AM curves for a range of output section length values

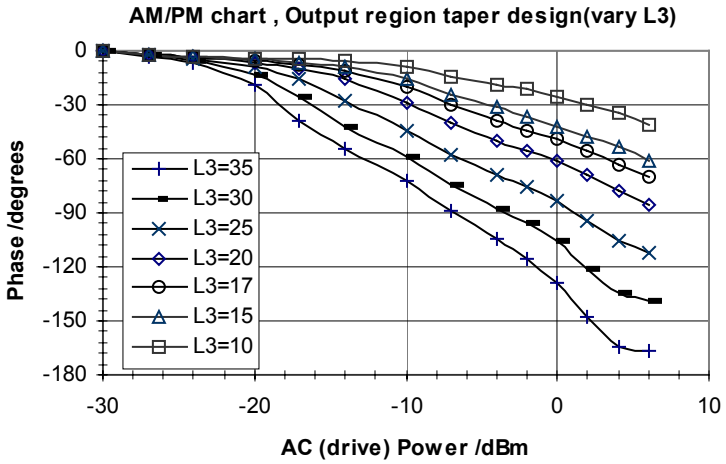

Fig 6.13 AM/PM curves for a range of output section length values

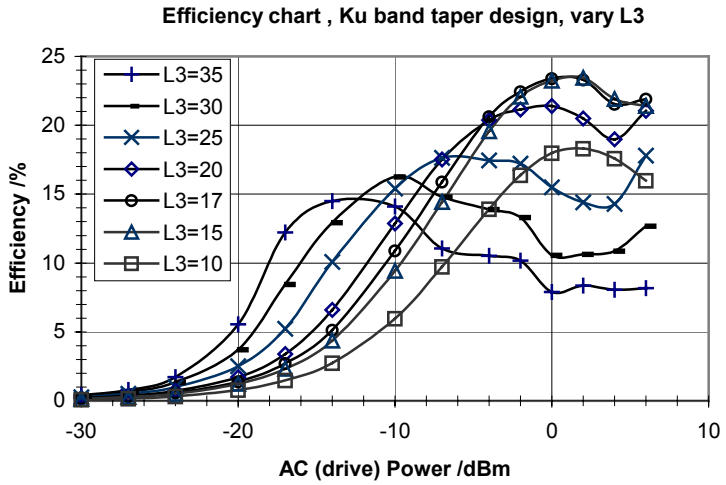

Fig 6.14 Efficiency curves for a range of output section length values

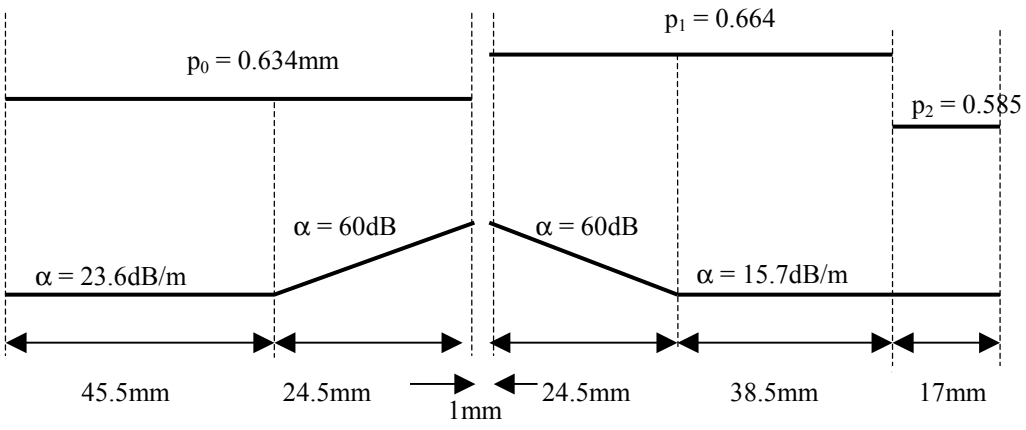

Fig 6.15 The pitch and attenuation /sever profiles of a double step taper design.

6.2.5 Design of a Linear Taper in a Non-Uniform Slow-Wave Structure

Towards the output end of the tube, the phase velocity of the electron beam must be reduced systematically to maintain the phase relationship between the beam and the helix and to maximise the saturated output power. The way in which the RF power is extracted from the beam by the helix is fundamental to the whole operation of a TWT and its nonlinear performance. The reduction of the forward wave phase velocity in the output region must therefore be done in a controlled way. This transition will be incorporated into the present three step design to complete the full slow-wave structure.

From the position in the tube where the bunch intensity is maximum, the pitch of the helix is reduced systematically from p_1 to the condition where maximum power extraction is achieved (at p_3). This linear pitch transition is shown in fig.6.16. The slope of the A-B transition must be chosen to maximise the transfer of energy from the beam to the helix. This power transfer should be consistent for each electron, so that the velocity distribution of the electrons is minimised thereby enhancing the recovery of the spent beam energy by the collector. The effect of the phase velocity reduction on the nonlinear properties of the TWT must also be investigated, so that the best trade-off between power extraction and linearity can be attained in the design.

Extensive modification had to be done to the LSM program to enable the helix propagation properties (i.e. the circuit attenuation, axial propagation constant and interaction impedance) to vary linearly with each plane in the structure.

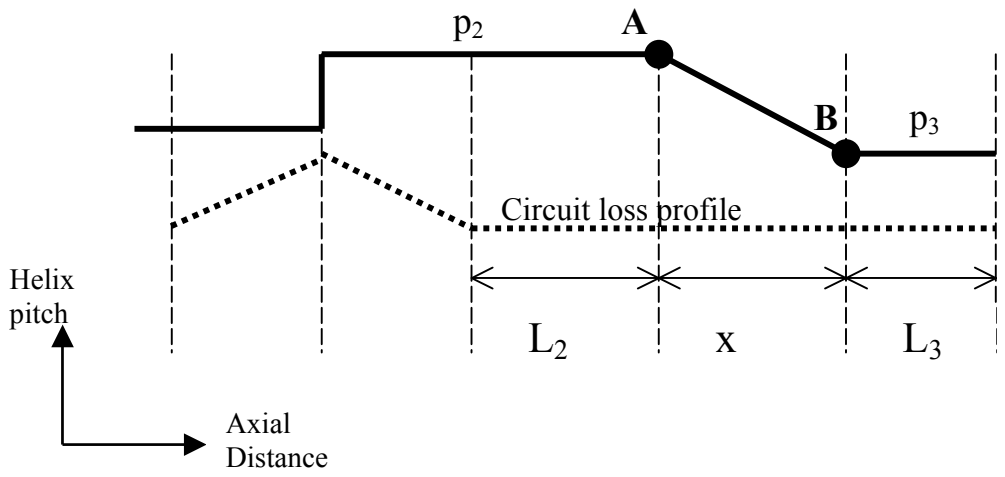

Fig 6.16 Helix pitch profile with a linearly decreasing circuit phase velocity region

The design procedure was as follows:-

1. Estimate x by considering the practical total length of the tube
2. Adjust the ratios L_2/x and L_3/x for maximum efficiency and linearity

The variation of L_2/x is equivalent to adjusting the point A (in fig. 6.16) in the axial direction, keeping everything else fixed. Likewise, varying the L_3/x ratio adjusts the position of B in the axial direction. Figures 6.17a-c show the AM/AM, AM/PM and efficiency transfer curves respectively, for a range of L_3/x values. When the ratio of L_3 to x is adjusted with L_2 set at 23.5mm, the nonlinear performance is affected across a wide dynamic range, as revealed in the AM/AM curves (see fig 6.17a). The phase conversion is increased from 2.8 to 4°/dB as L_3/x is increased across the wide range of values (in fig 6.17b). A positive-negative step taper gives a good phase performance of 2.8°/dB. These results reveal that this phase nonlinearity is not improved by including this linear taper transition from a stepped taper; this may be due to the initial chosen value of L_2.

As L_3/x is adjusted from the maximum of 20/10 to 6/24, the efficiency increases across the range of input powers (fig 6.17c). At approximately 4.5dB output backoff, the efficiency increases from 7 to 11%. As L_3/x is reduced further, the efficiency then reduces slightly until L_3 becomes zero, i.e. when there is no uniform pitch in the output region. The choice of the optimum L_3/x value of 6/24 was selected for maximum efficiency at the estimated output back-off level.

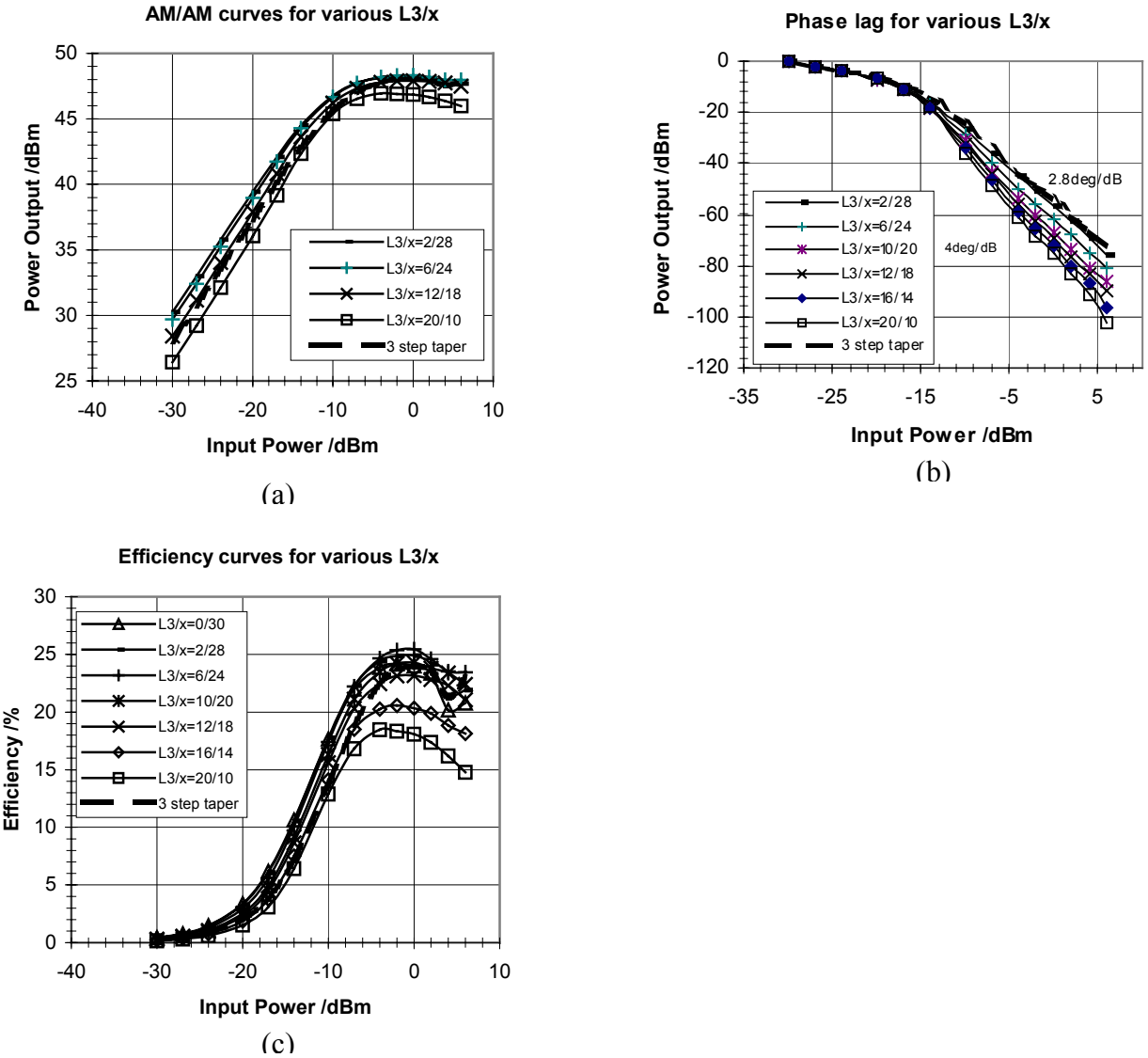

Fig. 6.17a-c AM/AM, AM/PM and efficiency transfer curves for various L_3/x.

Figures 6.18a-c show the AM/AM, AM/PM and efficiency transfer curves respectively, for a range of L_2/x values, with L_3 set at 6mm. Figures 6.18a-b show that L_2/x has a much less influence on the amplitude and phase transfer curves across the dynamic drive range. Some of the AM/AM transfer curves are not completely linear at 3dB or more of output backoff; the phase conversion is also increased to 3.5°/dB for L_2/x = 23.5/26. At saturation, the efficiency is enhanced (from 24 to 26.5%) when L_2/x is increased from L_2/x to 26.5%, as shown in fig. 6.18c. The choice of optimum L_2/x of 29.5/20 was based on a trade-off between linear AM/AM transfer curves and low phase conversion.

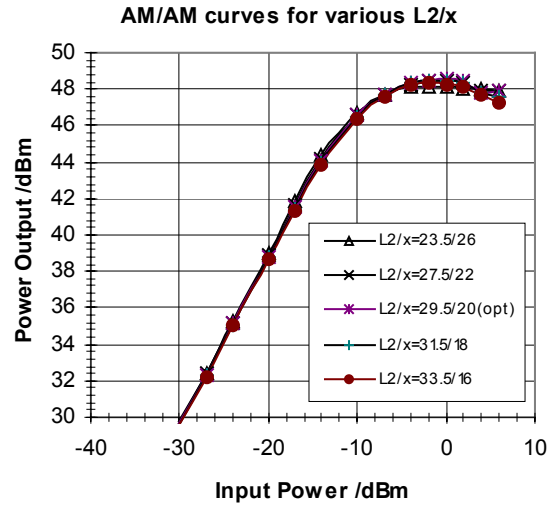

(a)

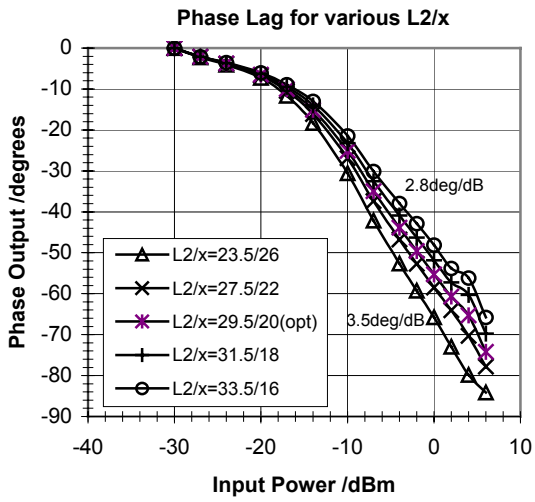

(b)

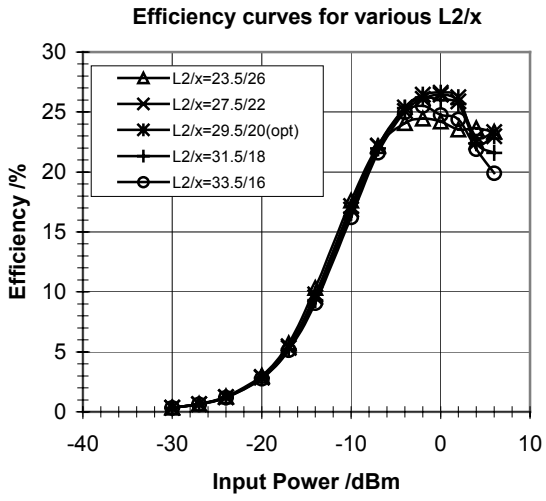

(c)

Fig 6.18a-c AM/AM, AM/PM and efficiency transfer curves for various L_2/x values.

The final values for the slow-wave structure were chosen to be: L_2 = 29.5mm, x = 20mm and L_3 = 6mm. The results reveal that including a linear taper to the structure, which is optimised for performance:-

- improves the backed-off conversion efficiency by around 3% from a stepped pitch profile. At power saturation, this efficiency improvement is actually slight less (2% improvement). This difference in performance between a stepped pitch profile and a linearly tapered one, is less than one might expect.
- does not improve the linear performance from a stepped pitch profile. A slow-wave structure where the helix pitch decreases uniformly until the very end of the structure produces an efficient performance which is close to the optimum.

The transfer characteristics for the final optimised design is shown in fig. 6.19a-b with one harmonic included in the simulation. This design will be used for a broadband and collector performance analysis in Sections 6.4 and 6.5. In the next section, an analysis will be carried out on the sensitivity of the 6 design parameters for a stepped pitch profile. Firstly: this will test the sensitivity of each parameter on the performance, secondly: provide an insight on the physical processes that are affected by each parameter and finally: verify the choice of parameters.

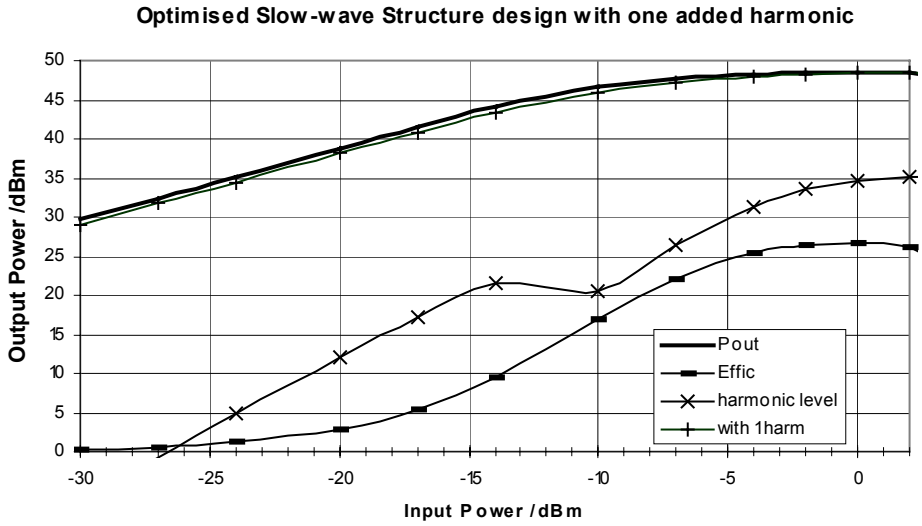

(a)

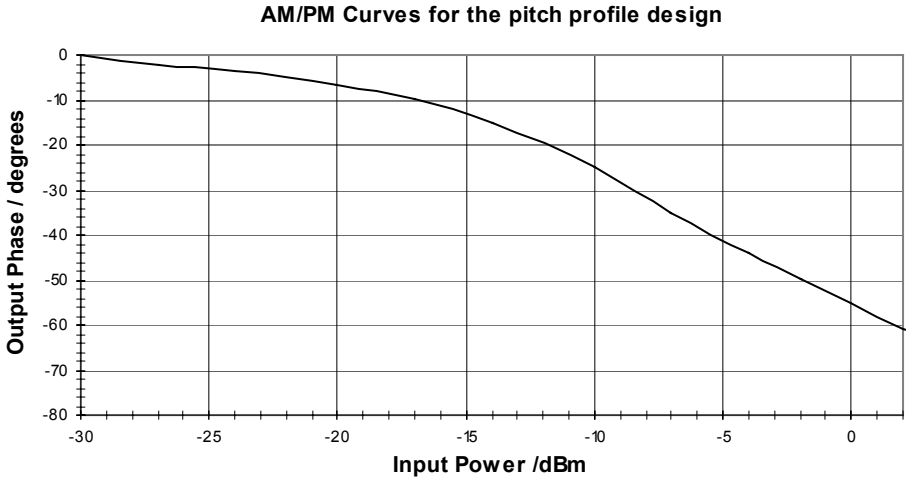

(b)

Fig 6.19 Transfer characteristics of the final tapered slow-wave structure design

6.3 The Effect of the Design Parameters on the Performance of a Double-Step Taper - a Sensitivity Analysis

This section covers a systematic investigation on the sensitivity of the section lengths and pitches on the nonlinear performance. The purpose is to determine and quantify which parameters have significant influence on the nonlinear characteristics. For example, the region of the TWT where the phase shift is most sensitive to the helix pitch adjustments. The Applegate diagrams and other information (versus axial distance z) will be provided to explain the physical influence the parameters have on the TWT nonlinear interaction processes. Simulations were carried out using three values for each parameter; the parameters being the helix pitches and lengths of the three regions: p_1, p_2, p_3 and L_1, L_2, L_3 respectively. Since this is a stepped pitch profile, the linear pitch transition length x = 0mm. The centre of the each of the three design values is the optimum. All parameters were set to their optimum value, apart from the parameter which is being varied. Table 6.1 lists the design parameters and their values.

Table 6.1

p_1 /mm	0.61	0.634	0.65
p_2 /mm	0.64	0.664	0.69
p_3 /mm	0.57	0.585	0.60
L_1 /mm	56	60	64
L_2 /mm	59	63	68
L_3 /mm	14	17	21

6.3.1 Effect of the Input Section Pitch on the Performance

The input section of the helix is where the growth of the RF signal occurs. Within this region, the amplitude of the RF signal is relatively small and linear. Therefore, the properties of the helix in this region mainly affect the growth of the low power signal. Figures 6.20 to 6.21 show the AM/AM, AM/PM, efficiency and gain. The shapes of the AM/AM curves appear to be similar for the different pitch values used, the phase conversion (i.e. the slope of the AM/PM curves) also remains constant. Therefore, this parameter has a minor influence on the transfer curves. The saturation efficiency (fig. 6.21a) is also unaffected by the variation in p_1. However, the gain at the small signal levels is noticeably different, as shown in fig 6.21b. The maximum small-signal gain is when p_1=0.634mm; this is the chosen optimum value. This advantage of having high small-signal gain is that less AC drive power is required for a given output power level. Saturation therefore takes place at a lower input level. This is useful for the amplification weak uplink signals in the satellite.

Fig. 6.22 shows the bunching of the beam phase (relative to the forward circuit wave) for the three input region pitch designs. These plots are all taken at around 3dB of output backoff (approximately corresponding to drive levels, (a) -7, (b) -10, (c) -7dBm) for the most effective comparison. The phase velocity transitions are clearly noticeable by the slopes of the curves, while the bunching intensity remains unaffected. The variation of the input region phase velocity also has noticeable effect on the relative phase plots in the input section of the tube (fig. 6.23); these show the phase of the RF beam current relative to the RF forward voltage versus axial distance. A value of p_1=0.634mm increases the initial growth phase to over 280°, and remains more flat in the growth region. This results in higher gain.

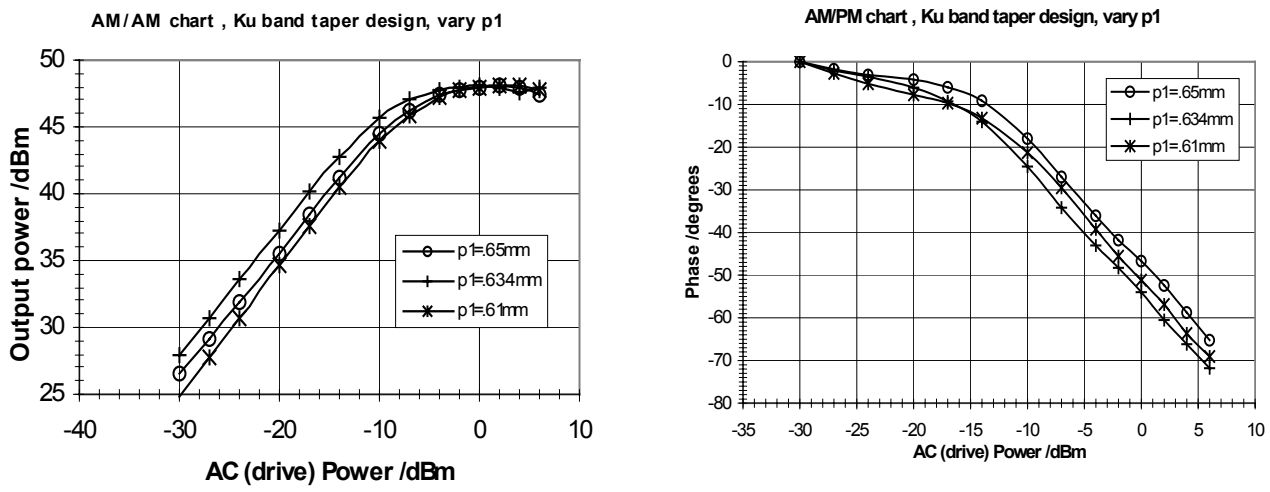

(a) (b)

Fig 6.20 AM/AM and AM/PM curves for a range of input section pitch values

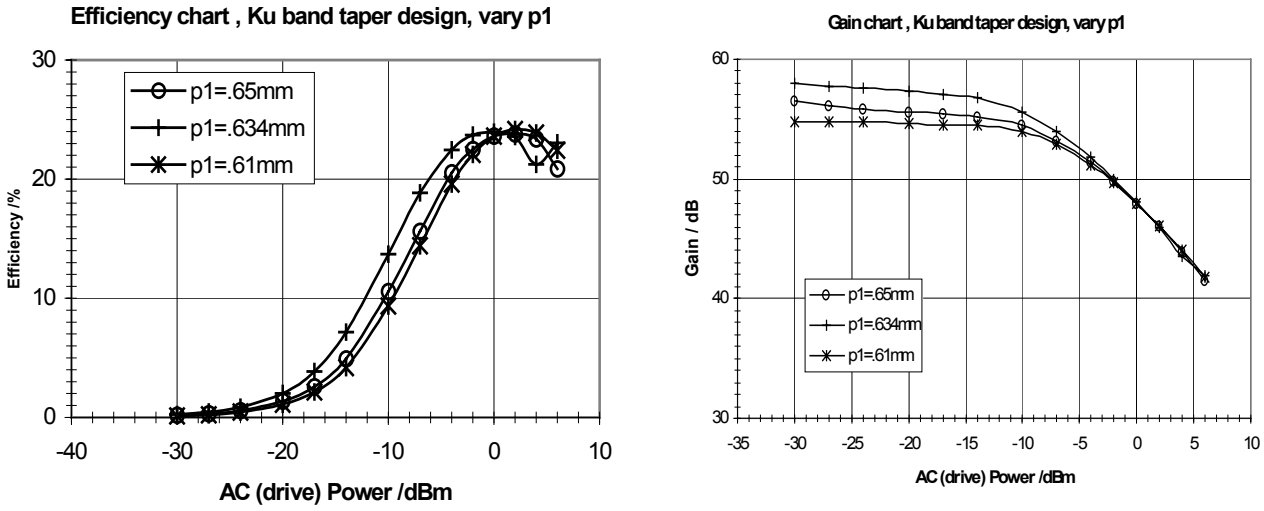

(a) (b)

Fig 6.21 Output efficiency and gain as a function of input RF power for a range of input section pitch values

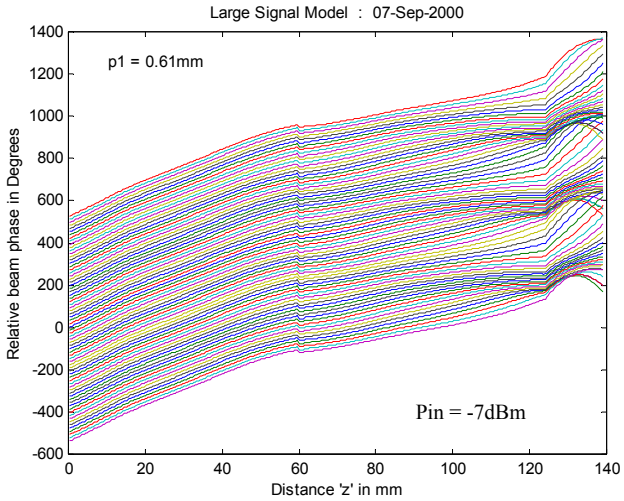

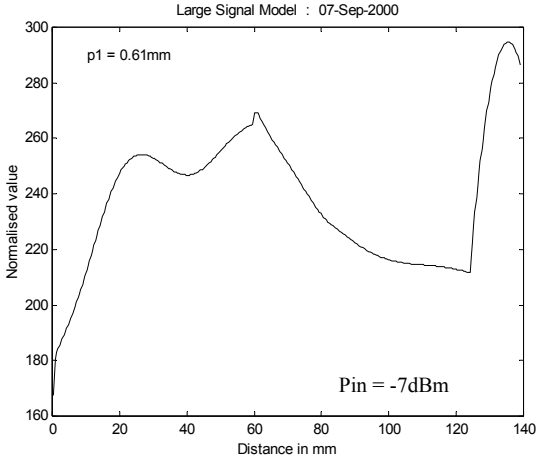

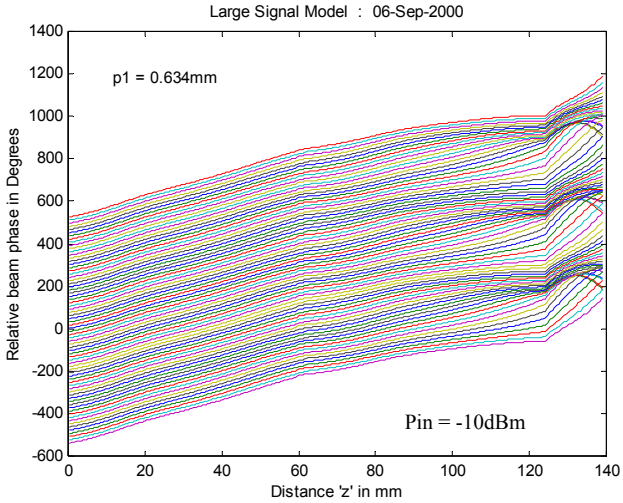

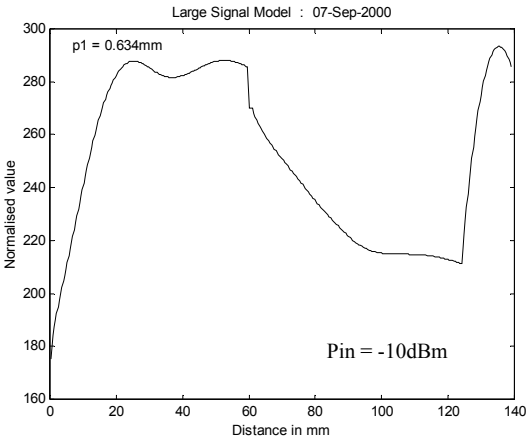

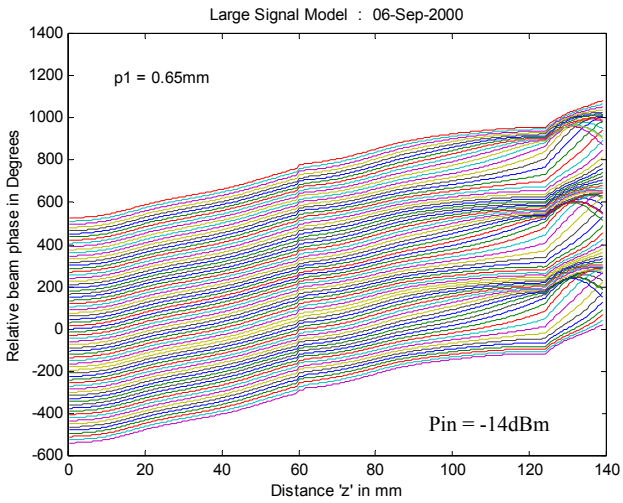

Fig 6.22 Beam bunching plots for the corresponding input section pitch values.

Fig 6.23 Relative phase profiles for the corresponding input section pitch values.

6.3.2 Effect of the Input Section Length on the Performance

When the input section length is varied, the phase properties of the RF structure are not affected. Instead, the initial gain is allowed to grow for a longer distance before it is severed. The change in the input section length therefore has a strong influence on the small signal gain. The behaviour is shown in fig. 6.25b

Figures 6.24a,b and 6.25a show the transfer curves and output conversion efficiency respectively. The change in the input section length has a very minor effect on these output characteristics as illustrated.

The change in the length L_1 of the initial pitch p_1 is clearly seen in the bunching profiles in fig 6.26 (all taken at approximately 3dB from saturation). The effect of L_1 on the bunching is minor however in the other two regions (whose lengths were kept constant throughout). The beam and circuit phases and velocities are therefore largely unaffected by L_1. The gain is affected however, and is shown in fig 6.27. Within the first region, the gain (and RF power) is allowed to grow, up to the point where it is severed. Therefore a longer initial section allows more growth in output RF power. Beyond the sever, the power growths are similar, as there is no variation in circuit parameters. At the output end, the gain does however slightly increase with L_1 (just below power saturation). Beyond power saturation, the gain output is independent of L_1.

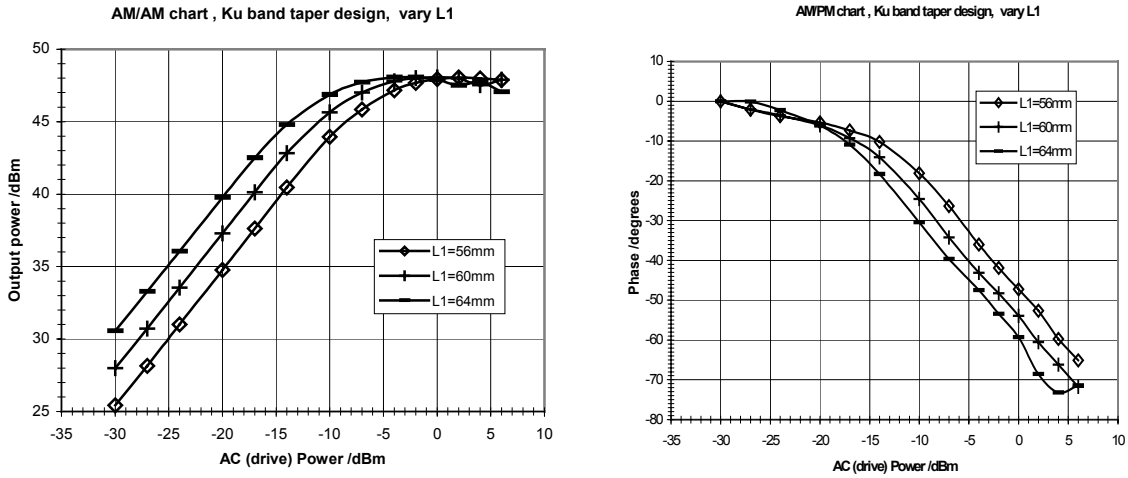

(a) (b)

Fig 6.24 AM/AM and AM/PM curves for a range of input section lengths

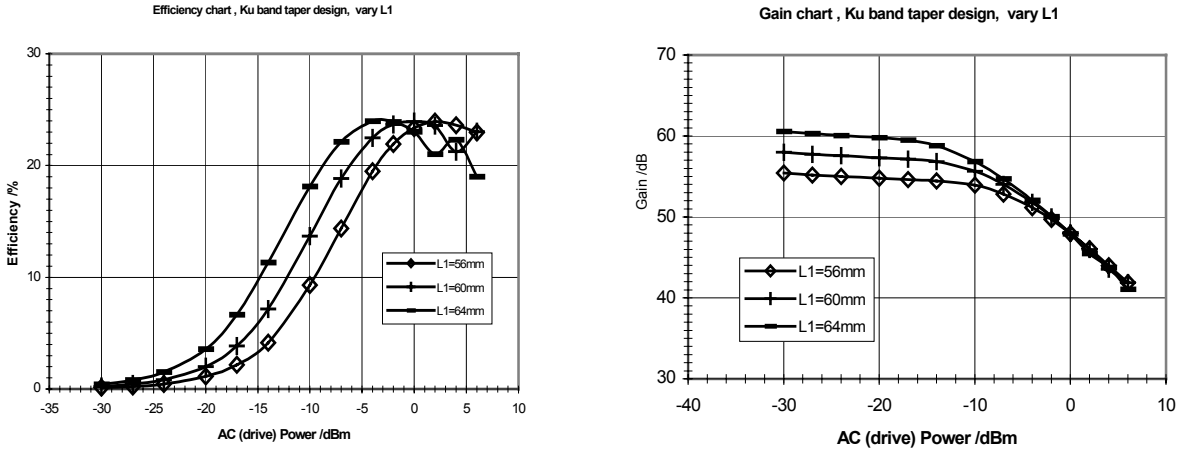

(a) (b)

Fig 6.25 Output efficiency and gain as a function of input RF power for different input section lengths

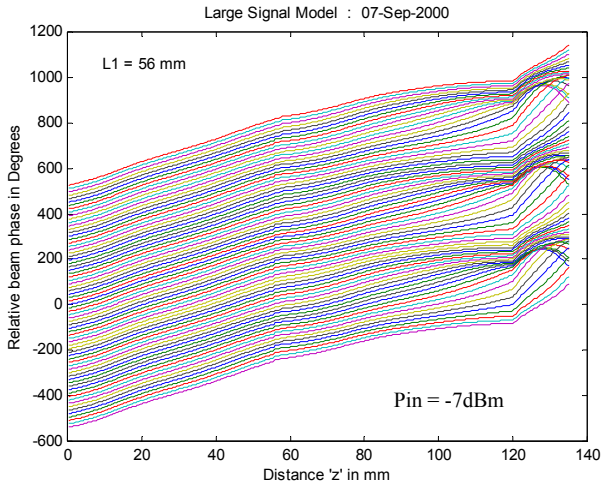

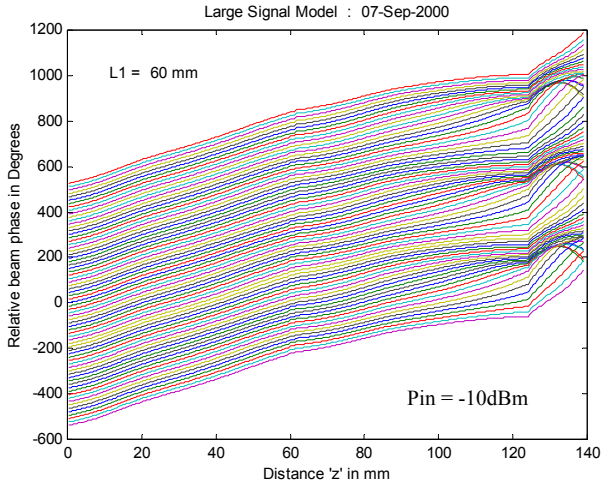

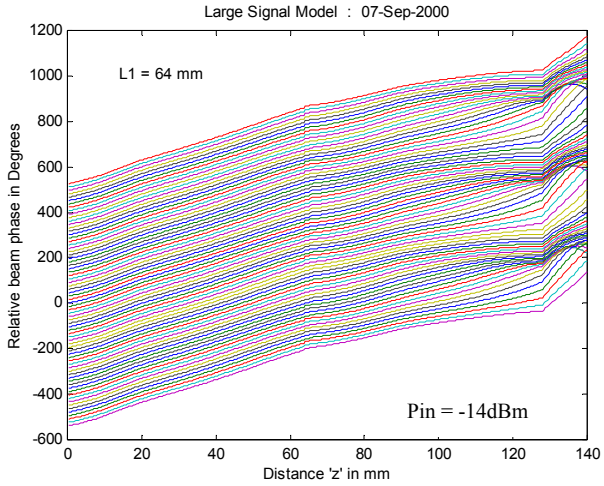

Fig 6.26 Beam bunching plots for the corresponding input section length values

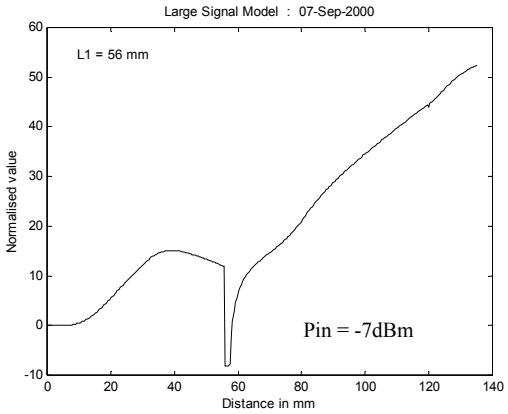

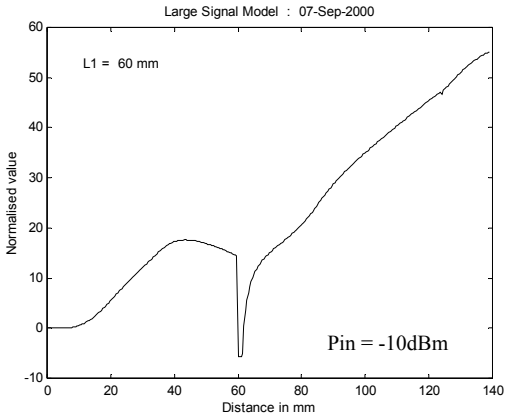

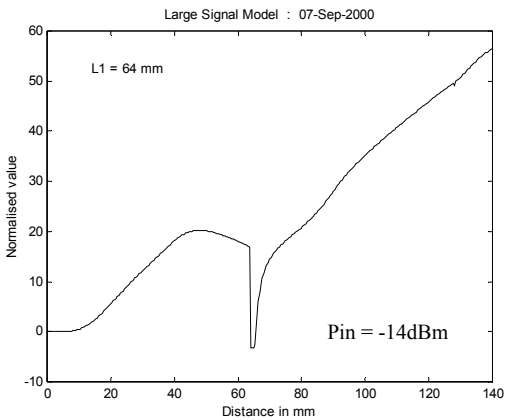

Fig 6.27 Gain growth versus axial distance for the corresponding input section lengths

6.3.3 Effect of the Centre Section Pitch on the Performance

The centre region is where beam phase variations occur and electron bunches develop. Since the helix pitch design in this region p_2 has a strong influence on the bunching and the non-linear performance, it is optimised for these purposes. The centre region pitch begins from the sever (for practical convenience) and ends where the pitch is lowered for power extraction. The simulation results show that the phase velocity of the helix has a major influence on the velocity of the electrons. The output power is affected and so is the output phase. The AM/AM curves for the three pitch values are shown in fig. 6.28a. As p_2 is increased, a higher drive level is needed to saturate the output power. The level at which the power saturates reaches its optimum at 0.664mm. This was the value chosen from the design method described earlier in Ch. 6.2.3. The trend of the AM/AM shapes for p_2 = –24μm and +26μm is also illustrated in the figure: the latter case reveals that the radial curvature of the AM/AM curve is the smallest, but the angle beyond saturation is the greatest.

The AM/PM curves are shown fig. 6.28. As the pitch is increased the phase conversion is reduced at a rate of 2.97° / dB between the two extreme cases; the rate is 0.59° / dB per mm decrease in p_2. The physical reason why the phase lag increases with decreasing pitch is uncertain. The bunching profiles (fig 6.30) reveal differences in the output section, which may provide insight into the physical interactions. When p_2=0.64mm (fig. 6.30a), the relative beam velocity seems constant up to the non-linear region. This forces the electrons with the least phase to be accelerated into a bunch. The electrons with the highest phase are not compressed into a bunch, but are just left to accelerate. When p_2=0.69mm (fig. 6.30c), the relative beam velocity is less, causing the electrons with the lowest phase to be left to accelerate, while the electrons with the highest phase are bunched. For the intermediate case, the RF circuit phase is such that there is the most electron bunch compression before the negative step taper. This results in optimum RF current induction in the helix, as shown in figure 6.31a. The optimum case also shows that there are a greater number of decelerating electrons at the output end. Thus more power is transferred to the circuit resulting in optimum efficiency as shown in fig. 6.29. Plots of the RF voltage phase relative to the current

phase as a function of axial distance are also shown in fig 6.31b to illustrate the change in the centre region phase velocities.

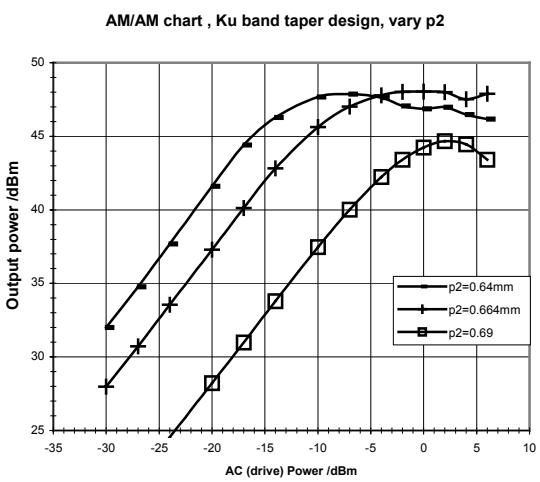

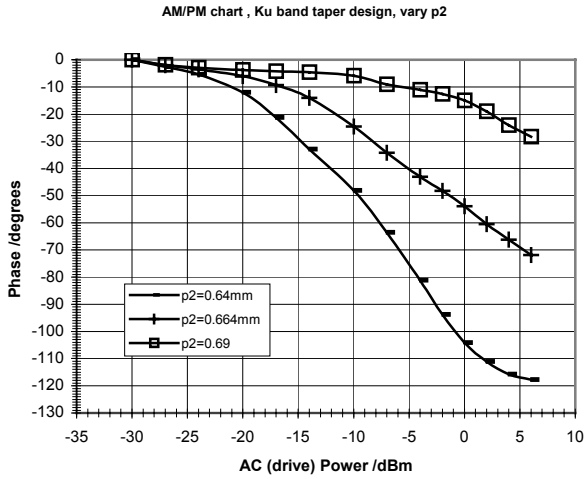

(a) (b)

Fig 6.28 AM/AM and AM/PM curves for a range of centre section pitch values

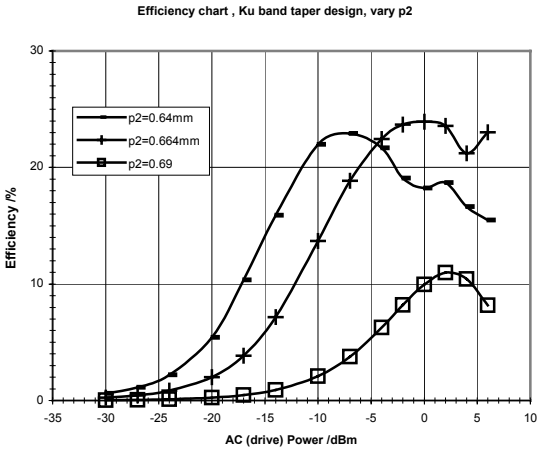

Fig 6.29 Efficiency curves for a range of centre section pitch values

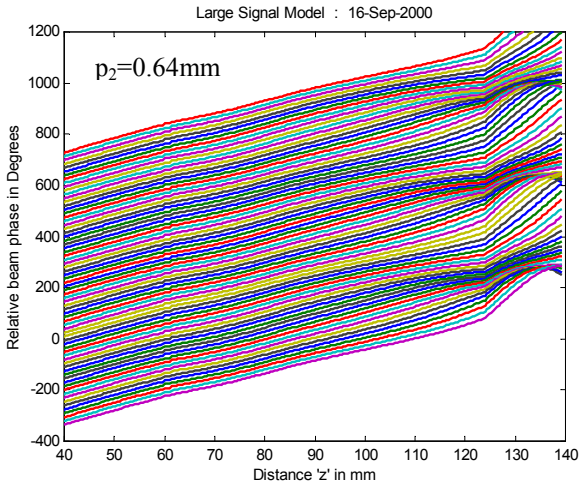

(a)

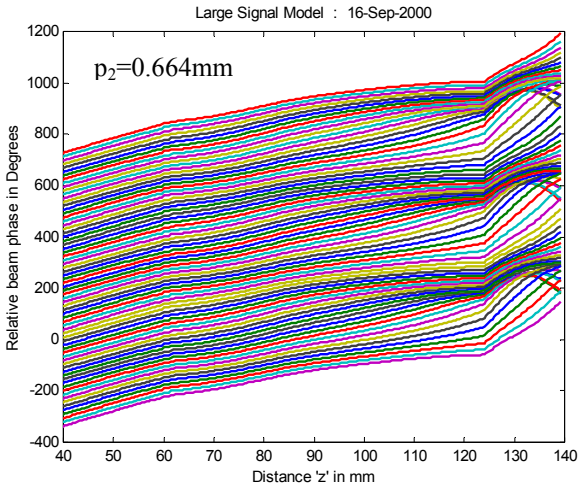

(b)

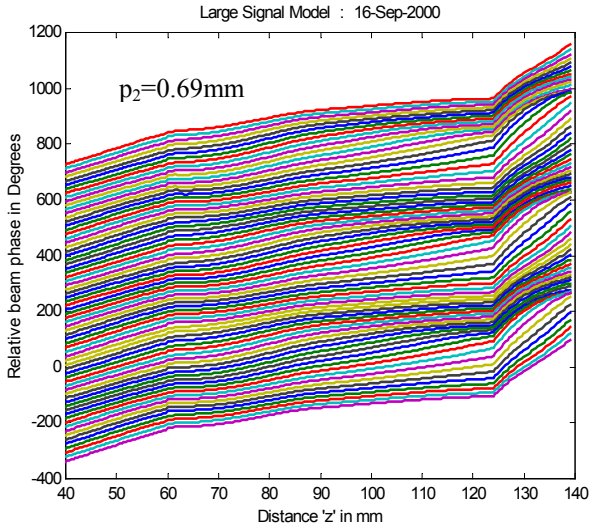

(c)

Fig 6.30 Beam bunching diagrams for the corresponding middle section pitch values: p_2 = (a) 0.64mm (Pin=-14dBm), (b) 0.664mm(-7dBm) and (c) 0.69mm(-3dBm).

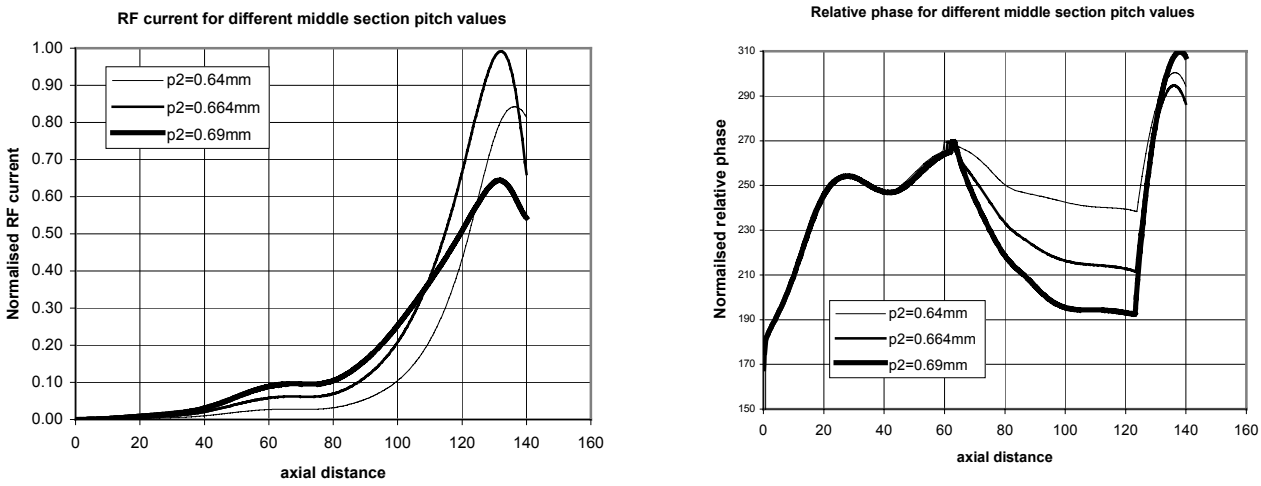

(a) (b)

Fig 6.31 RF current induction relative phase versus axial distance for the corresponding middle section pitch values

6.3.4 Effect of the Centre Section Length on the Performance

The influence of the centre section length on the nonlinearity of the amplifier is very minor. For the AM/AM shapes remain similar throughout the range of variation (9mm), as shown in fig 6.32a, and the phase conversion (fig 6.32b) is the same. This is mainly due to the unaffected relative beam phases at the output, as shown in the bunching diagrams (fig. 6.34). The intensity of bunching at the negative step transition however differs. This is clearly seen in fig 6.33b, which shows the RF current generation for the different cases. This length therefore influences the formation of electron bunches and the bunching intensity, but not the nonlinear performance at the output end. Fig. 6.33a shows that L_2 has a slight affect on the conversion efficiency: a length of 68mm results in about 1% more efficiency than that of 59mm. This is because the signal power is allowed to grow over the longer distance. In the design procedure, the length of this region is optimised for the most favourable bunching condition in the same way as the centre region pitch.

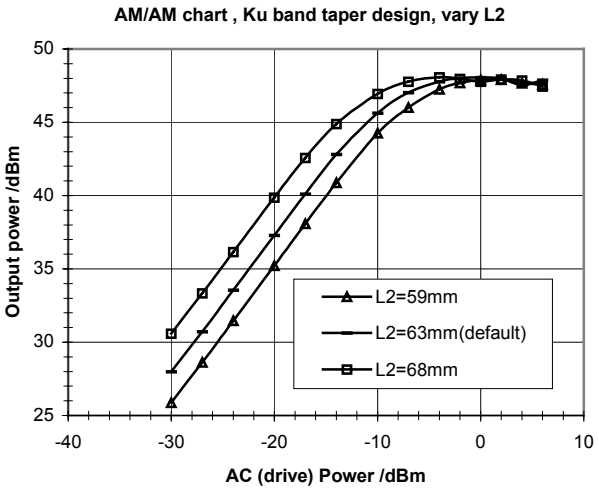

(a)

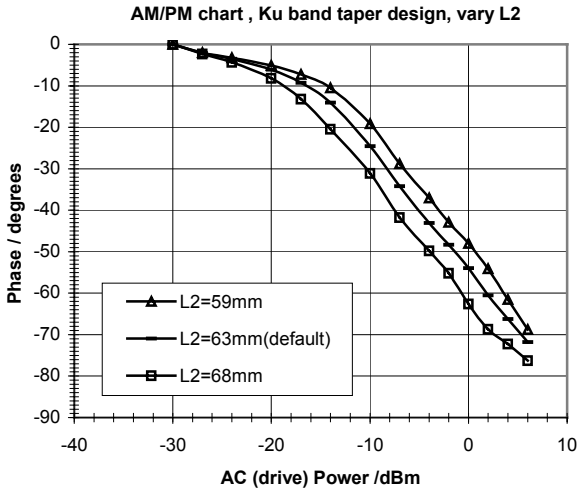

(b)

Fig 6.32 AM/AM and AM/PM curves for a range of middle section lengths

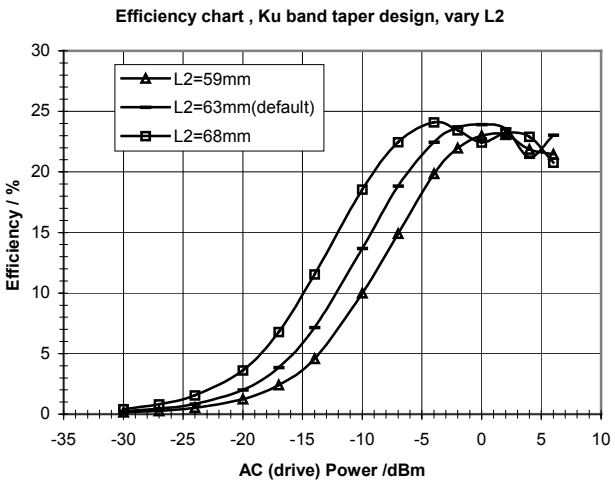

(a)

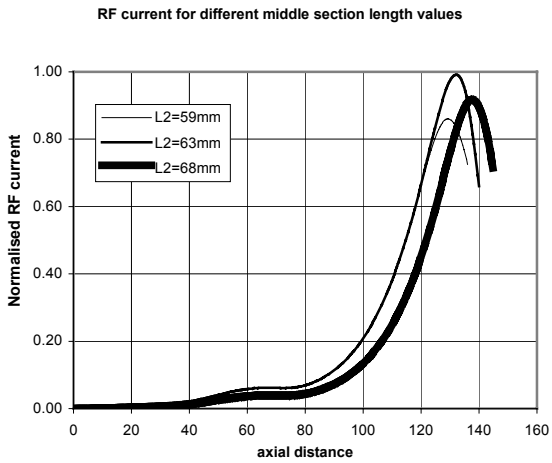

(b)

Fig 6.33 (a) Efficiency curves and (b) RF current curves versus axial distance for a range of middle section lengths

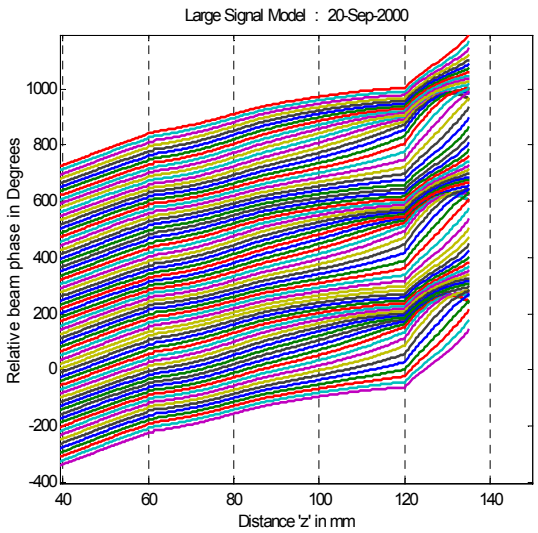

(a)

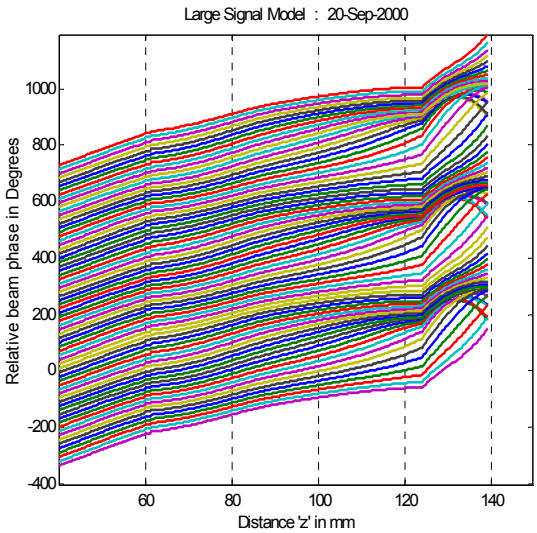

(b)

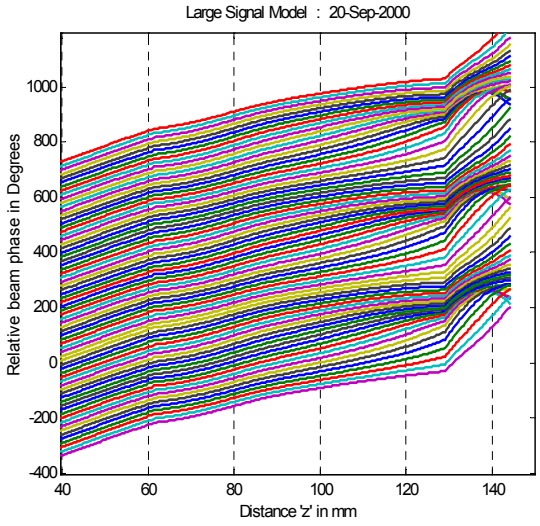

(c)

Fig 6.34a-c Applegate diagrams for L_2 = 59mm (Pin=-7dBm), 63 (Pin=-10dBm) and 68mm (-14dBm) respectively

6.3.5 Effect of the Output Section Pitch on the Performance

The output region is where the pitch is reduced to a point where, for an acceptable C/I, as much energy is extracted from the beam as possible. This region exhibits non-linear RF power growth in the tube. Varying the dimensions of the helix in this region therefore strongly influence the linearity of the output power and phase conversion. Since this region is where power extraction occurs, the output conversion efficiency is strongly dependent on the pitch.

As the pitch in the output region is increased, the output power saturates at lower drive levels as shown in fig 6.35a. The saturated output power reaches its maximum at around p_3=0.60mm. When the pitch is increased beyond this point, the saturated power drops rapidly (reducing the efficiency) and the angle of the AM/AM curve with the horizontal in overdrive is greater.

The corresponding AM/PM characteristics are shown in fig. 6.35b. The pitch corresponding to the minimum phase lag condition is relatively high, i.e. greater than 0.69mm (from fig. 6.28b). Therefore the phase conversion increases at a rate of about 0.25° per μm decrease in pitch. This is considerably less than that for the centre section, which implies that the nonlinear performance is more sensitive to any variations in the centre region.

The conversion efficiency characteristics are given fig 6.36. The peak efficiency is maximum at p_3=0.60mm. This differs to the single section determination (section 6.2.3), which predicted maximum tube efficiency at 0.585mm. This is probably due to the more inaccurate method taken at that time to determine the optimum value from one or two power levels. However the difference is only 0.6%.

Two Applegate diagrams are shown in fig 6.37 to compare the differences in phase and efficiencies at the same output backoff of around 2dB. The near optimum case in fig. 6.37b shows the bunching to be more confined, resulting in improved phase lag and efficiency.

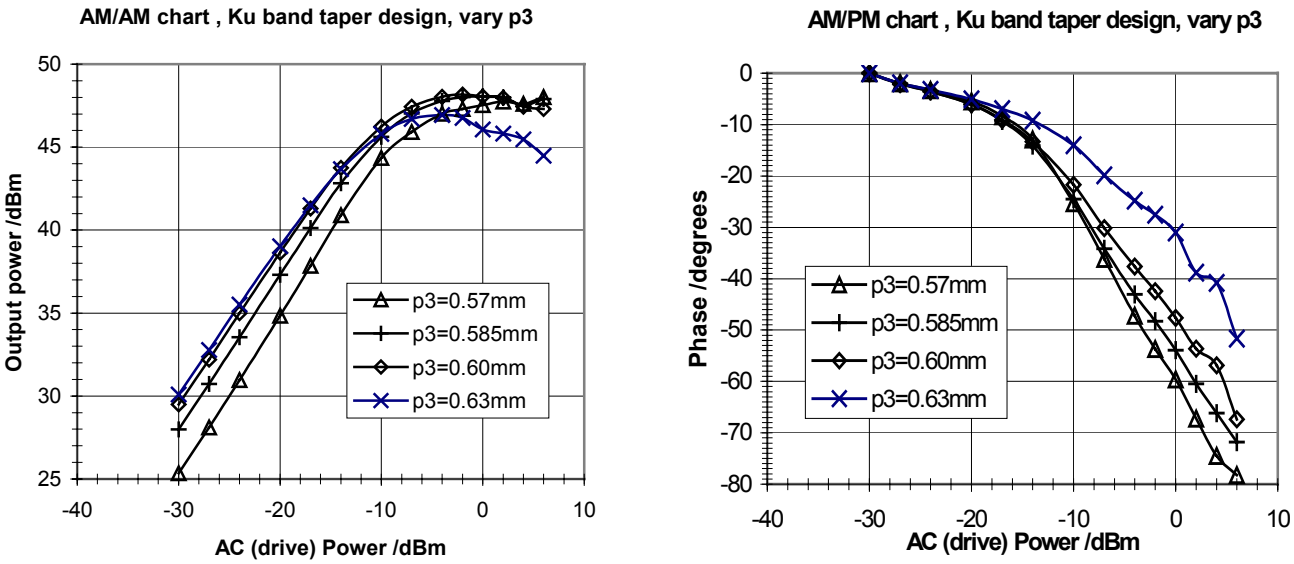

(a) (b)

Fig 6.35 AM/AM and AM/PM curves for a range of output section pitch values

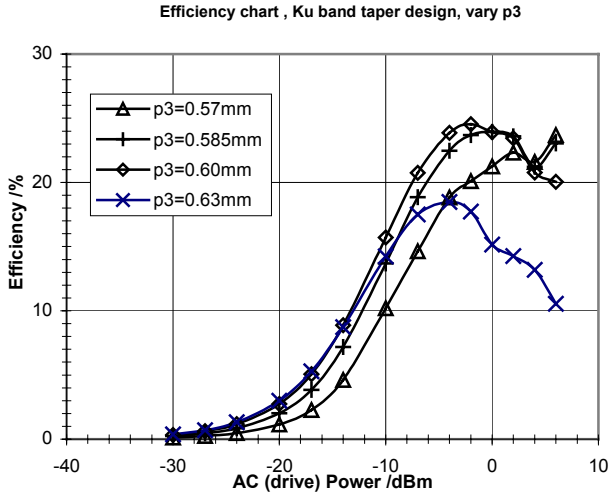

Fig 6.36 Efficiency curves for a range of output section pitch values

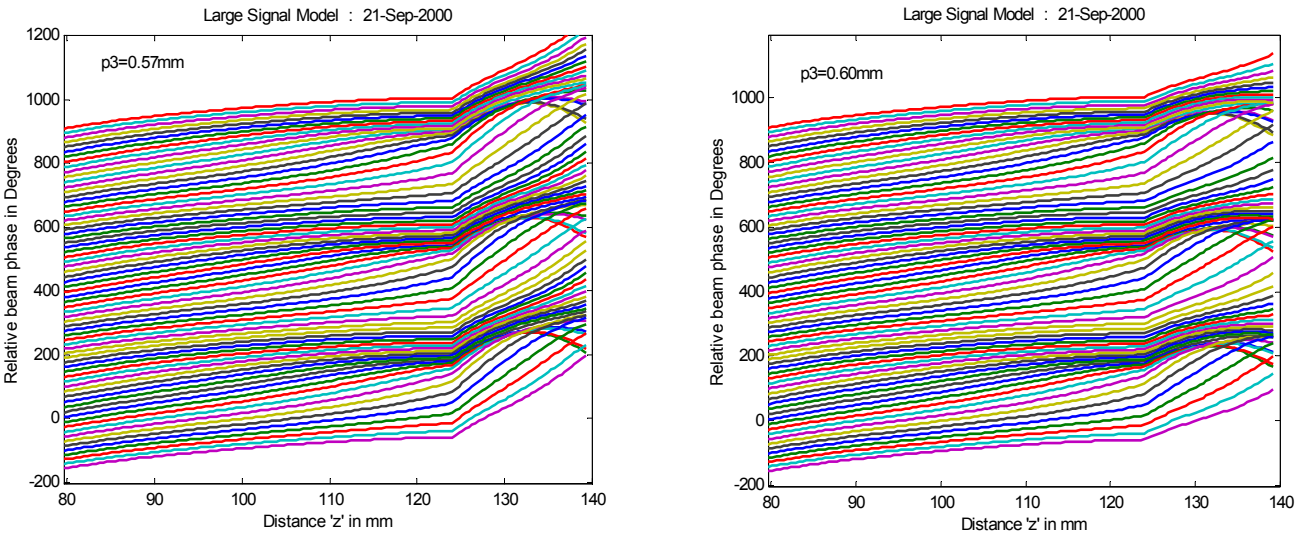

(a) (b)

Fig 6.37a-b Applegate diagrams for p_3 = 0.57 and 0.60mm respectively

6.3.6 Effect of the Output Section Length on the Performance

The effect of the output length on the performance is illustrated in fig.'s 6.38 to 6.40. When the length is extended, the trend of the RF current, phase, power and beam velocity along the axial direction continues in the same way, since the helix properties are not affected by L_3. For example, at an output backoff of say 3dB, the RF current and phase has reached its maximum when L_3=14mm, extending L_3 to 21mm therefore reduces these current and relative phase values at the output. Likewise, the beam velocity is reduced further when the output section length is increased. The consequence is a larger AM/PM conversion for a longer L_3 (fig. 6.38b). The saturation efficiency (fig. 6.39a) reaches its maximum at L_3=17mm, thereafter it deteriorates. Figure 6.39b illustrates this peak in performance as a function of axial distance for the case when L_3=21mm at an input drive level of 0dBm. At this drive level, the AM/AM curve shows the amplifier to be in overdrive with the RF power reduced. This is because the tube has been over extended such that the power has reached beyond its maximum as shown in the figure.

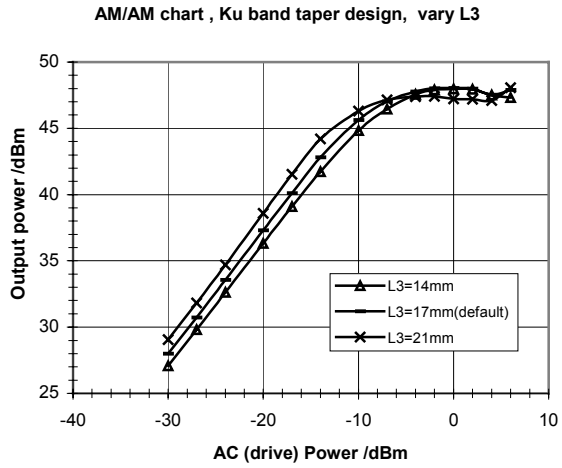

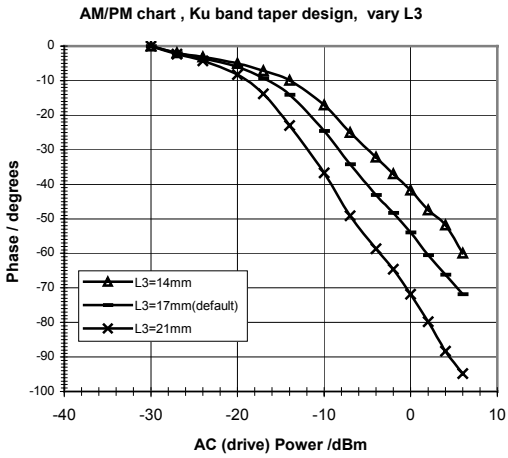

(a) (b)

Fig 6.38 AM/AM and AM/PM curves for a range of output section lengths

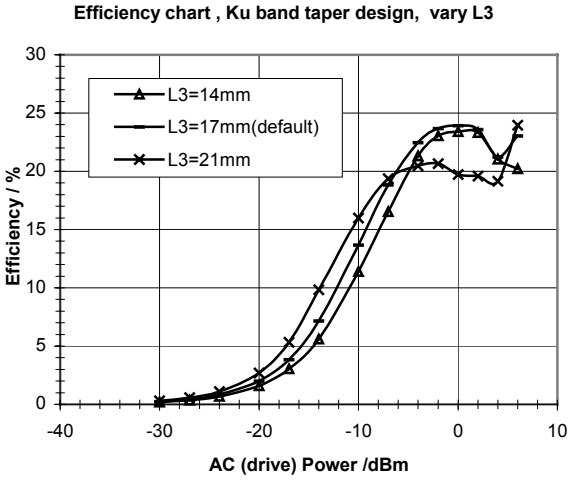

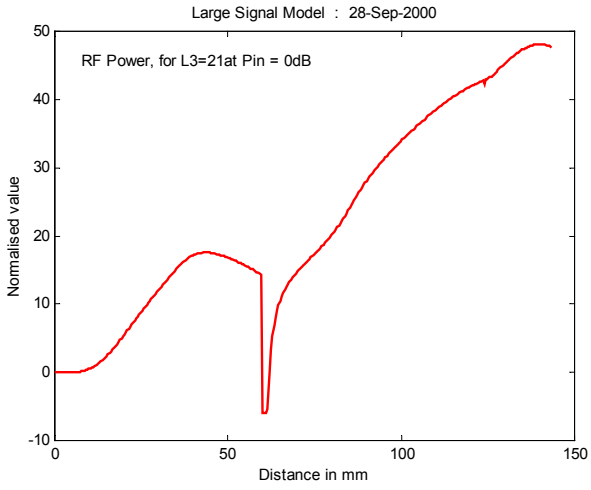

(a) (b)

Fig 6.39 (a) efficiency transfer curves for a range of output section lengths and (b) growth of RF power as a function of axial distance for L_3=21mm at Pin = 0dB

6.3.7 Summary of Results

The results and analysis covered in this section showed how the helix pitches and lengths of the input, centre and output regions affected the nonlinear performance of a helix TWT. It was discovered that the processes of power saturation are most strongly affected by p_2, p_3 and L_3; Phase lag is strongly affected by p_2, p_3 and L_3; and the conversion efficiency is affected by p_2, p_3, L_2 and L_3.

These results are of practical interest for tube manufacturers by identifying and quantifying the significance of variations (e.g. thermal vibrations) to the slow-wave structure at particular regions.

6.4 Broadband and Intermodulation Performance

This section investigates the broadband performance of the final design from Section 6.2.5. This was developed with a DC cathode voltage of 4.88KV (0.160μPerv). The results in this section also include the broadband performance across a range of beam perveances under constant DC power. By adjusting this slow-space charge parameter, the synchronisation between the beam and the helix is affected, effectively varying the trade-offs between the desired conditions. Note that this was also done in the uniform section analysis in Chapter 3.3. It was found that a synchronous beam-wave relationship gave a consistent operation across the 2GHz band.

Figure 6.41 shows the output tube efficiency versus input RF power across the frequency band of 10.7 to 12.75GHz for different beam voltages of 4.76 to 5.24KV (0.171 to 0.134μPerv). The band centre is at 11.7GHz. The output gain curves are also displayed across the bandwidth for the same range of beam voltages in fig 6.42.

For the slow-wave structure design at 4.88KV, the output efficiency is greater at the band centre than at the band edges from saturation to around 7 dB of input backoff. With further backed-off levels however, the frequency for maximum efficiency increases. Generally, this figure shows that a change in beam voltage has a considerable influence on the frequency for maximum output power. This frequency also depends on how close to power saturation the amplifier is driven.

As the beam voltage is reduced from 4.88 to 4.76KV (or beam perveance increased to 0.171μPerv), the conversion efficiency is consistent at saturation (fig 6.41). When the drive level is backed-off however, there is a sharp reduction in efficiency at the lower band edge (10.7GHz) and an increase in efficiency at the upper-band edge. At 4.76KV, the gain at the small signal levels (in fig. 6.42) also grows with frequency.

When the beam voltage is increased from 4.88KV to 5KV (or the perveance reduced to 0.151 μPerv), there is improved efficiency at the lower frequency band-edge, however this is at the expense of efficiency at the upper band-edge. As the DC voltage is increased further, the decline of RF output in the signal increases with frequency

within the band, especially at lower drive levels. The small-signal gain is also reduced when the voltage is increased from 4.88 to 5KV, especially at the upper frequency band-edge at 5.24KV (0.134 μPerv).

Since the slow-wave structure design was optimised for the best trade-off between linearity and efficiency, incorporating broadband optimisation into the tapering strategy as well was difficult. Varying the beam voltage however was found to be a direct way of improving the non-dispersive properties. However, as discussed in Chapter 2.4, the practical way of improving the broadband performance of any helix design in place is by the selection of dielectric material in the support rods as well as including anisotropic loading. Vanes in particular, are an effective practical means of reducing the frequency dependence on the electrical properties.

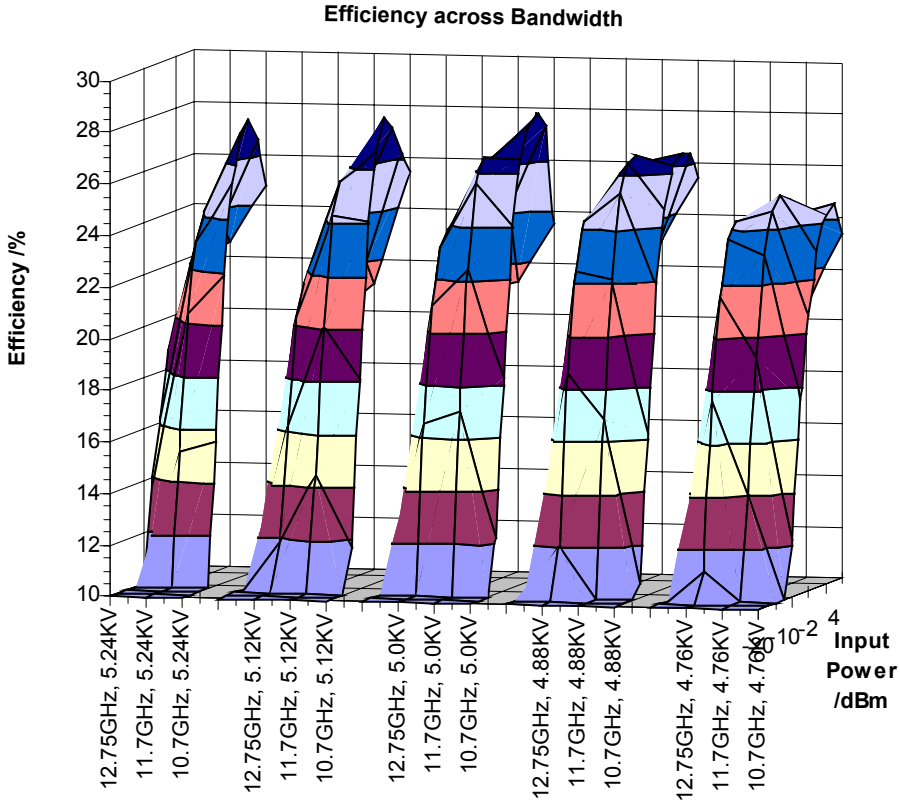

Fig 6.41 Efficiency characteristics across the band for various beam voltages

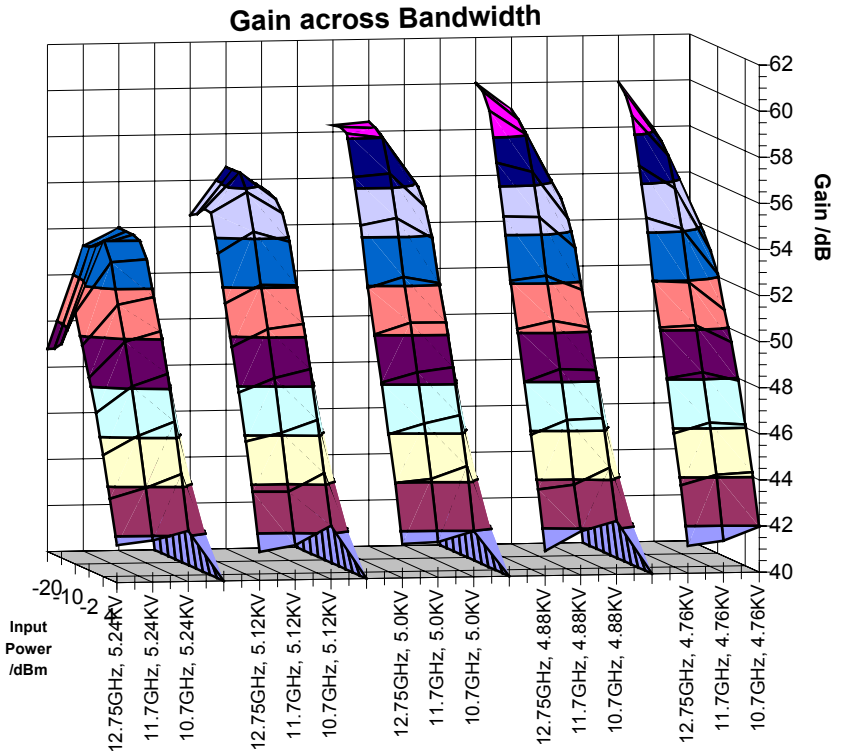

Fig 6.42 Gain characteristics across the band for various beam voltages

The carrier-to-intermodulation ratio at the band centre for a two-carrier signal is given in fig. 6.43. With a full slow-wave structure designed for a trade-off between linearity and efficiency, the output backoff for a C/I3 performance of –21dBc is around 5.5dB. With a lower beam voltage of 4.76KV, this output backoff for a multi-carrier system is improved to 4.9dB. But this is at the expense of reduced tube efficiency, especially at the lower band-edge, as shown in fig 6.41. The optimum choice of DC beam voltage for peak broadband performance at back-off, centred at 11.7GHz lies between 5KV and 4.88KV. However, when the linearity-efficiency trade-off criterion is considered, the optimum choice of beam voltage still remains at 4.88KV. The basic tube efficiency at the output backoff for C/I3=-21dBc across the band is plotted in fig 6.44. The efficiency performance for an acceptable linear performance exceeds 8% at the centre frequency. At say 12.2GHz, this performance could exceed 9%. The best uniform helix design (from Chapter 3) at synchronism (which gives a good efficiency-linearity trade-off) gave a basic backed-off efficiency of 6.5%. The tapered helix has therefore considerably improved the backed-off conversion efficiency.

Appendix C summarises results from a separate investigation which aimed to achieve a design which gives the highest linear performance. This was done purely by optimising the shapes of the AM/AM curves. The data was based on a single negative step taper taken from a design in a previous project. The results showed that it is possible to achieve a design which gives a good linear performance (just 3.8dB output back-off for a C/I3=-21dBc), but this is at the expense of bandwidth and basic tube efficiency.

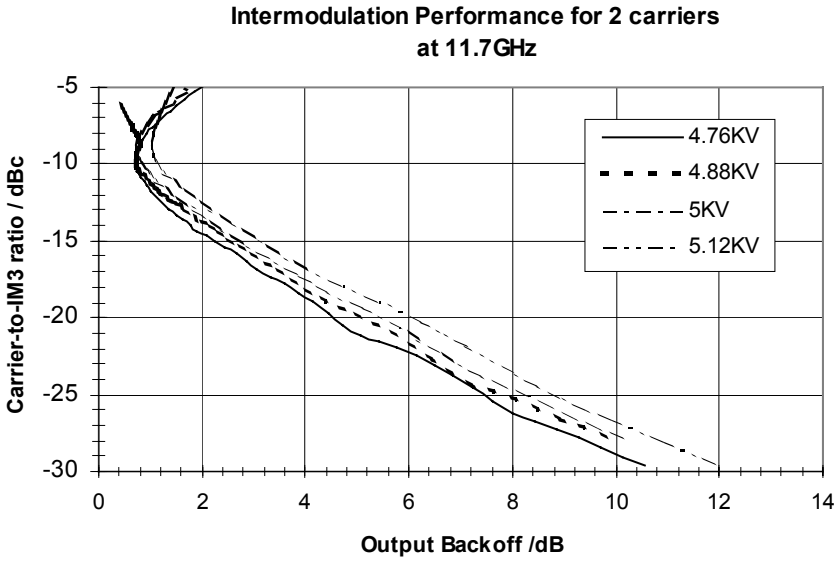

Fig 6.43 Carrier-to-IM3 ratio as a function of output backoff for various beam voltages

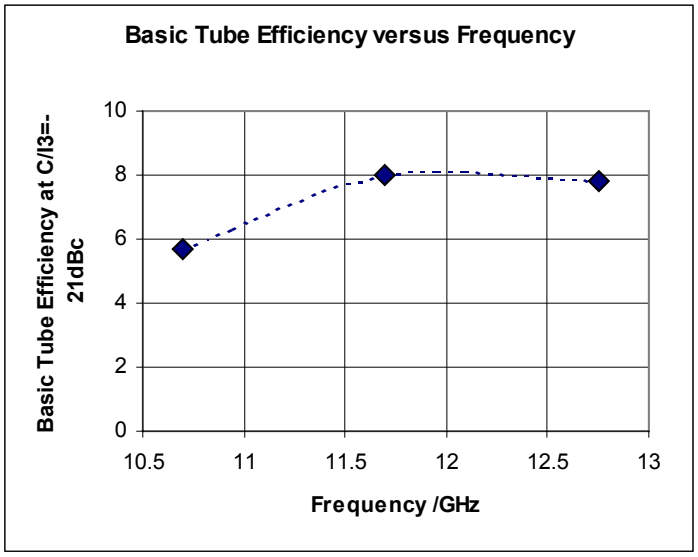

Fig 6.44 Conversion Efficiency at C/I3=-21dBc as a function of frequency

6.5 Design of the Multistage Depressed Collector

The multistage collector is an essential component of the TWT. Its design and operation is a major factor in determining the overall TWT efficiency. When the useful RF energy has been extracted from the electron beam by the slow-wave structure, the spent-beam then enters the collector. There is no axial magnetic field in the collector to control the spent-beam, therefore it is allowed to expand under the space-charge forces. A depressed collector contains electrodes whose potentials are depressed relative to the ground potential. If the collector is multistage, it consists of more than one electrode. The electrons in the beam face a retarding force and land on the electrode surfaces with a lower kinetic energy. Kinetic energy is thus effectively recovered from the electrons in the spent-beam, which is then reused again as DC input power.

The spent-beam energy distribution curves for the full pitch profile designs from Section 6.2 are shown in fig. 6.45. Three powers levels backed-off by 0.8, 1.98 and 4.46dB are displayed for the full helix profile (from Section 6.2.5). A positive-negative stepped pitch profile at 4dB of output backoff is also included for comparison. These spent-beam curves show a varying distribution of energies. The collector's geometry and its electrode potentials must be designed to collect these electrons with their different energies, such that maximum energy is removed from the spent-beam. This is achieved by optimising the voltages of the electrodes so that the electrons with their different energies are collected with the appropriate electrode. Because the spent-beam distribution changes with drive level, the collector must be optimised for consistent maximum power recovery across the dynamic operating drive level range. The spent beam distribution curves for the optimum pitch profile design (shown in fig. 6.45) was input into specialised software for modelling and optimisation of multistage collectors [7]. A four-stage collector was simulated whose potentials were optimised for the three different drive levels. Note that the effect of secondary electrons was not included in the simulations. Figures 6.46a-c show the spent energy distribution curves optimised for output backoffs of 0, 1.98 and 4.46dB respectively [8]. The shaded blocks represent the energy recovered by the different electrodes. Collector potentials optimised at 0dB output backoff have a collector

efficiency of 90.6% (fig 6.46a). To the right of the plot, the collector efficiencies for different drive levels (0, -2 –4, -7 –10, and –14dBm), with the same electrode voltages are shown. Collector potentials optimised at output backoffs of 1.98dB and 4.46 have collector efficiencies of 90.6 and 93.5 respectively (figs 6.46b-c).

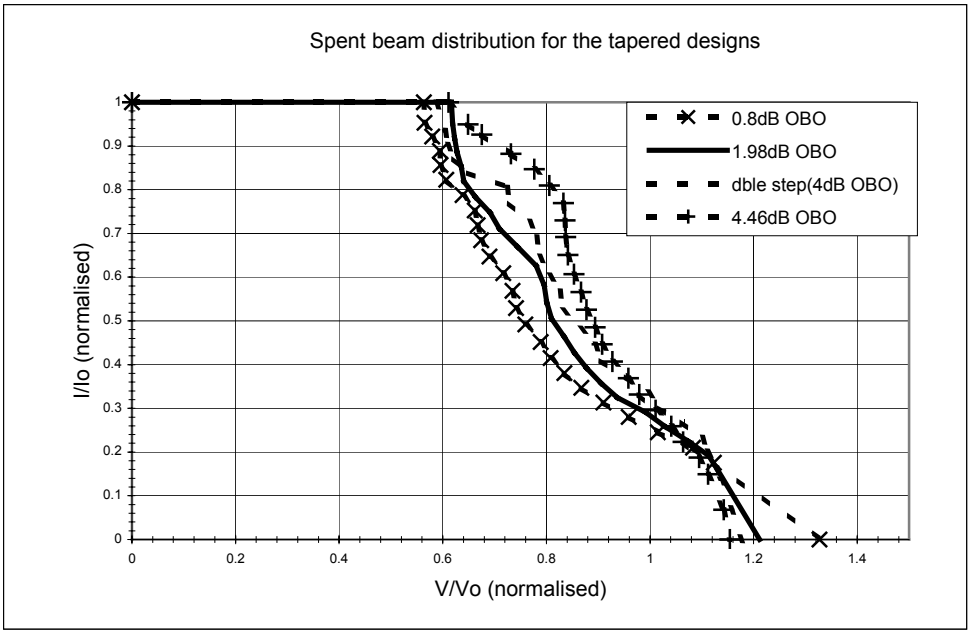

Fig 6.45 Spent-beam distribution curves with the optimum helix design at various output backoffs and a comparison with a stepped pitch profile.

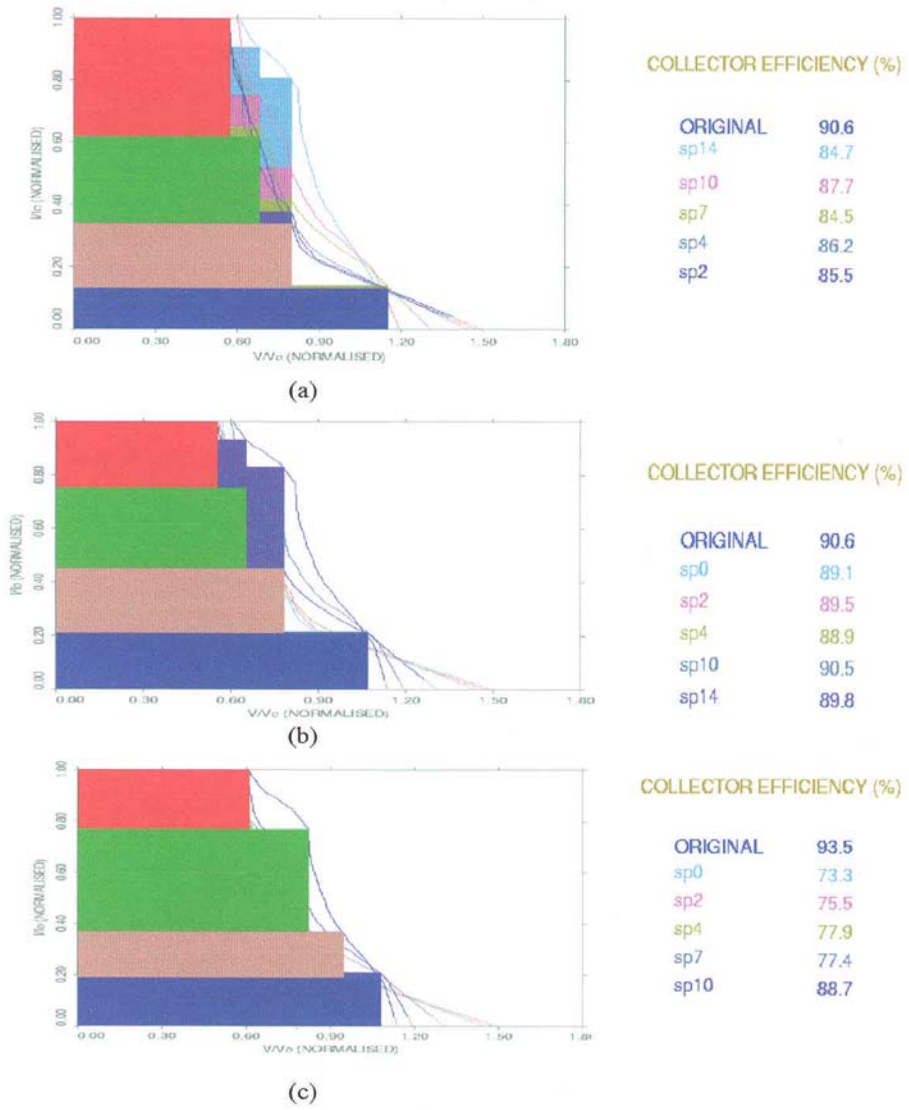

Fig 6.46 Optimisation of the electrode potentials for the spent-beam power distribution curves for output backoffs of (a) 0dB, (b) 1.98dB and (c) 4.46dB. [8]

These collector efficiencies are plotted as a function of input power as shown in fig. 6.47. The three curves represent different selections of electrode voltage optimised for certain output backoff levels. The results from the optimised collector model reveal that for the collector potentials optimised at saturation, the collector efficiency lies between 84% and 91%. When the electrodes are optimised for around 2dB output backoff, the collector performance is more constant – giving around 88 to 92% efficiency. A collector optimised at around 4.5dB of output backoff however, shows

the most dynamic variation in performance – ranging between 71 and 94%. The higher collector efficiency at lower drive levels is a desirable property of the beam collection, since the TWT will be operated across a dynamic drive range- centred at least 4dB of output backoff. It is desirable to maximise the collection of the beam across this dynamic range.

The overall efficiency of a TWT can be expressed as a function of the conversion efficiency η_o and the collector efficiency η_{coll} in the form shown in equation 6.1. The overall performance of the TWT can therefore be plotted. This is shown in fig. 6.48 versus input power.

$$\eta = \frac{\eta_o}{1 - \eta_{coll}(1 - \eta_o)} \qquad 6.1$$

The results of the overall TWT performance illustrate the significance that a well design collector has on the overall efficiency of a helix TWT. When the collector potentials are optimised for operation at around power saturation, the overall efficiency increases from 39 to 78% from –14dBm to saturation. For an optimised collector for around 2dB output backoff, the overall efficiency increases from 49 to 76% from –14dBm to saturation, but peaking at –2dBm with 77% efficiency. When the collector electrodes are optimised at 4.5dB output backoff however, the overall efficiency remains more constant at around 60% across the dynamic range. Note that inclusion of secondary electron modelling in the collector could decrease this value by 10% [8]. The final performance achieved across the band is given in table 6.2.

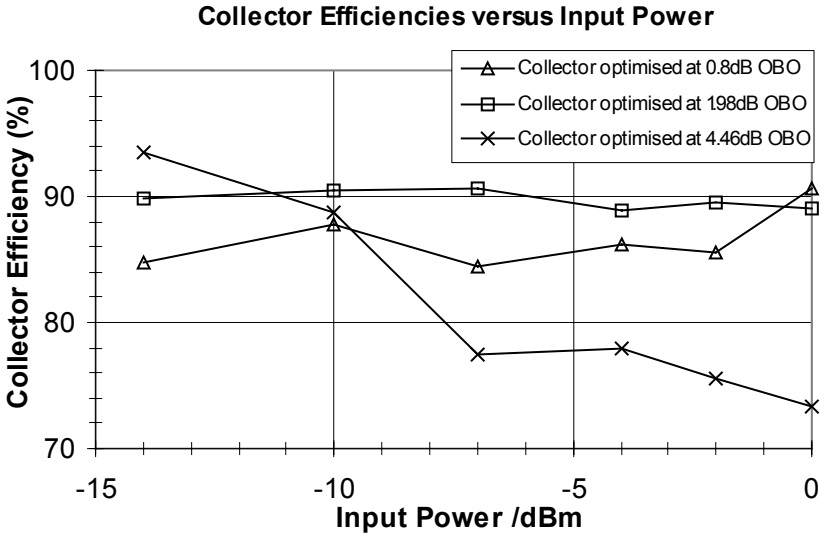

Fig 6.47 Collector efficiency versus input power for different optimised electrode potentials

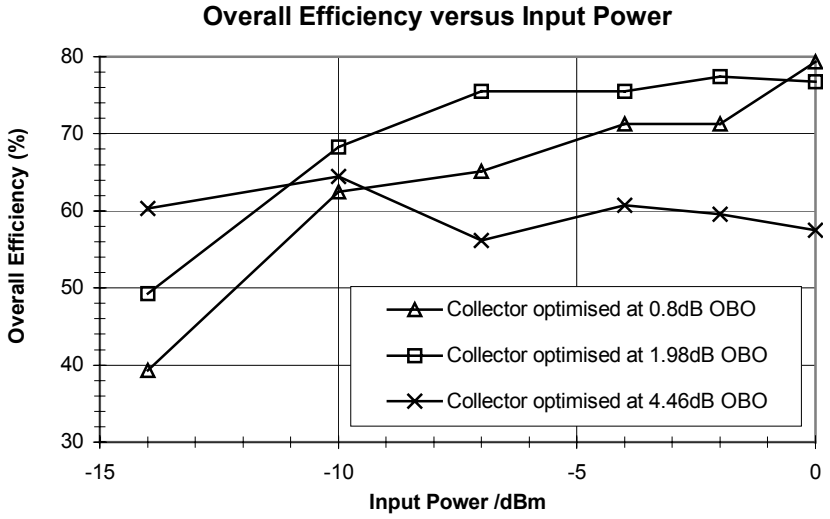

Fig 6.48 Overall efficiency versus input power for different optimised electrode potentials

Table 6.2

Frequency /GHz:	10.7	11.7	12.75
RF saturated output power /dBm	48.51	48.52	48.15
Saturated tube efficiency /%	26.57	26.62	24.45
Output power at C/I_3=-21dBc /dBm	41.18	43.32	43.15
Conversion efficiency at OBO/%	5.7	8	7.8
Estimated collector efficiency at OBO /%	90	92	90
Saturated overall efficiency /%	75	79	76
Overall efficiency at OBO /%	37.67	52.08	45.83

6.6 Conclusions

In this final research chapter, a full helix pitch profile was developed based on knowledge gained about the nonlinear processes in a TWT. It was shown in Chapter 3 that it is possible to meet each of the desired criteria in a helix TWT by optimisation of the helix pitch. This Chapter aimed to achieve the desired criteria in a complete design of the slow-wave structure. Initially in the linear region, the helix is optimised for maximum gain. By increasing the circuit phase velocity as the beam becomes nonlinear, the linearity and the bunching of the device are enhanced. When the bunching is of maximum intensity, the phase velocity is reduced to maximise the power extraction process from the beam. Since this is the highly nonlinear region, the design must be such that an appropriate trade-off between efficiency and linearity is achieved.

When optimising the lengths of the different tapered regions, it was found necessary to analyse the nonlinear behaviour across the dynamic drive range. Knowledge has therefore been gained on the nonlinear processes which are most sensitive to these length variations. It was found that the length of the input region is most sensitive to small signal gain which increases with length, 70mm was therefore chosen. The centre region length has most influence on the gain and bunching intensity, this parameter was therefore optimised for bunching. The length of the output region was shown to have a strong effect on the efficiency and transfer characteristics. The output length was chosen as a trade-off between optimum conversion efficiency and linearity. The sensitivity analysis in Section 6.3 confirms that the design values chosen produced the optimum results for the desired criteria. The six design

parameters were varied within the whole structure and the affect that these have on the nonlinear characteristics were analysed.

The linear pitch transition between the centre and output region has been optimised and incorporated into the final design and is shown in fig 6.48. It was previously thought that the transition in pitch between p_2 and p_3 was critical on the performance. The analysis in this chapter showed that compared with a stepped taper, this design gives just 3 percentage points of saturated efficiency improvement, with negligible improvement in the linear performance.

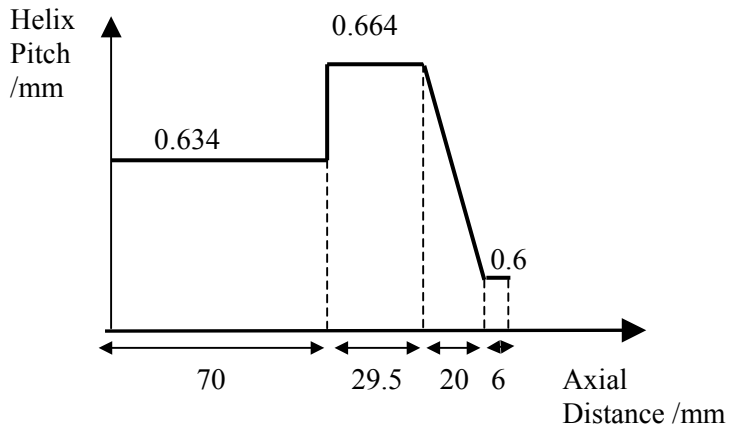

Fig 6.48 Full design of the helix pitch profile

The final design was tested across the bandwidth of 10.7 to 12.75GHz across different beam voltages. The carrier-to-intermodulation output was also given. It was found that a lower beam perveance from an optimised helix design improves the efficiency at the lower frequency, but this is at the expense of efficiency at both the centre and upper frequency band. If the beam perveance is increased, the linearity is also improved, but at the expense of tube efficiency at the lower frequency band. The conversion efficiency (at an acceptable linearity) of the tapered helix design was over 1.2 times that achieved by the best uniform helix design (from in Chapter 3). Backing-off the drive level to achieve an acceptable linearity was found to reduce the overall efficiency at the centre band from 79% down to 52%.

Determination of the overall non-linear performance was done by observing the transfer curves. This is due to convenience, since there are many effects of parameter variations on nonlinear performance to consider and a great deal more can be understood from observing the transfer curves rather than the carrier-to-IM ratio alone.

It is relatively straightforward designing a helix structure specifically for high linearity, high saturation efficiency or good broadband operation. It is common practice to use a computational optimisation routine to maximise one of these criteria. The aim of this research however is a much more challenging one: to observe the effect the different designs have on the bunching and other output characteristics in order to achieve high linearity, high efficiency and across a 2GHz band. These are all essential criteria for TWTs in present and future satellite systems. Careful trade-offs must be considered, for the propagation constants which correspond to the different conditions are separated. The design approach used in this report has successfully detected the important processes throughout the TWT, such that the helix can be designed to optimise all of them. This is the most effective approach to achieve the best possible trade-off.

References

[1] R. O. Jenkins and R. G. Carter, "Design of the Pitch Profile for High Linearity Helix TWT Amplifiers", in Proc. Conf. Displays and Vacuum Electronics, Garmisch-Partenkirchen, Germany, May 2001.

[2] R. O. Jenkins and R. G. Carter, "Optimisation of the Transfer Curves of Multi-Carrier Power Amplifiers for Low Intermodulation Distortion", in Proc. EPSRC-PREP 2001, April 9-11, 2001.

[3] J. E. Rowe and C. A. Brackett, "Efficiency, Phase Shift, and Power Limiting in Variable-Pitch Traveling-Wave Amplifiers", in Proc. National Electronics Conference, Chicago, Vol. 18, 1962

[4] A. S. Gilmour, Jr, "Principles of Travelling Wave Tubes", Artech House Inc., 1994.

[5] A. W. Scott, “Why a Circuit Sever Affects Traveling-Wave Tube Efficiency”, IRE trans. on Electron Devices, Jan. 1962.

[6] Strivastava V. & al., Design of Helix Slow-wave Structures for High Efficiency TWTs, IEEE Trans. on Electron Devices, pp. 2438-2443, Vol.47, Dec. 2000.

[7] T. K. Ghosh and R. G. Carter, “Improved Three Dimensional Simulation of Multistage Depressed Collectors for High Efficiency Travelling Wave Tubes”, in Proc. Vacuum Electronics Conf., pp 215-220, April 2-4, 2001.

[8] T. K. Ghosh and R. G. Carter, “Three Dimensional Modelling and Optimisation of Multistage Collectors”, Ph.D Thesis, Engineering Department, Lancaster University, May 2002.

Chapter Seven: Conclusions and Future Work

7.1 Introduction

This final chapter will summarise all of the methods and results and draw the general conclusions. The achievements and novelty of the thesis will be listed, followed by ideas and suggestions for future research in the same field.

7.2 Summary of the Thesis and Conclusions

Statement of the Problem and Project Objectives

Future satellite communications systems are designed to handle an ever-increasing flow of data traffic. Higher order modulation schemes, such as 16-QAM, are being employed across wider bands as a more effective means of transporting such vast quantities of data. In these schemes where the number of states is higher, it is more difficult to distinguish the different data locations, increasing the likelihood of the occurrence of bit-errors. The linear performance of the space TWT amplifier therefore becomes more essential and desirable in such systems, since it is the TWT nonlinearity that generates spectral noise, leading to bit-errors. For a signal comprising many carriers, the generation of intermodulation (IM) distortion is the main concern due to the level of carrier-to-IM ratio (C/I) and because they arise within the pass-band of the signal. Linearisation techniques are employed more frequently to improve the level of C/I. The drawbacks of linearisers in TWT amplifying systems include increased cost, added hardware complexity, signal phase-matching problems; in addition, their bandwidth limitations. The aim of this project was therefore to identify design methods of a helix TWT for optimising its linear performance without such drawbacks; two objectives were thus:-

1. To understand how nonlinearity arises in a helix TWT.
2. To recognise the desirable conditions in a helix TWT and the designs that can achieve these.

A TWT design which gives a highly linear performance is important, because, for an acceptable Carrier-to-intermodulation ratio, the power level has to be backed-off from saturation, reducing the conversion efficiency by more than half. A design methodology that achieves a high linear performance was therefore required. For an acceptable C/I3, present and future satellite communications systems also require helix TWTs that maintain maximum efficiency consistently across the allocated band (e.g. 2GHz). The following design objectives were targeted at an output backoff that gives an acceptable nonlinear performance .

1. To design for maximum conversion efficiency
2. To design for broad-band consistency (e.g. 10.7 to 12.75GHz)
3. To design the multistage collector based on the spent-beam distribution which gives maximum collector efficiency.

The outcome of this project was to achieve a final TWT design which meets the system's requirements and to improve understanding of the nonlinear behaviour in helix TWTs.

Simulation Tools

The Large Signal Program (LSM-1D) was the main tool to model the nonlinear interaction in the TWT. Based on the single transfer characteristics of the TWT, a quasi-memoryless model was used to quantify the intermodulation distortion (IMAL), since the results are in agreement with the LSM multi-carrier simulations.

Uniform TWT Analysis

The effect of the basic parameters of a uniform Ku-band helix TWT amplifier on its nonlinear performance was investigated in Chapter 3. For this purpose, the transfer curves and the carrier-to-IM ratio for a 2-carrier signal were generated; this is a useful and convenient way of identifying the trade-off between linearity and conversion efficiency.

For a non-uniform slow-wave structure, an initial approach was to synchronise the phase velocities of the beam and the forward circuit wave. This ensured active coupling thus high gain, which gives maximum tube efficiency in the linear power region; this strategy also gave a non-dispersive output RF power. A design spreadsheet was developed (in Excel) based on the Sheath Helix Model to compute the slow space-charge and forward-wave propagation constants (β- and β_0 respectively). The solver obtains a solution for the TWT parameters subject to the condition where β- = β_0. This design strategy is particularly useful when the TWTA is operated at well backed-off drive levels as this would also correspond to the maximum efficiency condition. It was found that the basic parameters resulting in maximum tube efficiency at an output backoff (where C/I3 = - 21dBc) whilst maintaining synchronism were as follows: -

1. A 6.2KV (or a 0.244μPerv) beam for a given DC Power of 800W
2. A corresponding helix radius of 0.778mm and a pitch of p=0.902mm
3. A beam filling factor (b/a) of 0.6

In practice, the two most effective design parameters for controlling β_o and β- are the helix pitch and beam voltage respectively. The results in Chapter 3 revealed how these parameters affect the nonlinear performance and the bunch intensity of a helix TWT. By plotting the nonlinear characteristics as a function of pitch with all other parameters fixed, the development of amplitude and phase nonlinearity has been revealed in a unique way as the amplifier is driven towards saturation. The results revealed how the pitches corresponding to maximum output power (or conversion

efficiency) and phase lag varied as power saturation is approached. As the tube becomes more non-linear, the peak RF beam current was shown to limit; this effectively increases the helix pitch corresponding to maximum electron bunch intensity. On the other hand, the nonlinearity in the TWT reduces the pitch corresponding to maximum phase shift and conversion efficiency. It has also been discovered from the results that for a given pitch, a condition occurs where the phase shift reverses sign and is therefore zero at this transition point. This condition is also independent to drive level up to power saturation. The pitches corresponding to the conditions for optimum AM/AM linearity and optimum phase linearity differed slightly: by about 20μm. In-between these two conditions therefore exists the condition for optimum overall linearity condition (or minimum generation of IM products). The pitch for zero phase shift was found to overlap that of maximum bunch intensity (or maximum RF beam current).

The above simulations were repeated for different beam voltages (or beam perveances). A number of trade-offs were concluded from the results. At the optimum AM/AM linearity condition, a higher beam perveance increases the conversion efficiency, but at the expense of greater phase conversion. At the zero phase condition however, the output power remains constant as the beam perveance is increased, but at the expense of AM/AM linearity.

Uniform un-severed helices are not used in practice, because the saturated output gain is too high for stable operation. But the results did provide a basis on which to fully optimise the design of a helix by identifying the parameters which correspond to the desirable conditions, such as high linearity and high efficiency, that are required in modern communications systems. The work has also contributed to our understanding on the development of nonlinearity in helix TWTs across a range of helix and beam designs.

Understanding the Nonlinear Mechanisms in a TWT

The key to developing a design strategy for a highly linear helix TWT is to understand what causes nonlinearity to arise in the tube. Helix TWTs are inherently nonlinear devices, since power saturation always occurs and the phase nearly always changes; either one of these will generate harmonics and IM distortion, which grow in amplitude as the drive level is increased. The issue of the causes of nonlinearity was addressed in Chapter 4, which gave an insight into the nonlinear beam phase mechanisms - as revealed by the Applegate diagrams. The Applegate diagrams provide a means with which to observe and understand the behaviour of the electrons and their interaction with the RF circuit field. These plots were used to compare the physical behaviour between the conditions of interest, for example maximum tube efficiency and minimum phase lag. The bunch profile for maximum efficiency, where there is large phase lag, revealed the greatest oscillation of electron velocities within the potential well. These results contributed to our understanding on the nonlinear behaviour in the beam, enabling the desirable processes to be identified. This is useful for the purpose of implementing a design strategy: an optimum design is therefore one where all of the electrons are strongly decelerated (i.e. high efficiency) without causing them to oscillate (i.e. achieving a reduced phase conversion).

New figures have also been produced that reveal the phase change of the electrons between successive drive powers. The development of phase nonlinearity throughout the beam is therefore shown. These were used to deduce the strong relationship between the change of phase of the electrons and the AM/PM conversion. For the purpose of TWT design, it is desirable to maintain the phase of the bunch across the dynamic signal fluctuations. The condition of zero phase-lag was also investigated in Chapter 4; such a design surprisingly gives over 40dBm of output RF power. This is because the bunch is very tight over a long axial distance of the tube and there is some energy extraction from the beam, resulting in net reduction of beam velocity. Decelerating electrons in the tube therefore does not necessarily result in phase conversion; but there has shown to be a link between the phase conversion and the change of beam velocity at the tube output as the drive level is increased.

The relationship between harmonics and intermodulation products was investigated in Chapter 5. The initially aim was to determine whether harmonic interaction in a TWT influences the amount of IM product generation. It was found that harmonic interaction in phase with the input carriers had a very minor effect on the level of intermodulation distortion. As expected, the amplitudes of the intermodulation products generated from a single carrier and a single harmonic were very small compared with those generated from two or more closely spaced carriers.

As the drive power is increased, the IM products and harmonic amplitudes always increase. The harmonic beam current, which is very sensitive to TWT nonlinearity however, becomes unpredictable as power saturation is approached. The harmonic current integrated along the tube always grows with the drive level however. The results showed that, as the drive power is increased, the C/I3 ratio increases with the LOG of integrated harmonic current; this relationship is valid for all drive levels.

Research has been carried out in order to discover the root causes of spectral distortion in the RF signal. Beam current and voltage waveforms containing harmonics were generated from the LSM program for a uniform structure corresponding to desirable conditions, i.e. minimum C/I3, maximum RF current and maximum efficiency. These results revealed the extent of the harmonic generation in both the beam current and helix voltage for different drive levels. For the maximum RF current condition, clipping of the waveform peak occurs at power saturation. For minimum C/I3 generation, the peak-to mean current is high (greater than 3 times the DC current) and for maximum basic tube efficiency the harmonic output is the greatest. Chapter 5 has contributed to our understanding on the nonlinear processes in the beam that results in spectral distortion in the output signal. However, this is an area where the physical processes are still not fully understood. Further work (discussed in Section 7.2) is therefore required to fully relate the nonlinear mechanisms in a TWT and its spectral distortion.

Practical TWT Design

The results in Chapter 3 demonstrated that it is possible to meet the desired criteria in a helix TWT by the control of the helix pitch. The aim of Chapter 6 was to achieve the desirable conditions in a single slow-wave structure design. Previous methods on the design of tapered helices were discussed, but these were focused on achieving the best efficiency at the saturated power level. The aim, therefore, was to modify the tapering design strategy for high linear performance as well as high efficiency, so that the amplifier achieves the best efficiency at the required output backoff.

It was necessary to determine the sensitivity of the TWT's nonlinear performance on the pitches and lengths at the input, centre and output regions of the tube. The maximum small-signal gain was found to be most sensitive to the pitch and length of the input region, while both the linearity and efficiency were most sensitive to the centre region pitch and output region pitch and length, and finally the optimum bunch intensity was found to be most sensitive to the centre region pitch and length and output region length.

The design tapering method for maximum efficiency [1] was modified so that in the region where the electrons become trapped, the circuit phase velocity is increased to optimise the bunch intensity in addition to optimising the transfer curves. When the bunch has maximum intensity, the phase velocity is then reduced to ensure that as much RF power is extracted from the beam whilst maintaining transfer curves that are as linear as possible. It was found however, that a trade-off was required between efficiency with linearity. A linear pitch transition between the centre and output region was then incorporated into the pitch profile design for an enhanced efficiency performance; the final design is shown in fig 6.48.

The output performance of the final design was tested across the bandwidth of 10.7 to 12.75GHz for a range of beam perveances (at constant beam power). It was found that with an optimised slow-wave structure design, a reduced beam perveance improves the efficiency at the lower frequency band, but at the expense of efficiency at both the centre and upper band. An increased beam perveance however improves the linearity, but at the expense of tube efficiency at the lower band.

Based on the spend-beam curves, a multi-stage collector whose electrode potentials are optimised for efficient beam collection gives an overall collection efficiency of over 90% (neglecting secondary electrons in the model). Achieving the acceptable linearity reduced the overall efficiency from 79% down to 52%. However, this backed-off efficiency is 7 percentage points more than the best uniform design achieved in Chapter 3.

The work in this thesis has identified the desirable conditions in a helix TWT and investigated them using Applegate diagrams, beam current and voltage waveforms, etc. This has contributed to our understanding of the physical processes in a helix TWT which result in high efficiency and power saturation and phase conversion. Based on this acquired knowledge it is fairly straightforward to design a uniform slow-wave structure specifically for high linearity, high saturation efficiency or a good broadband operation.

The aim of this project however was more challenging: to achieve simultaneous high linearity and high efficiency across a broad band of 2 GHz. It was found that careful trade-offs must be considered to achieve this. Alternative ways of achieving linearity and efficiency simultaneously is discussed in further work (in Section 7.3). However, a non-uniform slow-wave structure has been designed, where the pitches and lengths have been optimised for the best trade-off between conversion efficiency and linearity. An equally important achievement of the work included a better understanding of the basic TWT parameters on the nonlinear behaviour in the beam and in the output signal. Many of the results in this thesis have been well published in conferences on vacuum electronics (as listed in Appendix D).

7.3 Further Work

The research in this thesis has covered a broad range of issues. Hence, there are many ideas for future work to be carried out as a continuation of this research. Suggestions will be given in this section covering the fundamental understanding of the physics of a TWT, design method and linearisation techniques of a TWT amplifying system.

A lot of the fundamental nonlinear physical mechanisms of a helix TWT is not yet fully understood; this thesis has gone some way to improving this knowledge. Further modelling and understanding is required on the physical mechanisms in a TWT that generate harmonics at small-signal levels and towards power saturation. By relating this model to one in which the generation of intermodulation products occurs would give a more thorough understanding on the nonlinear mechanisms that cause harmonics and intermodulation products to arise and their relationship.

The improved understanding on the interaction processes in a TWT provided by this work gives a better idea of a design methodology for a simultaneously linear and efficient performance. An aim would now be to design a slow-wave structure where, if possible, the bunch intensity maintains consistency to minimise the phase lag whilst, at the same time, the bunch decelerates. Such a design would give low phase conversion and high efficiency, however achieving these two conditions simultaneously have, so far, been difficult.

Linearisers are gaining popularity despite their drawbacks. A useful insight into how a lineariser affects the nonlinear tube performance can be made. This can be compared to the performance without a lineariser incorporated. A band–pass filter is also a common device in a TWT amplifying system. By simulating signal reflections at the tube output at the out-of-band frequencies, the effect of a filter on the output TWT performance can be determined.

The types of modulation schemes in this project have been limited to single and multiple carriers with equal amplitude. NPR, 2-carrier and single carrier measurement have therefore been made. Investigating more complex amplitude and phase-varying modulation schemes, such as QPSK and QAM, on the nonlinear TWT performance may give a useful insight; IMAL can be used for this purpose.

This thesis has recognised the trade-offs that exist between linearity and efficiency in a single TWT design. Alternative linearisation methods for linearising helix TWTs have recently been published and patented [2,3]. In these methods, both phase and amplitude distortion are minimised by dynamic adjustment of the beam voltage and the beam current respectively. To minimise phase conversion, the electrons in the beam can be made to move along the interaction region at approximately the same velocities. Controlling the potential difference between the cathode and the anode effectively changes the beam velocity.

Figure 7.1(a) shows the phase transfer curves for different beam voltages. By adjusting the beam voltage from V_1 to V_3, a more constant phase is maintained across the dynamic drive range (from a to c), as shown by the bold line in the figure. AM/AM conversion can also be minimised by hard limiting the output RF power as a function of input RF power. Amplitude linearity can therefore be maintained across the dynamic range by adjusting the current in the beam. This is shown in fig. 7.1(b), where the amplitude transfer curves are plotted for different beam currents. Controlling the beam current (I_1 to I_3) effectively linearises the AM/AM transfer curve (from a to c). Control of the beam current can be achieved by adjustment of the potential difference between the cathode and the control grid.

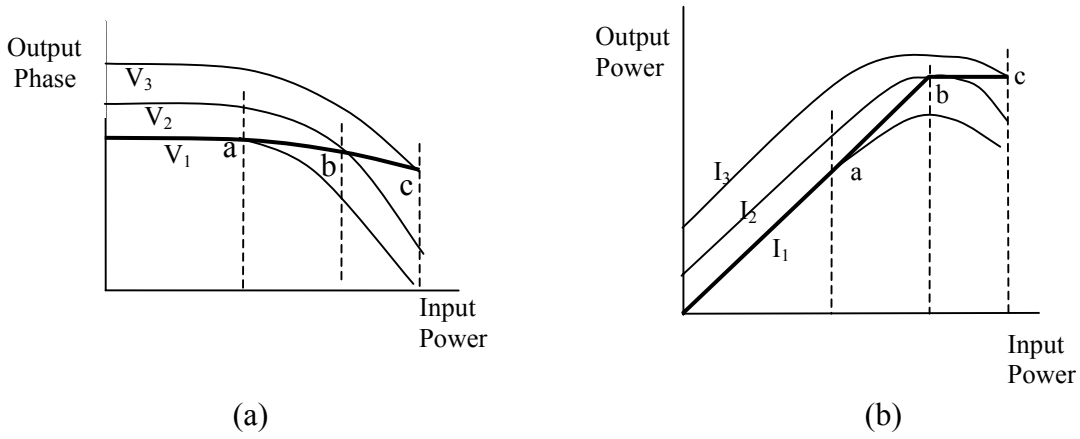

Fig 7.1 Linearised Phase and Amplitude characteristics by controlling the beam voltage and current respectively

A schematic layout of an example of such a system is shown in fig 7.2. The system includes a signal envelope detector, generators, Op Amps (with attached gain adjustment circuits) and variable voltage supplies. The input signal envelope is sent to two function generators, each containing pre-stored data about the amplitude and phase response of the TWT. One function generator determines the cathode potential to correct the beam voltage across the dynamic RF range, resulting in minimum phase delay. The other function generator modulates the voltage of the focussing electrodes relative to the cathode. The beam current is then controlled dynamically to linearise the power transfer curves. The RF signal line has a delay device fitted to account for the delay in the circuitry. All of the features described can be embodied into a single device such as a DSP or ASIC with a single input terminal coupled to the RF input signal and an output of two control signals.

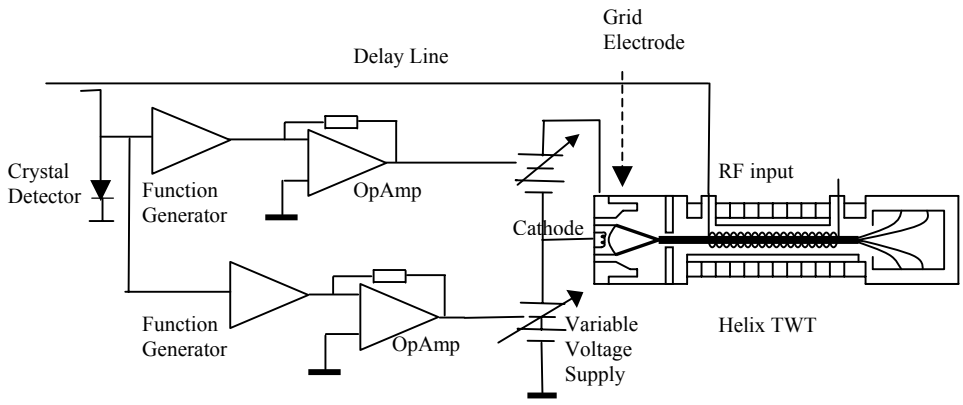

Fig 7.2 A schematic set-up of the linearisation technique for a helix TWT.

Experimental results from this technique show a dramatic improvement in the overall non-linear performance. A measured improvement of up to 23dB in the signal to intermodulation noise ratio for two carriers has been demonstrated [3]. The TWT amplifier can therefore be driven closer towards power saturation, providing a highly efficient operation (up to 70%), whilst maintaining a signal-to-intermodulation noise ratio of say -25dBc.

The technique has major limitations however, with regards to the frequency and bandwidth. Firstly, the cathode and grid corrections need to match with the variations in the RF envelope. This limitation of the reaction time will therefore restrict any variations in the signal envelope below a frequency of say 5GHz. The other limitation of this technique is the bandwidth due to the delay of the signal through the TWT. Testing of this technique has been demonstrated with a bandwidth of a few hundred kHz. Accounting for the transit time for the RF wave to maintain equilibrium in the TWT, a theoretical bandwidth of at least 100MHz is achievable. In practice, the bandwidth can be made considerably wider by restricting this transit time. Since the effect of the backward wave can assumed to be small compared to the forward wave, achieving a steady-state in the TWT is not necessary. Future work would be to find further ways of overcoming these bandwidth restrictions, so that this technique may be of practical use for future communications applications.

References

[1] Strivastava V. & al., Design of Helix Slow-wave Structures for High Efficiency TWTs, IEEE Trans. on Electron Devices, pp. 2438-2443, Vol.47, Dec. 2000.

[2] T. Chen and Y.Goren, "System and Method for Linearizing Vacuum Electronic Amplification", Pat.#6285254, September 2001.

[3] Y. Goren, C. Jensen, T.Chen, P. Lally, and D. Gagne, "A Novel Technology for Linearizing Traveling Wave Tube Amplifiers", Proc. Conf. Intl. Vacuum Electronics, Monterey, USA, April 2002.

Appendix A: Sheath Model Design Spreadsheet Parameters and the Calculation of the Plasma Frequency Reduction Factor

Table A.1: Input and output parameters of the 3 design spreadsheets

(1) Main Spreadsheet

Input		**Output**	
Frequency	f	current	Io
dc power	Pdc	perveance	Perv
Cathode Voltage	Vo	pitch angle	ϕ
Helix radius	a	beam radius	b
Fill factor	a/b	phase velocity(relativistic)	vp
Pitch	p	effective plasma frequency	
Tape width		(using Brewer diagrams)	ωq
to pitch ratio	δ/p	slow space charge-wave	β-

(2) Beam Spreadsheet

Input		**Output**	
Beam stiffness	m	charge density	ρo
Cathode loading	Lc	plasma frequency	ωp
Data from s.sheet (1)		Brillouin field	BB
		Axial Magnetic field	Bz
		Peak axial Magnetic field	Bz
		Cyclotron frequency	ωc
		g-factor	g
		Cathode radius	rc
		Cathode magnetic field	Bc
		cathode flux	ϕc

(3) Synchronism Spreadsheet

Input	**Output**	
Data from (1)	shield radius	c
Dielectric constant εr	Capacitance (incl. Support rods)	C2
Dielectric loading ϕN	inductance (incl.support rods)	L2
	Axial propagation constant (incl. Support rods)	βo

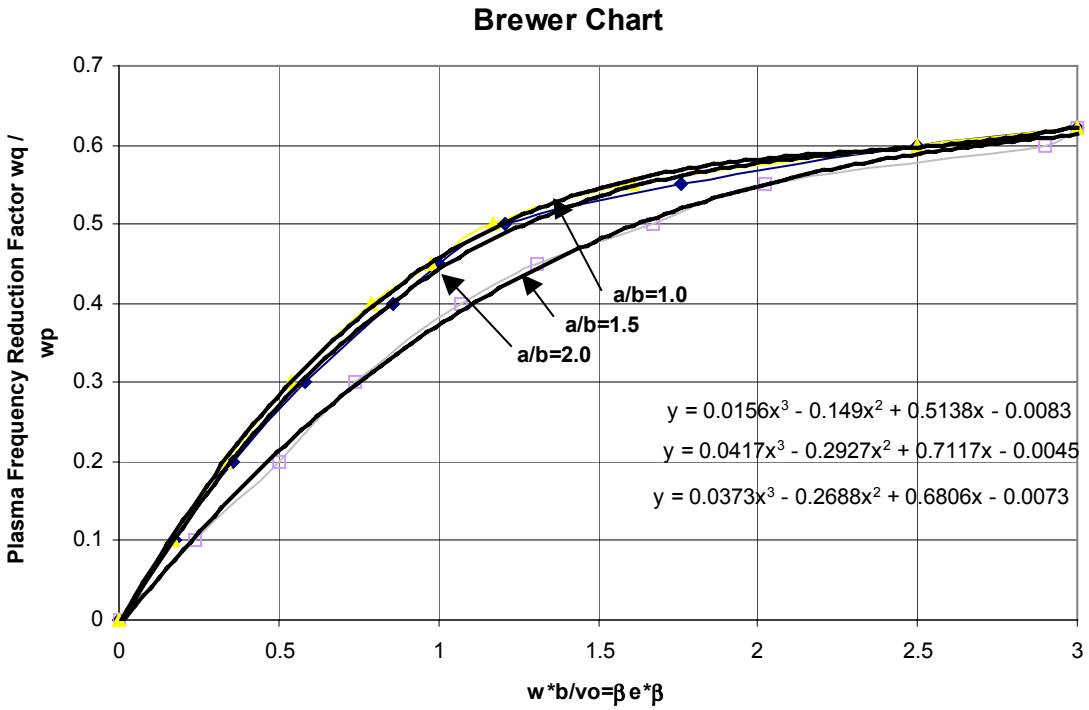

Fig A.1 Brewer diagram for the calculation of the plasma frequency reduction factor

Appendix B: Single Negative Step Taper Design

To ensure convergence and therefore reliable results, an attenuation α_i profile was introduced with a sever. The set up is shown as fig B.1.

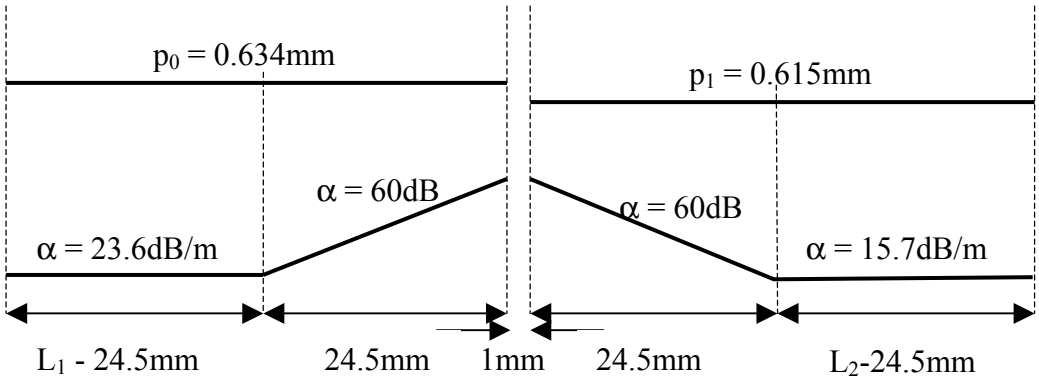

Fig B.1 Representation of the pitch and loss profiles for a single step negative taper

The length L_1 was adjusted for maximum RF current, which is an approximation to the condition of maximum bunching. This was done for a fixed drive power (around 3 dB below saturation power). For a range of L_1 from 55 to 65mm, the peak RF current was determined. The graph (fig B.2) shows the current distribution to be non-uniform, but contains a clear peak at L_1=60mm. Note that a constant loss profile was used in this case, explaining why the normalised current values are especially high.

When the input drive level is varied however, the RF current peaks at different power levels, as shown in fig B.3 (with the loss and sever profile now incorporated). This means that in order to determine the maximum current, it is necessary to scan across the input power range. Figure B.3 shows that L_1 = 70mm, gives the highest level of current, while L_1 = 65mm produces the most consistently high level of current. It is also observed that as the length of the first section is increased the maximum bunching condition is achieved at lower drive levels. A longer input section allows the gain to increase over a longer distance, thereby making the design more suitable for lower input signal levels.

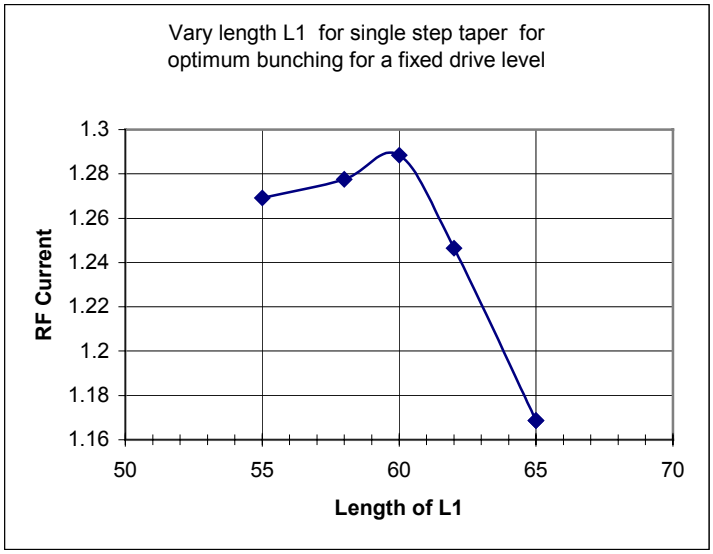

Fig B.2 RF current as a function of length L_1 for a single drive level

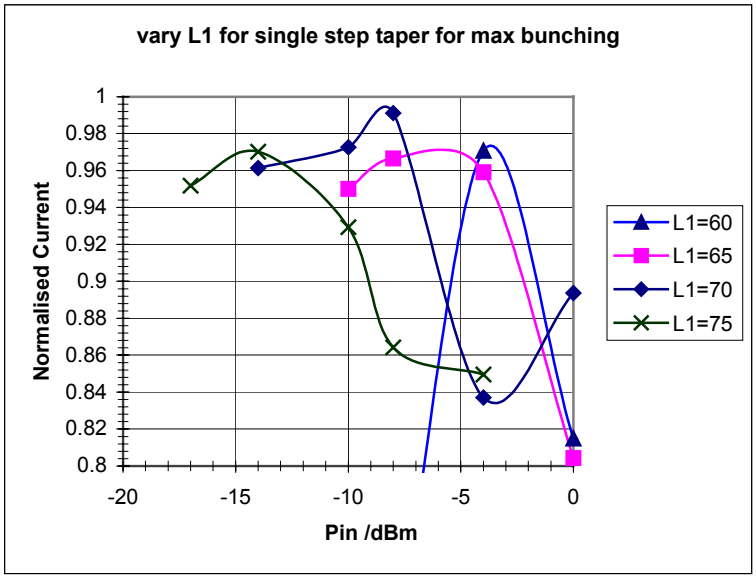

Fig B.3 RF current versus drive level for different lengths L_1

The Applegate diagrams for these three cases (shown in fig B.4) reveal similarities in their bunching. This is partly due the pitch profiles being the same and also due to the power levels at which the three cases were taken – each one corresponding to the point where the current is maximum. As soon as the electrons have passed through the positive phase velocity transition, the electrons become trapped. More electrons become fully captured, where they fall back into a decelerating phase. The trapping of

the electrons occurs over a large axial distance (50mm). After trapping has occurred, the relative phase of the electrons oscillate within a potential well, as clearly observed in the last figure. The current and relative phase for these three different designs are shown in fig.B.5. The maximum power output occurs when L_2=70mm, however the linear performance is poor.

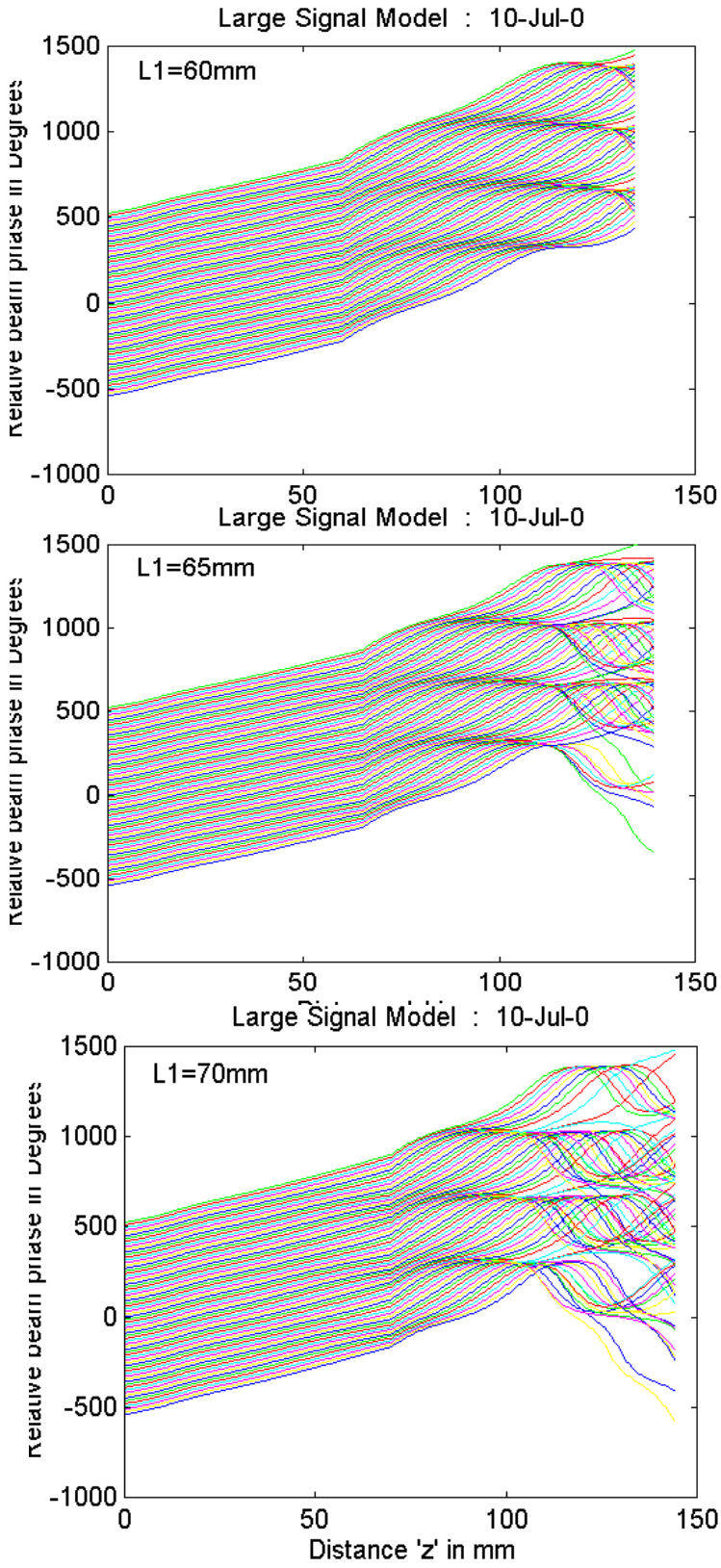

Fig B.4 Beam bunching diagrams for selected values of L_1 at drive levels where current is maximum.

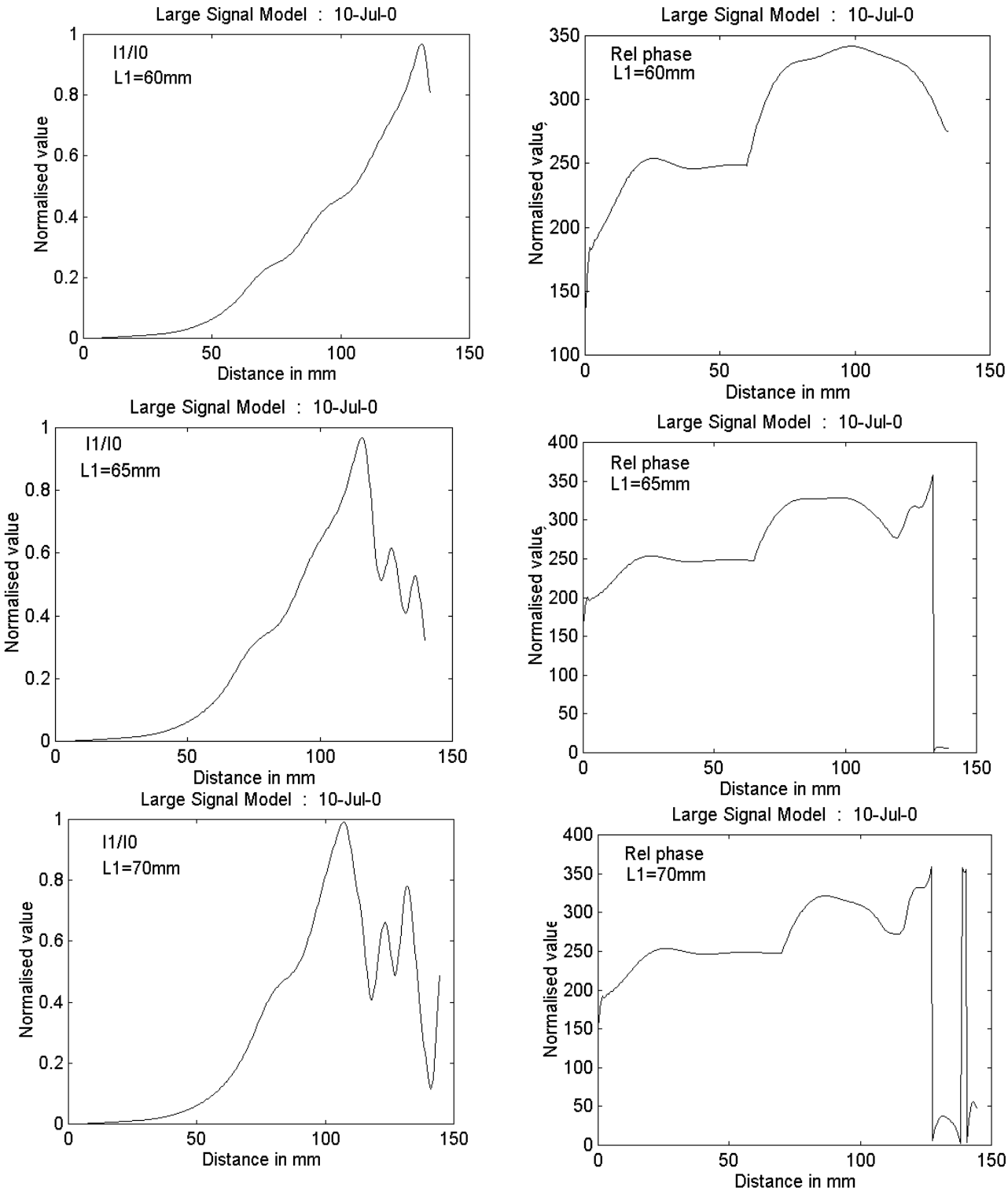

Fig B.5 Corresponding RF currents and relative phases for L_1=60, 65 and 70mm

Appendix C: A Single Negative Step Taper for High Linearity

This Appendix reports on a brief investigation based on selected design data from a previous TWT project (HEMTWT) which produced the most desirable transfer curves. This was found to be a single negative step taper with reasonably flat AM/AM transfer curves, however the broad-band performance was unreported. The axial propagation constants (β_0) and length variables were used to further improve the linearity of the transfer curves.

Fig C.1 shows the results for β values in the first section (β_1) plus and minus 50 of the HEMTWT design data. The effect of β on the AM/AM shapes is mainly due to the difference in gain in this region. In the second section however (fig C.2), the effect of β_2 on the AM/AM curves is more profound – strongly affecting linearity and efficiency. Fig C.3 shows the choice of L_1 has a minor effect on linearity, since the gain is affected in this region. L_2 however has an important influence on the AM/AM curves as shown in fig C.4. Beyond say L_2=15mm, a kink develops before saturation, which must be avoided.

When choosing the design with the most desirable AM/AM curves, based on these results, the dependence of the parameters on each other must be considered. For instance choosing a value of β_1 = 1700 will not result in a kink in the AM/AM curve if L_2 is below a certain limit.

After repeated tests to optimise the intermodulation based on the transfer curves, the final design for minimal IM distortion, h20, was as follows: β_1 = 1750, β_2 = 1900, L_1=90, L_2=15. The corresponding pitch values to the chosen β values are p_1=0.68mm and p_2=0.645mm, for a given helix and support rod design. The carrier-to-intermodulation produced from this is highly favourable as shown in fig C.5 as a function of output backoff: just 3.8dB output back for C/I3=-21dBc (an NPR measurement requires 5.5dB of output backoff). However the broadband performance is very poor as shown in fig C.6. In an attempt to improve the broadband performance, adjustments to the design were carried out, which caused deterioration

in the linearity as illustrated in fig C.5 for design h21. However the broadband performance of h21 was improved (fig C.7): an output power range of just 1.5 dB across the bandwidth (assuming operation at a backoff greater than 2dB).

This form of design approach was useful by determining the optimum AM/AM curves that could be achieved with a single taper. It has also demonstrated (using two extremes as an illustration) that the trade-off that exists between linearity and broadband performance.

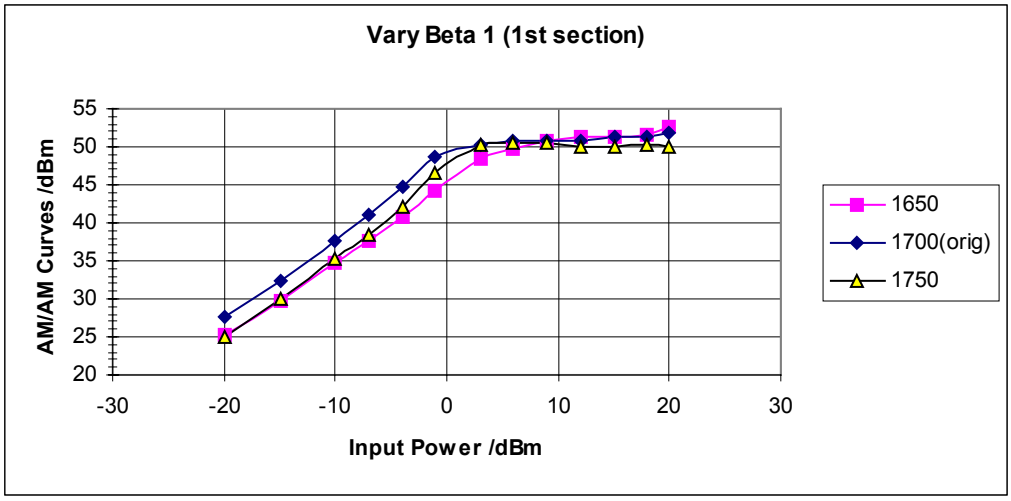

Fig C.1 AM/AM curves for β variation in the first section

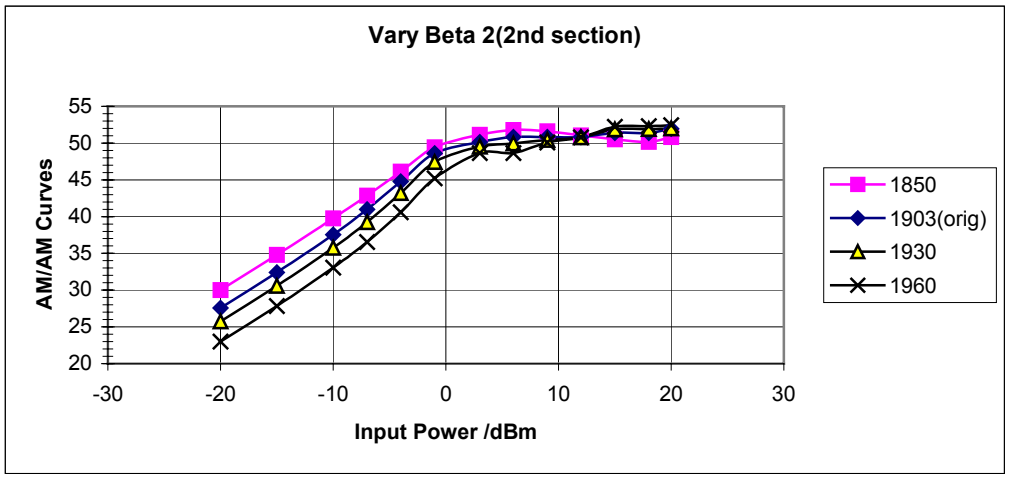

Fig C.2 AM/AM curves for β variation in the second section

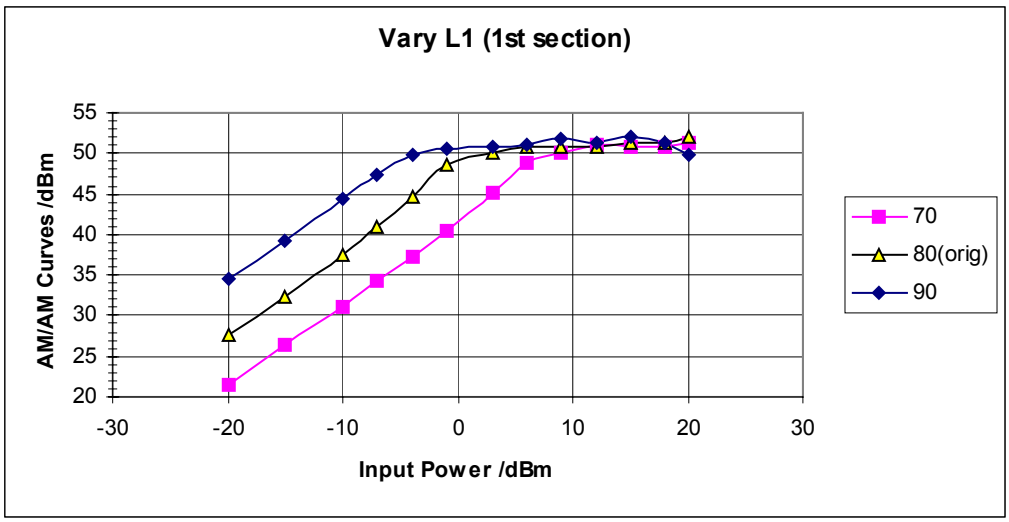

Fig C.3 AM/AM curves for different first section lengths in mm

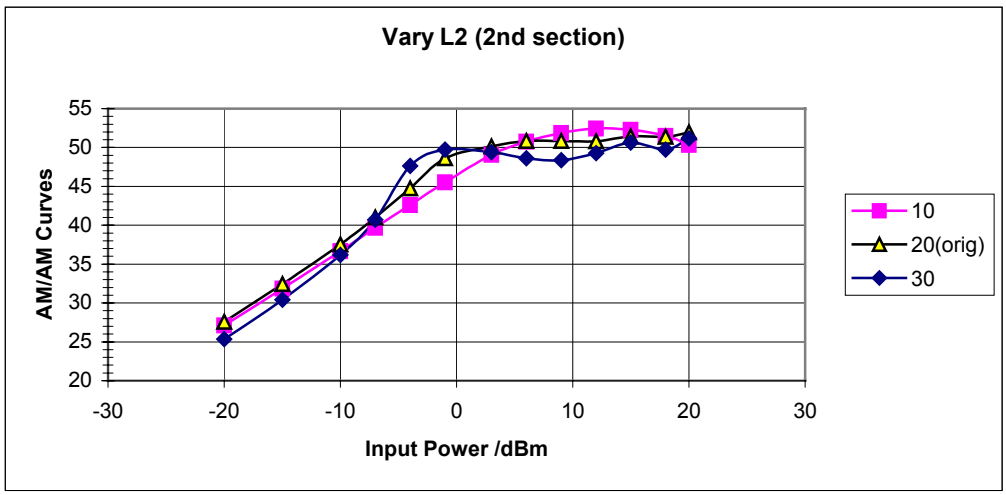

Fig C.4 AM/AM curves for different second section lengths in mm

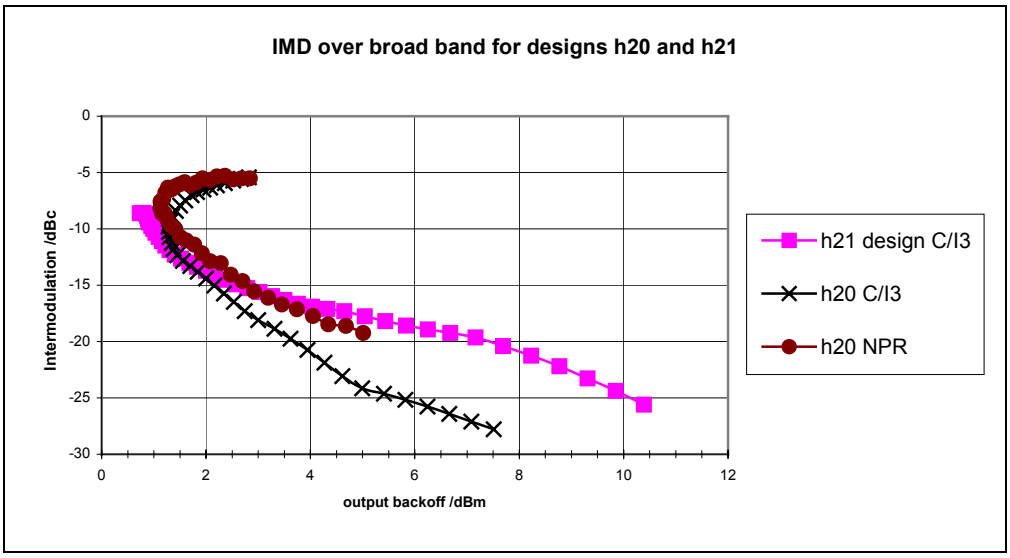

Fig C.5 Intermodulation performance for designs h20 and h21

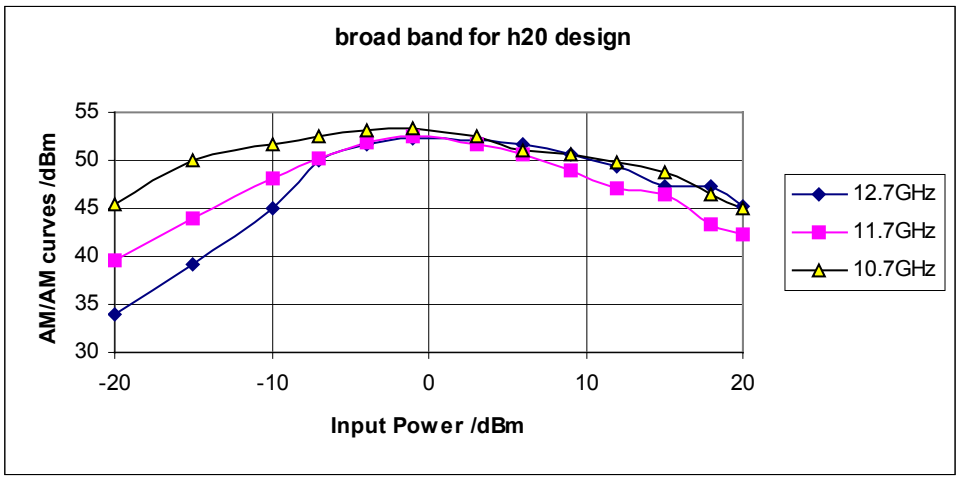

Fig C.6 AM/AM curves for across the allocated frequency bandwidth for design h20

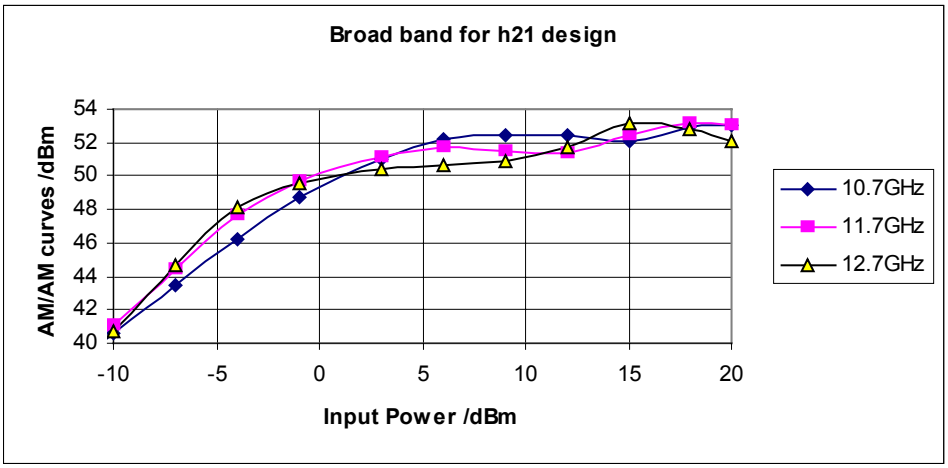

Fig C.7 AM/AM curves for across the allocated frequency bandwidth for design h21

APPENDIX D: PUBLICATIONS

During my PhD, I have presented my work in progress, at least five times to industrial collaborators and other academic staff and students. I have also written technical progress reports and presented my results at national and international conferences; the conference publications are listed below.

INTERNATIONAL CONFERENCE PUBLICATIONS

1. R. O. Jenkins and R. G. Carter, "Effect of the Beam Parameters on the Non-Linear Performance in Broadband Helix TWTs", IEEE International Vacuum Electronics Conferences, Monterey, USA, April 2002.

2. R. O. Jenkins and R. G. Carter, "Design of the Pitch Profile for High Linearity Helix TWT Amplifiers", ITG-Conf. on Displays and Vacuum Electronics, Garmisch - Partenkirchen, Germany, May 2001.

3. R. O. Jenkins and R. G. Carter, "Use of Electron Bunching Diagrams for the Design of Pitch Profiles in Helix TWTs", IEEE International Vacuum Electronics Conferences, ESA, Netherlands, April 2001.

NATIONAL CONFERENCE PUBLICATIONS

1. R. O. Jenkins and R. G. Carter, "Design of Helix TWTs for Optimum Linearity", 7th IEEE Postgraduate Student Colloquium, London, September 2002.

2. R. O. Jenkins and R. G. Carter, "High Linearity Broadband TWT Amplifiers for Satellites", Northern Vacuum Electronics Conference, Strathclyde University, Glasgow, July 2002.

3. R. O. Jenkins and R. G. Carter, "The Issues of Linearity in Helix TWTs", Northern Vacuum Electronics Conference, Lancaster University, Lancaster, July 2001.

4. R. O. Jenkins and R. G. Carter, "Optimisation of the Transfer Curves of Multi-Carrier Power Amplifiers for Low Intermodulation Distortion", Preparation of Event Digest Contribution (PREP-2001), EPSRC, Keele University, April 2001.

TECHNICAL REPORTS

1. R. O. Jenkins and R. G. Carter, "High Linearity Broad-band Helix TWT Amplifiers for Satellite Communications Systems", Progress Report 2, Engineering Department, Lancaster University, MRG/2001/11, November 2001.

2. R. O. Jenkins and R. G. Carter, "High Linearity Broad-band Helix TWT Amplifiers for Satellite Communications Systems", Progress Report 1, Engineering Department, Lancaster University, MRG/2001/1, January 2001.